Project B.14 – Demonstration of Enhanced Fire Safety Technology

Part 3: Full Scale Vehicle Fire Tests of a Control Vehicle and a Test Vehicle Containing an Intumescent Paint on its Underbody

Jeffrey Santrock and Douglas E. LaDue III
General Motors Corporation

Abstract

This report describes tests of an intumescent paint applies to the lower surface of the floor panel in a test vehicle. The test vehicle with added intumescent paint was subjected to a crash test where the vehicle was stationary and struck in the left front corner by a moving barrier. The crash tested vehicle was then subjected to a fire test, in which liquid gasoline pumped from an external reservoir onto the ground under the test vehicle was ignited with a pilot flame. When compared to a control test, the intumescent coating did not appear to substantially affect the timing of flame-spread into the passenger compartment or heat transfer through the floor panel.

Table of Contents

Appendicies

List of Figures

Report

List of Figures

Appendicies

List of Tables

Report

1 Introduction

The test described in this report was conducted by General Motors (GM) pursuant to an agreement between GM and the U.S. Department of Transportation. The purpose of this test was to evaluate the effects of an intumescent coating applied to the floor panel on propagation of flames from burning gasoline under the test vehicle into the passenger compartment. An intumescent material is one that bubbles or swells and chars when exposed to heat or flame. In so doing, gas bubbles are trapped in the charred residue of the expanded material, thus forming an insulating layer that can reduce heat transfer into and through the expanded (intumesced) material.

In a separate testing program, researchers at the Building and Fire Research Laboratory, National Institutes of Standards and Technologies (BFRL/NIST) evaluated a number of intumescent materials and coatings for possible application in slowing flame-spread into the passenger compartment in the event of a post-crash vehicle fire [1]. These tests concluded that the intumescent materials tested would not be effective in expanding to fill openings in the sheet metal structure of a vehicle because (1) the rate of expansion is too slow to be effective in preventing flame-spread through the openings and (2) the materials expand only in one dimension [1]. This report suggested that one potential application of intumescent materials in motor vehicles would be coatings designed to reduce heat transfer to metal surfaces exposed to flames, and thus conductive heating of materials in contact with these metal surfaces [1].

Testing conducted for Project B.3 showed that in a post-crash vehicle fire involving burning gasoline, flames could spread into the passenger compartment through openings in the sheet metal structure of the vehicle, resulting in the ignition of interior components [2 – 5]. Interior components such as the floor carpet in contact with metal bulkheads such as the floor panel could ignite without direct exposure to flames if the metal bulkhead was heated to sufficiently high temperatures. The test described in this report was designed to address this latter potential application, specifically to determine if an intumescent coating applied to the floor panel of an experimental vehicle would function as a thermal and fire barrier during a post-crash vehicle fire test, and reduce heat transfer and flame-spread into the passenger compartment.

In this report, results from a fire test of a crash-tested 1999 Ford Explorer (Experimental Vehicle) are compared to results from a fire test of a crash-tested 1997 Ford Explorer (Control Vehicle) conducted pursuant to project B.3 [4]. The crash test and fire test of the Experimental Vehicle were performed pursuant to project B.14. The test protocols used in the crash tests and fire tests of the Control and Experimental vehicles were identical. To prepare the Experimental Vehicle for

these tests, an intumescent coating was applied to its floor panel (**Section 2**). The Experimental Vehicle was crash tested using the same crash test protocol as used to crash test the Control Vehicle (**Section 3**). After the crash test, test instrumentation such as thermocouples, aspirated thermocouples, heat flux transducers, and gas sampling and analysis equipment was installed in the crash-tested Experimental Vehicle to track flame-spread during a fire test. The ignition protocol used in this fire test involved ignition of liquid gasoline pumped from an external reservoir under the vehicle and was the same as one used in the fire test involving the Control Vehicle conducted in Project B.3 (Section 4).

The results from this fire test were evaluated and compared to the results from the control fire test conducted in Project B.3.

2 Intumescent Coating

The intumescent coating used in this test was in the form of a water-based paint (nofire® A18, nofire® Technologies, Inc, Upper Saddle River, NJ). Technical literature from the supplier of this coating indicated that it is not suitable for application to surfaces painted with enamel paints. Visual inspection of the Experimental Vehicle indicated that the underbody was painted with an undercoat and an enamel base coat. Although some of the underbody also had a layer of top coat, it appeared this was due to over-spray. Before application of this intumescent coating, the existing underbody primer and base coat were removed from the lower surface of the floor panel of the Experimental Vehicle, including the floor panel in the passenger and rear cargo areas and the rear wheel wells

2.1 Removal of Existing Paint

The spare tire, gas tank and fuel lines, exhaust system assembly including catalytic converter, resonator, and mufflers, exhaust system heat shields, transfer case, and drive shaft were removed from the Experimental Vehicle to gain access to the floor panel for the paint removal. The undercoat and an enamel base coat were removed from the lower surface of the floor panel and coatings on the outer surface of the fuel tank by bead blasting with plastic beads followed by bead blasting with glass beads (Strip-It Co, Clinton Township, MI). This two-step process yielded an oil-free, scuffed surface on the metal. The exposed surfaces of the floor panel and fuel tank were cleaned with solvent before application of intumescent paint.

2.2 Application of Intumescent Coating

A water-based primer and nofire® A18 were applied to the exposed metal surfaces on the underbody of the test vehicle and to the fuel tank of the test vehicle by a technical representative of the manufacturer of this product using a pressurized spray gun. Table 1 lists the areas of the Experimental Vehicle where primer and nofire® A18 were applied, the number of applications of primer and nofire® A18 to each area, and the estimated total dry thickness of paint on these metal surfaces.

Table 1
Application of Primer, nofire® A18, and Estimated Coating Thickness

Component	Primer	NoFire A18	Estimated Total Dry Thickness (mils)
Floor Pan	1 Application	2 Applications	40
Rear Wheel Wells	1 Application	2 Applications	30
Gas Tank	1 Application	2 Applications	30
Steel Frame	1 Application	1 Application	20

2.3 Application of Top Coat

Commercial aftermarket primer and base coats were applied (Showcase Collision, Warren, **MI)** over the intumescent paint on the underbody of the Experimental Vehicle. The primer was a two-part, catalyzed, lead free, epoxy (PPG DP402LF, PPG Industries, Inc.) applied to the underbody using a hand-held pressurized spray gun. The primer completely covered the intumescent coat. The base coat was a non-reactive, acrylic cellulose paint (PPG DBC500, PPG Industries, Inc) applied over the primer using a hand-held pressurized spray gun. An aftermarket, solvent-based, rubberized chip-resistant protective coating was applied over the base coat in the rear wheel wells and over the intumescent paint on the fuel tank.

The spare tire, gas tank and fuel lines, exhaust system assembly including catalytic converter, resonator, and mufflers, exhaust system heat shields, transfer case, and drive shaft were removed from the Experimental Vehicle before application of the primer, base coat, and rubberized protective coating.

3 Crash Test

The Experimental Vehicle was a 1999 Ford Explorer (VIN: 1FMDU34E2XUB70063). The Experimental Vehicle was crash tested (C12820) on November 24, 1999 at the General Motors Proving Ground in Milford, Michigan. In the crash test, this vehicle was stationary and was struck in the left front (driver's side) by a moving barrier. The moving barrier had a deformable aluminum honeycomb face as described in FMVSS214 [6]. The test vehicle was parked with the brakes on and positioned at a 21 ± 2° angle relative to the velocity vector of the moving barrier. so that the barrier face struck the front left corner of the test vehicle. A schematic representation of the crash test protocol used in these tests is shown in Figure 1.

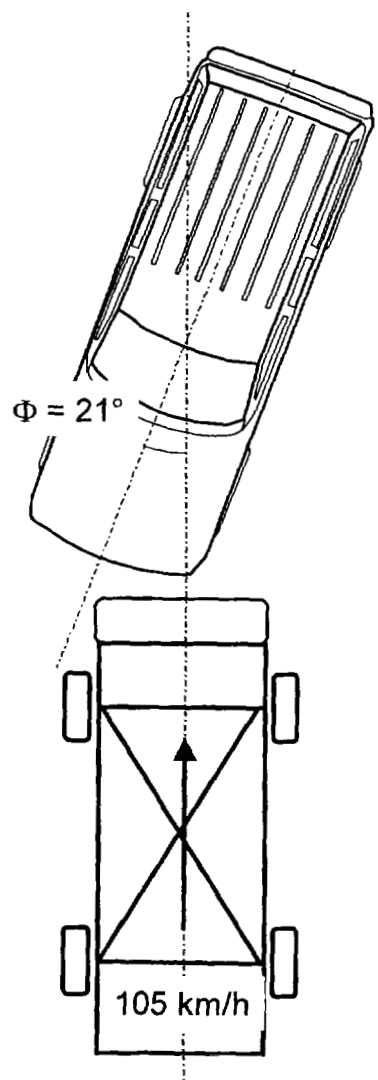

Figure 1. Schematic representation of crash test protocol used in the crash tests of the Control and Experimental Vehicles.

A static (vehicle stationary) engine warm-up procedure was used in these tests to achieve underhood temperatures greater than ambient for the Control and Experimental Vehicles. The Control and Experimental Vehicles contained the factory fills of motor oil (4.3 L), transmission fluid (4.7 L), engine coolant (10.8 L), brake fluid (0.78 L), power steering fluid (0.72 L), and windshield washer fluid. Gasoline for the engines was supplied from a secondary fuel tank with a capacity of 8 L mounted in the rear compartment area for these tests. The secondary fuel tank was fitted with a new service parts fuel pump for a 1999 Ford Explorer. The wiring harness and fuel lines were connected to the fuel pump in the secondary fuel tank. The ignitions were on and the engines were idled at 1500 - 1800 rpm for approximately 1 hour before impact. At impact, the ignition in the Experimental Vehicle was on and the engine was running at approximately 1800 rpm. The transmission was in neutral. The brakes were on. The heater was on with the blower set on high. The Hi-beam headlights were on. The radio was on. The crash test did not result in a fire or a leak in the fuel system. Table 2 summarizes the pre-impact warm-up schedules for the Control and Experimental vehicles.

Table 2
Pre-Impact Vehicle Warm-Up Schedule for the Control and Experimental Vehicles

	Elapsed Time (hr:min:sec)	
	Control (C11687)	**Experimental (C12820)**
Start Engine	00:00:00	00:00:00
Increase Engine Speed	00:18:00	00:01:00
Start Background Vapor Sampling	00:18:00	00:02:00
End Background Vapor Sampling	00:31:00	00:12:00
Power-Down Vapor Sensors / Shut Engine	00:31:00	00:48:00
Begin Instrumentation Calibration	00:31:40	00:49:00
Instrumentation Calibration Complete	01:01:00	00:51:00
Restart Engine	01:01:30	00:52:00
Increase Engine Speed	01:02:00	00:52:00
Power-Up Vapor Sensors	01:05:30	00:52:00
Impact	01:17:40	01:02:00

3.1 Crash Test Data

One triaxial accelerometer was attached to the front and rear of each rocker panel on the Experimental Vehicle, and two tri-axial accelerometers were located on the moving barrier to measure vehicle and barrier accelerations during the crash test. Flammable vapor sensors were located in the engine compartment of the Experimental Vehicle to measure flammable vapor concentration. Sampling devices to acquire air samples for GC/MS analysis were co-located with the flammable vapor sensors to identify organic vapors in the engine compartment. Thermocouples were intrinsically welded to the exhaust manifolds and exhaust pipes of the Experimental Vehicle to measure surface temperature before, during, and after the crash test.

Data recorded from accelerometers located on the rocker panels is in **Appendix A**. Data recorded from the flammable vapor sensors is in **Appendix B**. Data from analysis of gas samples from the engine compartment is in **Appendix C**. Data recorded from the thermocouples on the exhaust system is in **Appendix D**.

Table 3 summarizes the vehicle mass, vehicle speed at impact, engine speed at impact, location of impact, average change in velocity, and maximum dynamic crush for the Control and Experimental Vehicles. The masses of the Control and Experimental Vehicles included two 50^{th} percentile adult male Anthropomorphic Test Devices (ATD) in the front seats for ballast, test instrumentation, and 76.5 L of Stoddard solvent in the fuel tank. The mass of each ATD was 75.7 kg. The ATD's were belted and the supplemental restraint systems in each vehicle were active and deployed during both tests. Data recorded from the ATD's in the crash test of the Control Vehicle are documented in another report [7]. No data was recorded from the ATD's in the crash test of the Experimental Vehicle.

The data summarized in Table 3 show that the masses of the Control and Experimental Vehicles differed by 1 kg (0.04%). The barrier speeds at impact differed by 0.6 kmh (0.05%). The angle between the velocity vector of the barrier and the longitudinal centerline of the vehicle differed by 2° (8.7%). The average change in velocity recorded from accelerometers on the rear right and left rocker panels was 42 kmh @ 105 msec for the Control Vehicle and 48 kmh @ 85 msec for the Experimental Vehicle, a difference of 3 kmh (6.3%). The crash test of the Control Vehicle was conducted in July with an ambient air temperature of approximately 40 to 45°C. The crash test of the Experimental Vehicle was conducted in November with an ambient air temperature of – 5 to 0°C.

Table 3

Summary of Vehicle Mass, Vehicle Speed at Impact, Engine Speed at Impact, Location of Impact, Average Change in Velocity, and Maximum Dynamic Crush for the Control and Experimental Vehicles

	Control C11687	Experimental C12820
Vehicle Test Mass - Front	1152 kg	1152 kg
Vehicle Test Mass – Rear	1080 kg	1081 kg
Vehicle Test Mass – Total	2232 kg	2233 kg
Barrier Mass	1638 kg	1648 kg
Barrier Speed at Impact[1]	104.4 kmh	105.0 km/h
Barrier / Vehicle Angle[2]	23 ± 2°	21 ± 2°
Engine Speed at Impact	approx. 1800 rpm	approx. 1800 rpm
Average Change in Velocity[3]	42 kmh @ 105 msec	48 kmh @ 85 msec

[1] Vehicle Speed at Impact was determined by the radar speed measurement at time zero.

[2] Barrier / Vehicle Angle was the angle between the velocity vector of the moving barrier and the longitudinal center liner of the vehicle.

[3] Average Change in Velocity was determined from the difference between the maximum and minimum average velocities in the direction of the X-axis calculated from the accelerometers on the left and right rear rockers (Plots A25 and A26, Appendix A).

Figures 2 and 3 show photographs of the Control and Test vehicles before and after the crash test, respectively. Results summarized in Tables 3, show that the vehicle masses, barrier masses, barrier speeds at impact, and average change in velocities of the Control and Experimental Vehicles were similar in Crash Tests C11687 (Control) and C12820 (Experimental). The crash damage observed in Figures 2 and 3 show that impact damage to the Control and Experimental Vehicles from these crash tests was similar.

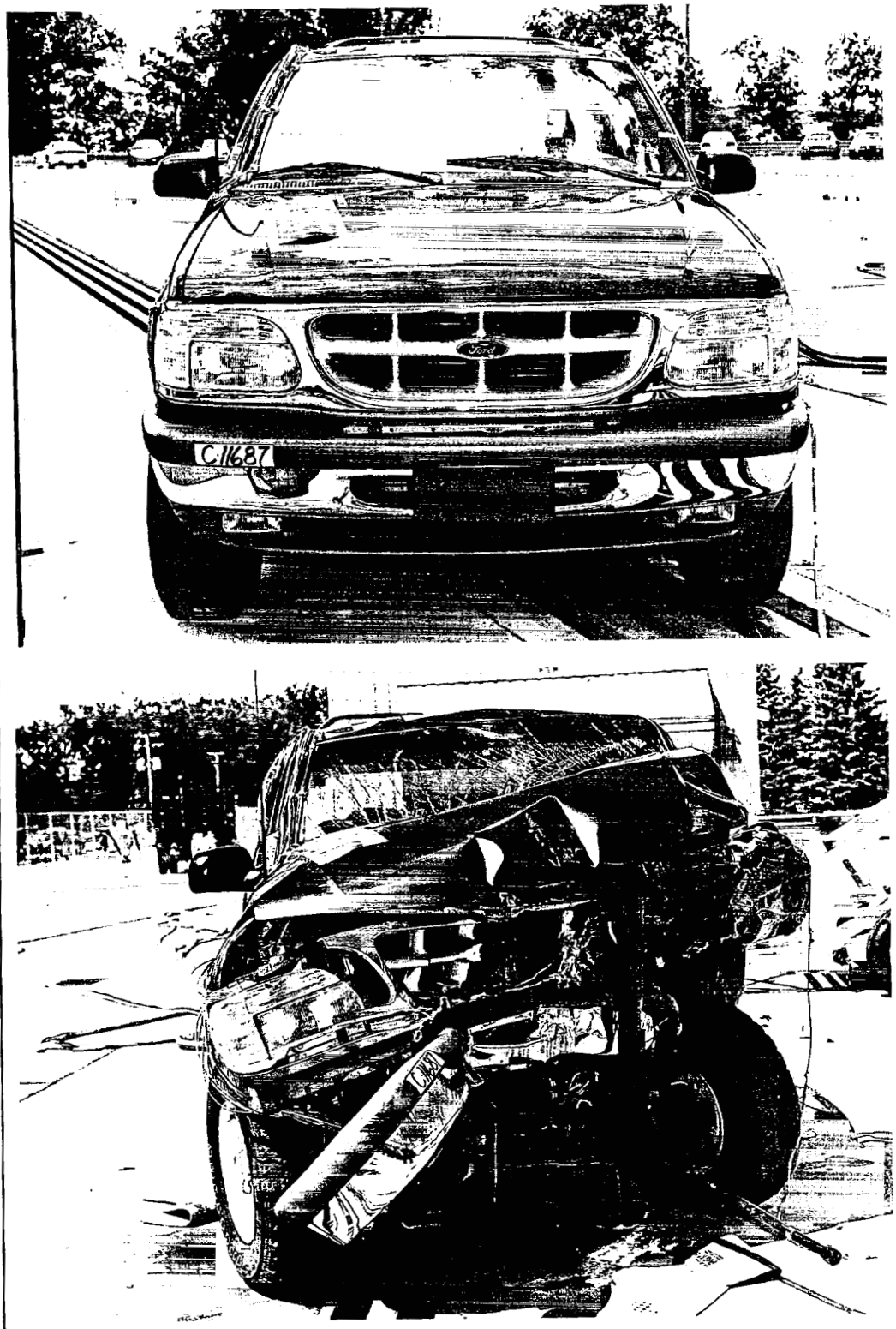

Figure 2. Crash Test C11687. Photographs of the Control Vehicle before (upper) and after (lower) the crash test.

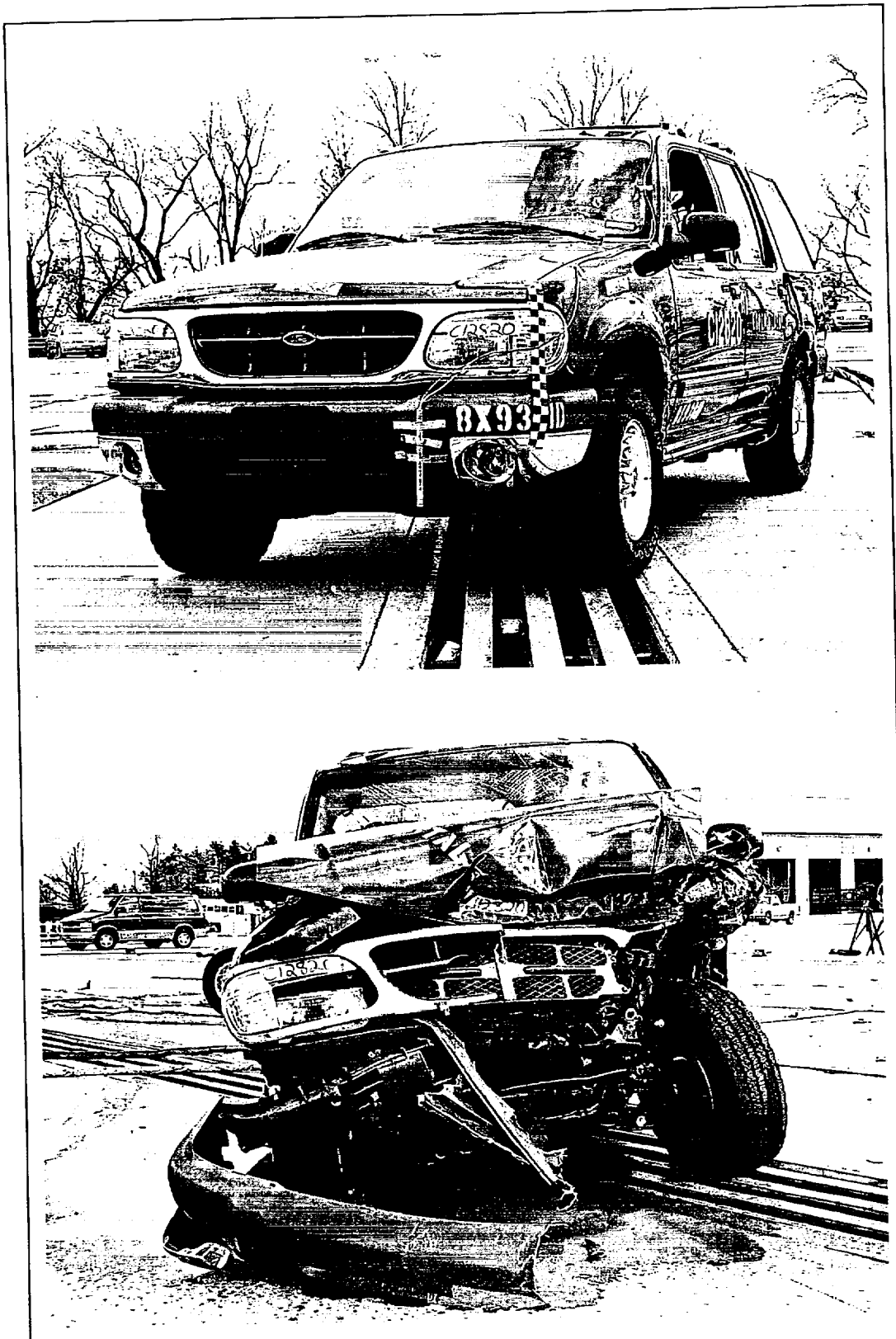

Figure 3. Crash Test C12820. Photographs of the Experimental Vehicle before (upper) and after (lower) the crash test.

4 Fire Tests

The conditions of the Control and Test Vehicles after the crash tests were similar (see Fig.'s 2 and 3). Thermal instrumentation such as thermocouples and heat flux transducers were installed in both vehicles after the respective crash tests and before the respective fire tests. Both fire tests were conducted at the Factory Mutual Global Test Center in West Glocester, Rhode Island. The vehicle conditions and test protocols in both fire tests were substantially similar.

The fire test of the Control Vehicle (F980611) was conducted on June 11, 1998 [4]. An analysis of data collected during Fire Test F980611 (Control Vehicle) appears in another report [4].

The fire test of the Experimental Vehicle (F99B1403) was conducted on February 23, 2000. A description of the video camera set-up used in Fire Test F99B1403 appears in **APPENDIX E**. A description of the thermocouples installed in the test vehicle and data collected from these thermocouples in Fire Test F99B1403 appears in **APPENDIX F**. A description of the aspirated thermocouple probe installed in the test vehicle and data collected from the aspirated thermocouples in Fire Test F99B1403 appear in **APPENDIX G**. A description of the heat flux transducer/radiometer assemblies installed in the test vehicle and data collected from these transducers in Fire Test F99B1403 appears in **APPENDIX H**. A description of the Fourier Transform Infrared Gas Analysis System used during Fire Test F99B1403 and data collected during Fire Test F99B1403 appear in **APPENDIX I**. A description of the Fire Products Collector (FPC) at the Factory Mutual Global Test Center, data analysis procedures, and FPC data collected during Fire Test F99B1403 appear in **APPENDIX J**.

4.1 Vehicle Condition and Test Protocol

The crash-tested vehicle was prepared for the fire tests at the General Motors Research and Development Center (GM R&D Center) in Warren, Michigan, and shipped to the Factory Mutual Test Center in West Glocester, Rhode Island where this fire test was conducted. The test vehicle was returned to the GM R&D Center after the fire test, where it was systematically disassembled to permit closer inspection of the fire damage and identification of flame-spread paths into the passenger compartment that were not obvious from observations made during this fire test.

The vehicle was placed in a rectangular steel pan (length = 25 ft., width = 15 ft., height = 4 in.) to prevent spilled and leaking automotive fluids from spreading in the test facility. This fluid containment pan was fabricated from two sheets of carbon steel. Angle-braces were welded to the under-side of the pan to keep it from flexing under the weight of the vehicle. The corners of

the support frame rested on load cells. Mass loss was determined from data acquired from the load cells during the test.

A layer of fiberglass-reinforced cement construction board (DuraRock, USG Corporation) was placed on bottom of the fluid containment pan. A thin layer of sand was used to level the concrete board so that the grade of the surface measured from the center to the edges along the major and minor axes was no greater than 1%. The joints between boards were sealed with latex caulking. The test vehicles were placed in the center of the pan (Fig. 4).

All doors were closed. Except for the left front door, the door window glasses were raised to their fully closed position in each door. An air horn was sounded to signal three events during the test: (1) the start of gasoline flow, (2) ignition of the gasoline pool by a propane torch, and (3) the end of the test and start of fire suppression. The air horn was used to synchronize the data acquisition systems used in this test. The air horn was audible on the videotapes and infrared imaging systems. One channel of the data acquisition system for vehicle instrumentation monitored a normally open switch, which was depressed at each sounding. The real-time clock in the FTIR data system was synchronized to the real-time clock in the vehicle instrumentation data system.

The original fuel tank was removed from the test vehicle after the crash test, the fuel sender assembly was removed from the fuel tank, stainless steel tubing (o.d. = 0.125 in) was installed in the fuel tank, and the modified fuel tank was re-installed in the test vehicle for this fire test (Fig. 5). The dispersion and drip patterns of fuel flowing from the outlet of the tubing in the fuel tank in the Experimental Vehicle were similar to the dispersion and drip patterns of fuel flowing from the outlet of the tubing in the fuel tank observed in the Control Vehicle. The tubing in the modified service parts fuel tank was connected to an external gasoline reservoir. In the test of the Control Vehicle, the external gasoline reservoir was a pressurized cylinder containing approximately 4 L of liquid gasoline [7]. In the test of the Experimental Vehicle, the external gasoline reservoir was an aluminum tank fitted with an electric fuel pump. The capacity of the aluminum tank was approximately 10 L. In both systems, the flow rate of gasoline was controlled by adjusting a Rotometer® calibrated for gasoline.

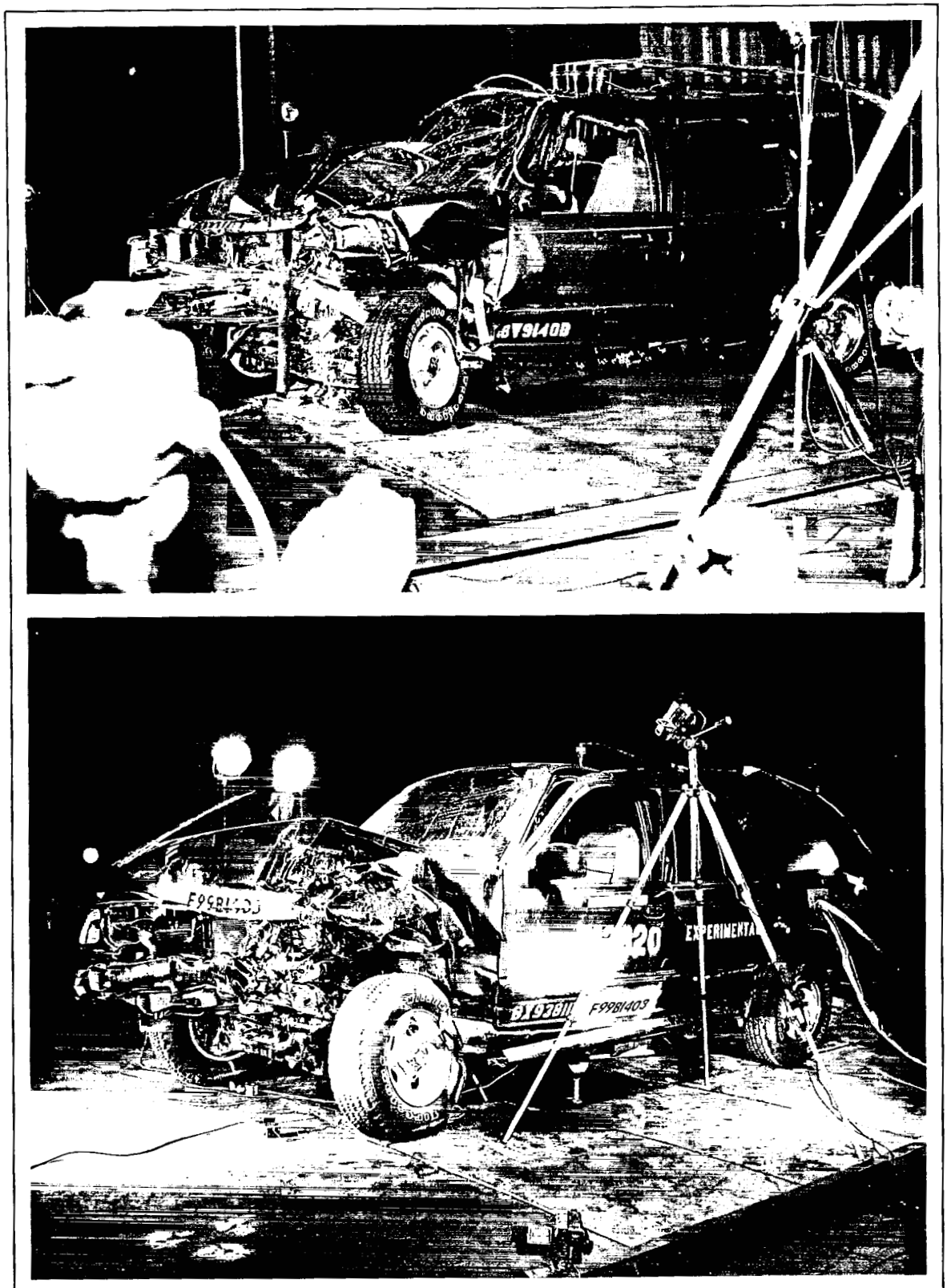

Figure 4. Photograph of the Control Vehicle (upper) and Experimental Vehicle (lower) on the fluid containment pan before the respective fire tests.

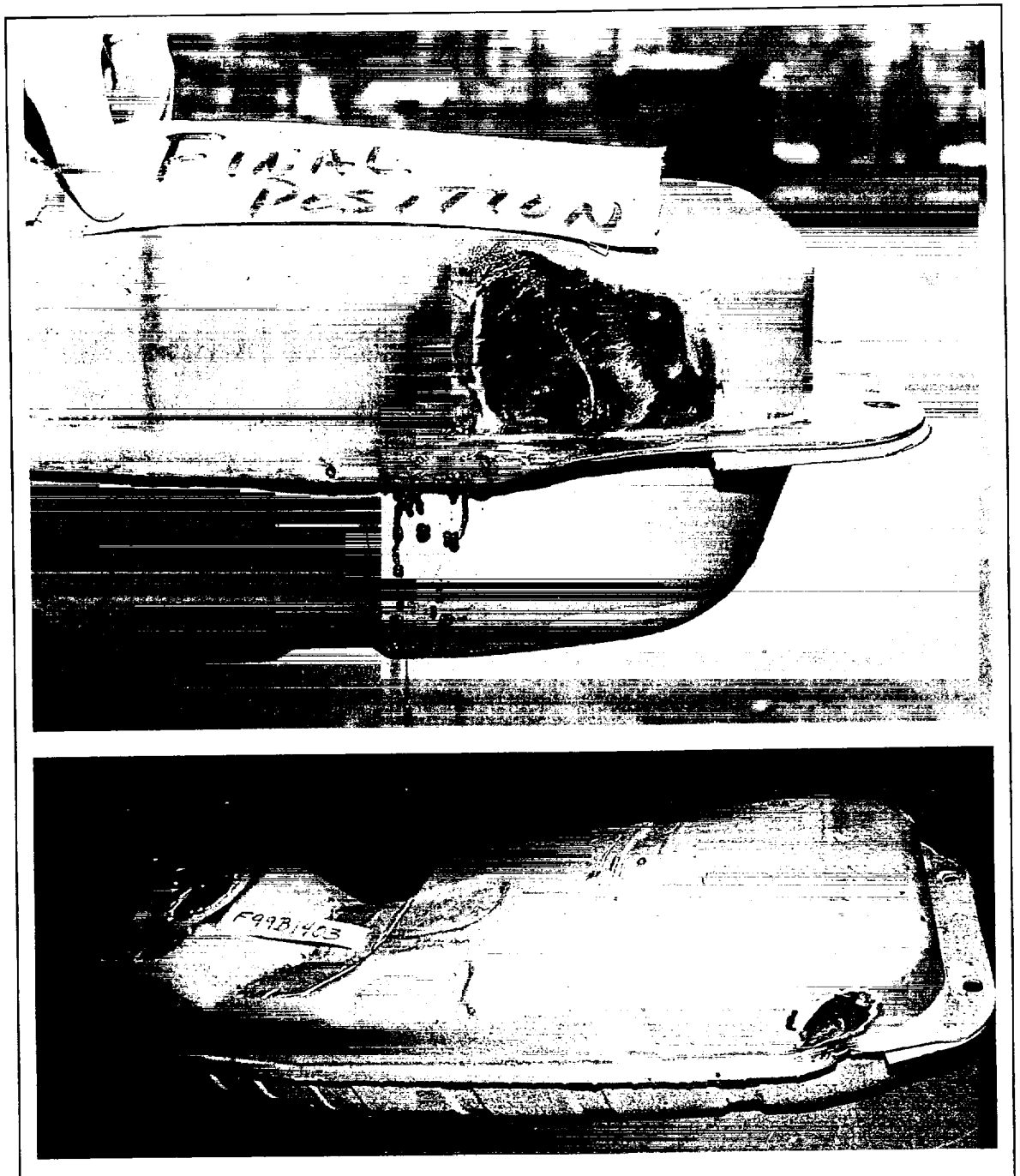

Figure 5. Photographs of the modified fuel tank used in the fire test of the Control Vehicle (upper) and the modified fuel tank with intumescent and rubberized coatings used in the Experimental Vehicle (lower).

The test protocol used in the fire tests of the Control and Experimental Vehicles was as follows:

Start	Start gasoline flow from the outlet of the tubing installed in the fuel tank.
Ignition	Ignite gasoline vapor under the vehicle with a propane torch approximately 30 seconds after the start of gasoline flow.
End	End the test and start fire suppression after flames are observed in the passenger compartment.

4.2 Ignition

At the start of each test, gasoline started to flow from the outlet of the tubing installed in the fuel tanks in the test vehicles into the fuel tank skid plate and onto the cement board surface under the test vehicle. The target flow rate in both tests was 300 cm^3/min. The gasoline delivery system used in Fire Test F99B1403 yielded a more accurate and controllable flow rate than the gasoline delivery system used in Fire Test F980611. A propane torch was used to ignite gasoline vapor above the liquid gasoline pool under the test vehicles (Fig. 6). Table 4 summarizes the flow rates of gasoline, ignition times, and cumulative volumes of gasoline that exited the tubing outlet at the time of ignition in these fire tests.

Table 4

Summary of Gasoline Flow Rates, Ignition Times, and Cumulative Gasoline Volumes for the Control and Experimental Vehicles

	Control F980611	Experimental F99B1403
Gasoline Flow Rate	350 ± 10 cm^3/min	300 ± 5 cm^3/min
Ignition Time	28 seconds	38 seconds
Cumulative Gasoline Volume	163 cm^3	190 cm^3

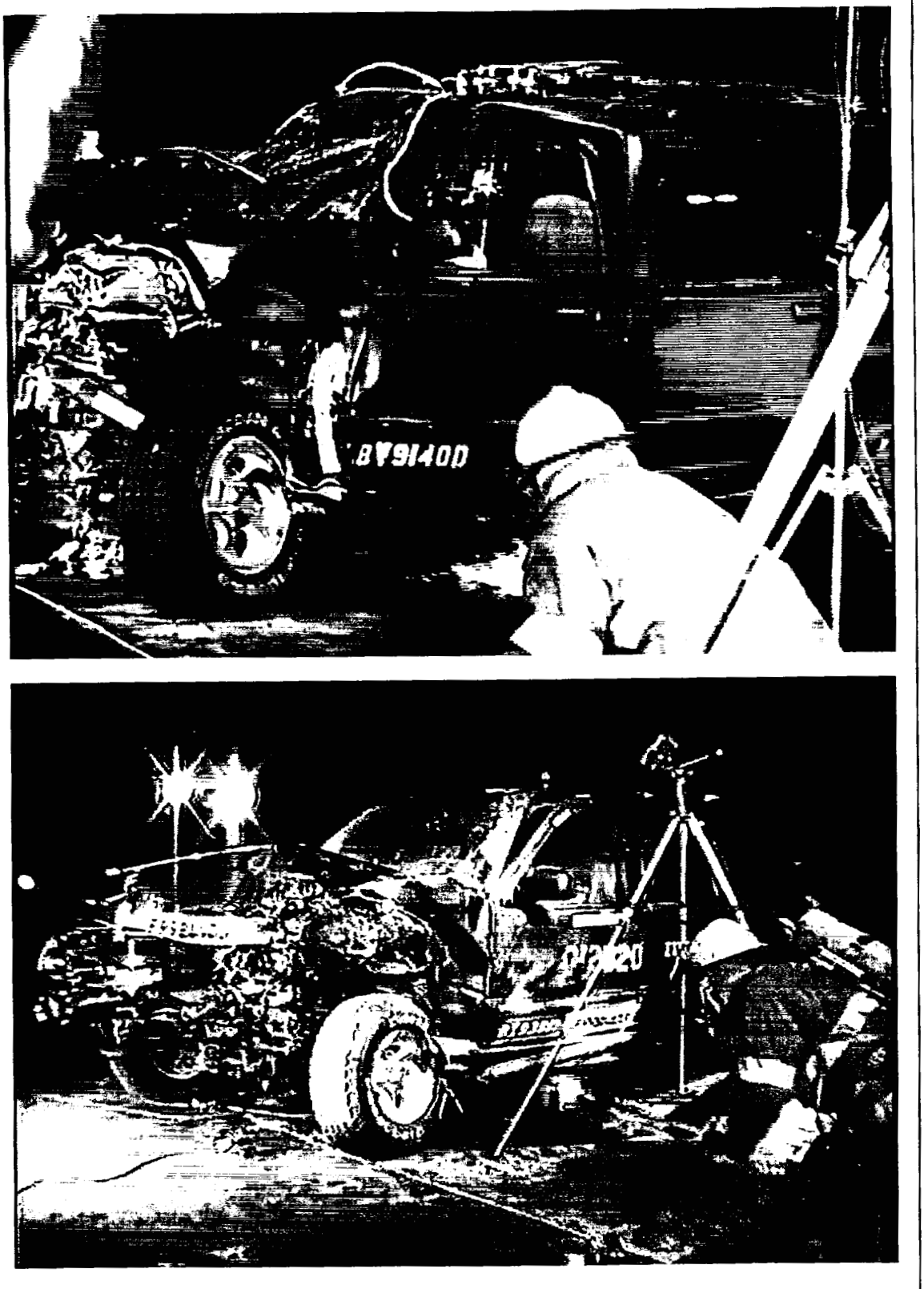

Figure 6. Video stills from F980611 Camera 3 (upper) and F99B1403 Camera 7 (lower) at the time of ignition.

4.3 Distribution of Flames on the Underbody

Liquid gasoline flowed from the outlet of the stainless steel tubing installed in the fuel tank into the fuel tank skid plate and onto the cement board surface below the forward section of the fuel tank. After ignition, flames were observed on the cement board surface and in the fuel tank skid plates in both test vehicles. Figures 7 through 16 show a series of video stills from F980611 Camera 3 (upper) and F99B1403 Camera 7 at 15, 30, 60, 90, 120, 150, 180, 210, 240, and 243/245 seconds post-ignition. In both tests, the flames attached to the gasoline pool on the cement board appeared to be between 10 and 15 inches wide[1] from the time of ignition through about 30 seconds post-ignition (video stills, Fig.'s 7 through 8). The amount of gasoline flowing from the fuel tank skid plate onto the cement board surface decreased as this test progressed, resulting in a decrease in the width of flames on the cement board surface (Fig.'s 8 through 16). This observed behavior suggests that the rate of consumption by fire of liquid gasoline in the fuel tank skid plate was greater than the flow rate of liquid gasoline onto the skid plate, resulting in a decrease in the flow of liquid gasoline out of the fuel tank skid plat onto the cement board surface under the test vehicle. By 210 seconds post-ignition in F980611 (upper video still, Fig. 14) and 150 seconds post-ignition in F99B1403 (lower video still, Fig. 12), the size of the burning gasoline pool on the cement board surface had decreased substantially and flames from the cement board surface did not appear to reach the lower surface of the fuel tank skid plate. Flames from burning gasoline in the fuel tank skid plate could be seen spreading along the underbodies of the test vehicles inboard of the left rocker panel.

It was not possible to determine accurately the distribution of flames on the underbodies of the test vehicles from the video records alone. Review of the videos from these tests showed flames from the burning gasoline on the cement boards spreading out along the lower surface of the fuel tank skid plate and the underbody between the fuel tank and left rocker panel. None of the video cameras in F990611 were positioned to view directly the underside of the test vehicle. The number of thermocouples located below the floor panel in F980611 was not adequate to estimate the temperature distribution, and thus the distribution of flames on the lower surface of the test vehicle. It was therefore not possible to determine the area of the floor panel that was exposed to flames during F980611.

[1] This dimension is perpendicular to the line-of-sight of F980611 Camera 3 and F99B1403 Camera 7, and was estimated by comparison to the left front wheel (diameter = 15 in.).

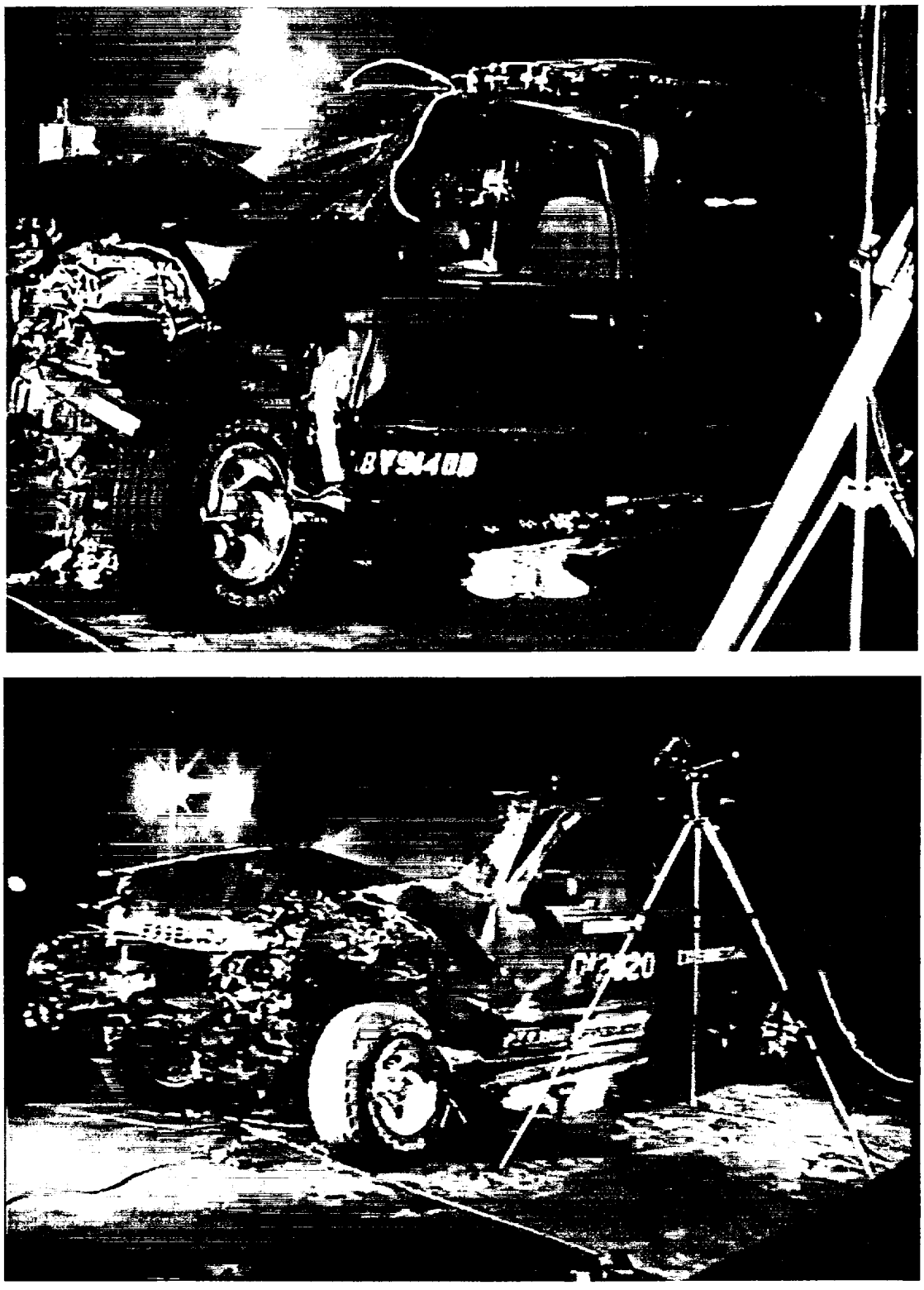

Figure 7. Video stills from F980611 Camera 3 (upper) and F99B1403 Camera 7 (lower) at 15 seconds post ignition.

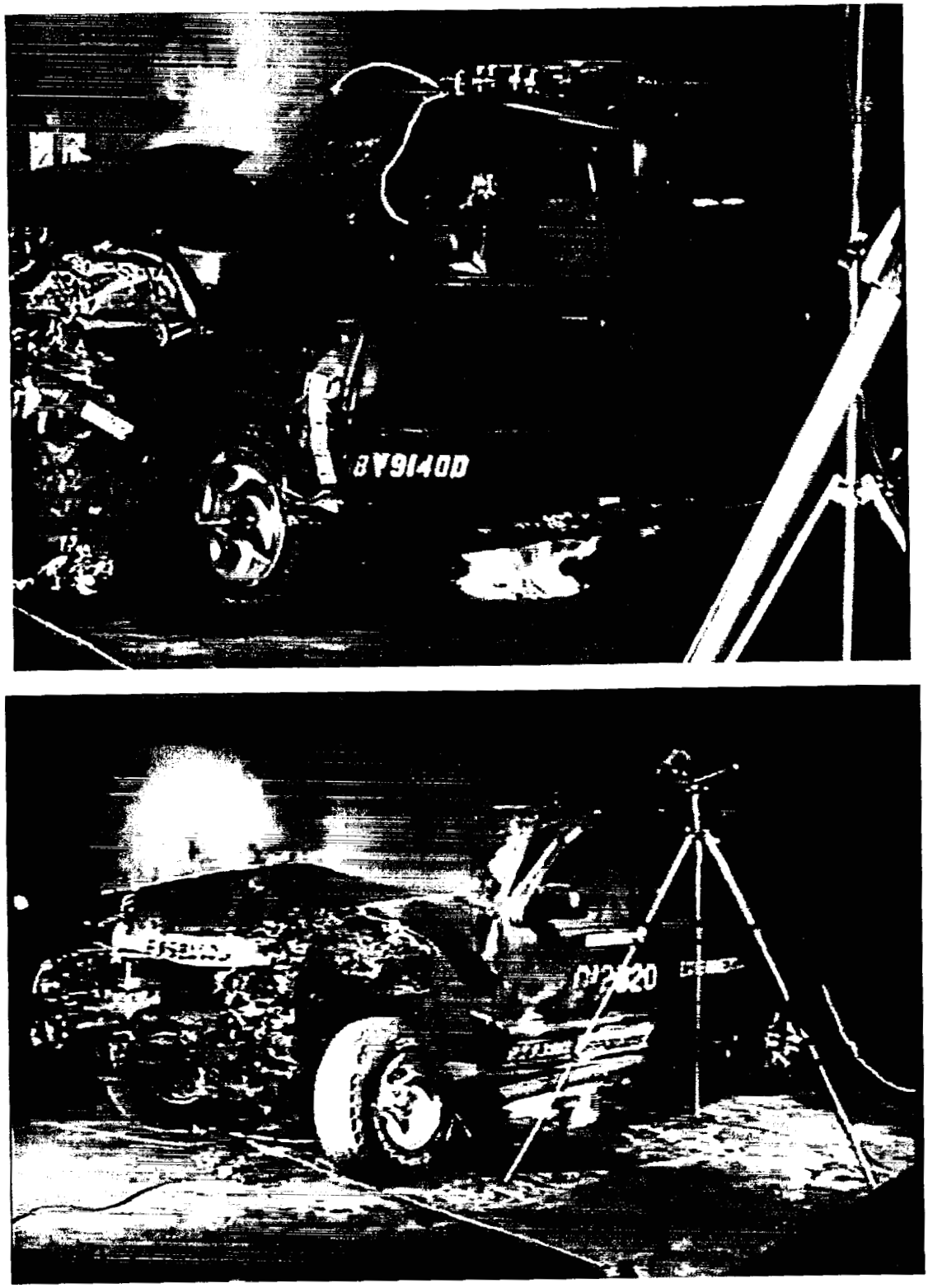

Figure 8. Video stills from F980611 Camera 3 (upper) and F99B1403 Camera 7 (lower) at 30 seconds post ignition.

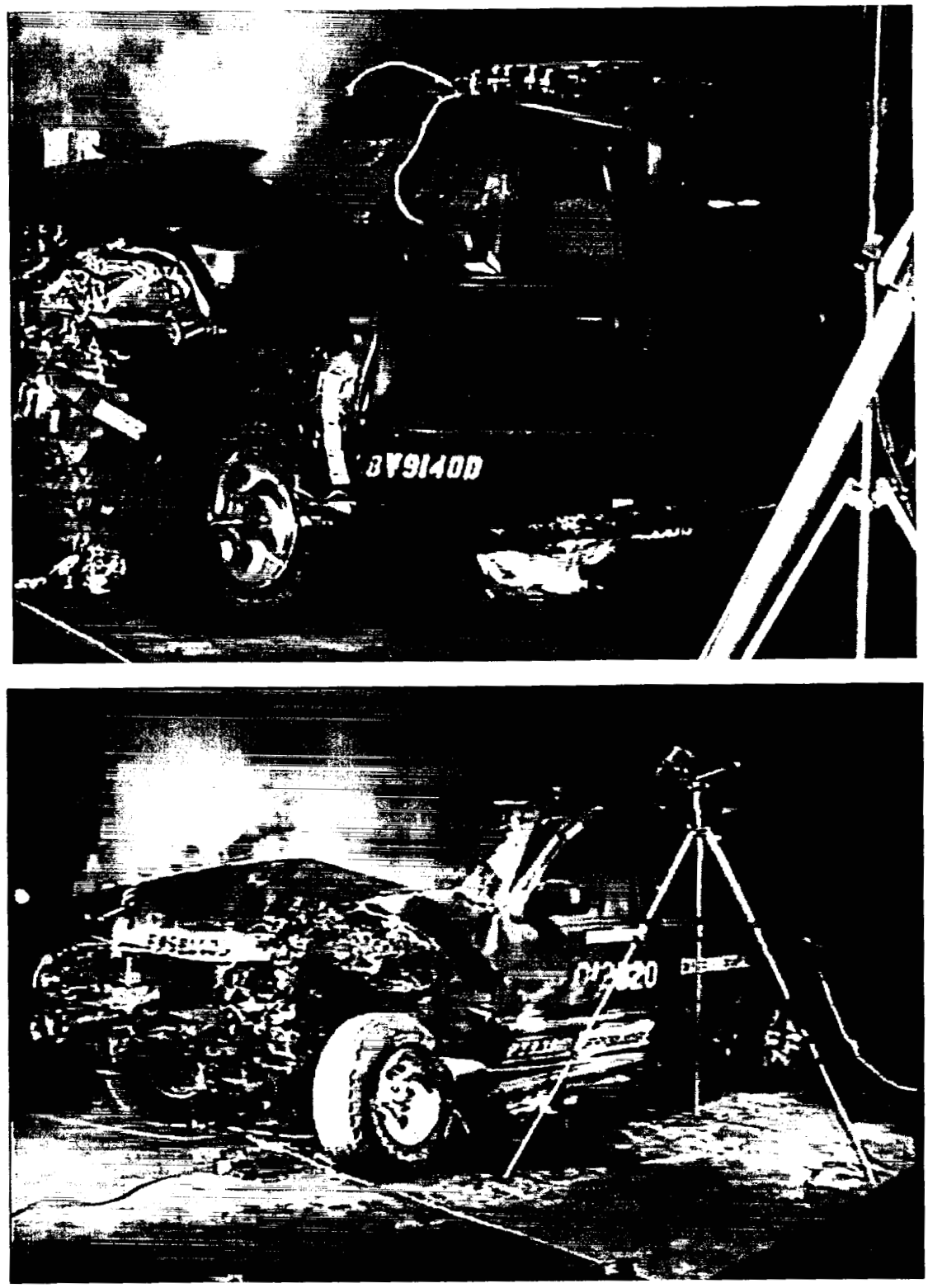

Figure 9. Video stills from F980611 Camera 3 (upper) and F99B1403 Camera 7 (lower) at 60 seconds post ignition.

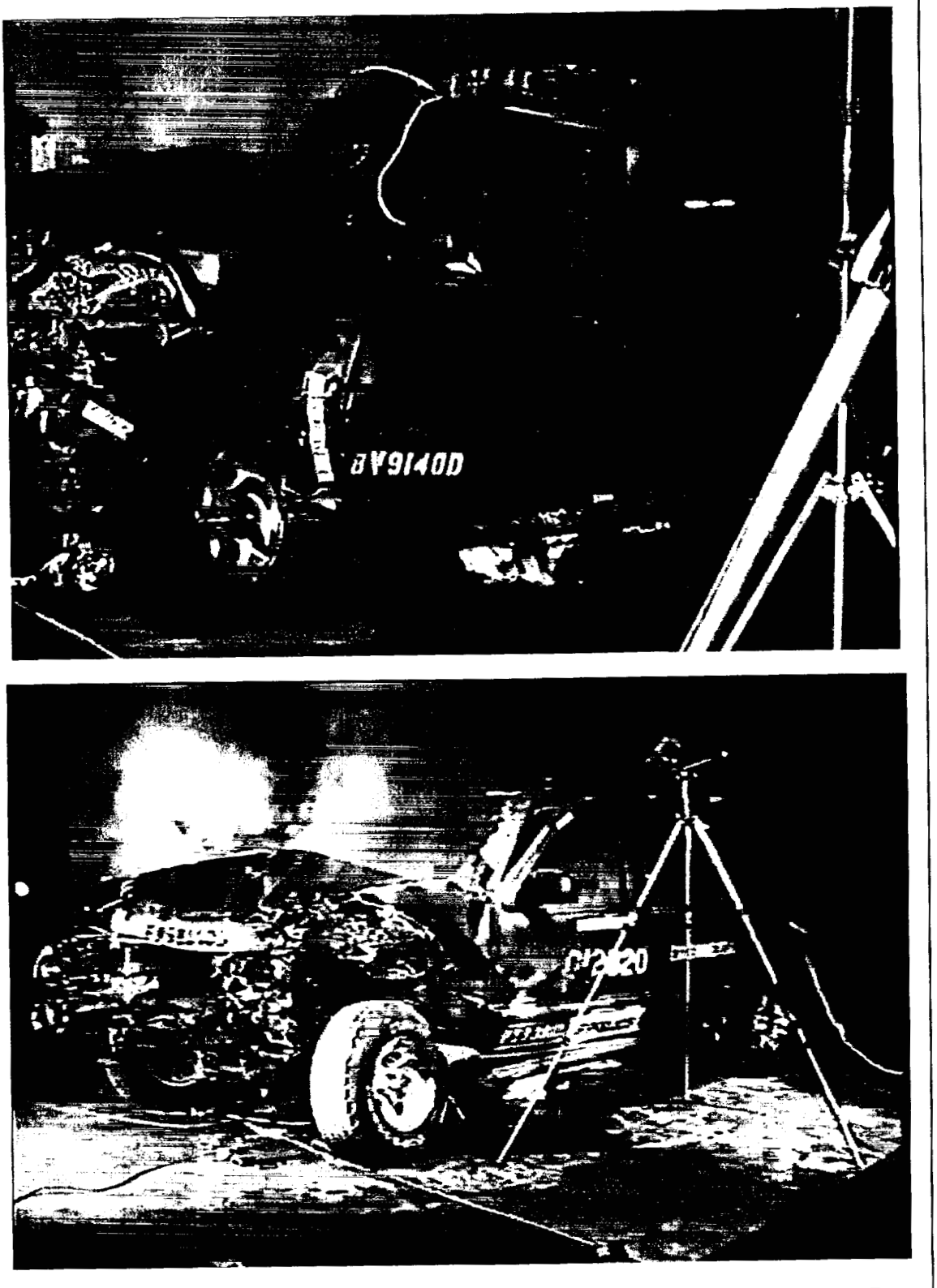

Figure 10. Video stills from F980611 Camera 3 (upper) and F99B1403 Camera 7 (lower) at 90 seconds post ignition.

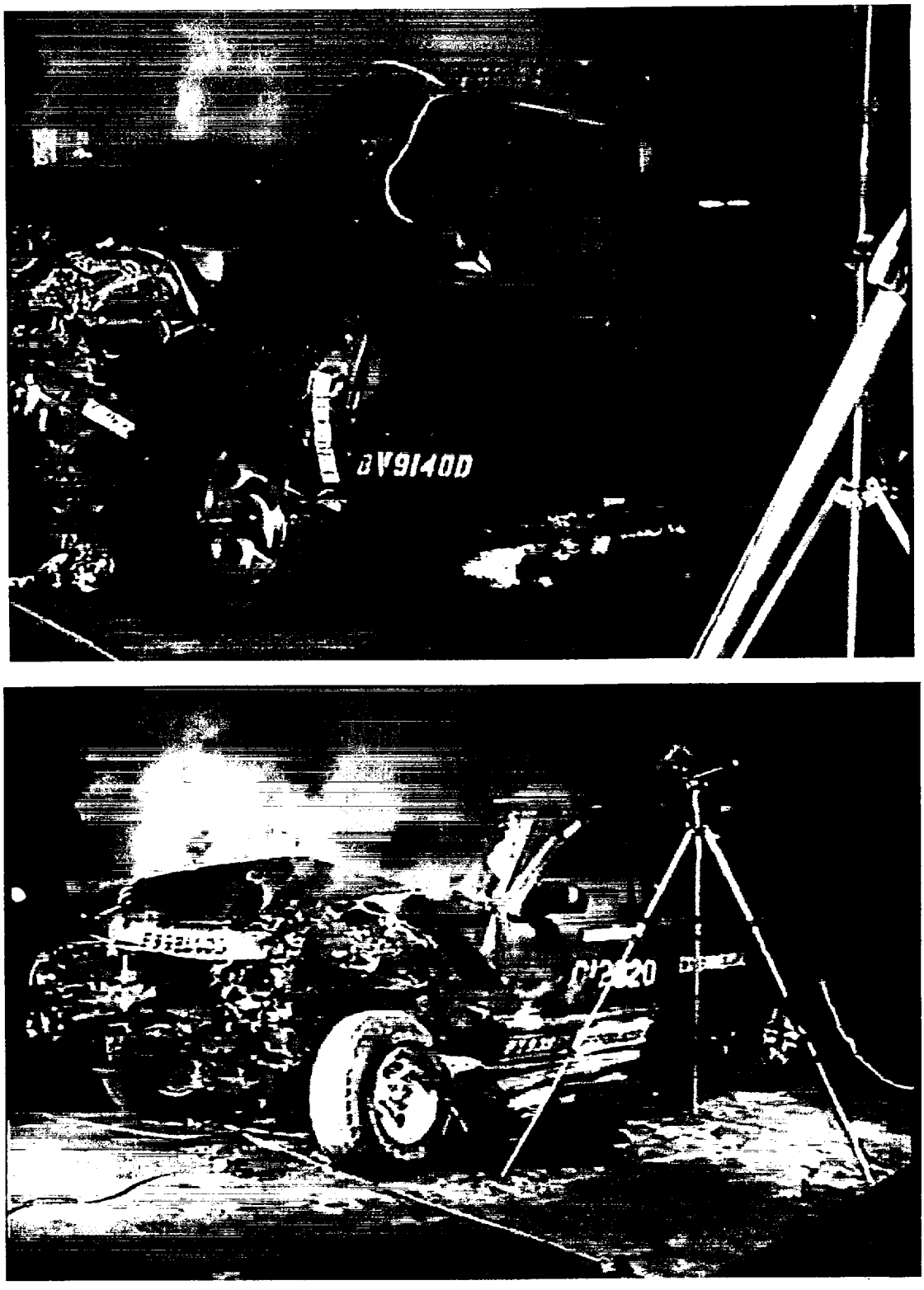

Figure 11. Video stills from F980611 Camera 3 (upper) and F99B1403 Camera 7 (lower) at 120 seconds post ignition.

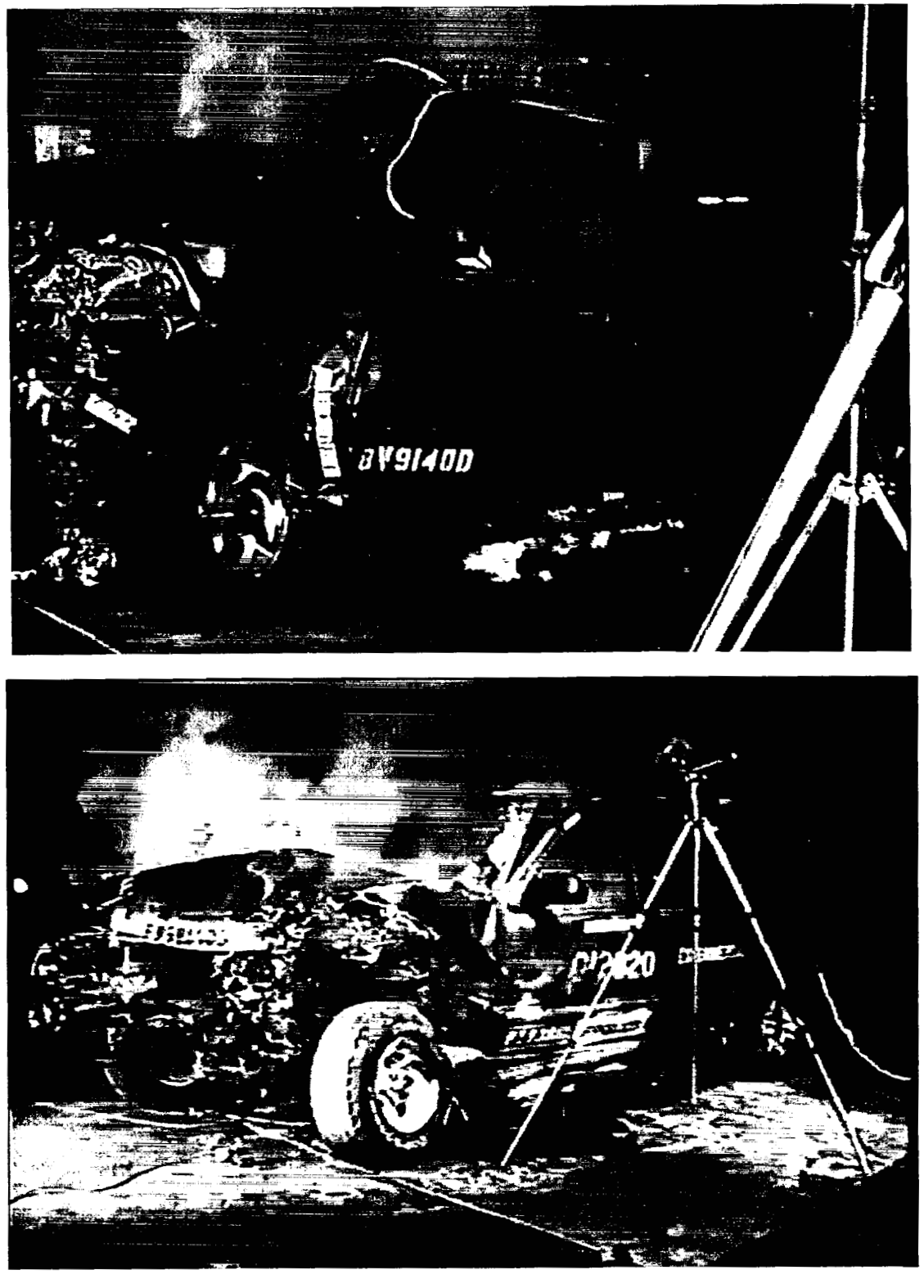

Figure 11. Video stills from F980611 Camera 3 (upper) and F99B1403 Camera 7 (lower) at 120 seconds post ignition.

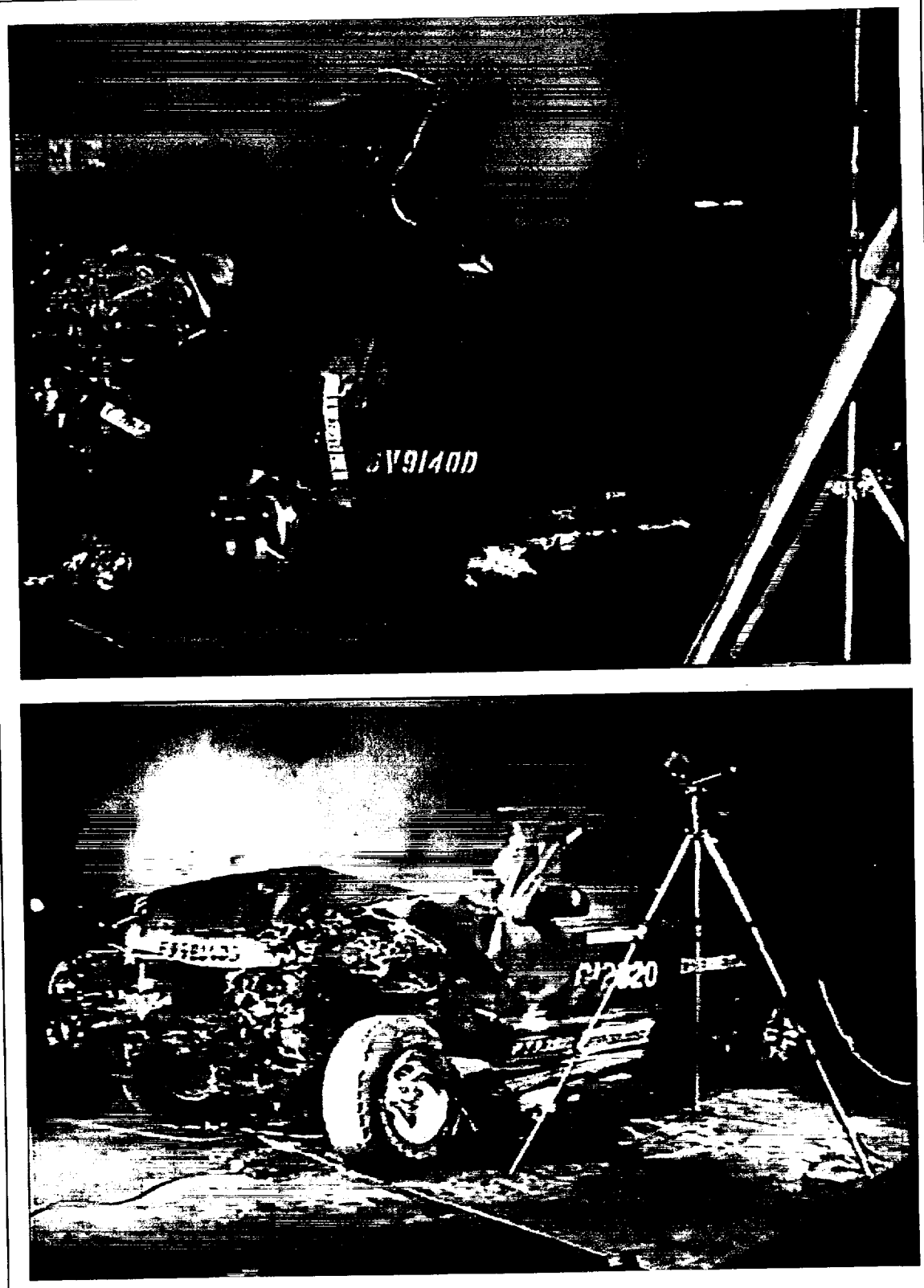

Figure 13. Video stills from F980611 Camera 3 (upper) and F99B1403 Camera 7 (lower) at 180 seconds post ignition.

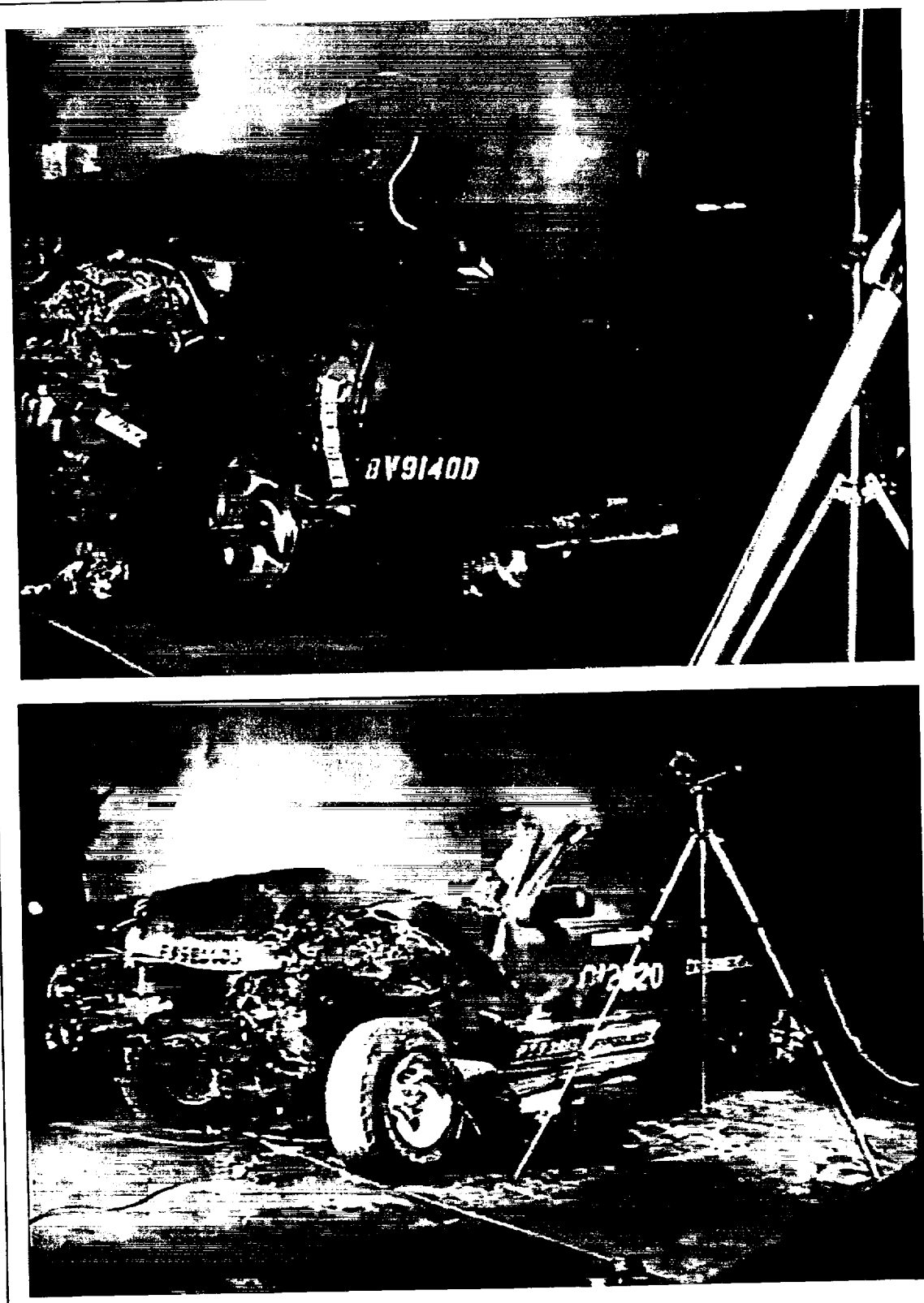

Figure 14. Video stills from F980611 Camera 3 (upper) and F99B1403 Camera 7 (lower) at 210 seconds post ignition.

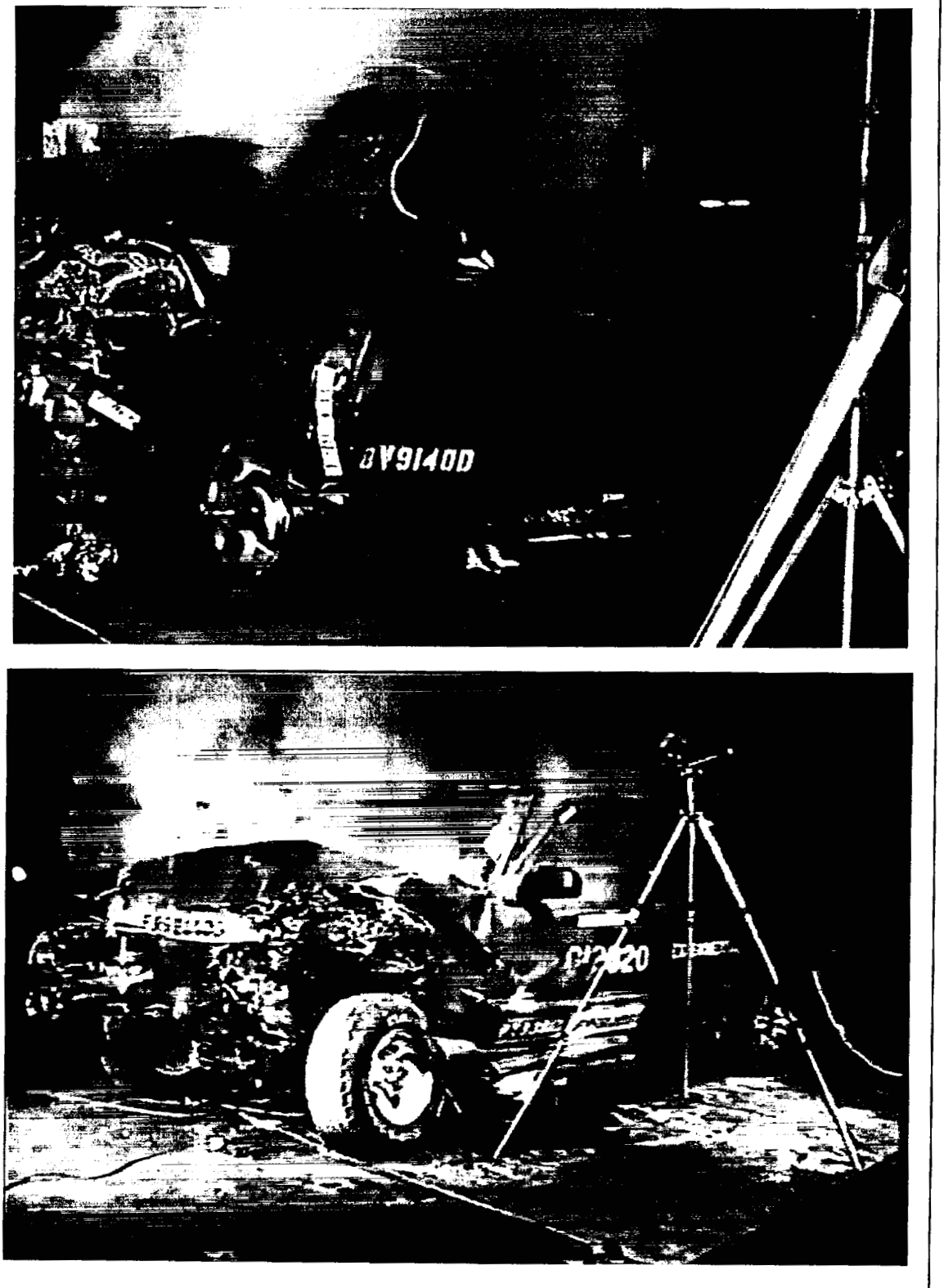

Figure 15. Video stills from F980611 Camera 3 (upper) and F99B1403 Camera 7 (lower) at 240 seconds post ignition.

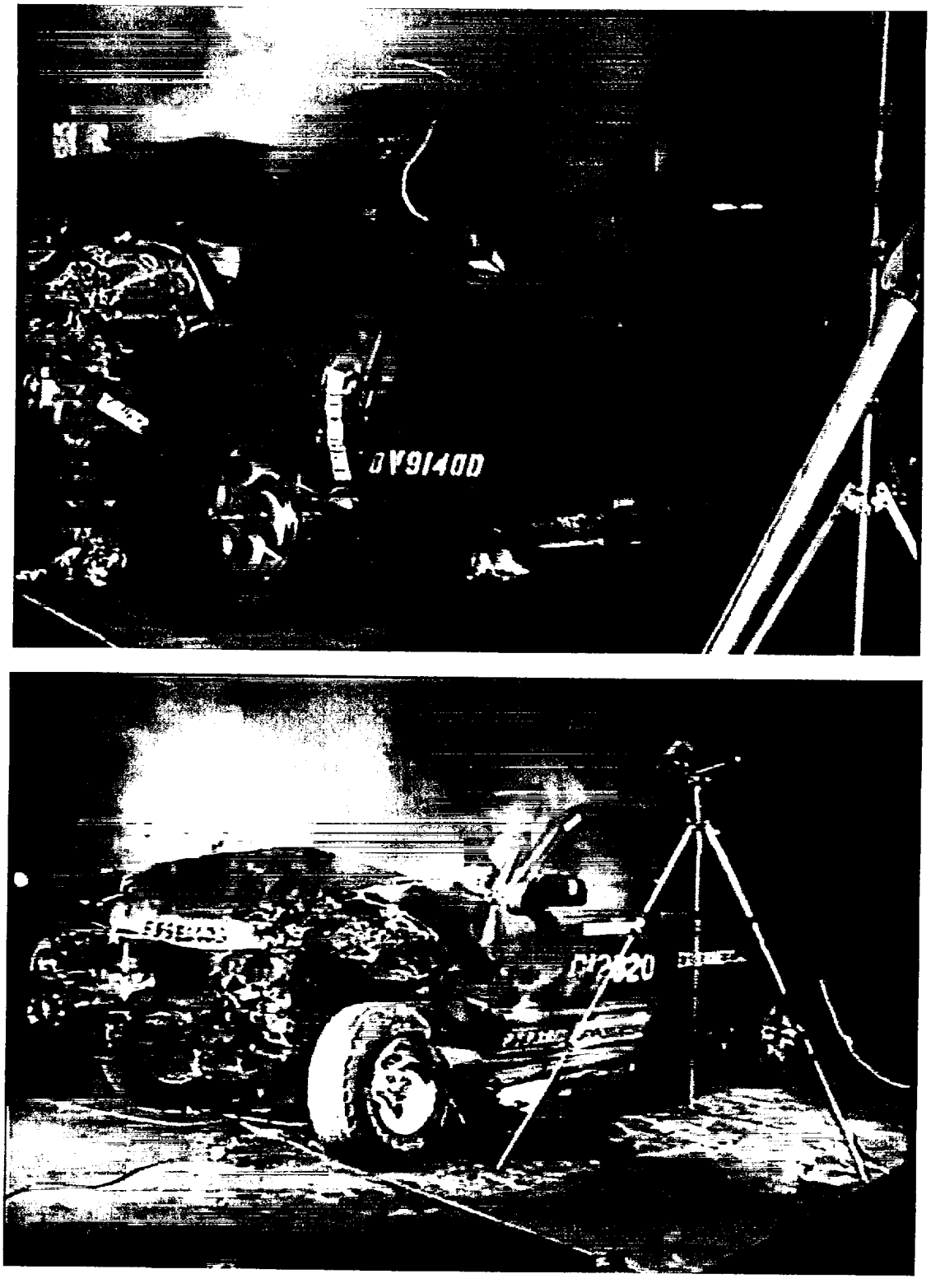

Figure 16. Video stills from F980611 Camera 3 at 243 seconds post ignition (upper) and F99B1403 Camera 7 (lower) at 245 seconds post ignition.

The number of thermocouples in F99B1403 was sufficient to estimate isothermal contours[2] of temperatures below the floor panel of the test vehicle. Figure 17 shows some of the structures forming the underbody of the test vehicle after the crash test and isothermal contour plots of temperature below the floor panel in the passenger compartment during this test.

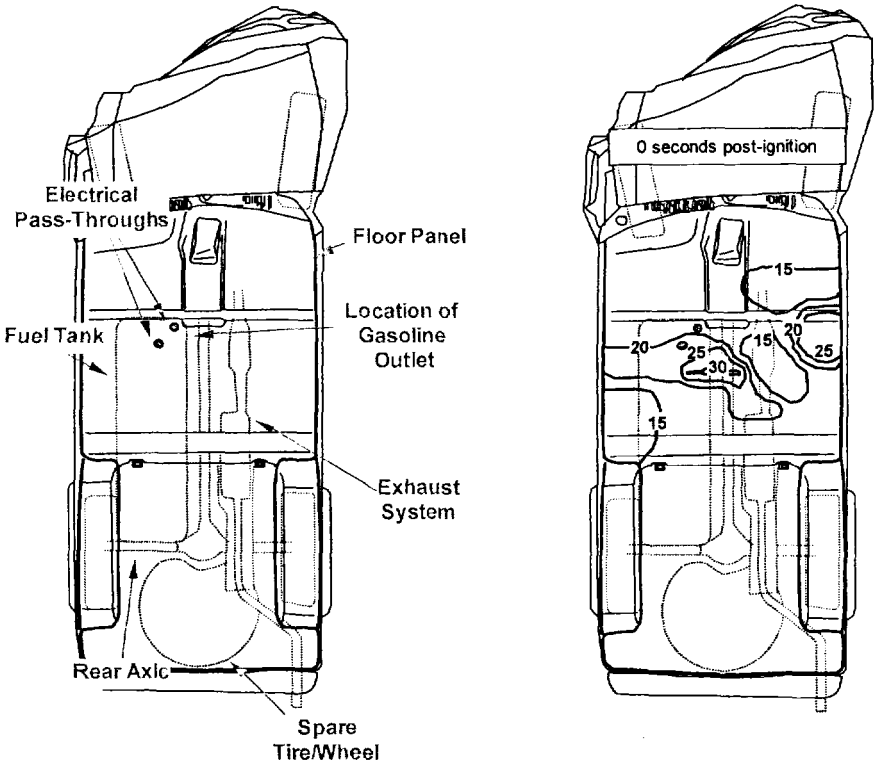

Figure 17. Fire Test F99B1403. View from above the test vehicle showing the floor panel, electrical pass-through openings in the floor panel, and outlines of the fuel tank, exhaust system, rear axle, and spare tire, and isothermal contour plots showing estimated temperatures below the floor panel at 0, 15, 30, 45, 60, 90, 120, 150, 180, 210, 240, 270, and 300, seconds post-ignition.

[2] Isothermal contours of the temperature below the floor panel were estimated from the temperature data recorded from the F-Thermocouples located below the floor panel using a three-dimensional interpolation algorithm available in SigmaPlot for Windows Version 4.00 [8]. This algorithm uses an inverse distance method to generated temperature values for points on a uniformly spaced Cartesian grid from the [x,y,t] data from these thermocouples. Refer to **APPENDIX C** for the approximate locations of the F-thermocouples on the floor panel and the data recorded from the F-thermocouples.

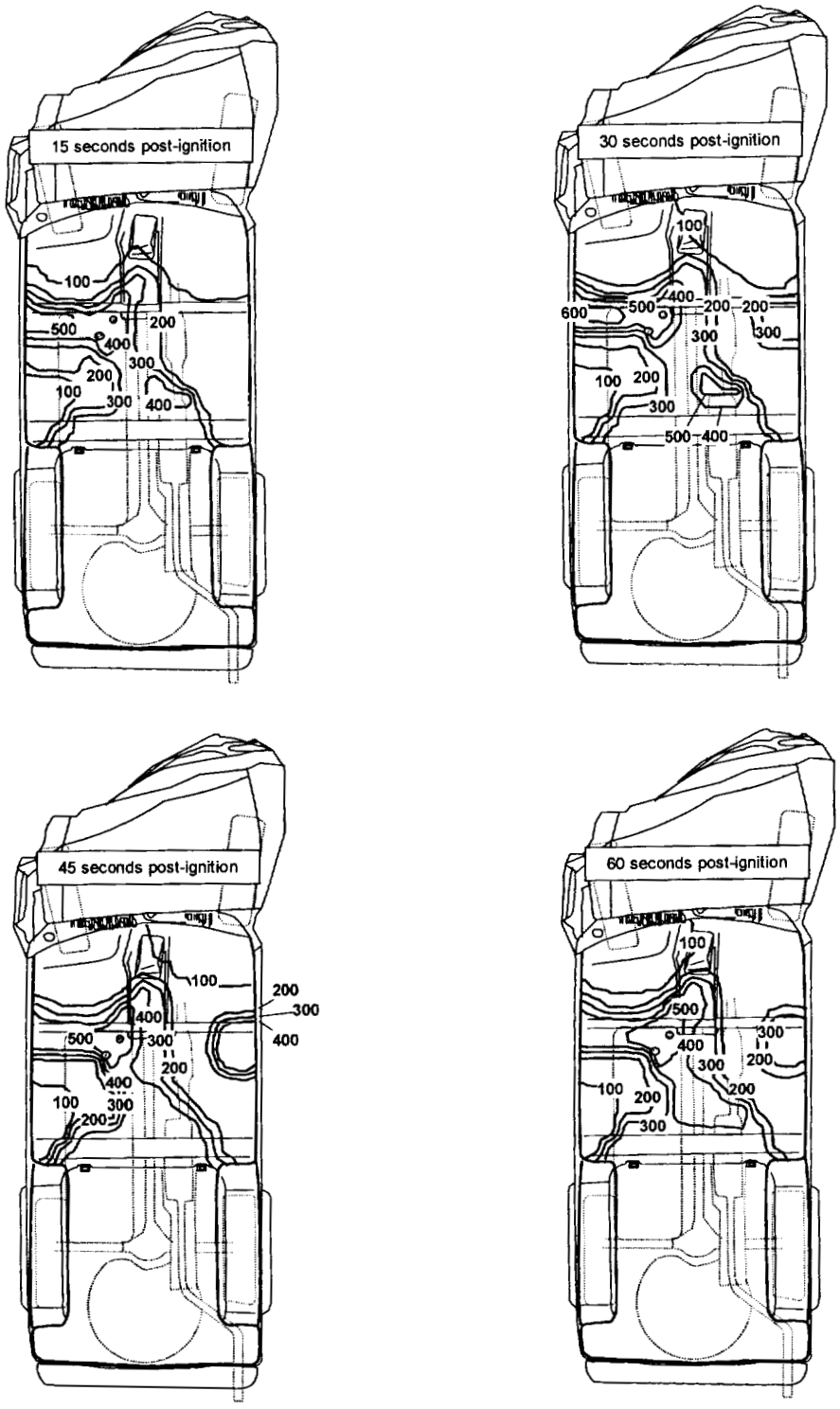

Figure 17, continued. Fire Test F99B1403. View from above the test vehicle showing the floor panel, electrical pass-through openings in the floor panel, and outlines of the fuel tank, exhaust system, rear axle, and spare tire, and isothermal contour plots showing estimated temperatures below the floor panel at 0, 15, 30, 45, 60, 90, 120, 150, 180, 210, 240, 270, and 300, seconds post-ignition.

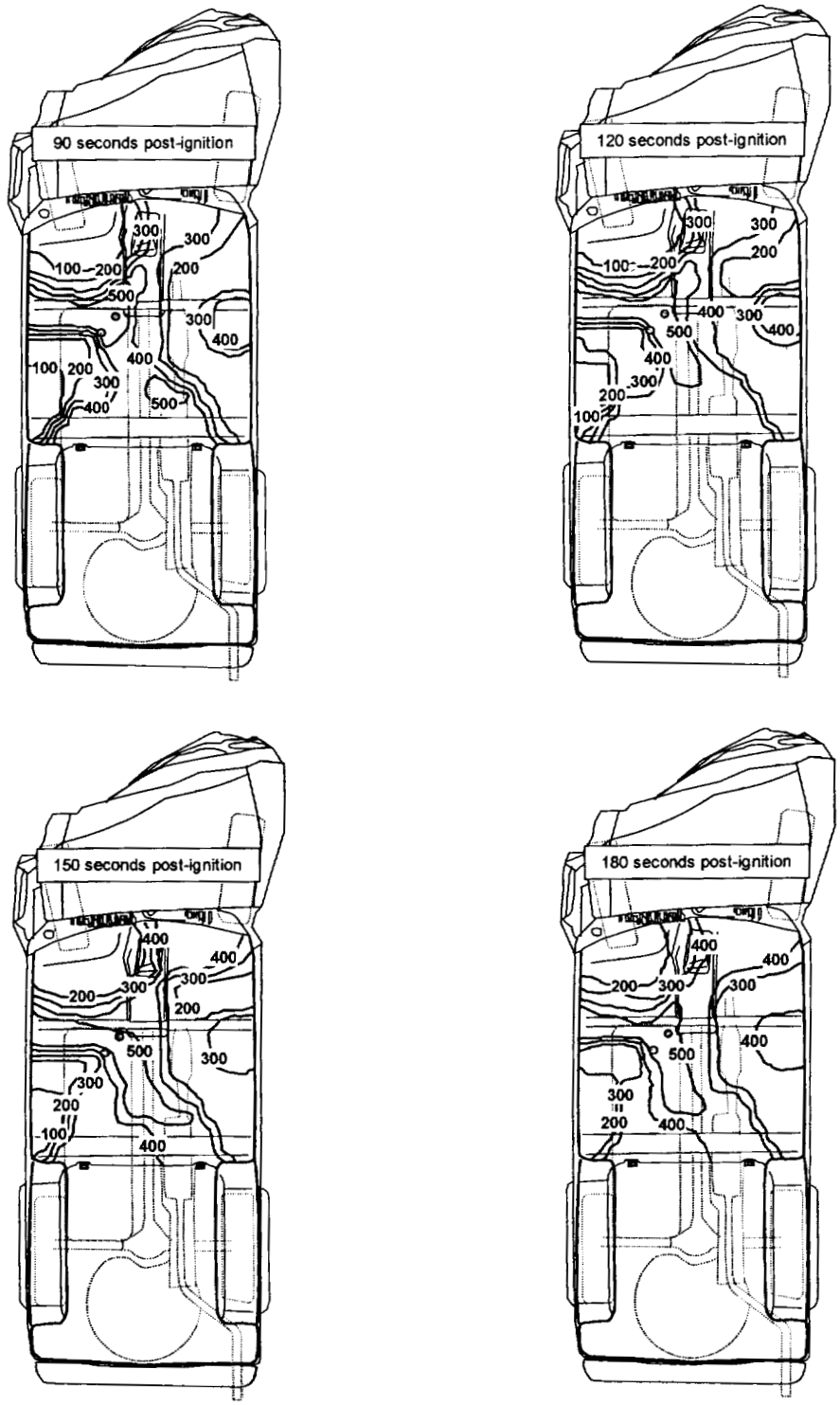

Figure 17, continued. Fire Test F99B1403. View from above the test vehicle showing the floor panel, electrical pass-through openings in the floor panel, and outlines of the fuel tank, exhaust system, rear axle, and spare tire, and isothermal contour plots showing estimated temperatures below the floor panel at 0, 15, 30, 45, 60, 90, 120, 150, 180, 210, 240, 270, and 300, seconds post-ignition.

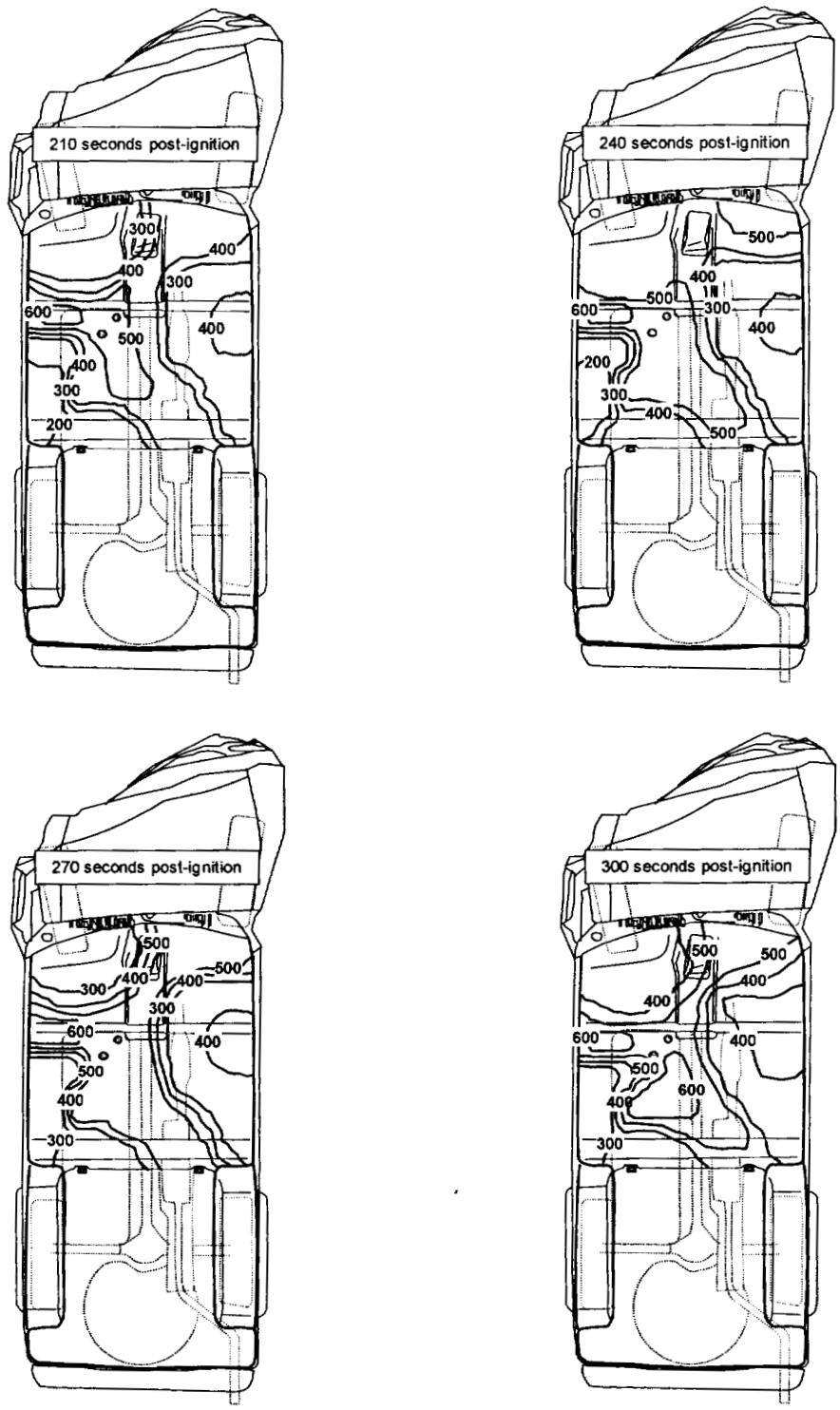

Figure 17, continued. Fire Test F99B1403. View from above the test vehicle showing the floor panel, electrical pass-through opeings in the floor panel, and outlines of the fuel tank, exhaust system, rear axle, and spare tire, and isothermal contour plots showing estimated temperatures below the floor panel at 0, 15, 30, 45, 60, 90, 120, 150, 180, 210, 240, 270, and 300, seconds post-ignition.

A threshold temperature of 600°C was used to indicate the presence of flames in the analysis of temperature data collected for Project B.3 [2 – 5]. These tests showed that temperatures recorded from thermocouples in flames may be less than 600°C when the amount of fuel load is relatively low and airflow into the flame is restricted causing an under ventilated flame. Based on analysis of the data collected in these previous tests, a threshold of 500°C appeared appropriate when the flames were under ventilated, as would be expected in this test for flames in restricted spaces along the underbody of the test vehicle. Using this criteria, areas of the floor panel were exposed to flames in the test vehicle with $t \geq 500$°C in Figure 17.

The isothermal contours in Figure 17 indicate that the area of the floor panel in F99B1403 above the front inboard corner of the fuel tank that contained two electrical pass-through openings was exposed to flames from about 30 seconds post-ignition through the end of this test. Estimated temperatures in this area were > 500°C between 15 and 30 seconds post-ignition, and increased to > 600°C between 270 and 300 seconds post-ignition (Fig. 17). The area of the underbody in the test vehicle exposed to flames appears to have increased during this test, extending to the right of the inboard side of the fuel tank and rearward in the drive train tunnel (Fig. 17). Differences in temperatures recorded from thermocouples located below the floor panel in several areas (see for example Section 4.4) suggests that there were differences in the distribution of flames on the underbodies of the control and experimental vehicles during these tests.

4.4 Flame-Spread Propagation into the Passenger Compartment

The intumescent coating was not applied to the drain hole and pass-through closures in the floor panel of the Experimental Vehicle and thus did not effect flame-spread into the passenger compartment through the electrical pass-through openings in the floor panel. Heat and fire damage to the floor panel and floor carpet observed during inspection of both test vehicles after these tests indicated that flames spread into the passenger compartment through electrical pass-through openings under the left front seat. Figure 18 shows the approximate locations of thermocouples and heat flux transducers located around this area of the floor panel of the test vehicles. In each test vehicle, one of the closures was dislodged from the electrical pass through during the crash test. In F980611, Thermocouple F9 was located approximately ½ in. below the lower surface of the floor panel, Thermocouple F10 was attached to the upper surface of the floor panel using a thermally conductive adhesive, Thermocouples P6 and P7 were located in the electrical pass-through opening where the grommet dislodged from the opening during the crash test, and Thermocouple P5 was located above the grommet in the other electrical pass-through opening (Fig. 18).

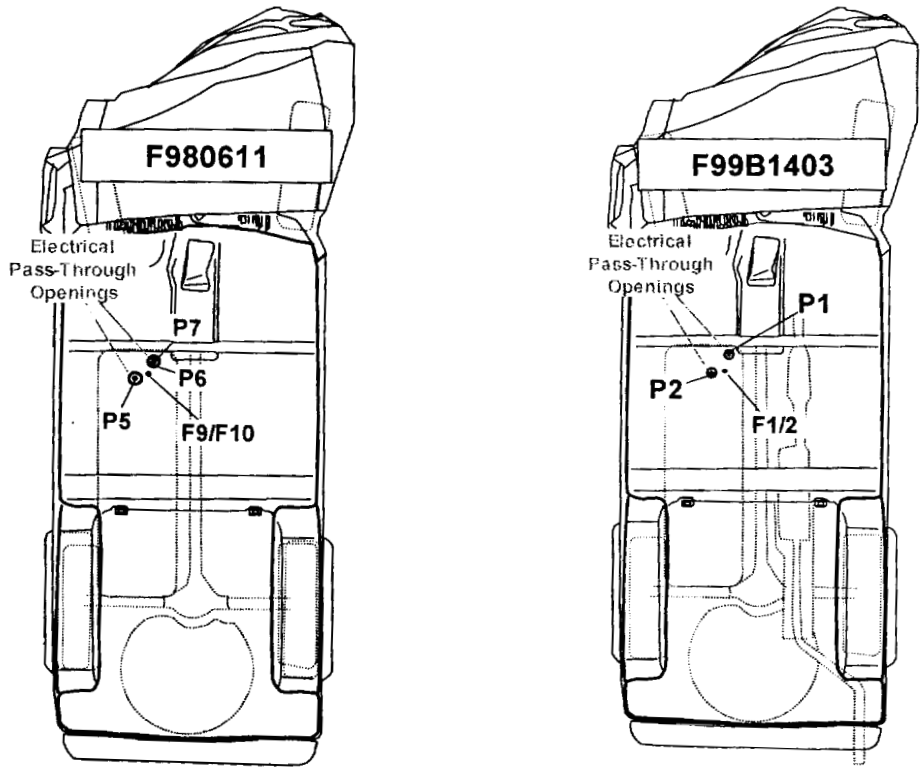

Figure 18. The diagram on the left shows the approximate locations of Thermocouples F9 and F10 and a HFT2 in the floor panel and Thermocouples P5, P6, and P7 in electrical pass-through openings in the floor panel of F980611. The diagram on the right shows the approximate locations of Thermocouples F1and F2 in the floor panel and Thermocouples P1 and P1 in the electrical pass-through openings in the floor panel of F99B1403.

In F99B1403, Thermocouple F1 was located approximately ½ in. below the lower surface of the floor panel, Thermocouple F2 was attached to the upper surface of the floor panel using a thermally conductive adhesive, Thermocouple P1was located in the electrical pass-through opening where the grommet dislodged from the opening during the crash test, and Thermocouple P2 was located above the grommet in the other electrical pass-through opening (Fig. 18).

Temperature data recorded from thermocouples located below the floor panel indicated that this area of the floor panel was exposed to flames within 15 seconds post-ignition (Fig.'s 19 and 20). Temperatures below the floor panel were between 650 and 750°C from 15 through 280 seconds post-ignition in F980611 (Fig. 19) and between 500 and 600°C from 15 through 380 seconds post-ignition in F99B1403 (Fig. 20).

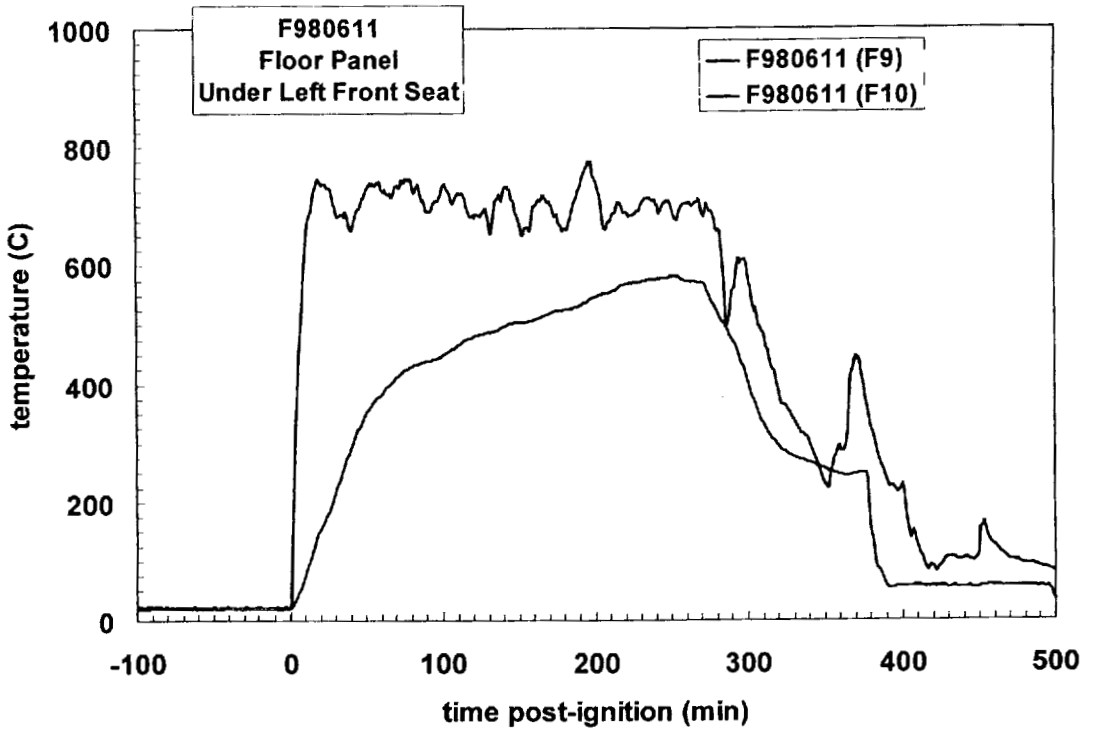

Figure 19. Fire Test F980611. Plots of temperature data recorded from Thermocouples F9 and F10.

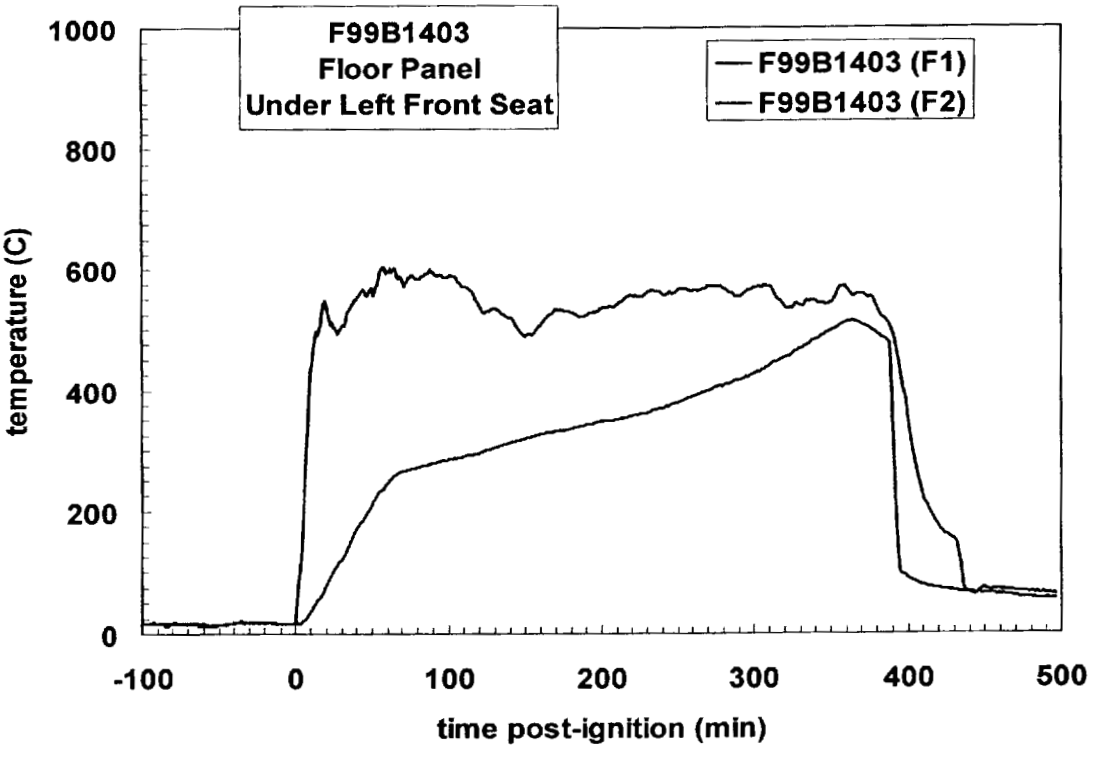

Figure 20. Fire Test F99B1403. Plots of temperature data recorded from Thermocouples F1 and F2.

The test was ended and fire suppression began at approximately 150 seconds post-ignition in F980611 and 300 seconds post-ignition in 99B1403. By the end of the test, the temperature of the floor panel in the area of the electrical pass-through openings was approximately 580°C in F980611 and 430°C in F99B1403.

The timing of flame-spread into the passenger compartments of the Control and Experimental Vehicles was approximately the same. For example, smoke started to flow out of the interior of from top of the left front door between 90 and 120 seconds post-ignition in both tests (Fig.'s 10 and 11). The density of the smoke visible in the interiors of the test vehicles and flowing out of the vehicles increased as both tests progressed (Fig.'s 12 through 16), indicating that materials in the passenger compartments of both vehicle were being heated to the point of pyrolysis and possibly had ignited by this time.

Data from thermocouples located under the seat cushions in the left front seats indicates that, in F980611, heated gases starting flowing onto the lower surface of the foam pad at about 20 seconds post-ignition (Fig. 21). Temperatures > 600°C, indicating flames along the lower surface of the surface of the foam pad in the seat cushion, were recorded from Thermocouple S19 at about 220 seconds post-ignition (Fig. 21). In F99B1403, heated gases starting flowing onto the lower surface of the foam pad between 50 and 60 seconds post-ignition (Fig. 22). Temperatures > 600°C were recorded from Thermocouple FS1 at about 215 seconds post-ignition, Thermocouple FS3 at about 260 seconds post-ignition, Thermocouple FS2 at about 340 seconds post-ignition, and Thermocouple FS4 at about 250 seconds post-ignition (Fig. 22)

Figure 23 is a video grab from Camera 10 F980611 at 250 seconds post-ignition and Figure 24 is a video grab from Camera 5 F99B1403 at approximately 270 seconds post-ignition showing flames burning through the cushions in the left front seats of the Control and Experimental Vehicles, respectively. Figure 25 is a photograph of the front seats removed from the Control Vehicle after F980611. Figure 26 is a photograph of the front seats removed from the Experimental Vehicle after F99B1403.

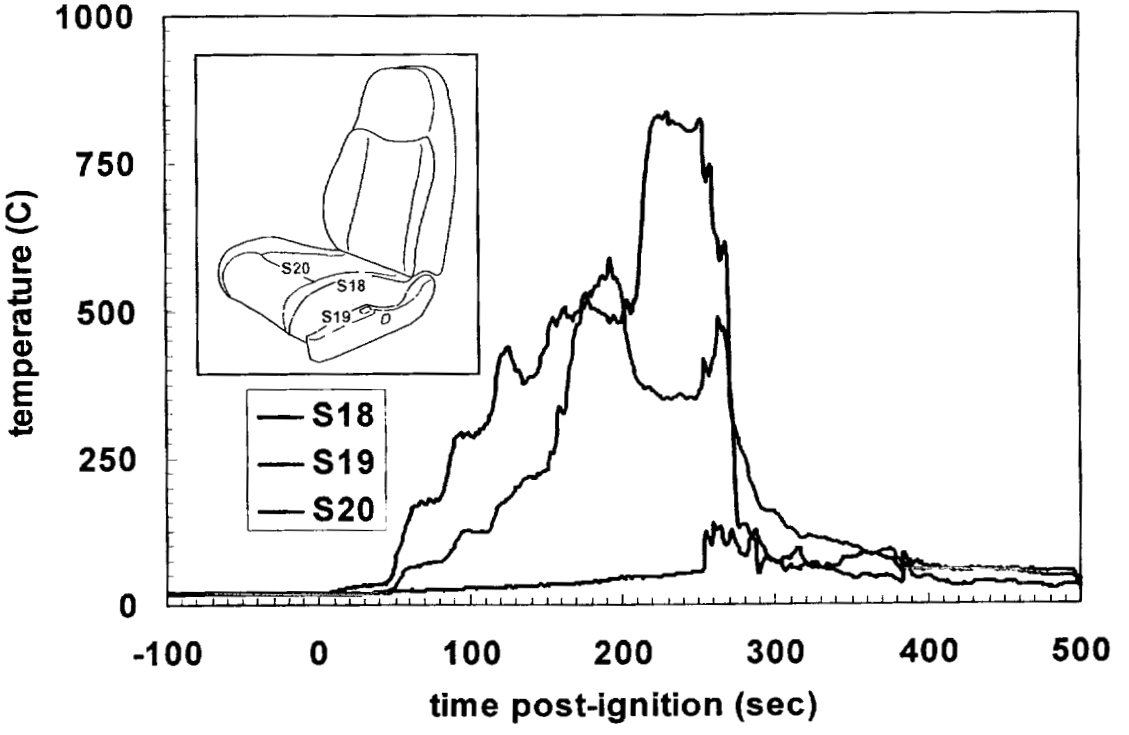

Figure 21. Fire Test F980611. Plots of temperature data recorded from Thermocouples S18, S19, and S20.

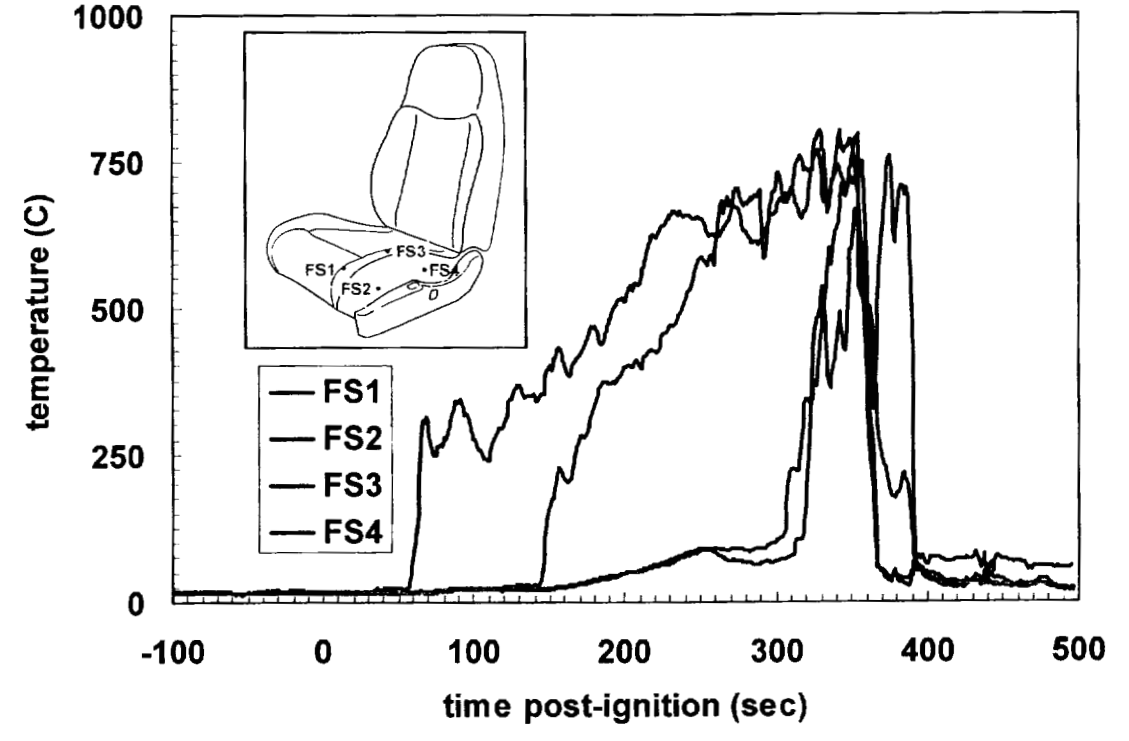

Figure 22. Fire Test F99B1403. Plots of temperature data recorded from Thermocouples FS1, FS2, FS3, and FS4.

Figure 23. Fire Test F980611. Video stills from Camera 10 at 250 seconds post-ignition.

Figure 24. Fire Test F99B1403. Video stills from Camera 5 at approximately 270 seconds post-ignition.

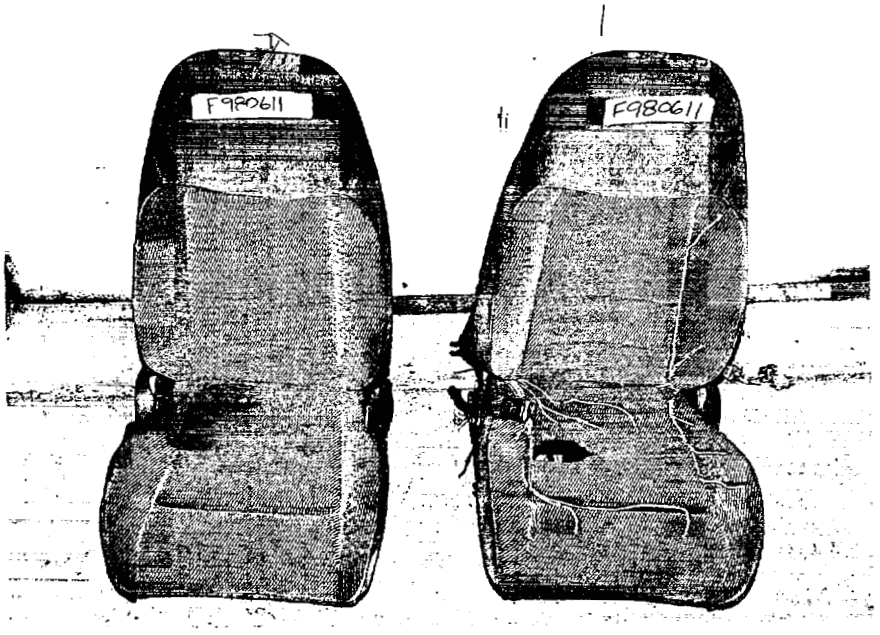

Figure 25. Fire Test F980611. Photograph of the left front seat in the test vehicle after Fire Test F980611.

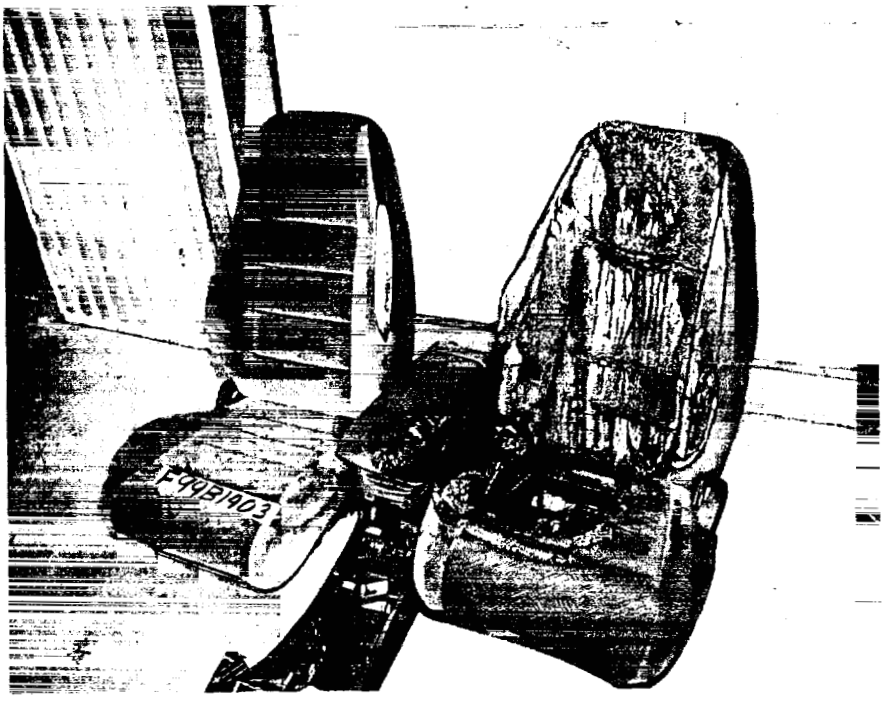

Figure 26. Fire Test F99B1403. Photograph of the left front seat in the test vehicle after Fire Test F99B1403.

5 Flame-Spread and Heat Transfer

Heat flux and thermocouple data from F980611 and F99B1403 was analyzed to determine the effect of intumescent coating on the apparent hot-side surface thermal resistance of the floor panel without and with intumescent paint using an approach similar to that used to determine insulation R values described in ASTM C1045 – 01 [9]. Figure 27 shows the approximate locations of heat flux transducers and thermocouples in the drive train tunnel in the floor panels of the Control and Experimental Vehicles.

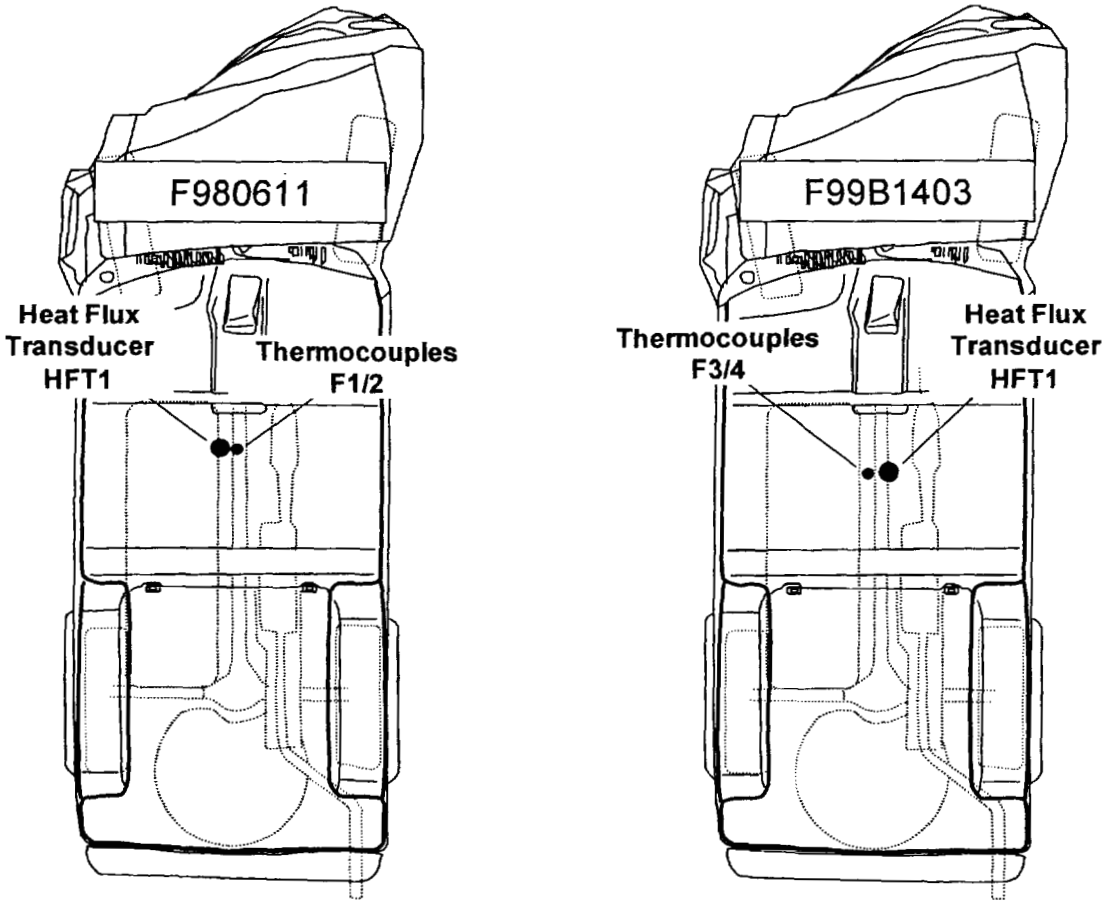

Figure 27. Approximate locations of heat flux transducers and thermocouples in the Control and Experimental Vehicles.

Figure 28 is a schematic cross section of the floor panel showing the relative locations and orientation of the heat flux transducers and thermocouples in the Control and Experimental Vehicles. The heat flux transducers were inserted through clearance holes in the floor panels so that the transducer faces were flush with the lower surfaces of the floor panels. One

thermocouple was located approximately 5 cm below the lower surface of the floor panel (TC1 in F980611 and TC3 in F99B1403), and one thermocouple was attached to the upper surface of the floor pane with thermally conducting cement TC2 in F980611 and TC4 in F99B1403). The paint on both surfaces of the floor panel in F980611 consisted of the production undercoat, base coat, and clear coat. The paint on the upper surface of the floor panel in F99B1403 consisted of the production undercoat, base coat, and clear coat and the paint on the lower surface of the floor panel in F99B1403 consisted of a non-production intumescent coating, base coat, and clear coat.

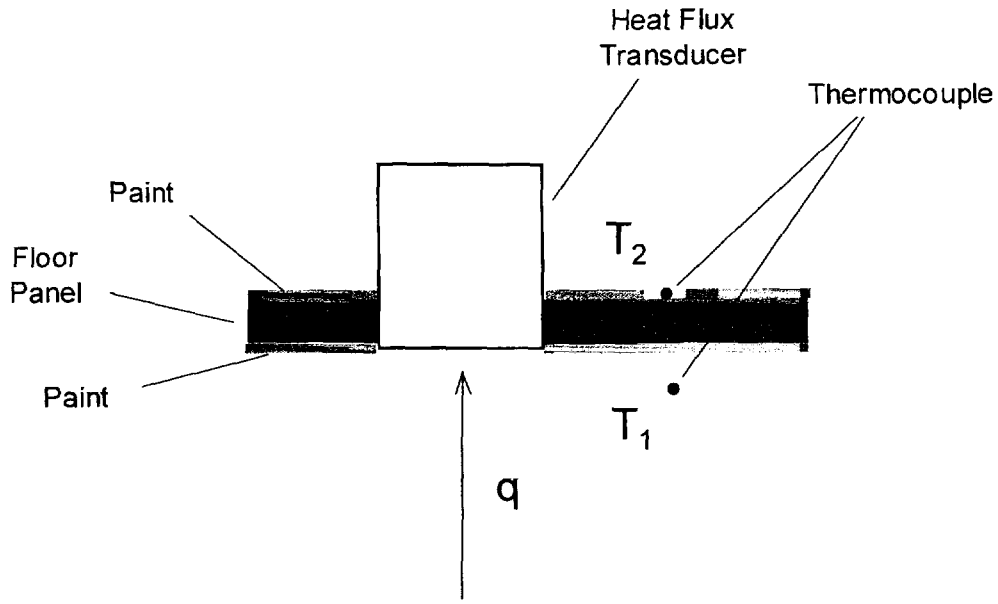

Figure 28. Schematic cross section of the floor panel containing the heat flux transducer and thermocouples

Data recorded from these transducers includes the heat fluxes to the lower surfaces of the floor panels, temperatures approximately 5 mm below the lower surface (hot-side) of the floor panels, and the temperatures of the upper surfaces (cold-side) of the floor panels.

The approach to calculating thermal transmission properties described in ASTM C1045 – 01 is applicable to test conditions that produce a steady-state, one-dimensional heat flux with isothermal temperatures on both surfaces of the material being tested and materials where the thickness and thermal transmission properties of the material being tested are constant during the measurement. These conditions were not met by the tests described in this report. For example, the heat flux to the underbodies of the test vehicles was not uniform or constant (steady-state) in these tests. As a result, isothermal surface temperatures were not achieved over the entire floor panel. When exposed to heated gases and flames, an intumescent material forms an expanded layer of char that alters heat transfer from heated gases and flames to that surface. Thus, the

thickness of the intumescent coating and its thermal transmission properties were not constant during F99B1403. A theoretical model of heat transfer in a multi-layered system exposed to a non-steady-state, three-dimensional heat flux, where the thickness and thermal transmission properties of some of the layers are not constant that would allow comparison of the heat transfer characteristics of the floor panels from the data acquired in these tests, has not been developed at this time. Thus, the approach described in ASTM C1045 – 01 was used here to estimate time-dependent changes in the hot-side thermal resistance of the floor panels in the test vehicles in F980611 and F99B1403.

Hot-side surface thermal resistance is defined in ASTM C1045 – 01 as "the quantity determined by the temperature difference at steady-state between an isothermal surface and its surrounding air that indicates a unite heat flow per unit area to or from the surface":

$$R_h = \frac{A(T_1 - T_h)}{Q} \qquad (1)$$

where R_h is the hot-side surface thermal resistance, A is surface area, T_1 is the area-weighted air temperature on the hot side of the surface, T_h is the area-weighted temperature of the surface exposed to the heated air, and Q is the one dimensional heat flux through the surface [9]. Thus, R_h is a measure of the resistance to heat transfer through a material exposed to heated air on one of the surfaces.

Figure 29 shows plots of the hot-side surface thermal resistances (R_h) in F980611 and F99B1403 calculated for a 1 cm^2 area of the floor panel in the drive train tunnel using equation (1). The calculated hot-side surface thermal resistance of the floor panel in F980611 (Control Vehicle) was greater than the hot-side thermal resistance of the floor panel in F99B1403 (Experimental Vehicle). Differences in the calculated R_h shown in Figure 29 were due to a smaller temperature gradient ($T_1 - T_h$) through the floor panel in F99B1403 than in F980611. (See Appendix C in [4] for thermocouple data acquired in F980611 and Appendix F in this report for thermocouple data acquired in F99B1403). The measured heat fluxes to the floor were similar in the Control and Experimental vehicles. (See Appendix F in [4] for heat flux transducer data acquired in F980611 and Appendix H in this report for heat flux transducer data acquired in F99B1403).

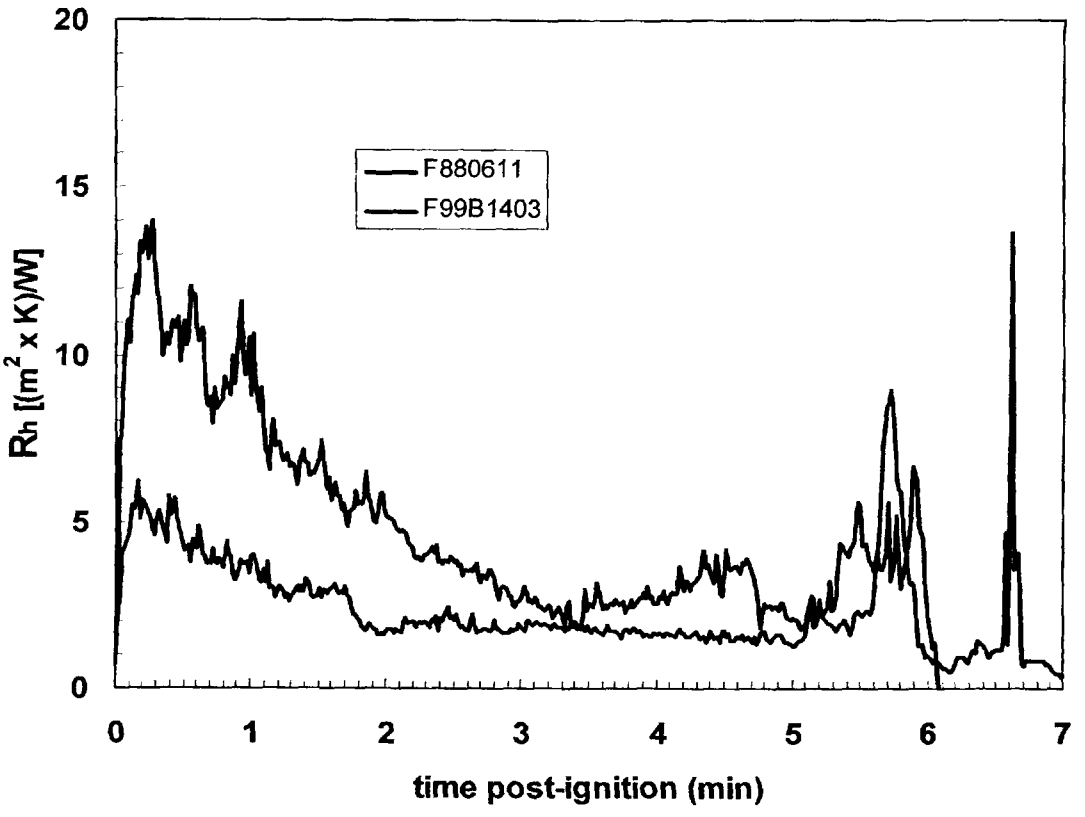

Figure 29. Hot-side surface thermal resistances (R_h) calculated for a 1 cm^2 area of the floor panel in the drive train tunnels in F980611 and F99B1403.

Figures 30 and 31 are photographs of the floor carpets (upper) and floor panels with the carpets removed (lower) in the Control and Experimental Vehicles after F980611 and F99B1403, respectively. The outlines in these photographs show the approximate locations of the front seats, the center console, and the rear bench. The floor carpet under the left front seat was burned in both vehicles. This was caused by flame-spread through electrical pass-through openings in the floor panel under the left front seat. Sections of the floor carpet at the rear of the center console and under the inboard side of the right front seat were discolored and melted in both vehicles. This appeared to have been caused by heating of the carpet by conduction through the floor panel. The section under the right side of the rear bench were burned in the Control Vehicle and melted in the Experimental Vehicle. During F980611, flames spread through a drain hole under the right side of the rear bench (labeled G in Fig. 30) and ignited the carpet in this area. Flames did not spread through this drain hole (labeled P9) in F99B1403. The carpet in this area of the Experimental Vehicle was melted from heating by conduction through the floor panel. Melted and charred residue from the carpet was observed on the floor panels of both the Control Vehicle (lower photograph, Fig. 30) and Experimental Vehicle (lower photograph, Fig. 31) after the carpets had been removed.

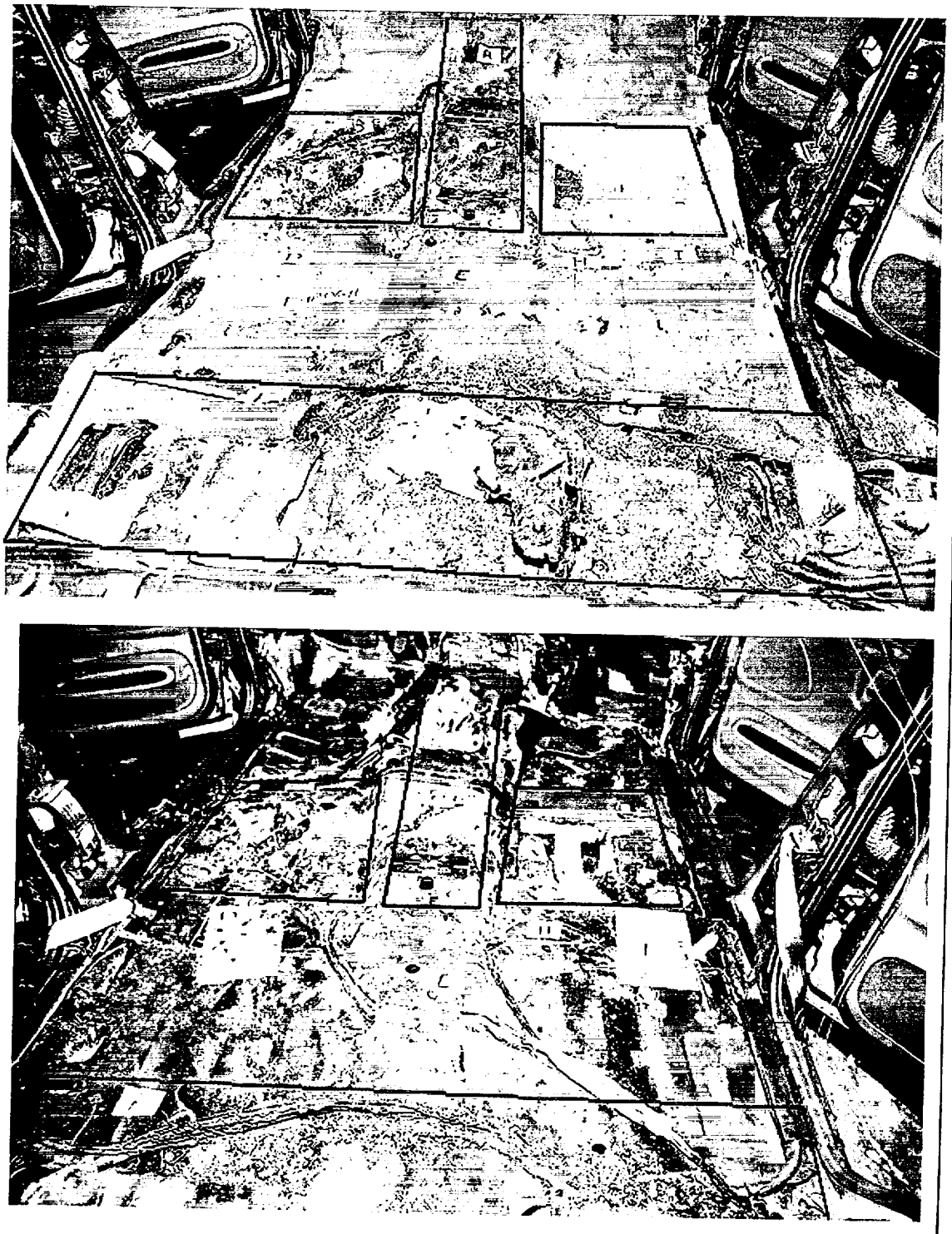

Figure 30. Fire Test F980611. Photograph of the floor carpet (upper) and floor panel (lower) in the test vehicle after F980611.

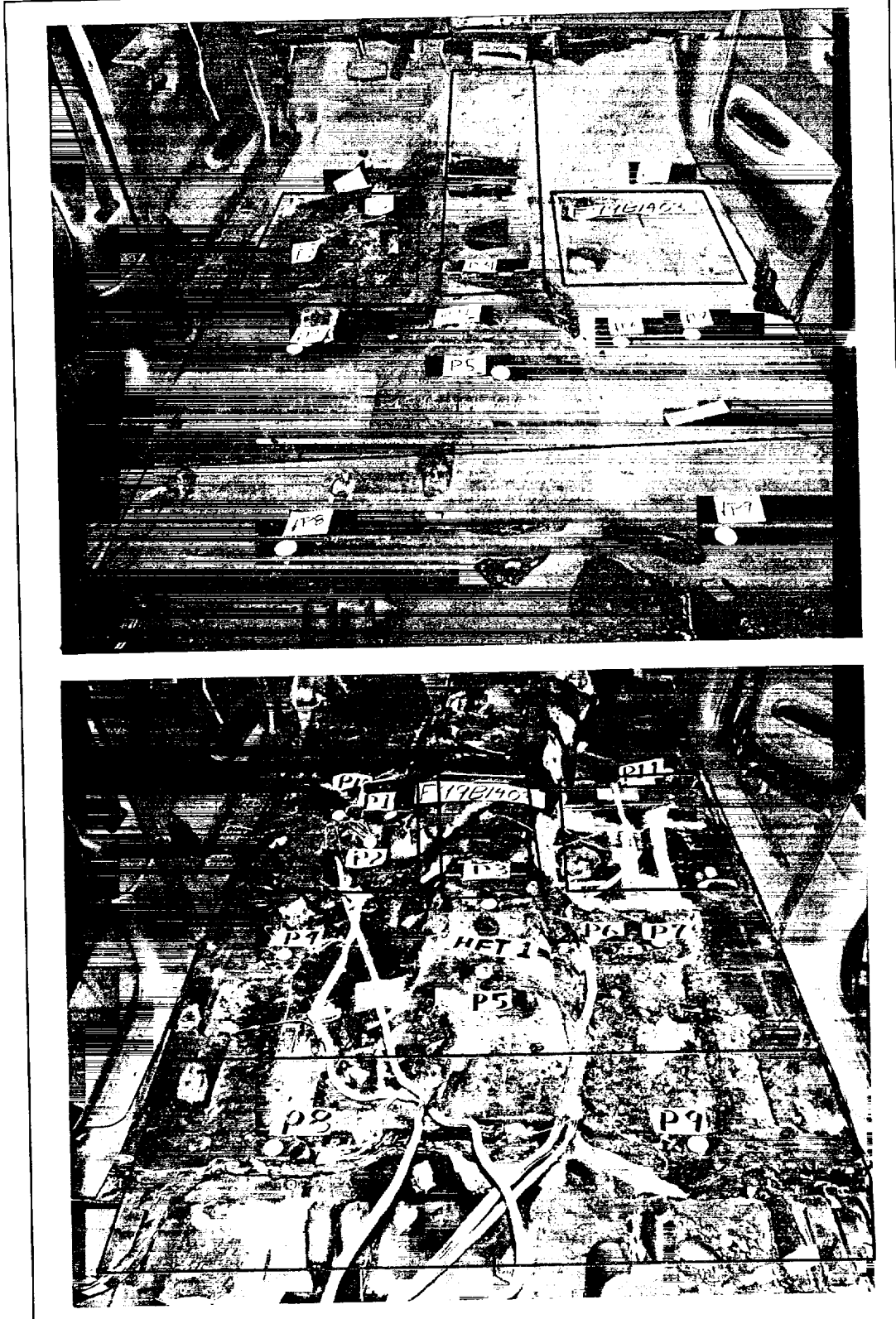

Figure 31. Fire Test F99B1403. Photograph of the floor carpet (upper) and floor panel (lower) in the test vehicle after F99B1403.

Inspections of the Control and Experimental Vehicles after these tests showed that their underbodies were coated with soot (Fig.'s 32 and 33). In the Control Vehicle, the base coat and clear coat were charred (Fig. 32). The undercoat was exposed and thermally degraded (white color) on the right side of the floor panel under the rear bench (Fig. 32). In the Experimental Vehicle, the intumescent coating has charred and expanded, and detached from several areas of the underbody exposing the metal floor panel (Fig. 33).

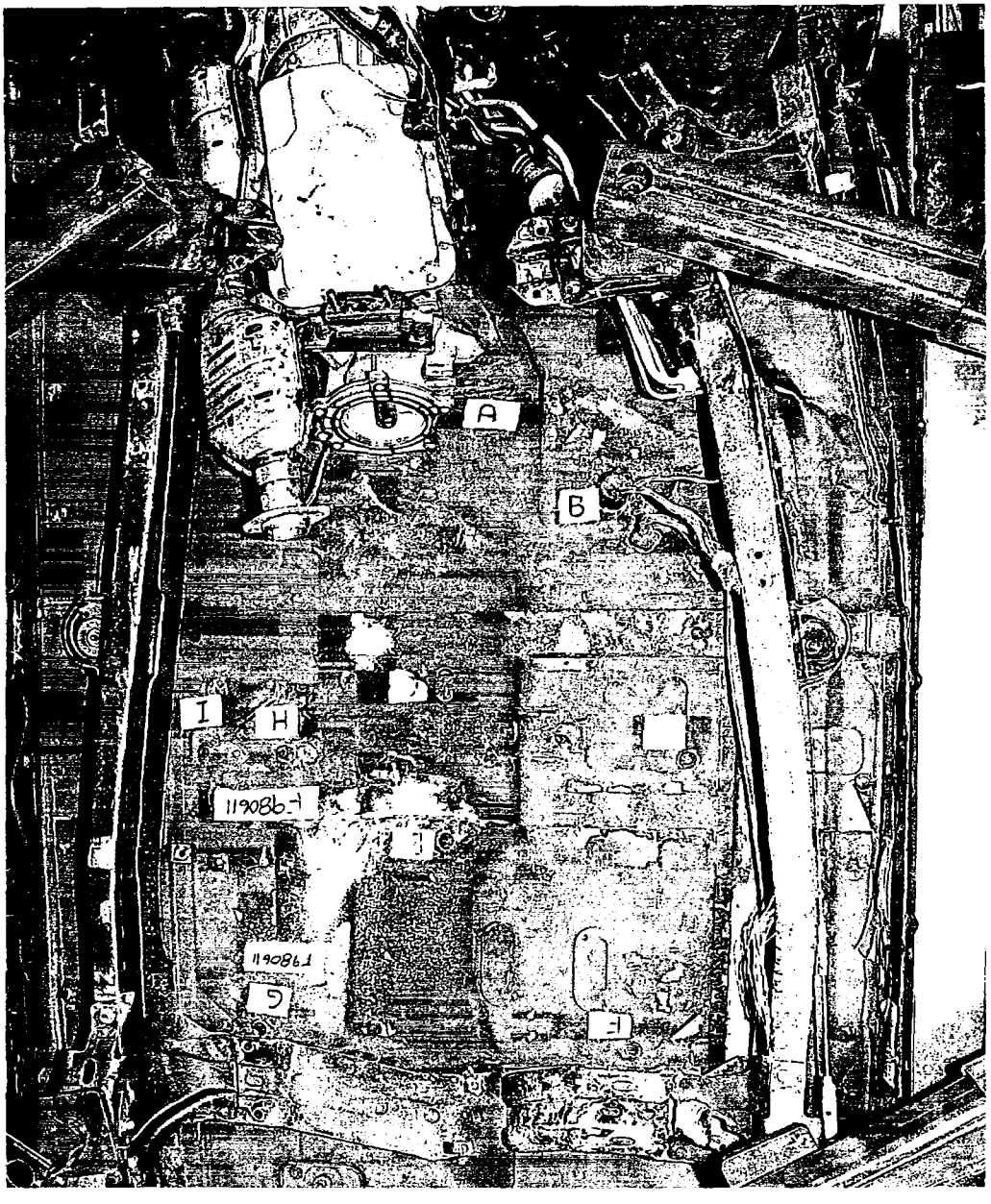

Figure 32. Fire Test F980611. Photograph of the underbody of the Control Vehicle after F980611.

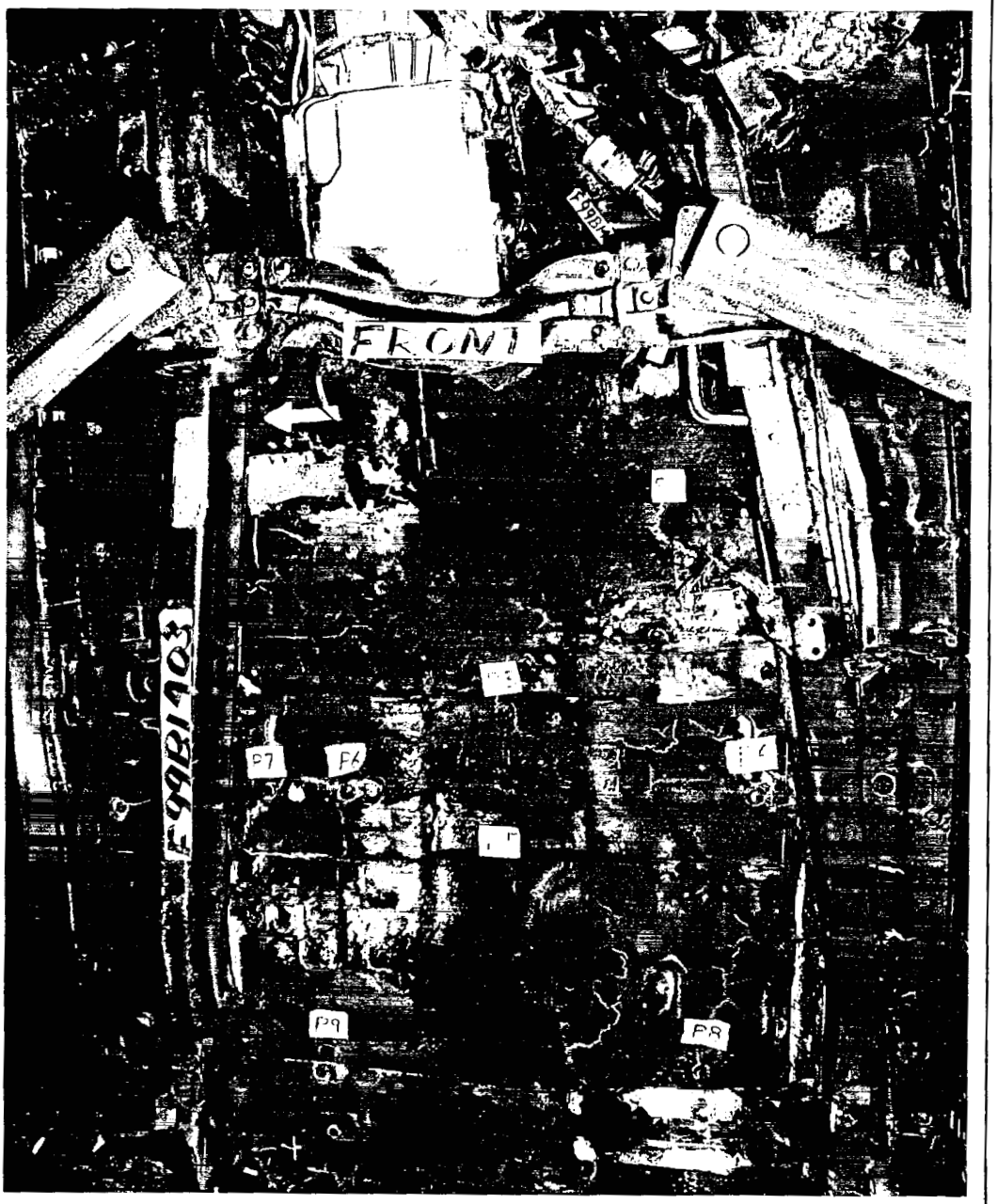

Figure 33. Fire Test F99B1403. Photograph of the underbody of the Experimental Vehicle after F99B1403.

Measurements done after F99B1403 showed that intumescent coating exposed to flames during this test expanded between about 1 and 10 mm. For example, Figures 34 and 35 show close-up views of the underbody of the Experimental Vehicle in the areas of P1 / P2 (Fig. 34) and P3 / P5 (Fig. 35).

Figure 34. Fire Test F99B1403. Photograph of the underbody of the Experimental Vehicle in the area of P1 / P2 after F99B1403.

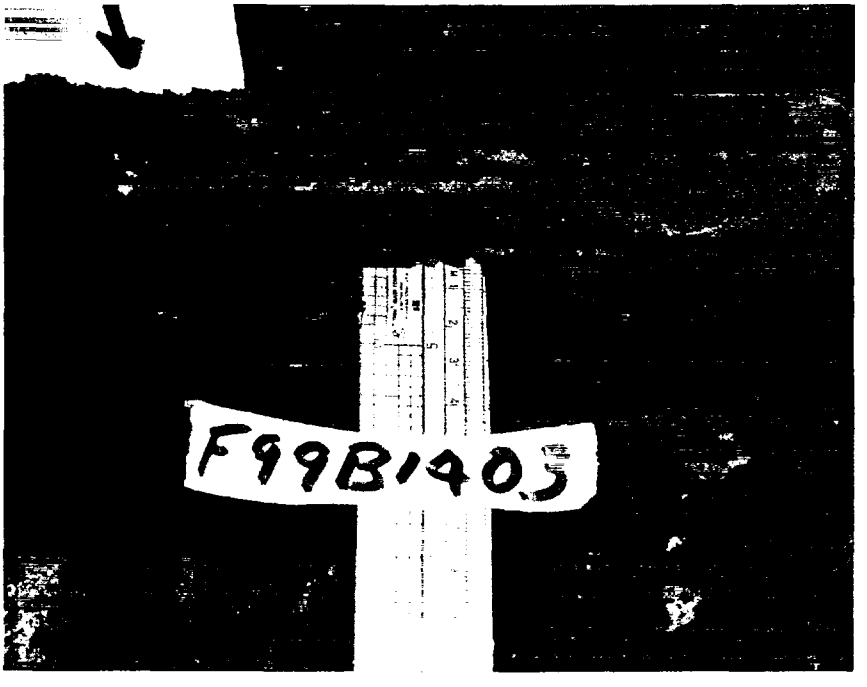

Figure 35. Fire Test F99B1403. Photograph of the underbody of the Experimental Vehicle in the area of P3 / P5 after F99B1403.

The intumescent coating had expanded to approximately 7-8 mm (Fig. 34) and 3-5 mm (Fig. 35), respectively, in these areas. Figure 36 shows a close-up view of the underbody in the drive-train tunnel. The intumescent coating had detached from several areas of the floor panel and flaked off during F99B1403, exposing the metal floor panel (Fig. 36).

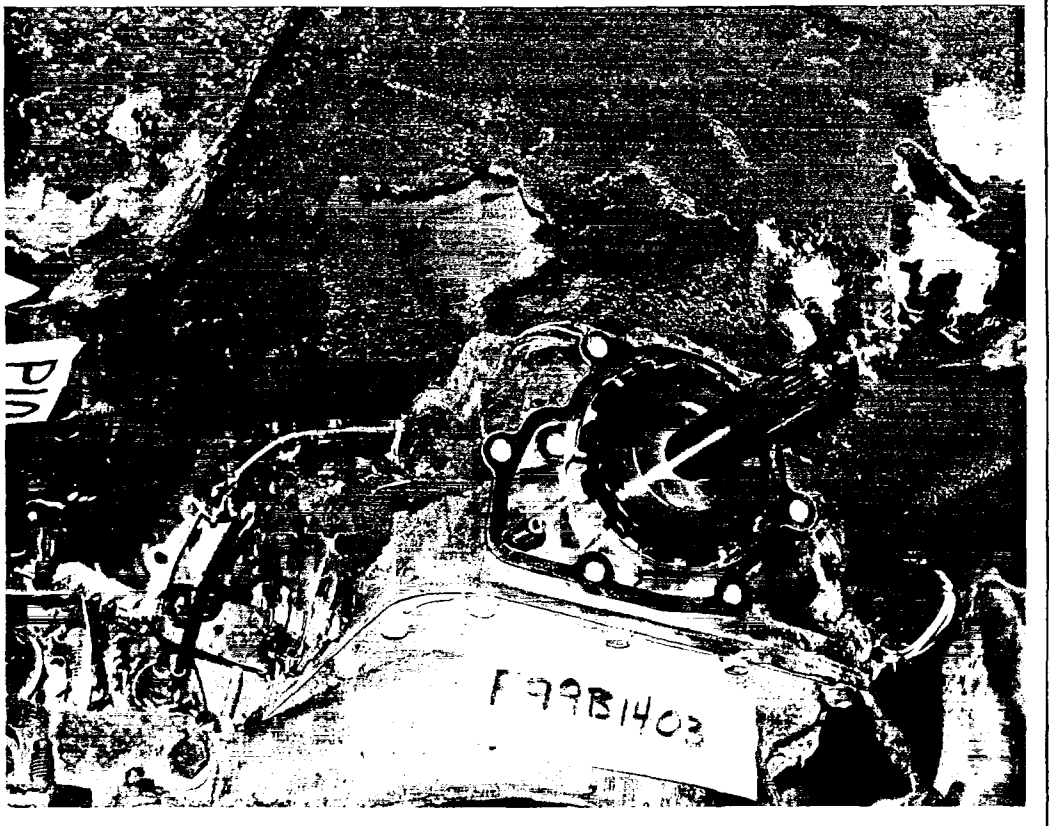

Figure 36. Fire Test F99B1403. Photograph of the underbody in the drive train tunnel of the Experimental Vehicle after F99B1403.

The concentrations of gaseous combustion products in the passenger compartment of the Experimental Vehicle during F99B1403 were generally greater than the concentrations of gaseous combustion products in the passenger compartment of the Control Vehicle during F980611. For example, Figure 37 shows plots of the concentration of carbon monoxide in the passenger compartments of Control Vehicle during F980611 and in the Experimental Vehicle during F99B1403.

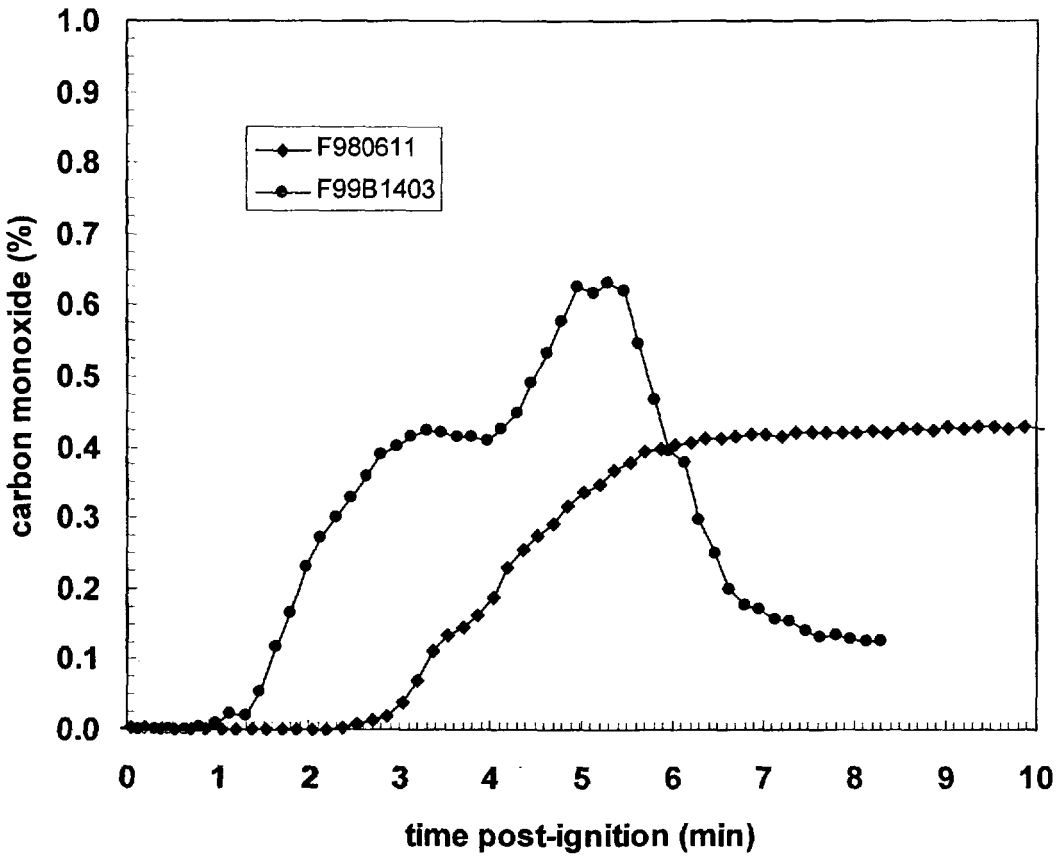

Figure 37. Plots of the carbon monoxide concentrations in the passenger compartments in the Control Vehicle in F980611 (—♦—) and in the Experimental Vehicle in F99B1403 (—●—).

These plots show that the concentration of carbon monoxide in the Control Vehicle during F980611 was always less than the concentration of carbon monoxide in the Experimental Vehicle during F99B1403 from the time of ignition to the time when these tests were ended and fire suppression began (Fig. 37).

6 Summary and Conclusions

The timing of flame-spread into the passenger compartment in the Experimental Vehicle during F99B1403 was not substantially different than the timing of flame-spread into the passenger compartment of the Control Vehicle during F980611. In both of these tests, flames spread through electrical pass-through openings in the floor panel under the left front seat, resulting in ignition of materials in the seat cushions and seat backs.

Any effect of the inumescent coating on heat transfer through the floor panel in these tests was small and difficult to quantify. Calculation of R_h from heat flux transducer and thermocouple data recorded during these tests suggests that the hot-side surface thermal resistance of the floor panel in the Control Vehicle was greater than the hot-side surface thermal resistance of the floor panel in the Experimental Vehicle. Temperature data recorded from the thermocouple located below the lower surface of the floor panel in F99B1403 may have been effected by expansion of the intumescent coating, thus yielding a lower value for $(T_1 - T_h)$ and R_h.

The floor carpet under the rear bench in the Control vehicle ignited during F980611. The equivalent area of floor carpet in the Experimental Vehicle did not ignite during F99B1403. This area of the floor carpet in the Control and Experimental Vehicles was melted and showed evidence of thermal degradation because of heat transfer from the burning gasoline under the test vehicle through the floor panel. The thermally degraded carpet in the Control Vehicle ignited because flames burned through a plug in a drain hole opening in the floor panel under the right side of the rear bench during F980611 (G in the lower photograph of Fig. 30). Flames did not burn through this drain hole plug in the Experimental Vehicle during F99B1403 (P9 in the lower photograph in Fig 31). An intumescent coating was not applied to the drain hole plugs in the Experimental Vehicle. Thus, this difference in behavior appears to have been the result of test-to-test variability, which resulted in greater exposure to flames of this area of the underbody of the Control Vehicle.

References

1. Anthony Hamins. Evaluation of Intumescent Body Panel Coatings in Simulated Post-Accident Vehicle Fires. Submitted to the National Highway Transportation Safety Administration pursuant to the Settlement Agreement between General Motors and the Department of Transportation. Submitted October 1, 1998.

2. Jeffery Santrock. Evaluation of Motor Vehicle Initiation and Propagation. Part 4. Propagation of an Underbody Gasoline Pool Fire in a 1996 Passenger Van. Submitted to the National Highway Transportation Safety Administration pursuant to the Settlement Agreement between General Motors and the Department of Transportation. Submitted August 3, 2001.

3. Jeffrey Santrock. Evaluation of Motor Vehicle Initiation and Propagation. Part 6. Propagation of an Underbody Gasoline Pool Fire in a 1997 Rear Wheel Drive Passenger Car. Submitted to the National Highway Transportation Safety Administration pursuant to the Settlement Agreement between General Motors and the Department of Transportation. Submitted February 20, 2001.

4. Jeffrey Santrock. Evaluation of Motor Vehicle Initiation and Propagation. Part 10. Propagation of an Underbody Gasoline Pool Fire in a 1998 Sport Utility Vehicle. Submitted to the National Highway Transportation Safety Administration pursuant to the Settlement Agreement between General Motors and the Department of Transportation. Submitted May 31, 2002.

5. Evaluation of Motor Vehicle Initiation and Propagation. Part 12. Propagation of an Underbody Gasoline Pool Fire in a 1998 Front Wheel Drive Passenger Car. Submitted to the National Highway Transportation Safety Administration pursuant to the Settlement Agreement between General Motors and the Department of Transportation. Submitted October 31, 2002.

6. Federal Safety Standards. Motor Vehicle Safety Standard No. 214 Side Impact Protection - Passenger Cars, Trucks, Buses & Multipurpose Passenger Vehicles with GVWR of 10,000 Pounds or Less. 60FR57838-39 (November 22, 1995).

7. Jack L. Jensen and Jeffrey Santrock. Evaluation of Motor Vehicle Fire Initiation and Propagation. Part 8: Crash Tests on a Sport-Utility-Vehicle. Submitted to the National Highway Transportation Safety Administration pursuant to the Settlement Agreement between General Motors and the Department of Transportation. February 15, 2001.

8. SigmaPlot® 4.0 for Windows®, SPSS Inc., 444 North Michigan Avenue, Chicago, IL 60611. Copyright © 1997 by SPSS Inc..

9. ASTM C1045 – 01. Standard Practice for Calculating Thermal Transmission Properties Under Steady-State Conditions. American Society for Testing and Materials, 100 Barr harbor Drive, West Conshohocken, PA.

Appendix A

Crash Test C12820 – Accelerometer Data

I. Crash Test C12820 - Accelerometer Data

Four tri-axial (longitudinal, lateral, and vertical) accelerometers were mounted to the test vehicle in the following locations:

- Right front rocker panel
- Left front rocker panel
- Right Rear Rocker Panel
- Left Rear Rocker Panel

Figure A1 shows the approximate locations of the accelerometers on the test vehicle.

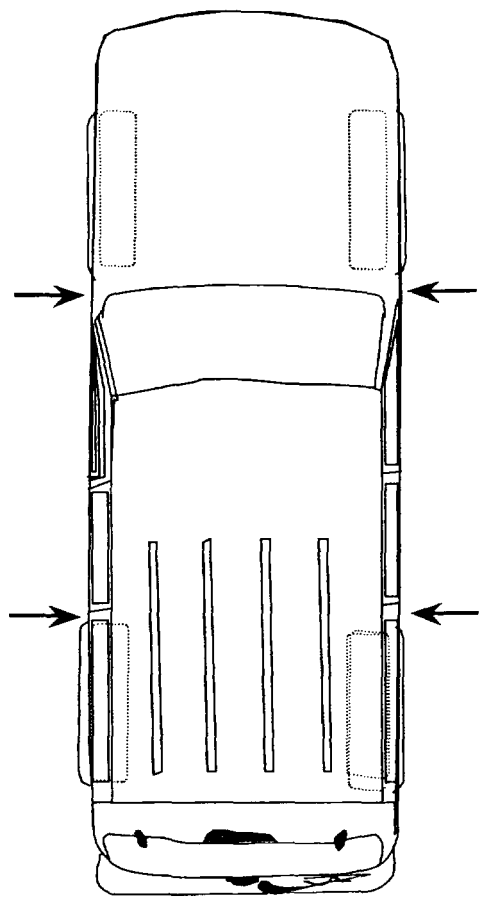

Figure A1. Diagram showing the approximate locations of the accelerometers on the test vehicle.

Two tri-axial (longitudinal, lateral, and vertical) accelerometers were mounted on the Adjustable Moving Deformable Barrier (AMDB) in the following locations:

- Rear cross member
- Center of Mass

Figure B1 shows the approximate locations of the accelerometers on the Adjustable Moving Deformable Barrier.

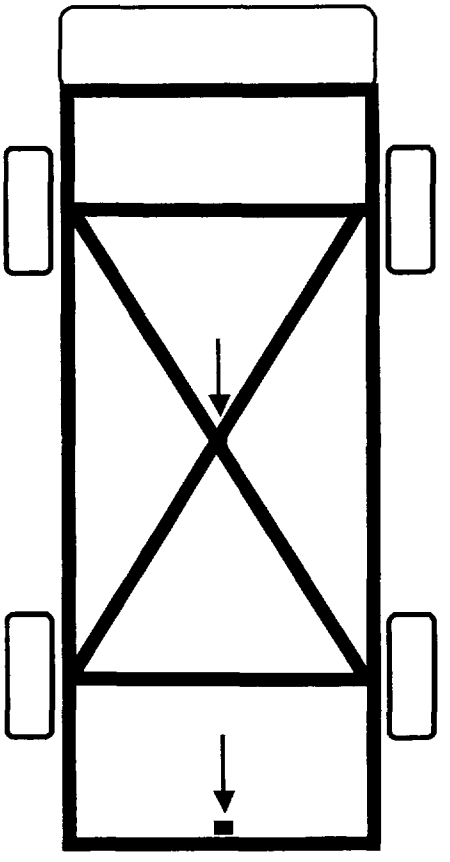

Figure A2. Diagram showing the approximate locations of the accelerometers on Adjustable Moving Deformable Barrier.

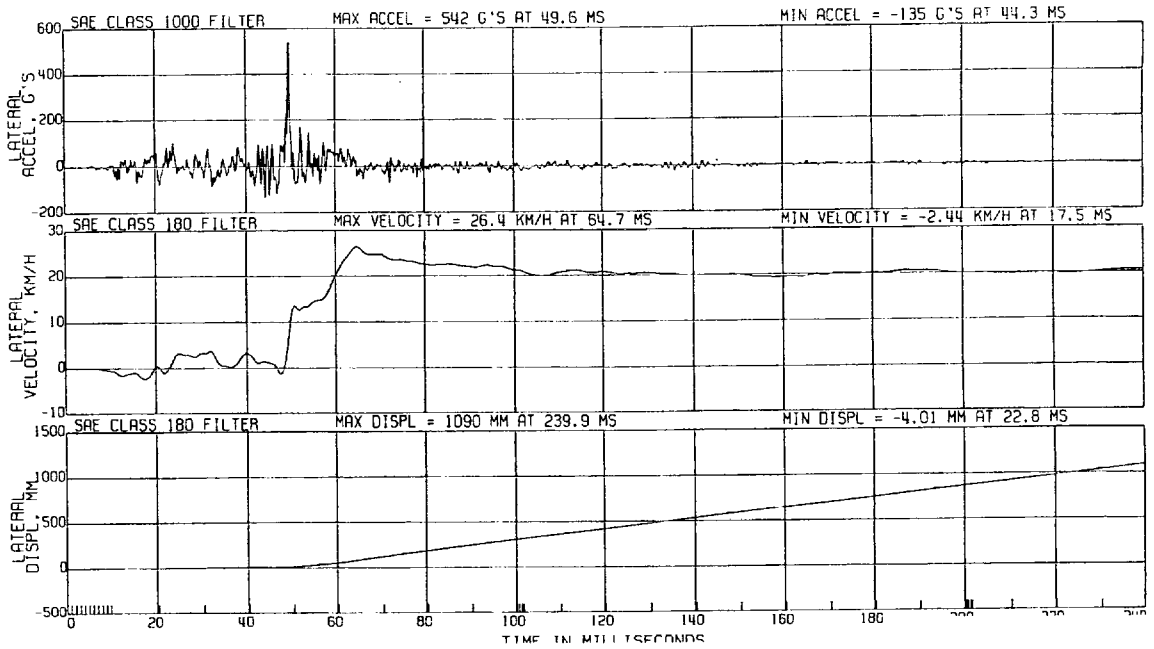

Plot A1. Crash Test C12820. Plots of acceleration, velocity, and displacement in the direction of the lateral-axis calculated from the accelerometer on the left front rocker.

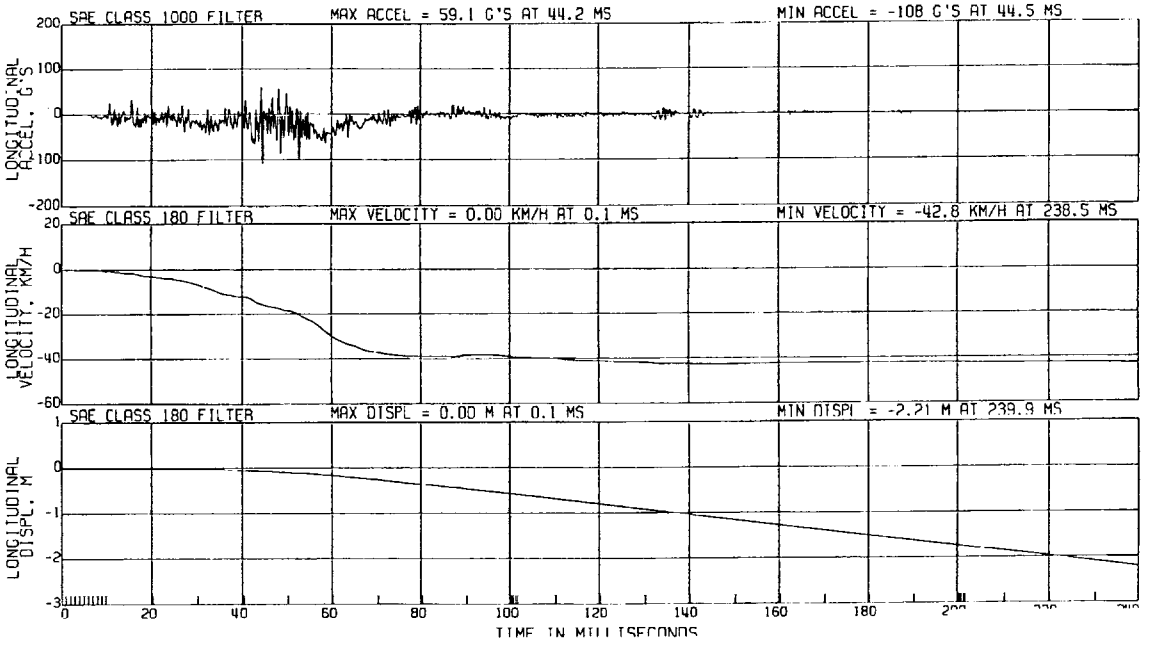

Plot A2. Crash Test C12820. Plots of acceleration, velocity, and displacement in the direction of the longitudinal-axis calculated from the accelerometer on the left front rocker.

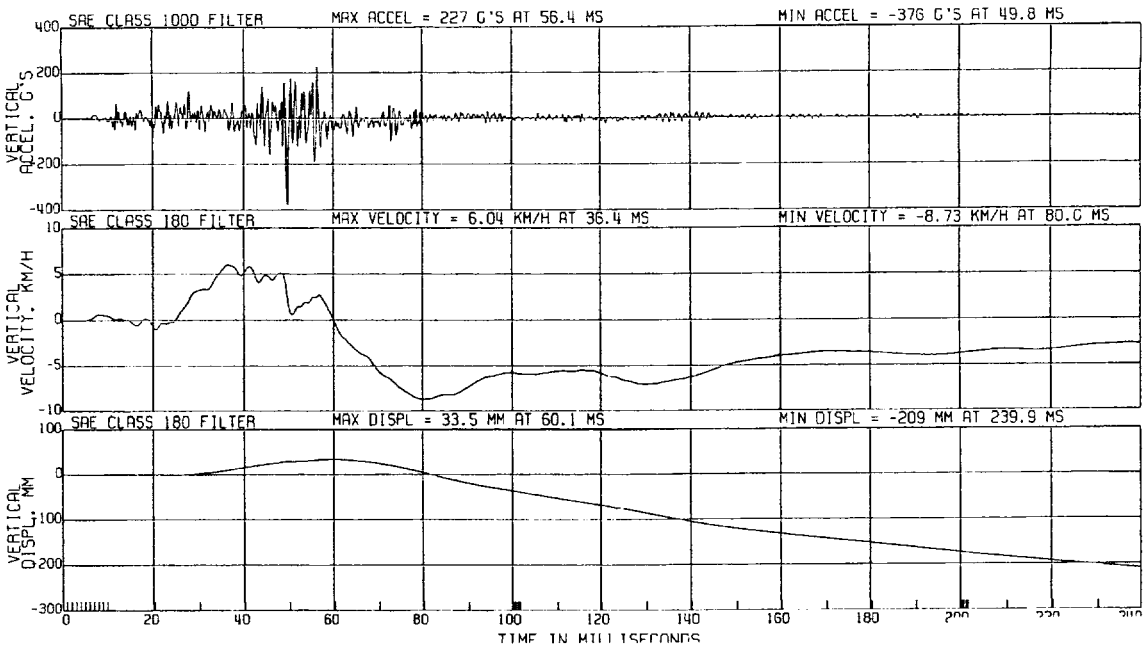

Plot A3. Crash Test C12820. Plots of acceleration, velocity, and displacement in the direction of the vertical-axis calculated from the accelerometer on the left front rocker.

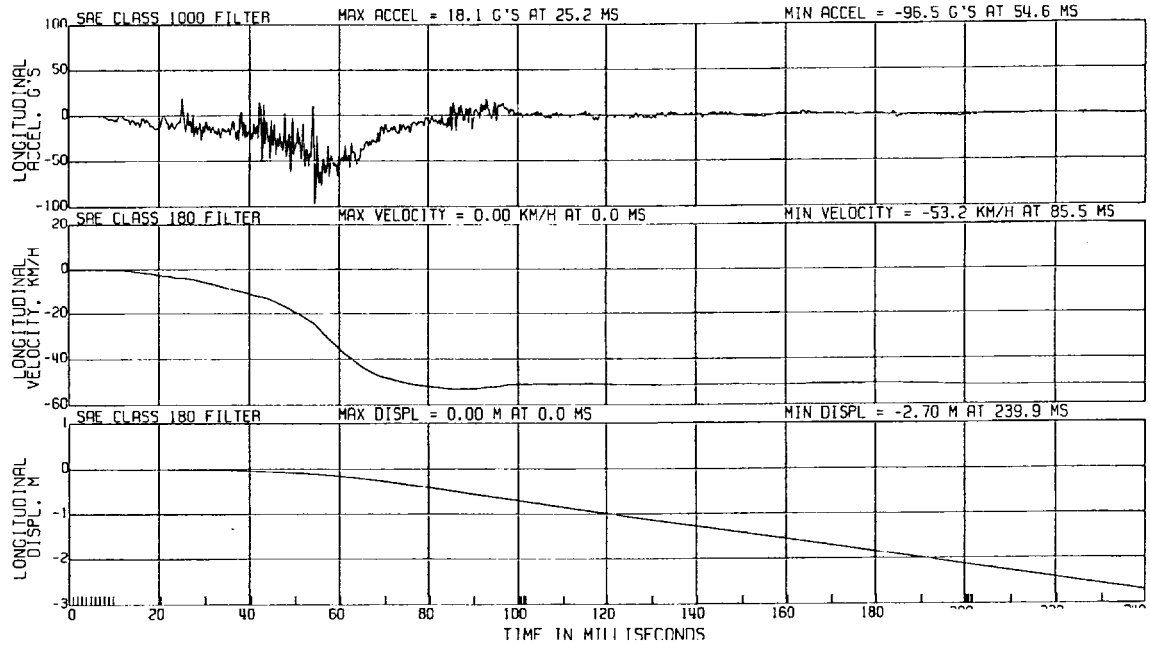

Plot A4. Crash Test C12820. Plots of acceleration, velocity, and displacement in the direction of the longitudinal-axis calculated from the accelerometer on the right front rocker.

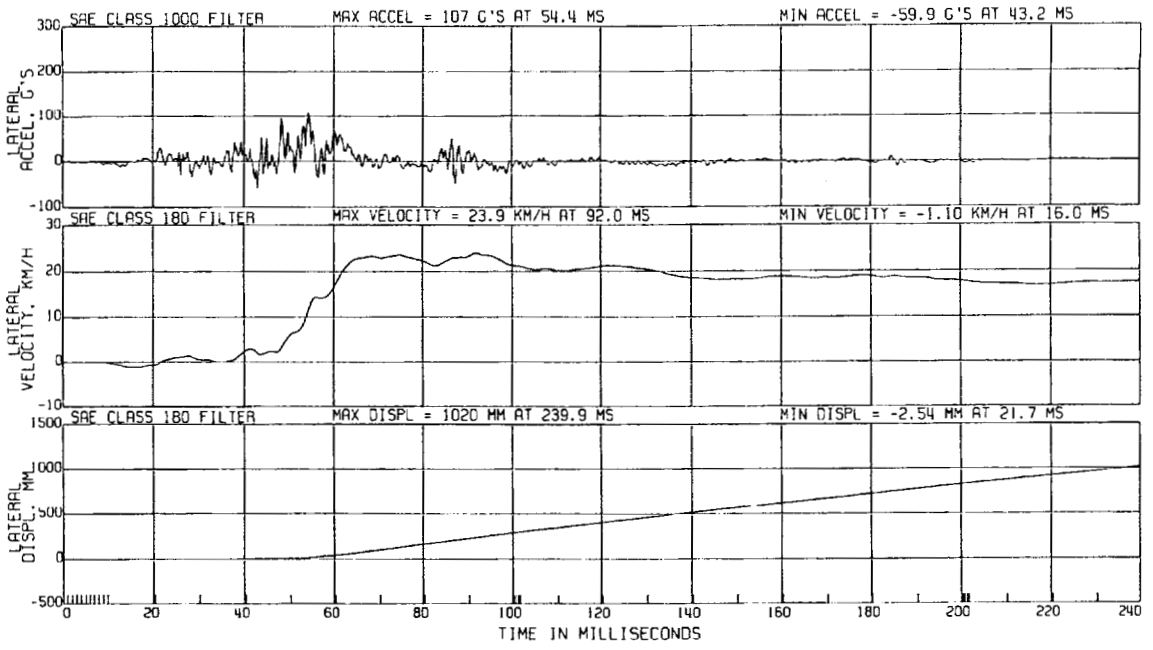

Plot A5. Crash Test C12820. Plots of acceleration, velocity, and displacement in the direction of the lateral-axis calculated from the accelerometer on the right front rocker.

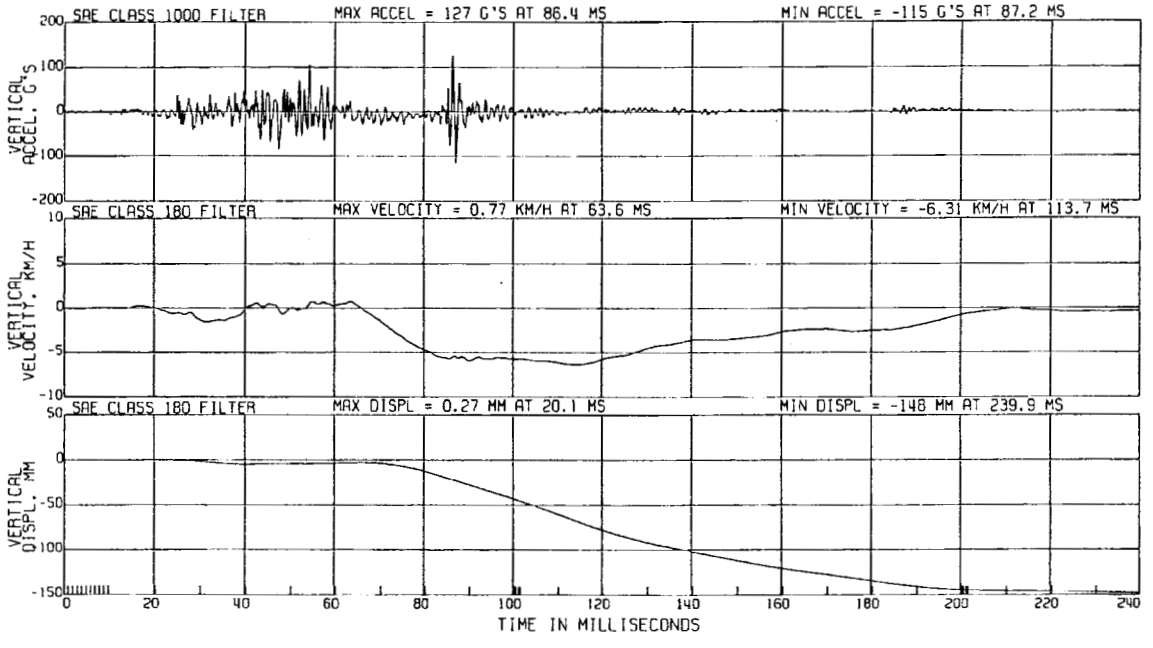

Plot A6. Crash Test C12820. Plots of acceleration, velocity, and displacement in the direction of the vertical-axis calculated from the accelerometer on the right front rocker.

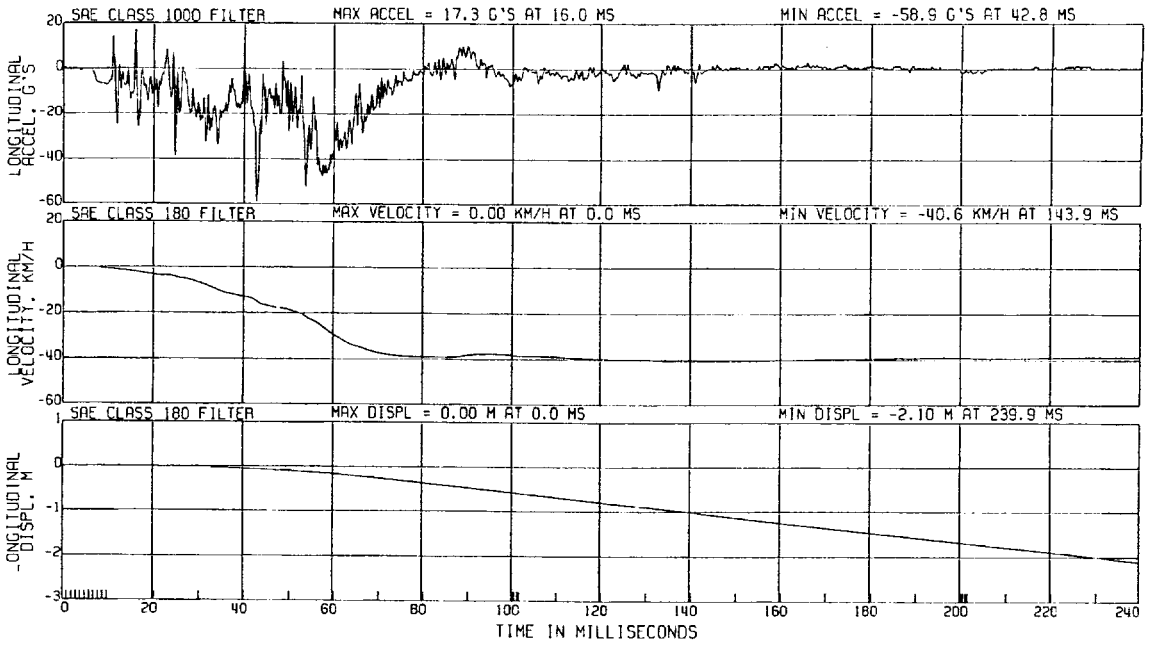

Plot A7. Crash Test C12820. Plots of acceleration, velocity, and displacement in the direction of the longitudinal-axis calculated from the accelerometer on the left rear rocker.

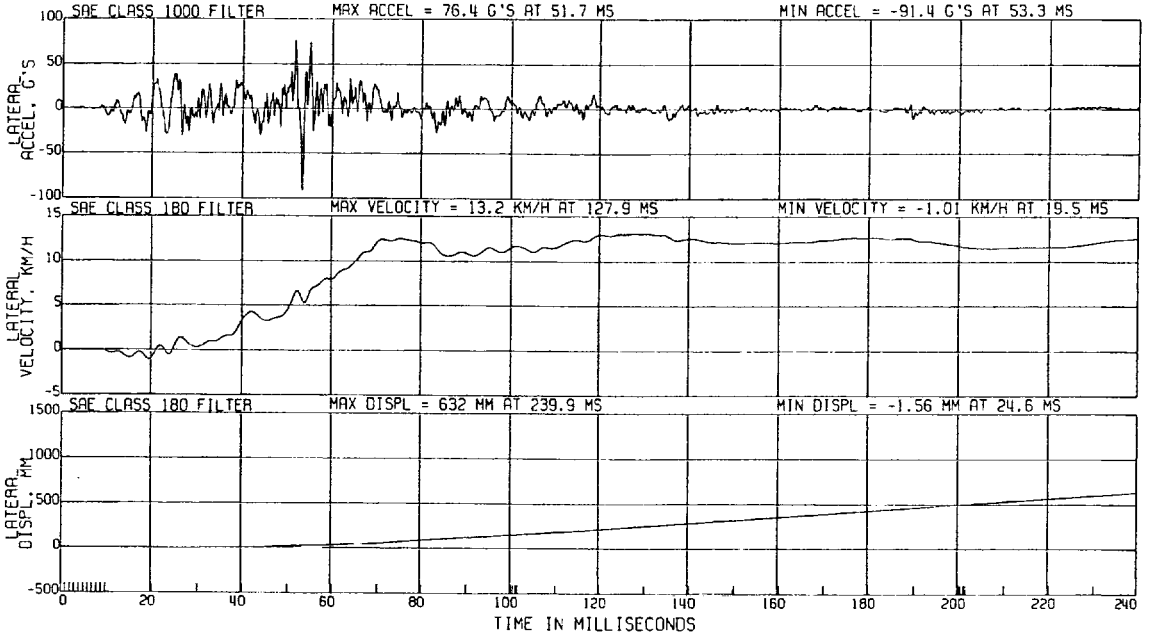

Plot A8. Crash Test C12820. Plots of acceleration, velocity, and displacement in the direction of the lateral-axis calculated from the accelerometer on the left rear rocker.

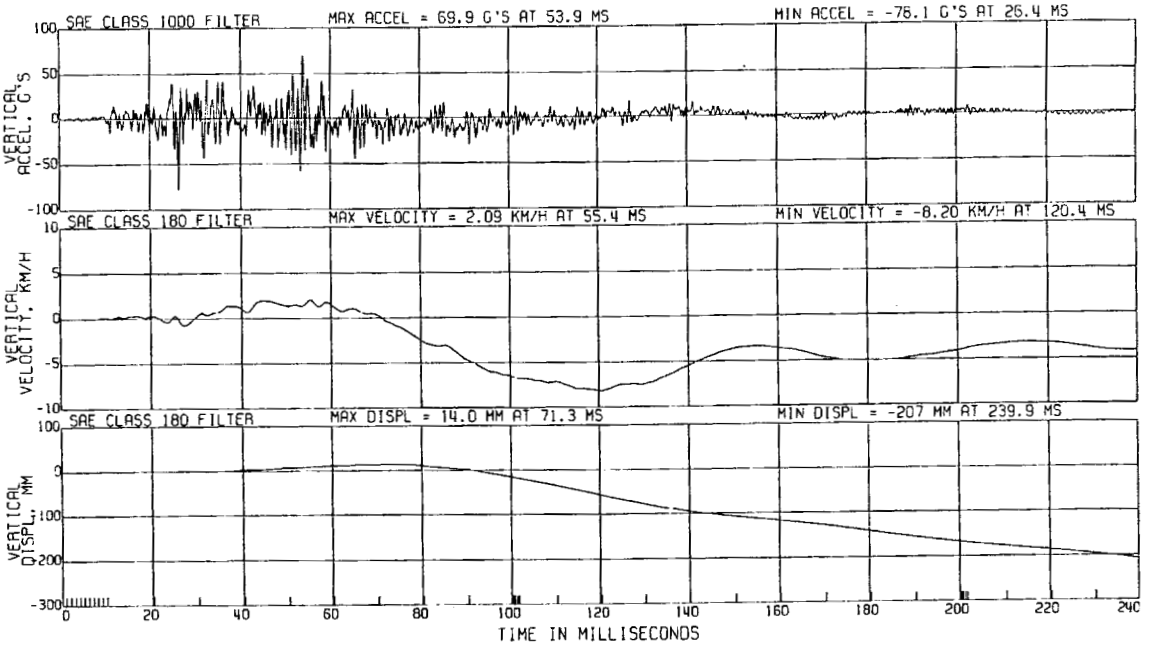

Plot A9. Crash Test C12820. Plots of acceleration, velocity, and displacement in the direction of the vertical-axis calculated from the accelerometer on the left rear rocker.

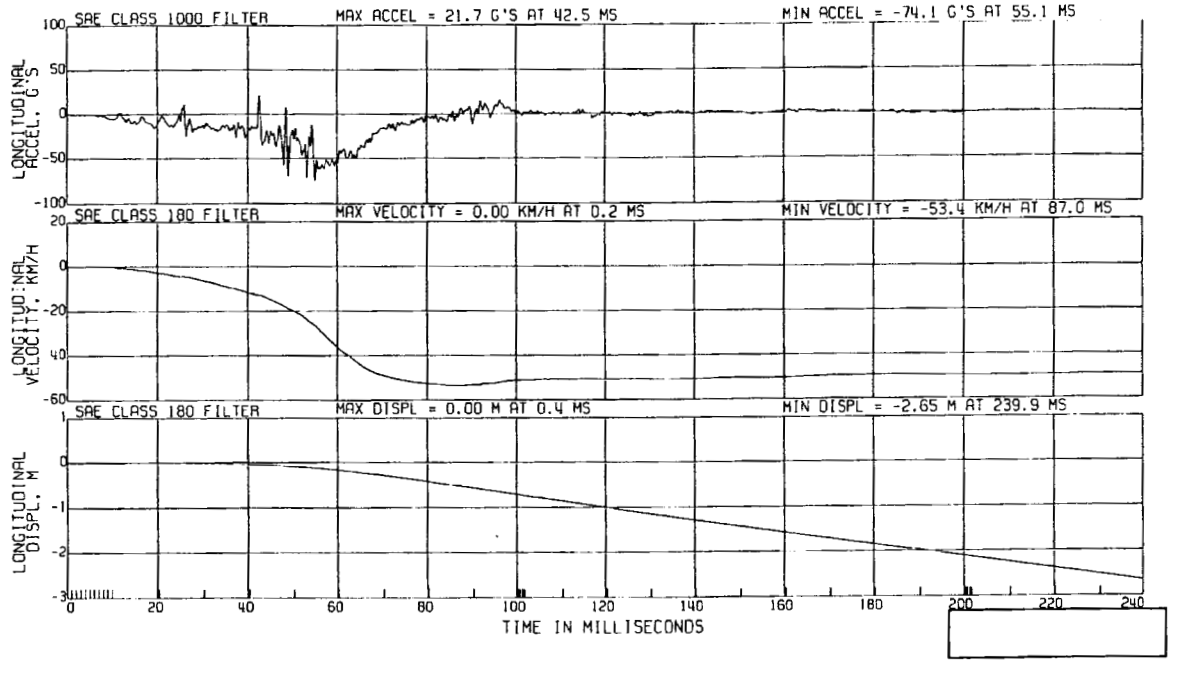

Plot A10. Crash Test C12820. Plots of acceleration, velocity, and displacement in the direction of the longitudinal-axis calculated from the accelerometer on the right rear rocker.

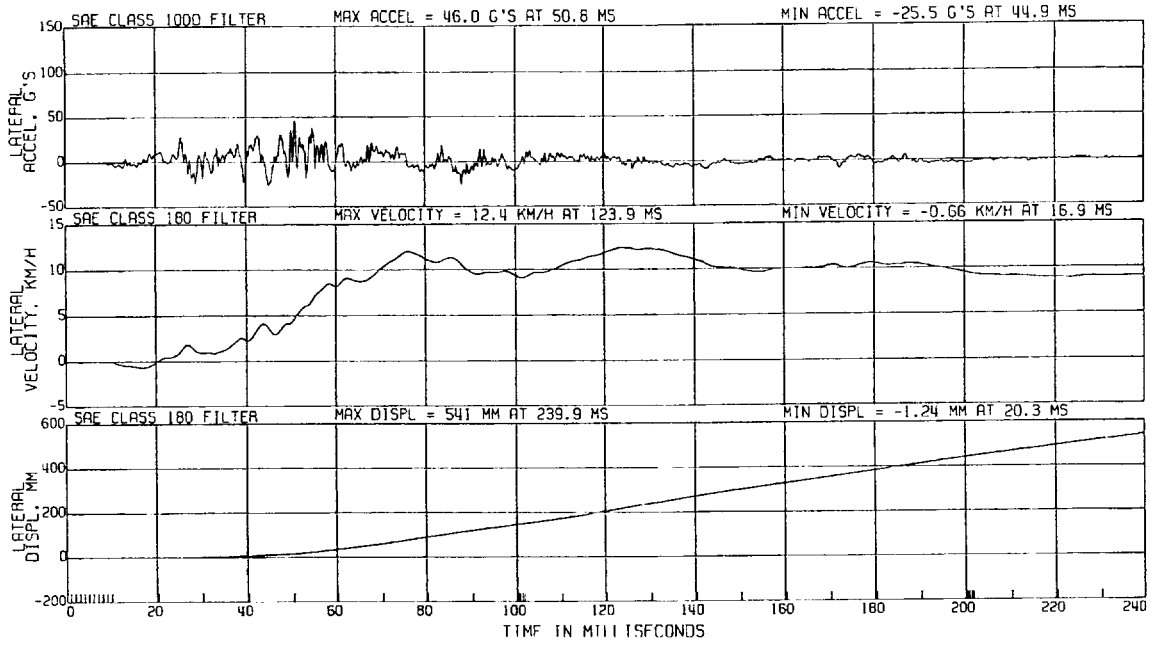

Plot A11. Crash Test C12820. Plots of acceleration, velocity, and displacement in the direction of the lateral-axis calculated from the accelerometer on the right rear rocker.

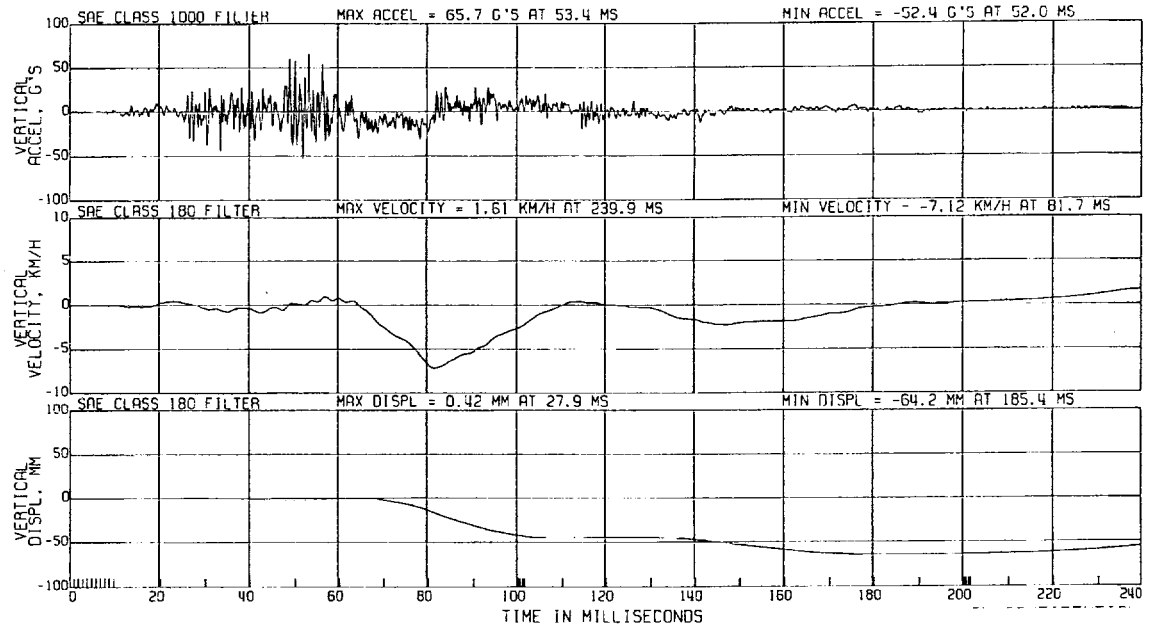

Plot A12. Crash Test C12820. Plots of acceleration, velocity, and displacement in the direction of the vertical-axis calculated from the accelerometer on the right rear rocker.

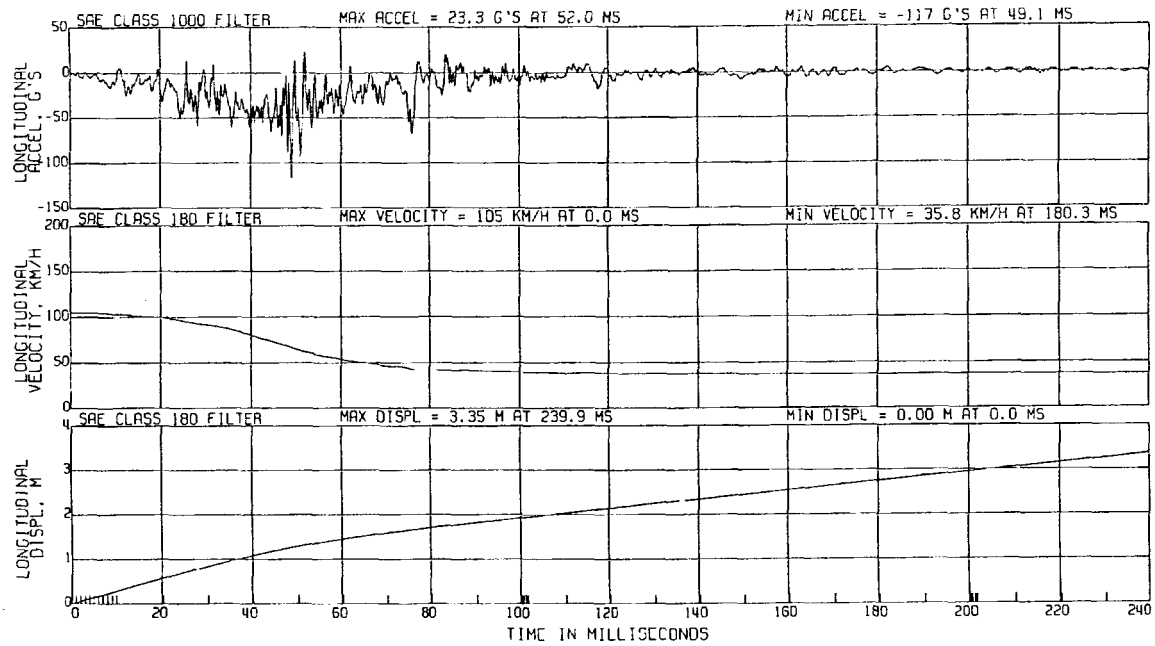

Plot A13. Crash Test C12820. Plots of acceleration, velocity, and displacement in the direction of the longitudinal-axis calculated from the accelerometer at Center of Mass on the AMDB.

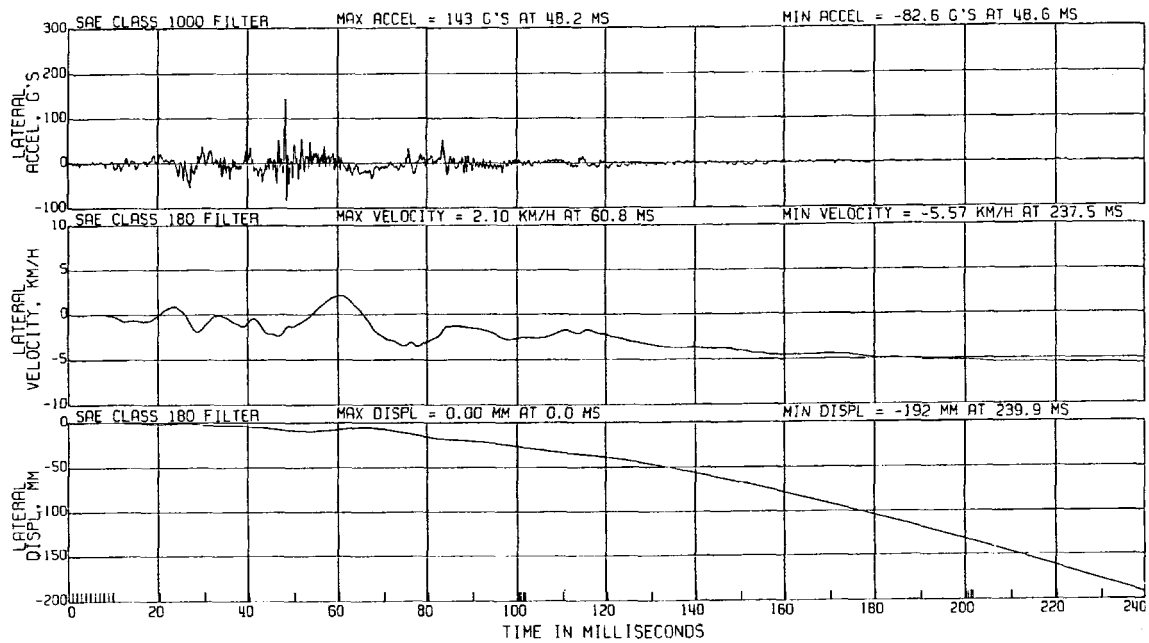

Plot A14. Crash Test C12820. Plots of acceleration, velocity, and displacement in the direction of the lateral-axis calculated from the accelerometer at Center of Mass on the AMDB.

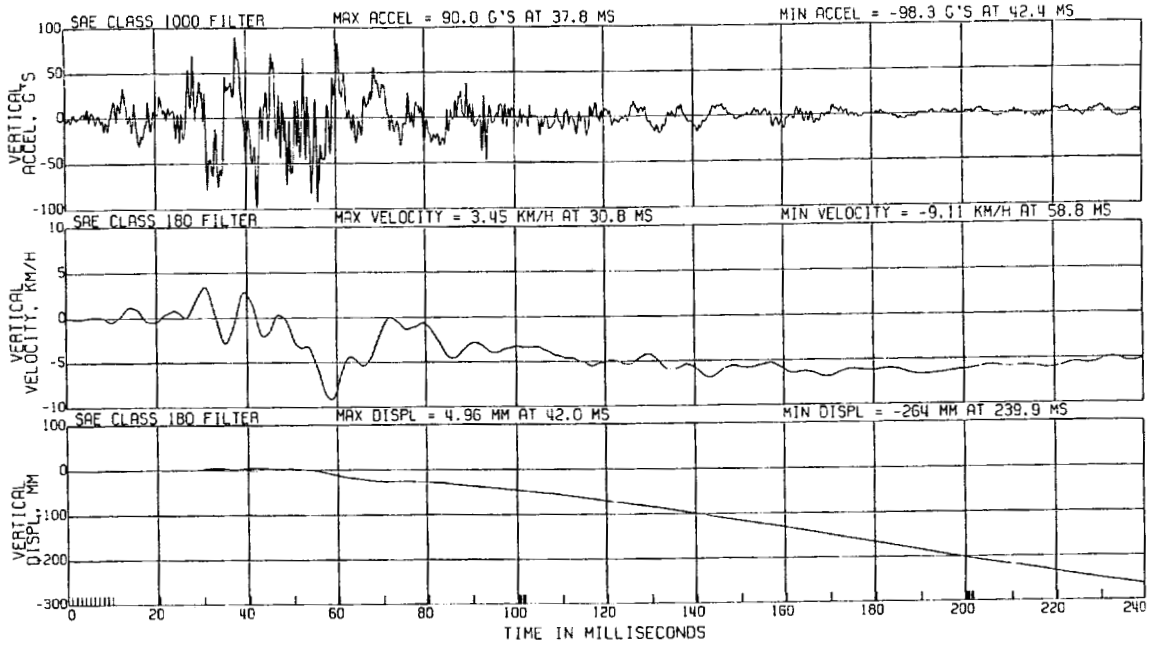

Plot A15. Crash Test C12820. Plots of acceleration, velocity, and displacement in the direction of the vertical-axis calculated from the accelerometer at Center of Mass on the AMDB.

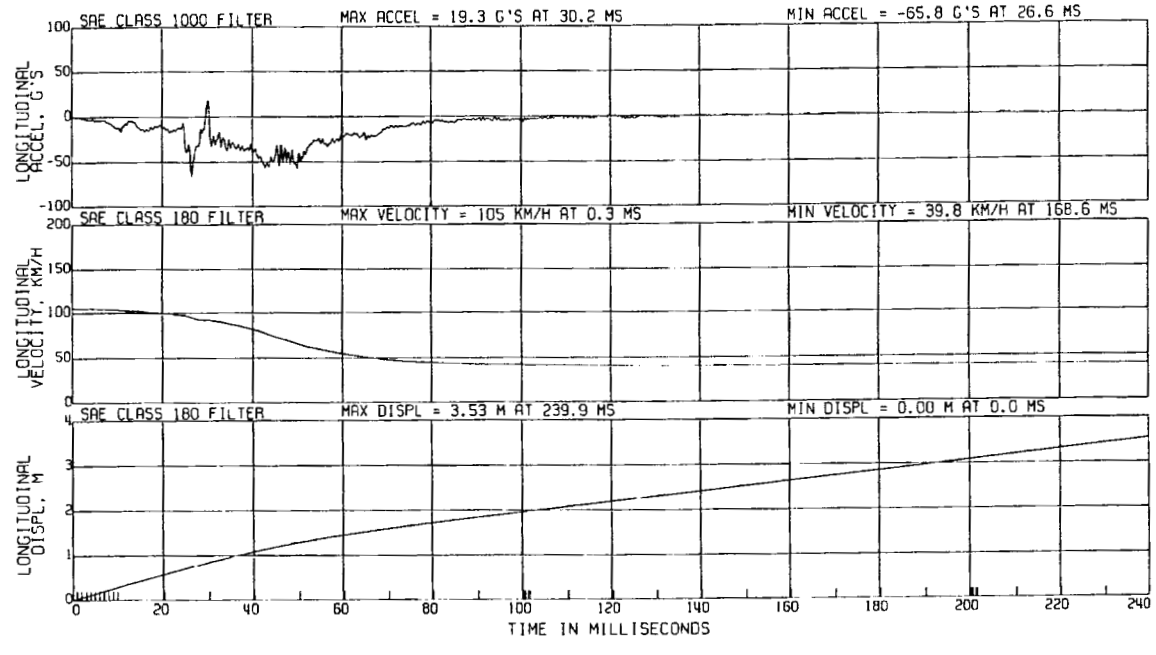

Plot A16. Crash Test C12820. Plots of acceleration, velocity, and displacement in the direction of the longitudinal-axis calculated from the accelerometer on the rear cross member on the AMDB.

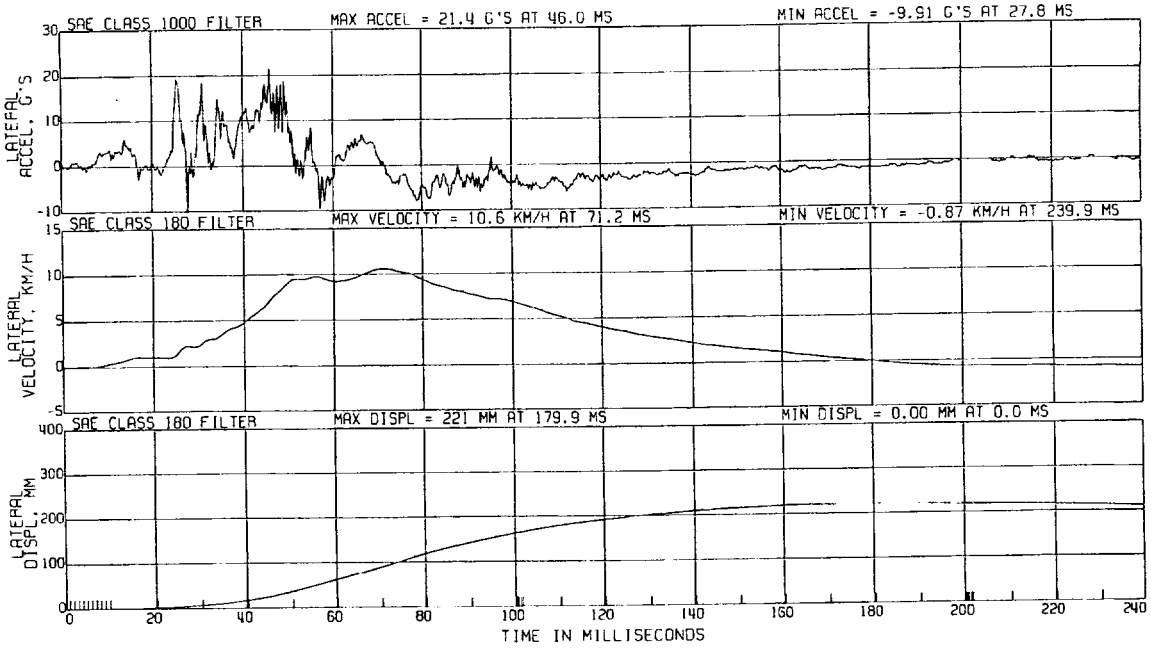

Plot A17. Crash Test C12820. Plots of acceleration, velocity, and displacement in the direction of the lateral-axis calculated from the accelerometer on the rear cross member on the AMDB.

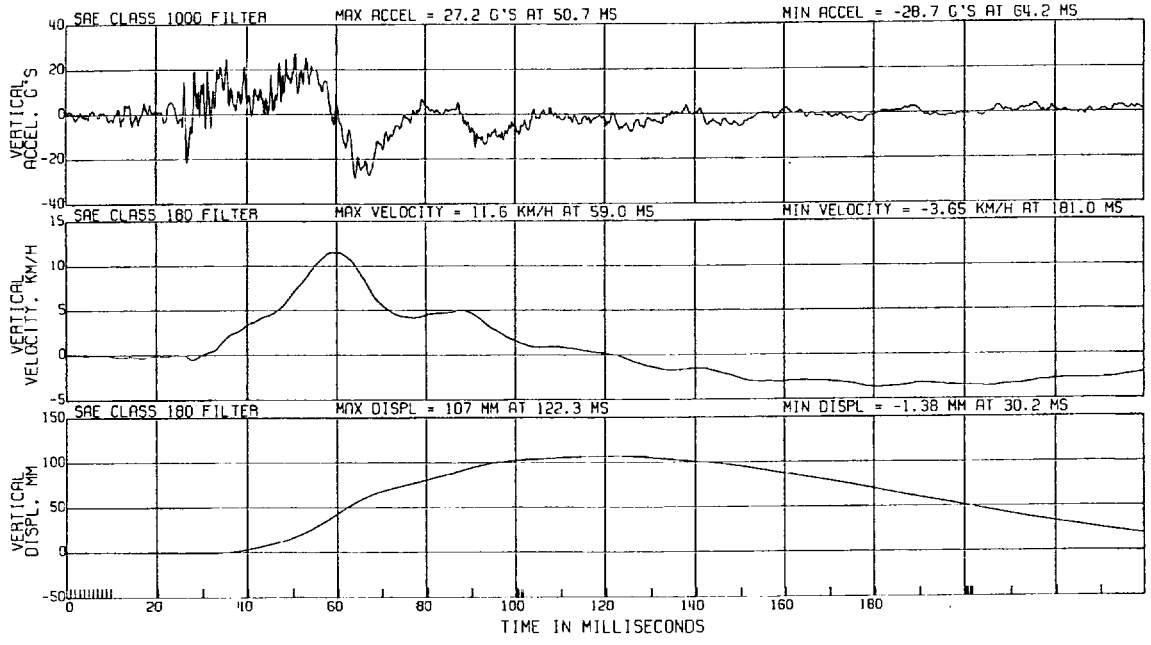

Plot A18. Crash Test C12820. Plots of acceleration, velocity, and displacement in the direction of the Vertical-axis calculated from the accelerometer on the rear cross member on the AMDB.

Appendix B

Crash Test C12820 – Flammable Vapor Sensor Data

Five flammable gas sensors (TGS 813, FIGARO USA, Inc, Wilmette, IL) were installed in the engine compartments of the test vehicle in the following locations:

- Location 1: Above the left exhaust manifold at rear
- Location 2: Above the left exhaust manifold at front
- Location 3: Above the left fuel rail
- Location 4: Above the right fuel rail
- Location 5: Above the right exhaust manifold

Gas phase concentration – sensor output voltage calibration data was obtained using heptane in the range of 0 to 5% (V/V). Estimates of the flammable gas concentration at each location in the engine compartment of both test vehicles using this calibration data are shown in Plots B1 through B10.

The tin oxide semiconductor elements in these sensors also respond to changes in temperature. Exposure to heated vapor or aerosol of a non-flammable fluid, such as electrolyte from the battery (20% sulfuric acid in water) expelled from a battery being crushed during the crash test, will cause the sensor output voltage to increase as if it was exposed to a flammable gas. Interpretation of the flammable sensor data therefore must include a consideration of the results of the gas chromatography/mass spectrometry analysis of gas samples acquired from these locations during the crash test shown in APPENDIX C.

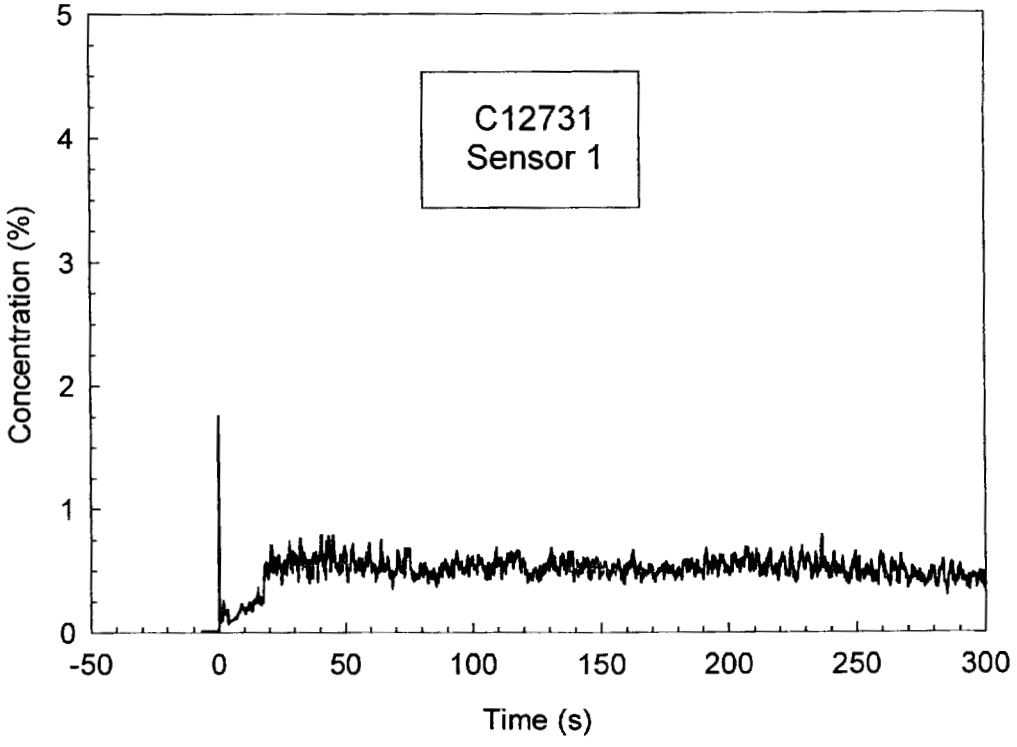

Plot B1. Crash Test C12820. Plot of flammable vapor concentration recorded by the flammable gas sensor at Location 1.

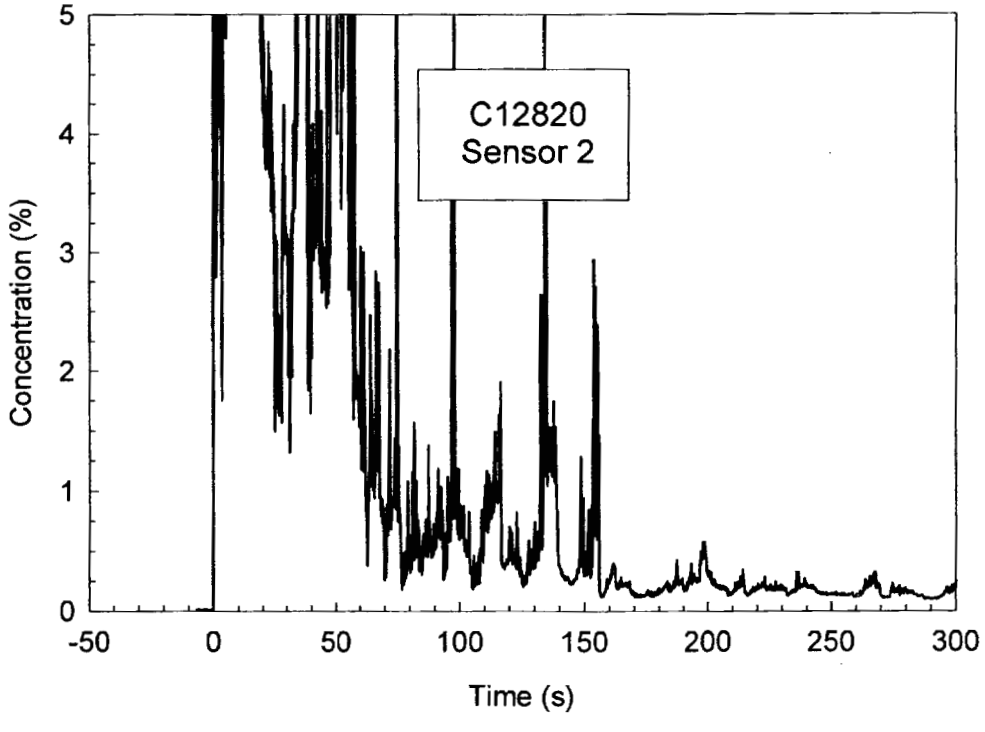

Plot B2. Crash Test C12820. Plot of flammable vapor concentration recorded by the flammable gas sensor at Location 2.

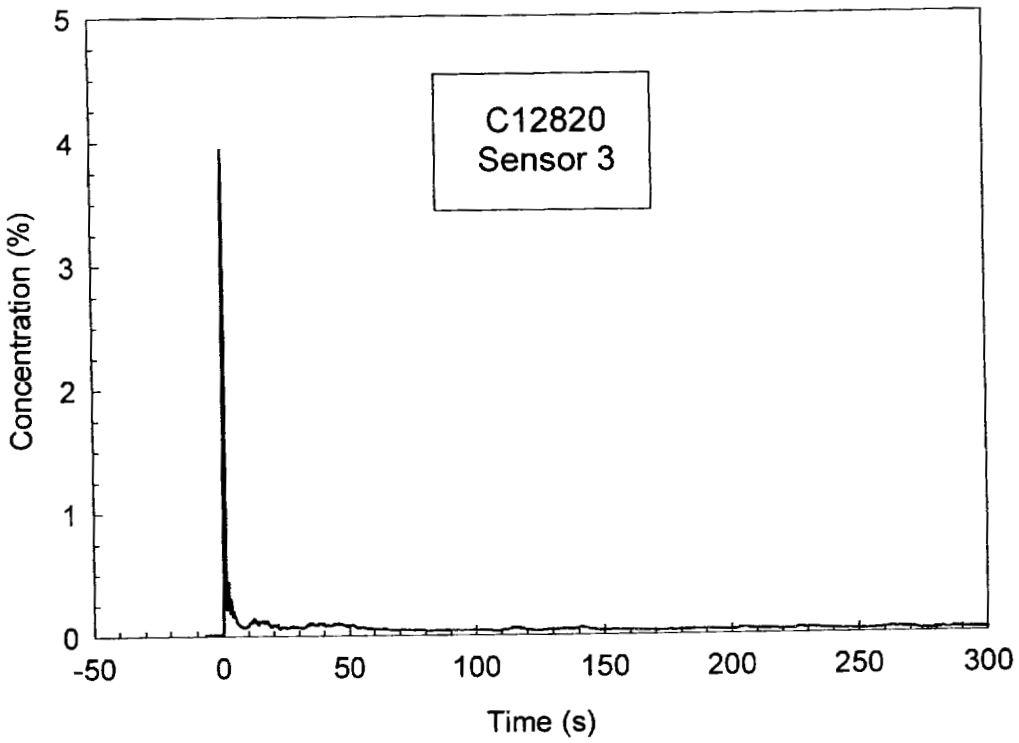

Plot B3. Crash Test C12820. Plot of flammable vapor concentration recorded by the flammable gas sensor at Location 3.

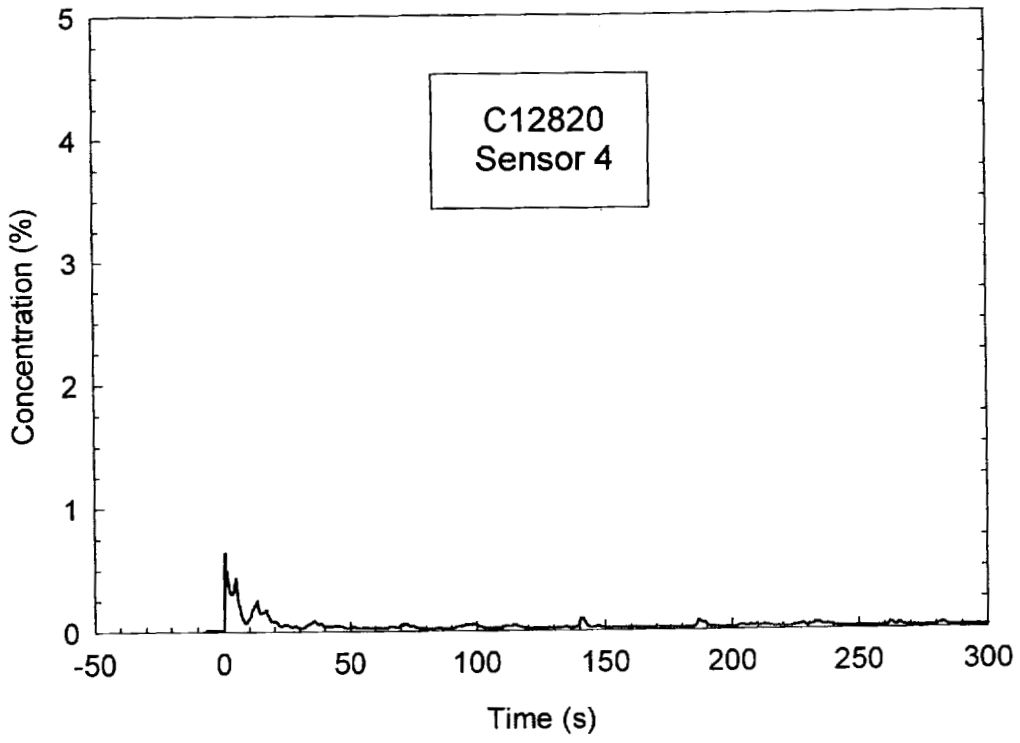

Plot B4. Crash Test C12820. Plot of flammable vapor concentration recorded by the flammable gas sensor at Location 4.

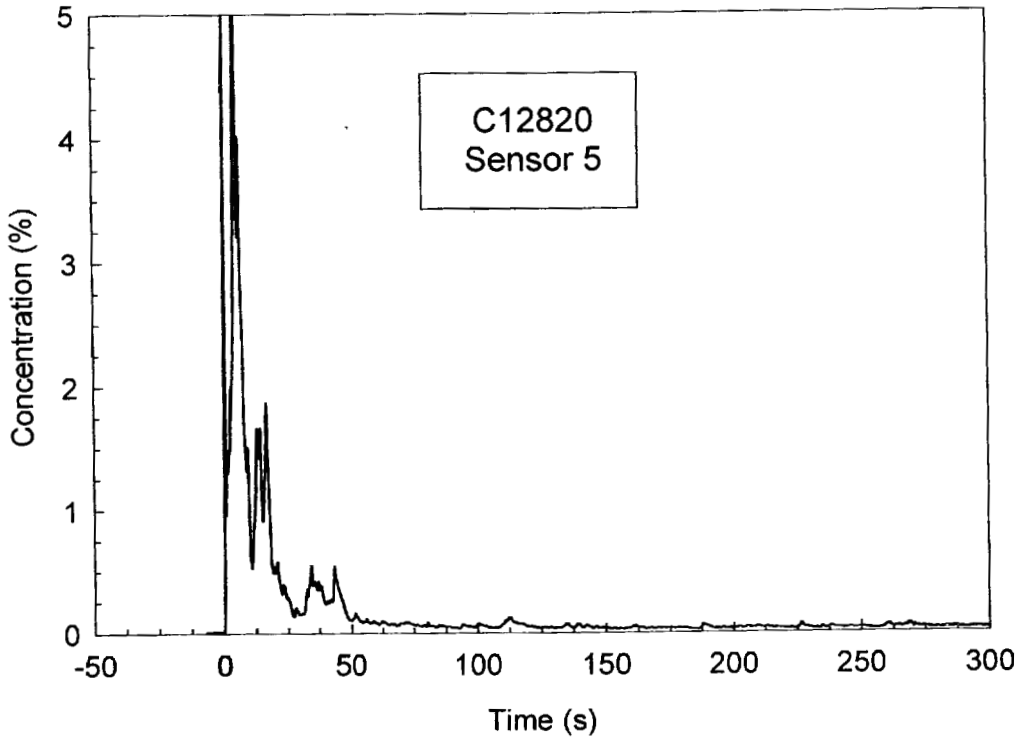

Plot B5. Crash Test C12820. Plot of flammable vapor concentration recorded by the flammable gas sensor at Location 5.

Appendix C

Crash Test C12820
Gas Chromatography / Mass Spectroscopy Analysis of
Engine Compartment Air Samples

Air was samples from were acquired from five locations in the engine compartments of the test vehicles during these crash tests. Sample cartridges packed with an absorbent media were connected to a pumping manifold located in the rear compartments of the test vehicles. A sample cartridge consisted of a glass-lined stainless steel tube (i.d. = 4 mm; length = 10 cm; Scientific Instrument Services, Inc, Ringoes, NJ) packed with 25 mg of Carbotrap™ C Graphitized Carbon Black (Supelco, Inc.; Bellefonte, PA) in series with 15 mg of Carbotrap™ Graphitized Carbon Black (Supelco). The inlet of each sample cartridge was connected to a stainless-steel tube (o.d. = 0.125 in. (3.18 mm), i.d. = 0.085 in. (2.16 mm)), which ran from the rear compartment into the engine compartment. The inlets of the sample tubes were located one of the flammable sensors:

- Location 1: Above the left exhaust manifold at rear
- Location 2: Above the left exhaust manifold at front
- Location 3: Above the left fuel rail
- Location 4: Above the right fuel rail
- Location 5: Above the right exhaust manifold

The airflow rate through each cartridge was adjusted to 250 cm^3/min with a rotometers mounted to the pumping manifold. Blank samples were acquired for a 10 minute period during the engine warm-up before the crash test. Samples during the crash test were acquired for a 22 minute period starting approximately 12 minutes before impact and ending approximately 10 minutes after impact.

Organic substances retained by the absorbent media in the sample cartridges were analyzed by thermal desorption/gas chromatography/mass spectrometry after the crash tests. Deuterated standards dissolved in deuterated methanol were added to each sorbent cartridge to monitor sample recovery. A modified purge-and-trap concentrator was used for thermal desorption (Model 600 Purge-and-Trap Concentrator, CDS Analytical, Oxford, PA). The gas chromatograph was a Model 5890 Series II Plus Gas Chromatograph (Hewlet Packard, Palo Alto, CA). The mass spectrometer was a Hewlet Packard Model 5989B Mass Spectrometer (Hewlett Packard). The thermal desorption unit was interfaced directly to the split/splitless injector of the gas chromatograph through a cryo-focusing unit. The injector was operated in the split mode with a split of approximately 10 mL/min. The chromatographic column was a fused silica capillary column coated with 100% methyl silicone (HP-1 ; length = 30 m; i.d. = 0.25 mm; film thickness = 0.25 μm).

The sample was desorbed at 320°C for 10 min, and cryofocused onto the head of the chromatographic column -80°C. The temperature of the analytical column was maintained at 0°C

while the sample was desorbed and cryo-focused. To start the chromatographic analysis, the cryo-focusing unit was heated ballistically to a temperature of 320°C. The column temperature was programmed from 0 to 325°C at a rate of 5°C/min. Mass spectra were obtained by scanning from m/z 40 to 600 at a rate of 1.2 scan/s.

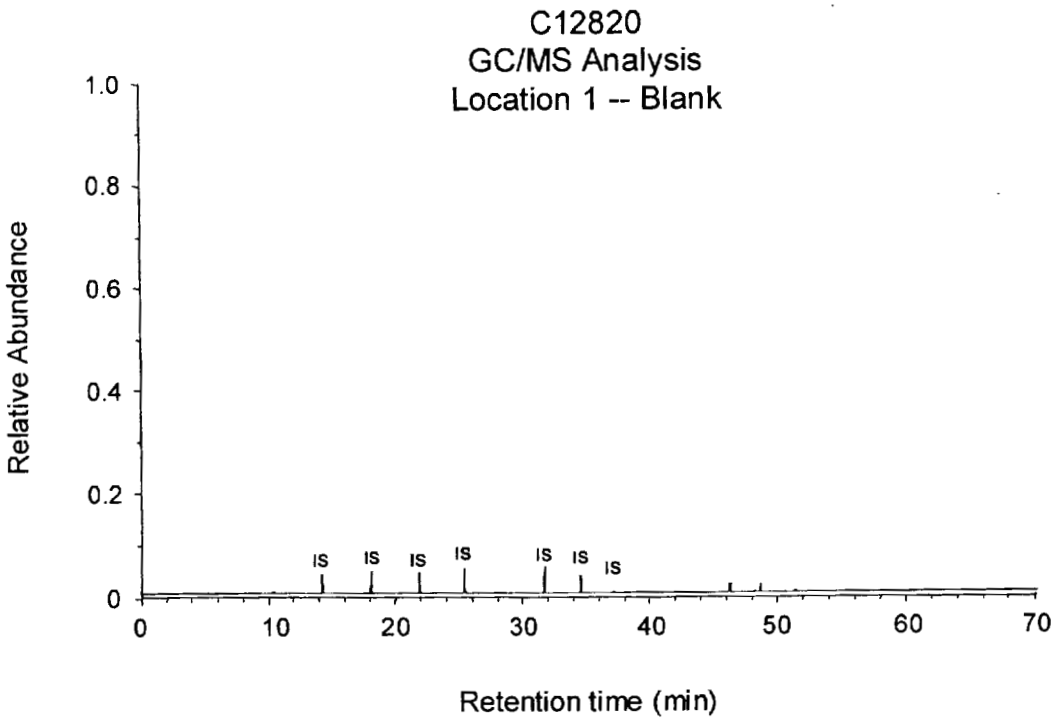

Plot C1. Crash Test C12820. Chromatogram of blank from Location 1 acquired before impact.

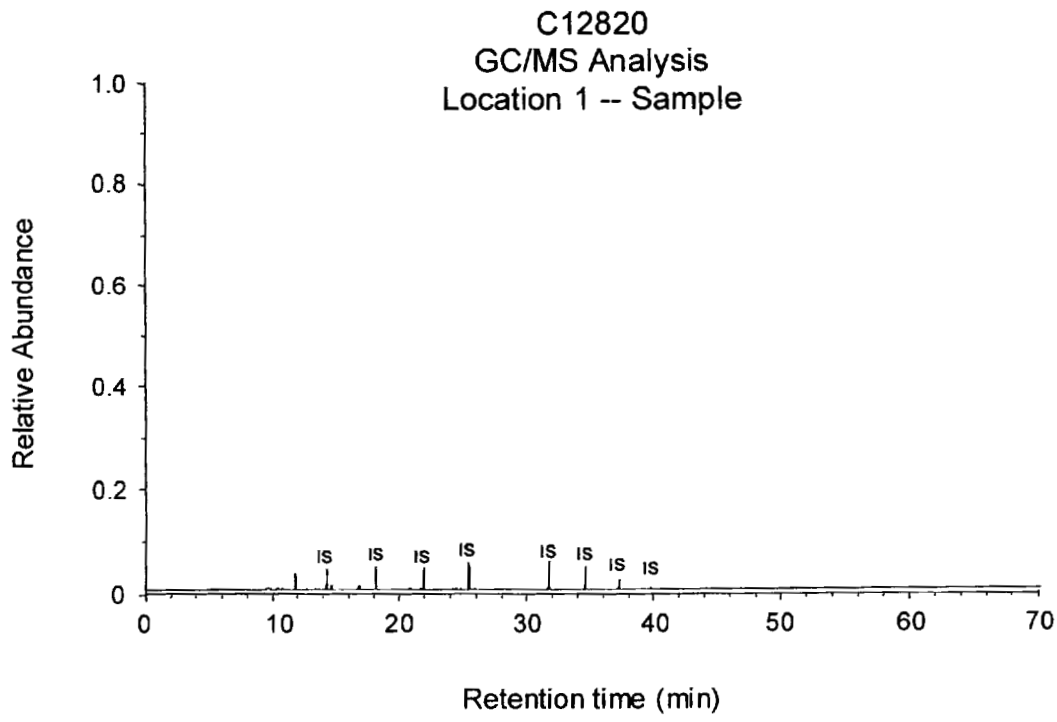

Plot C2 Crash Test C12820. Chromatogram of sample from Location 1 acquired during and after impact.

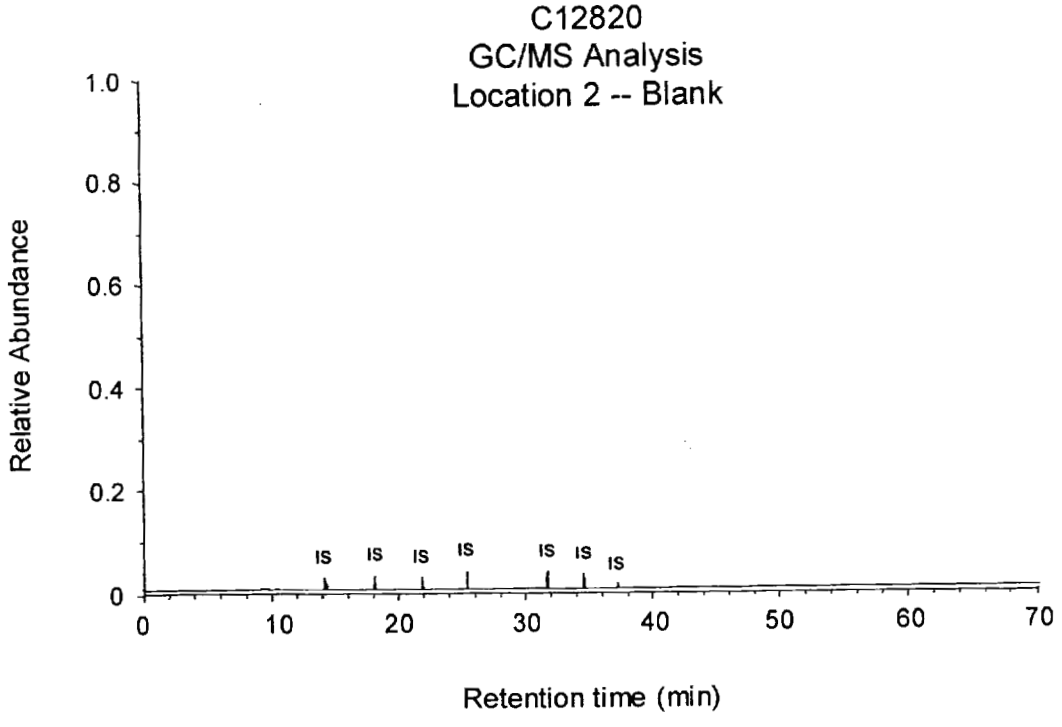

Plot C3. Crash Test C12820. Chromatogram of blank from Location 2 acquired before impact.

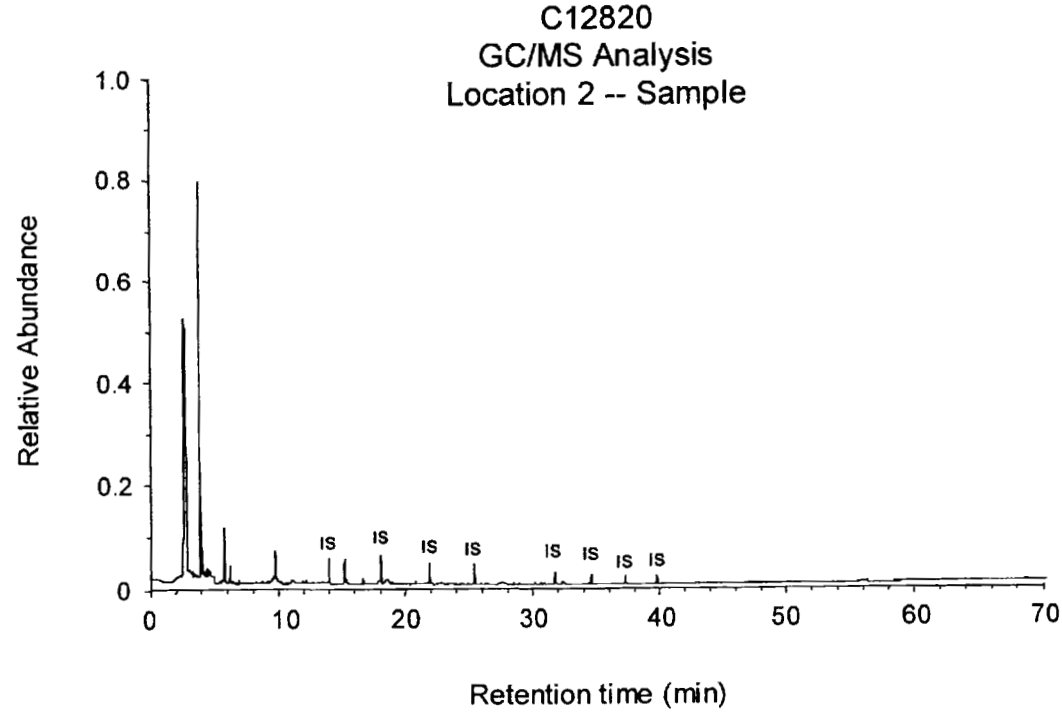

Plot C4. Crash Test C12820. Chromatogram of sample from Location 2 acquired during and after impact.

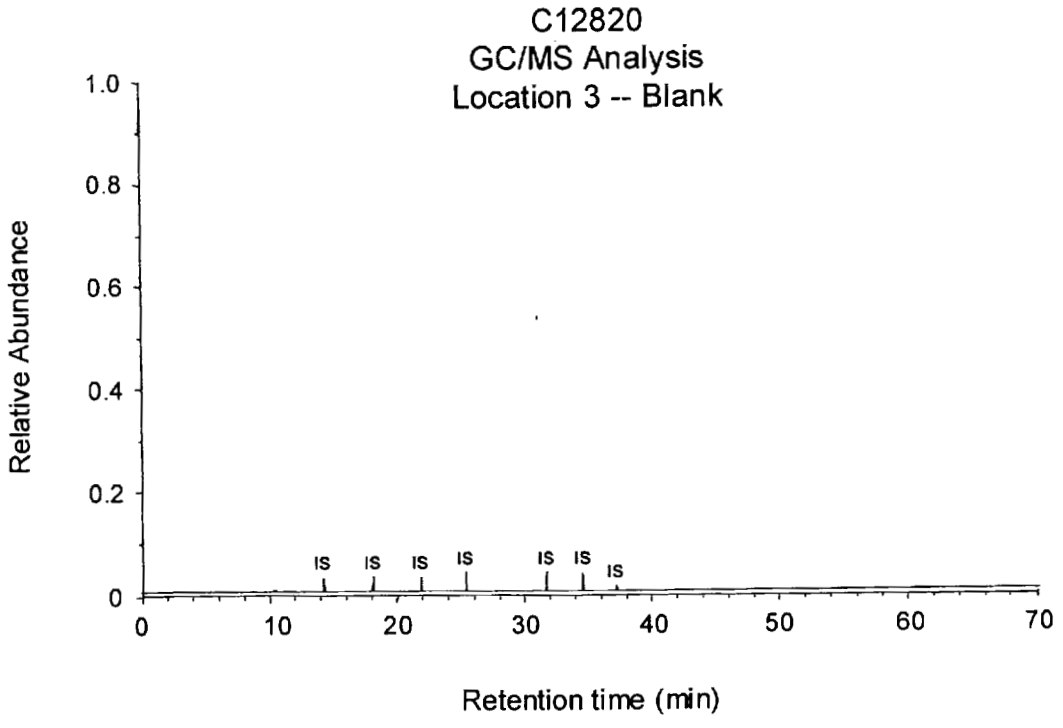

Plot C5. Crash Test C12820. Chromatogram of blank from Location 3 acquired before impact.

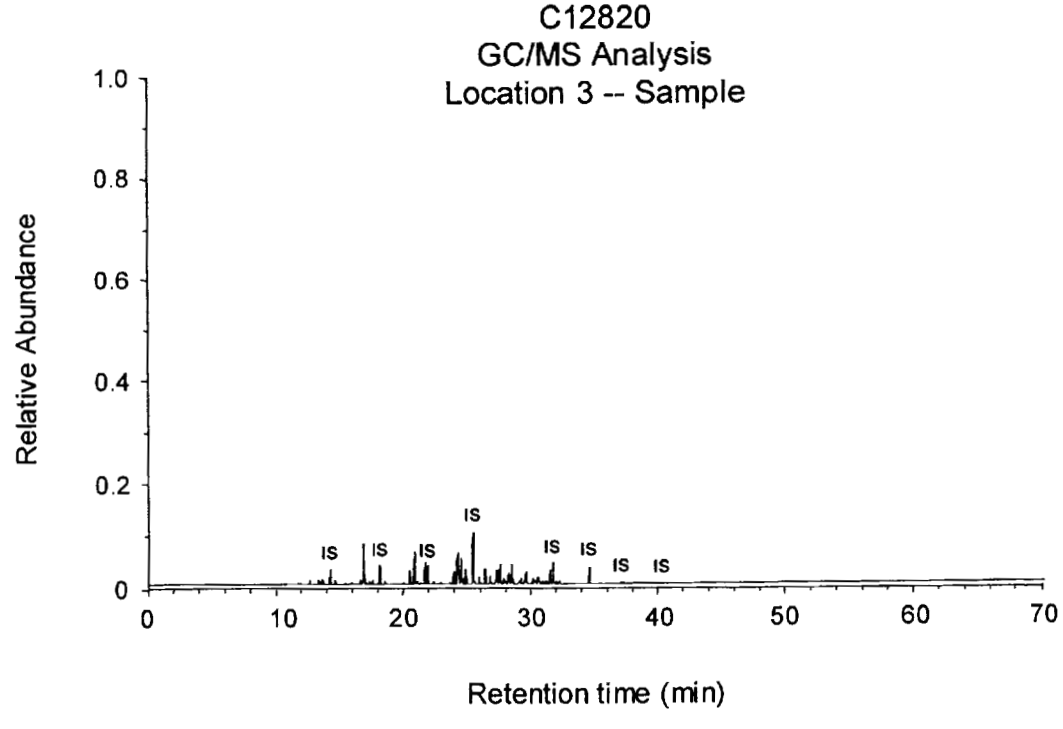

Plot C6. Crash Test C12820. Chromatogram of sample from Location 3 acquired during and after impact.

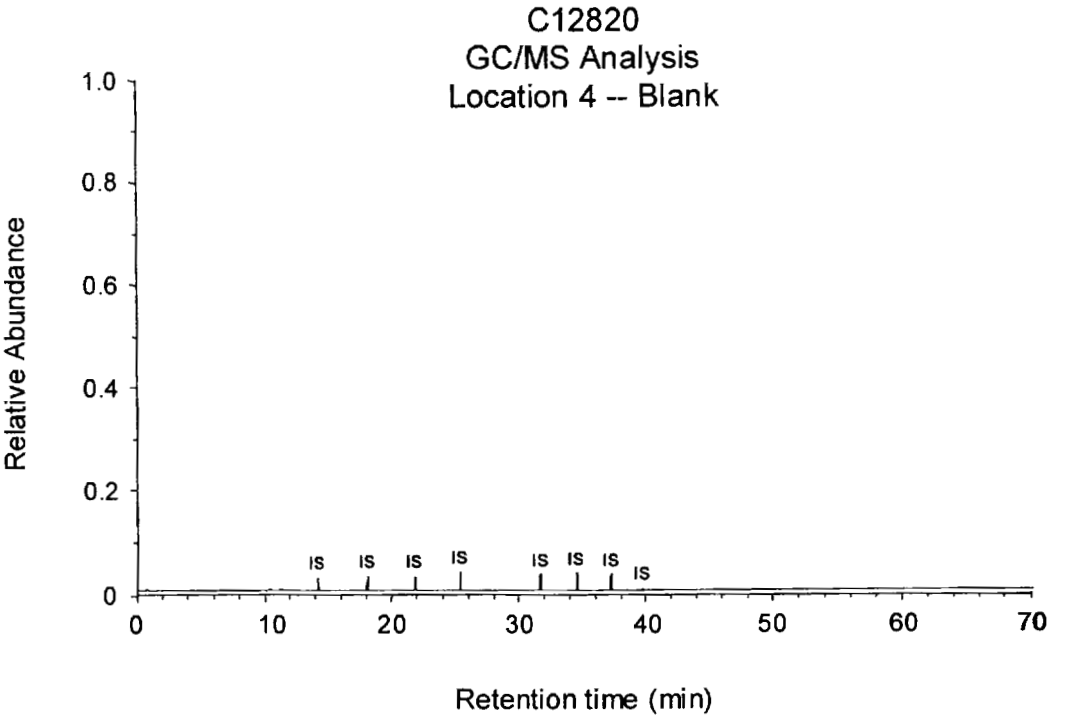

Plot C7. Crash Test C12820. Chromatogram of blank from Location 4 acquired before impact.

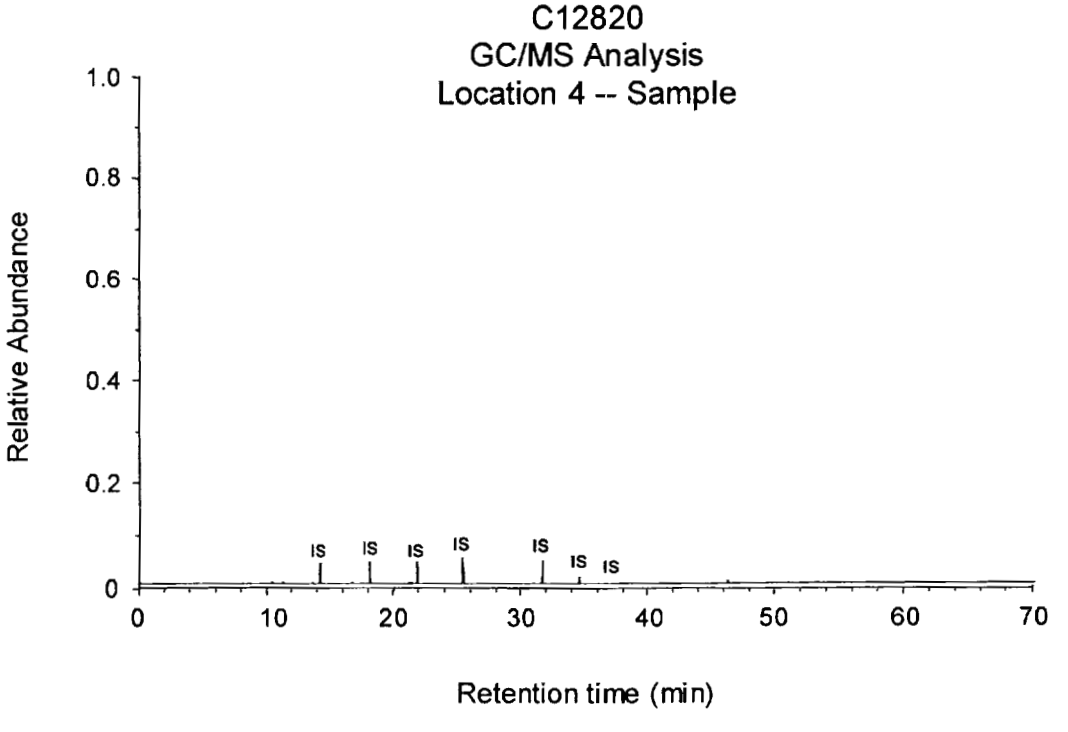

Plot C8. Crash Test C12820. Chromatogram of sample from Location 4 acquired during and after impact.

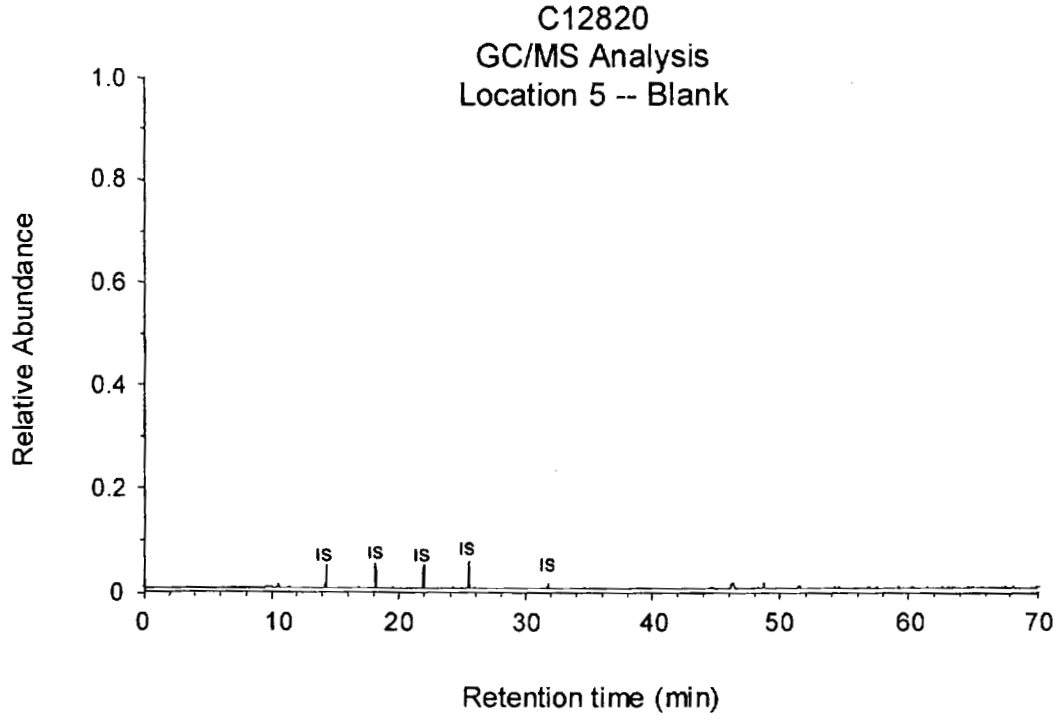

Plot C9. Crash Test C12820. Chromatogram of blank from Location 5 acquired before impact.

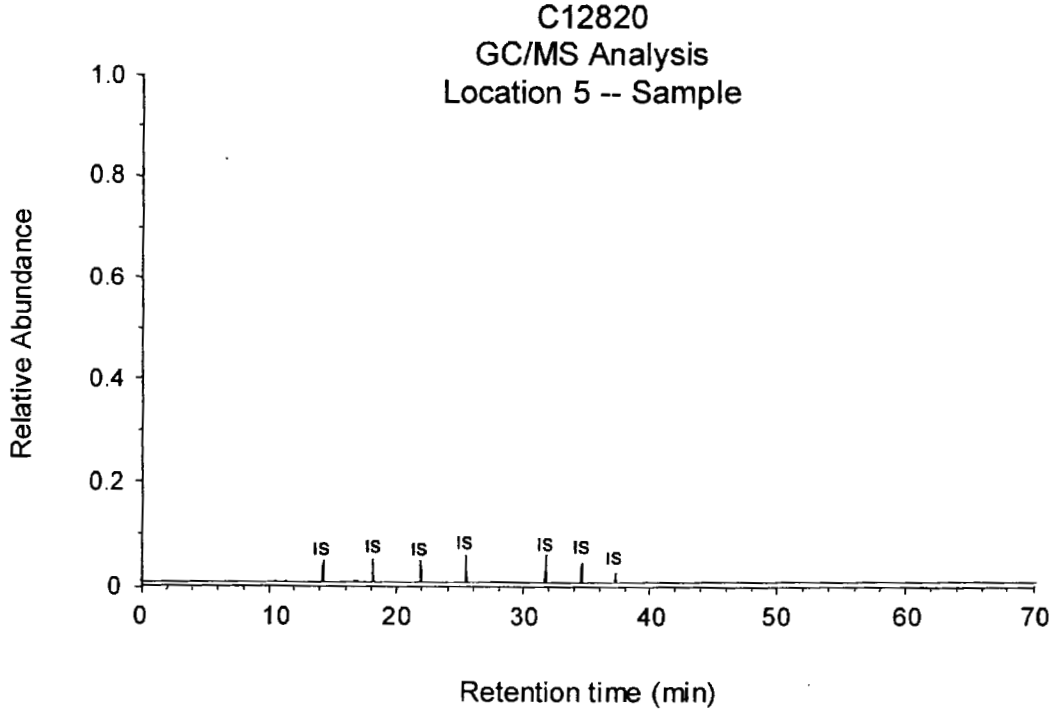

Plot C10. Crash Test C12820. Chromatogram of sample from Location 5 acquired during and after impact.

Appendix D

Crash Test C12820 – Exhaust System Temperature Data

Type-K thermocouples were intrinsically welded to the exhaust system at the following locations:

- Thermocouple 1: Left Exhaust Manifold Runner – Cylinder 3
- Thermocouple 2: Left Exhaust Manifold Collector
- Thermocouple 3: Right Exhaust Manifold Runner – Cylinder 2
- Thermocouple 4: Right Exhaust Manifold Collector
- Thermocouple 5: Left Exhaust Take-Down Pipe

Each thermocouple was connected to a thermocouple amplifier (OMNI-AMP IV, Omega Engineering, Stamford, CT) and calibrated using a thermocouple calibrator (Model CL27, Omega) at 0, 100, 200, 300, 400, 500, 600, 700, 800, 900, and 1000°C. The output signals from the thermocouple amplifiers were recorded by the data acquisition system at the crash test facility.

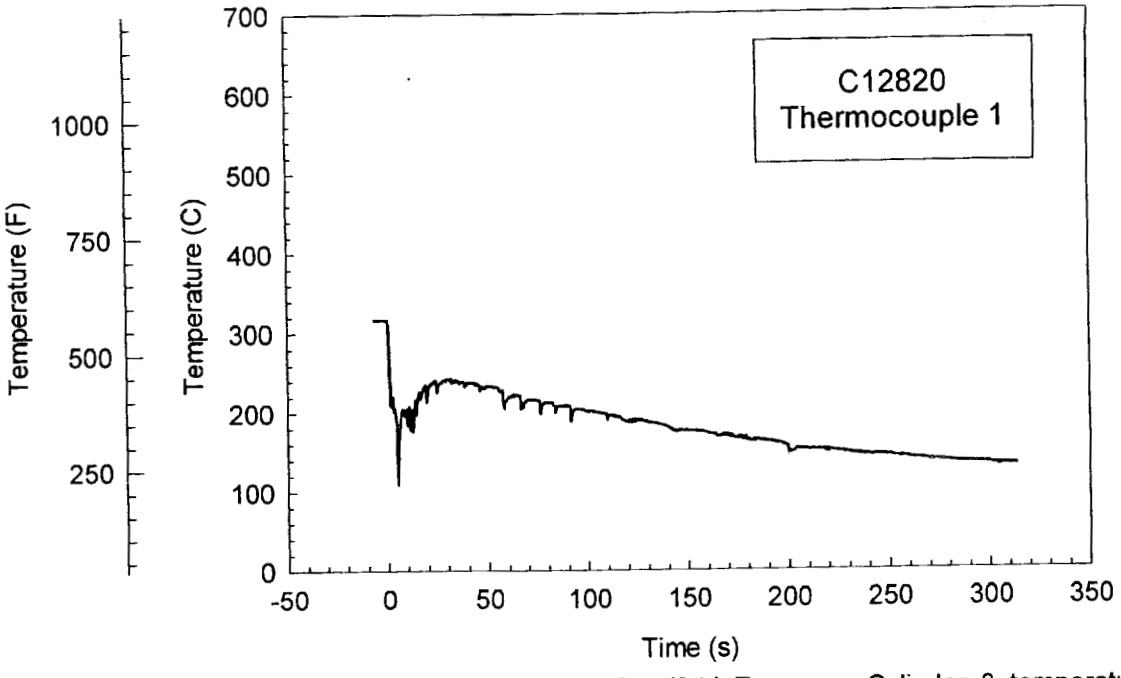

Plot D1. Crash Test C12820. Left Exhaust Manifold Runner – Cylinder 3 temperature recorded from Thermocouple 1.

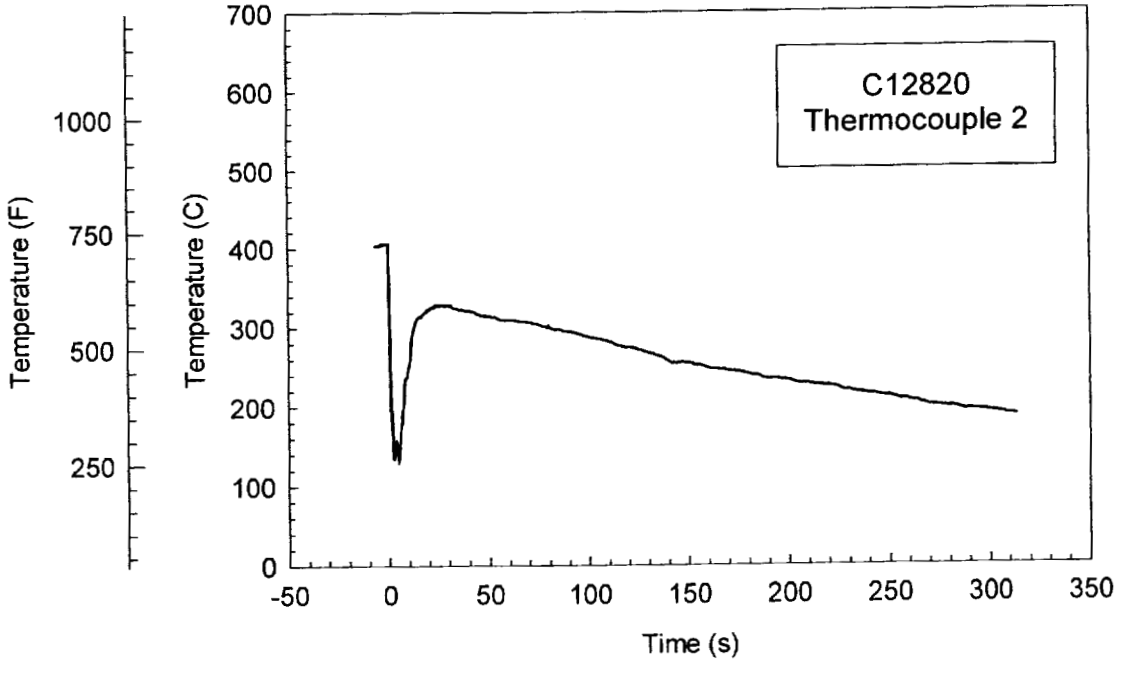

Plot D2. Crash Test C12820. Left Exhaust Manifold Collector temperature recorded from Thermocouple 2.

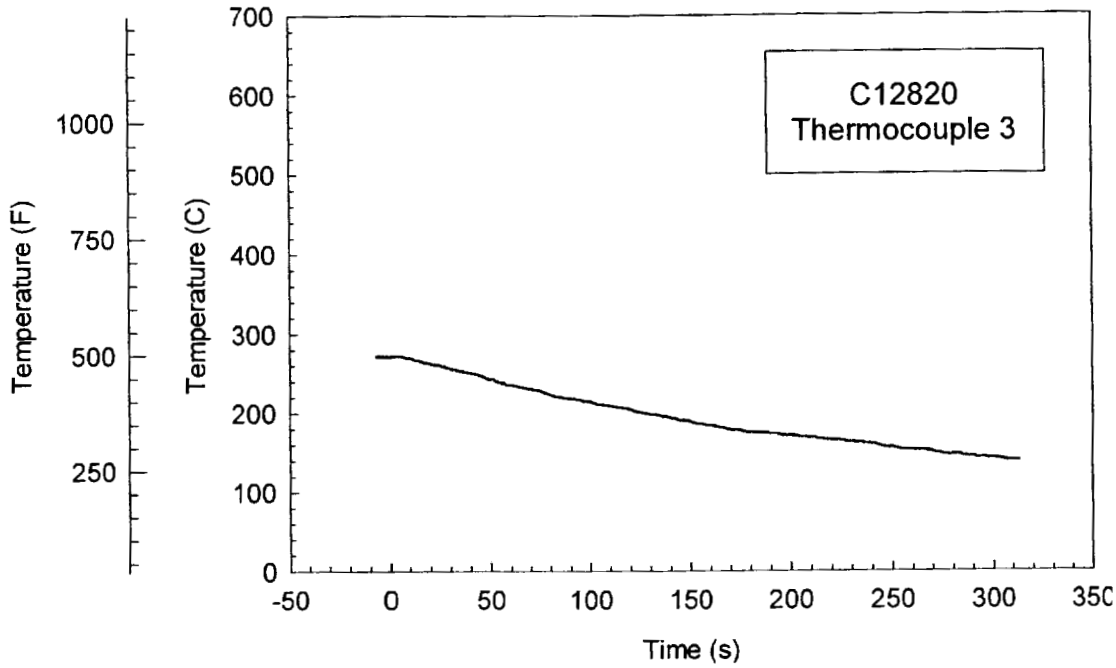

Plot D3. Crash Test C12820. Right Exhaust Manifold Runner – Cylinder 2 temperature recorded from Thermocouple 3.

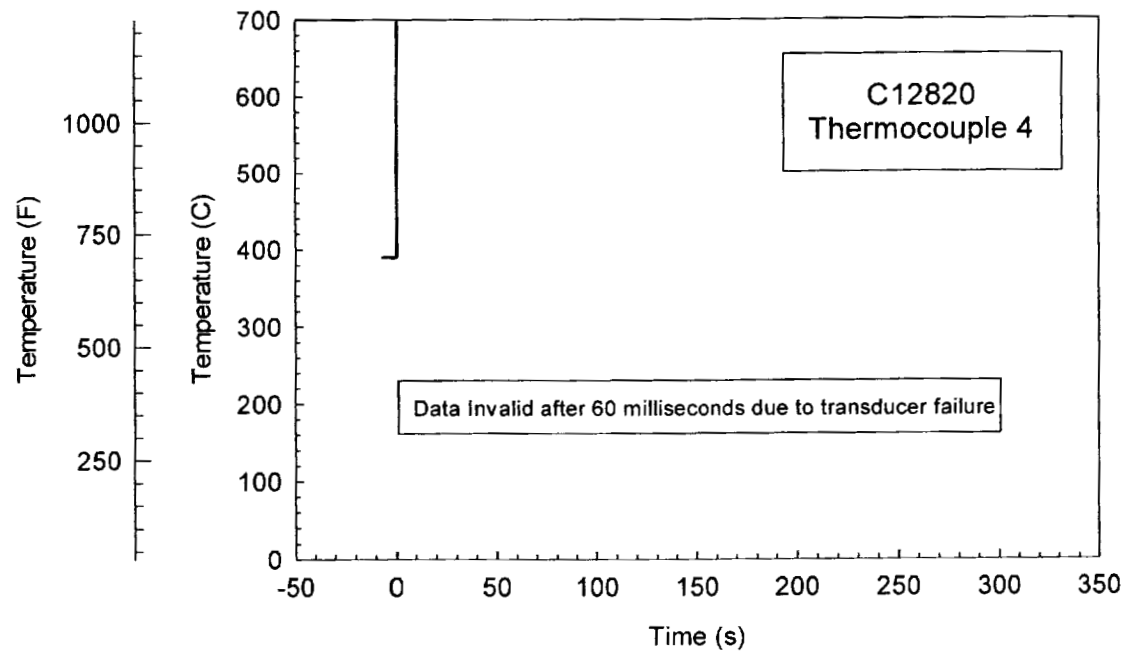

Plot D4. Crash Test C12820. Right Exhaust Manifold Collector temperature recorded from Thermocouple 4.

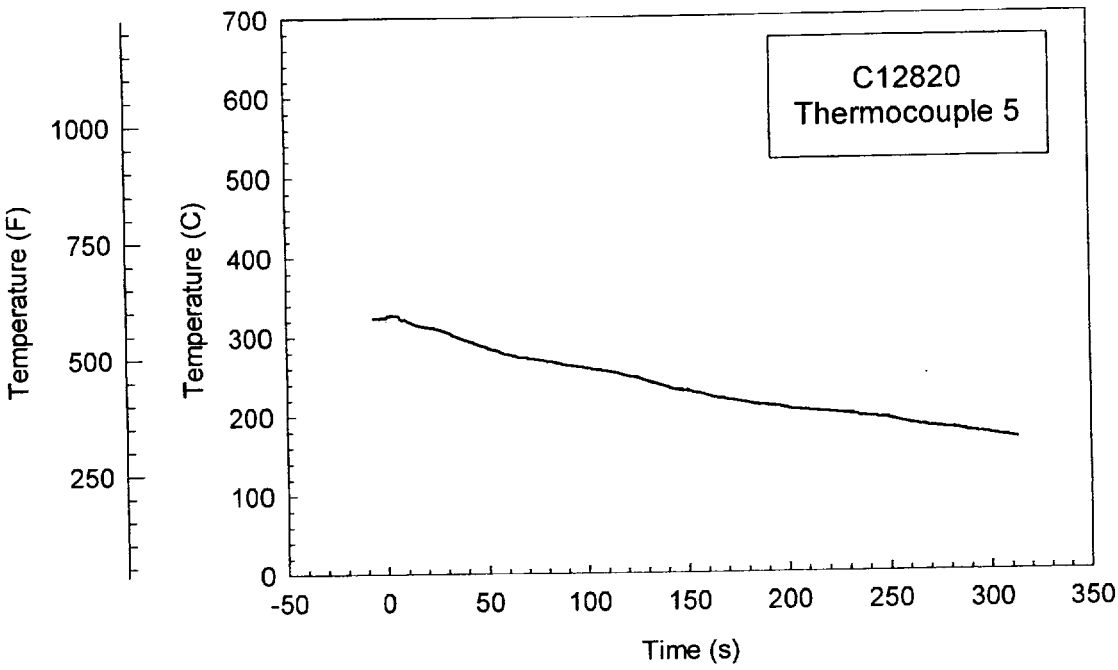

Plot D5. Crash Test C12820. Left Exhaust Take-Down Pipe temperature recorded from Thermocouple 5.

Appendix E

Fire Test F99B1403 – Video Camera Set-Up

Eight video cameras were used in Fire Test F99B1403. Figure E1 shows the approximate locations of the video cameras relative to the test vehicle during this test.

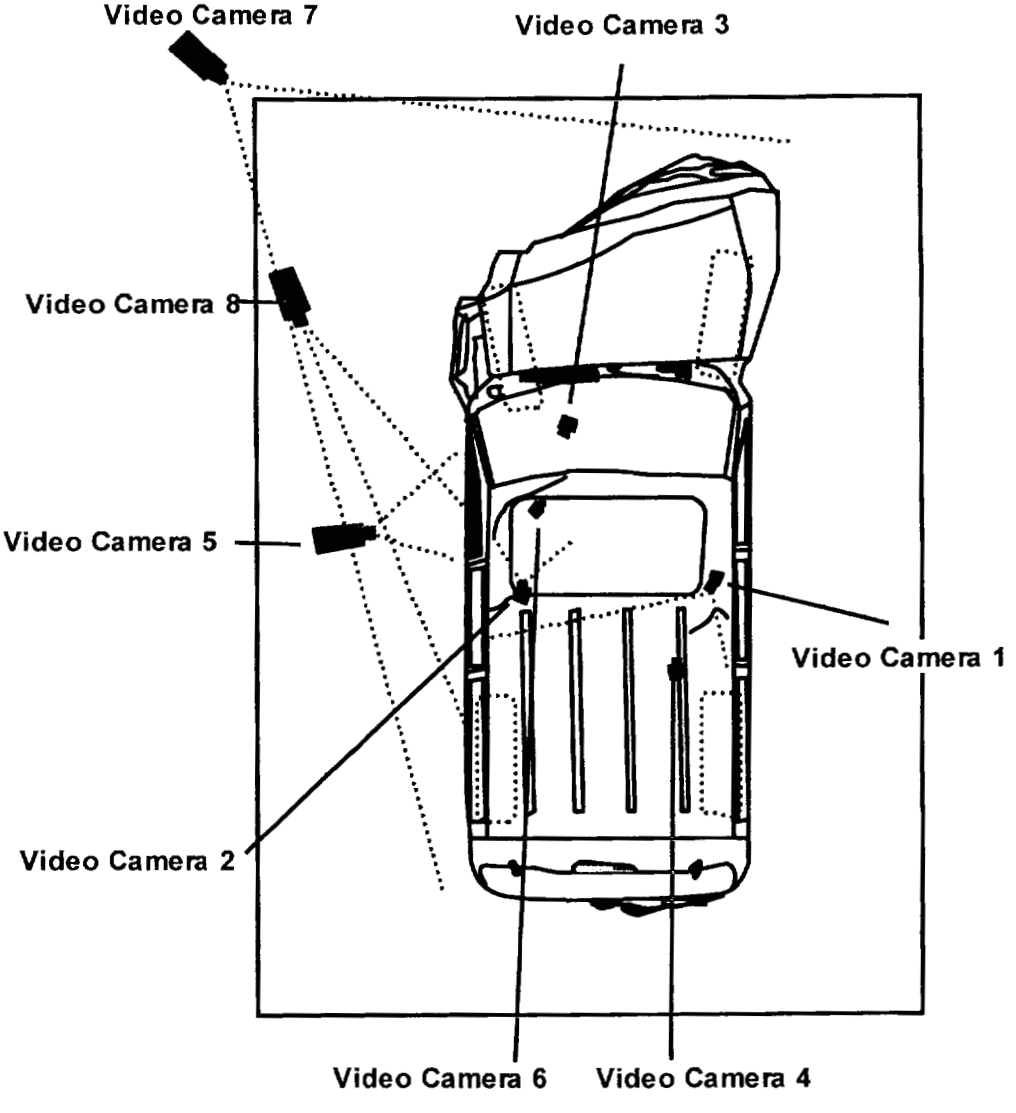

Figure E1. Video camera layouts in Fire Test F99B1403. Distances in this figure are not to scale in this diagram. All height measurements are referenced to the surface of the fluid containment pan.

Camera 1 was a CCD camera mounted on the floor under the rear of the right front seat, inside the passenger compartment. It had a field-of-view that included the rear seat area from the head-rest to the floor and from door to door in the test vehicle. Camera 2 was a CCD camera mounted under the left front driver seat cushion. It had a field-of-view that included the area under the left front seat. Camera 3 was a CCD camera mounted on a tripod located under the left side of the engine compartment. It was focused on a section of the floor panel that contained the electrical pass-throughs under the left front seat of the test vehicle. Camera 4 was a CCD camera mounted on a tripod located under the test vehicle. Its field-of-view included the area between the drive shaft and the frame from the rear axle to the transfer case. Camera 5 was a Hi-8 camcorder mounted on a tripod approximately 5ft. 10in. above the test surface of the fluid containment pan, and 1ft. 8in. from the test vehicle. Its field of view included the left side of the passenger compartment. Camera 6 was a CCD camera mounted to the underbody of the test vehicle looking forward. Its field-of-view included the shift lever pass through cover plate. Camera 7 was a Hi-8 camcorder mounted on a tripod approximately 4ft. 1in. above the test surface and approximately 11ft. 6in. from the test vehicle. Its field-of-view included the left side of the test vehicle. Camera 8 was a Hi-8 camcorder mounted on a stand approximately 6.5in. above the test surface and 5ft. from the test vehicle. Its field of view included the test surface under the fuel tank of the test vehicle from the front tire to the rear of the left front door.

All video cameras were started before the test. A microphone on Cameras 5, 7 and 8 recorded an air horn signal, which indicated the start of gasoline flow, ignition, and the end of the test. Since the CCD cameras had no audio capabilities, the main circuit breaker at the transformer supplying power to the video lighting was switched off and on momentarily before the start of this test to obtain a visual time reference on all videos of this test

Quartz-halogen floodlights were used to illuminate the exterior of the vehicle. One 12V halogen light with a magnetic base was located on the floor behind the right front passenger seat to illuminate the area under the rear seat on the right side in the test vehicle. One 12V halogen light with a magnetic base was located on the floor behind the left front driver seat to illuminate the area under the front seat on the left side in the test vehicle. One 12V halogen light with a magnetic base was located on the test surface to illuminate the shift lever pass through cover plate under the test vehicle. One 12V halogen light with a magnetic base was located on the test surface to illuminate the area between the drive shaft and the muffler under the test vehicle. One 12V halogen light with a magnetic base was located on the test surface to illuminate the electrical pass through under the driver seat of the test vehicle.

Camera 5 in was inadvertently plugged into a switched power outlet before the start of this test, which caused it to stop recording when the main circuit breaker at the transformer supplying power to the video lighting was switched off to produce a time reference.

APPENDIX F

Fire Test F99B1403 – Thermocouple Data

The thermocouples used in this test were type-N thermocouples fabricated by Medtherm Corporation (Huntsville, AL). Each thermocouple consisted of an ungrounded thermocouple junction (30 AWG thermocouple wire) enclosed in an Inconel 600 sheath insulated with magnesium oxide (o.d. = 0.040 in. (1 mm), length = 50 ft. (15.2 m)). A transition was made through a stress-relief bushing to a duplex thermocouple extension cable (24 AWG) with fiberglass insulation and a stainless steel over-braid (length = 1 ft. (0.28 m)). Each thermocouple wire terminated in a grounded, compensated Type-N thermocouple plug. The thermocouples were connected to the data acquisition system using Type-N thermocouple extension cables (length = 50 ft. (15.2 m)).

The data acquisition system consisted of a PC (75 MHz Pentium Processor, 16 MB RAM, an 814 MB hard disk, and a 16-bit, Model BG45-AP5CP, ACER Inc., Taiwan R. O. C.) with a 100 kHz I/O board with 16 analog input channels (DaqBoard 200A, IOTech, Inc., Cleveland, OH). Thermocouple multiplex expansion cards (DBK-19, IOTech, Inc., Cleveland, OH) were used for data acquisition from the thermocouples. The expansion cards were mounted in an electronics cabinet and hard-wired to a panel containing compensated Type-N thermocouple jacks.

To reduce electronic noise on the thermocouples, the ground leads from each thermocouple jack were connected to the electronic chassis ground of the thermocouple mutliplex extension cards. The vehicle chassis was connected to the electronic chassis ground by a large-gauge cable. The electronic chassis ground was connected to an isolated earth ground.

The data acquisition software (DASYLab, Daten System Technik GmbH, Mönchengladbach, Germany) was configured to sample each channel at a rate of 10 Hz and store the data in 10-point block averages.

Figures F1 through F6 show the approximate locations of thermocouples in the test vehicle. Plots F1 through F60 show plots of the temperature data recorded from these thermocouples during this test.

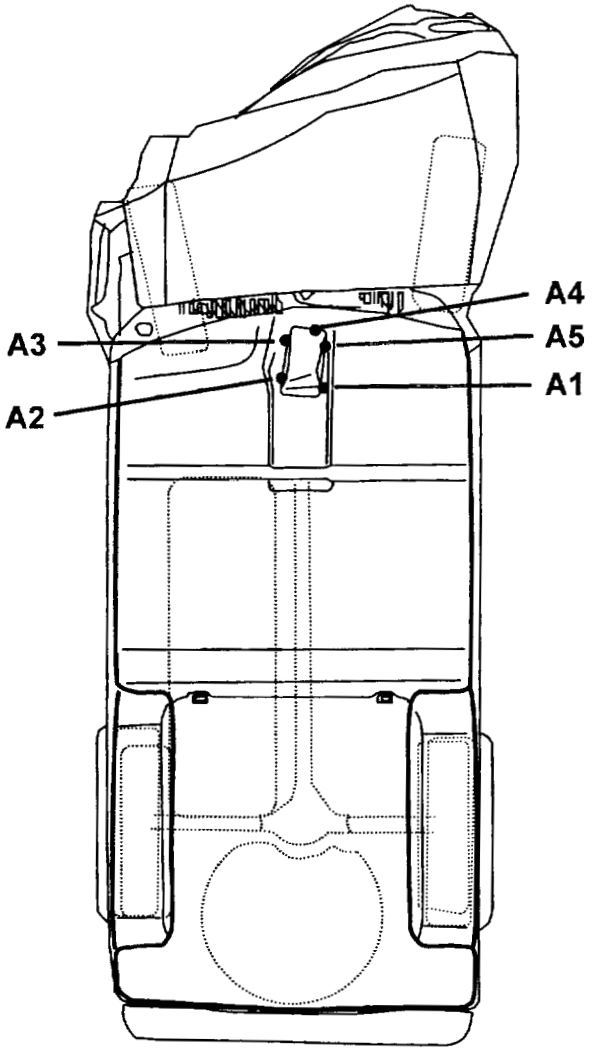

Figure F1. Fire Test F99B1403. Diagram showing the approximate locations of thermocouples on the lower surface of the manual transmission shift lever pass-through cover plate on the Experimental Vehicle. Thermocouples A1, A2, A3, A4, and A5 were located in gaps between the cover plate and floor panel caused by deformation of the cover plate and floor panel in the crash test.

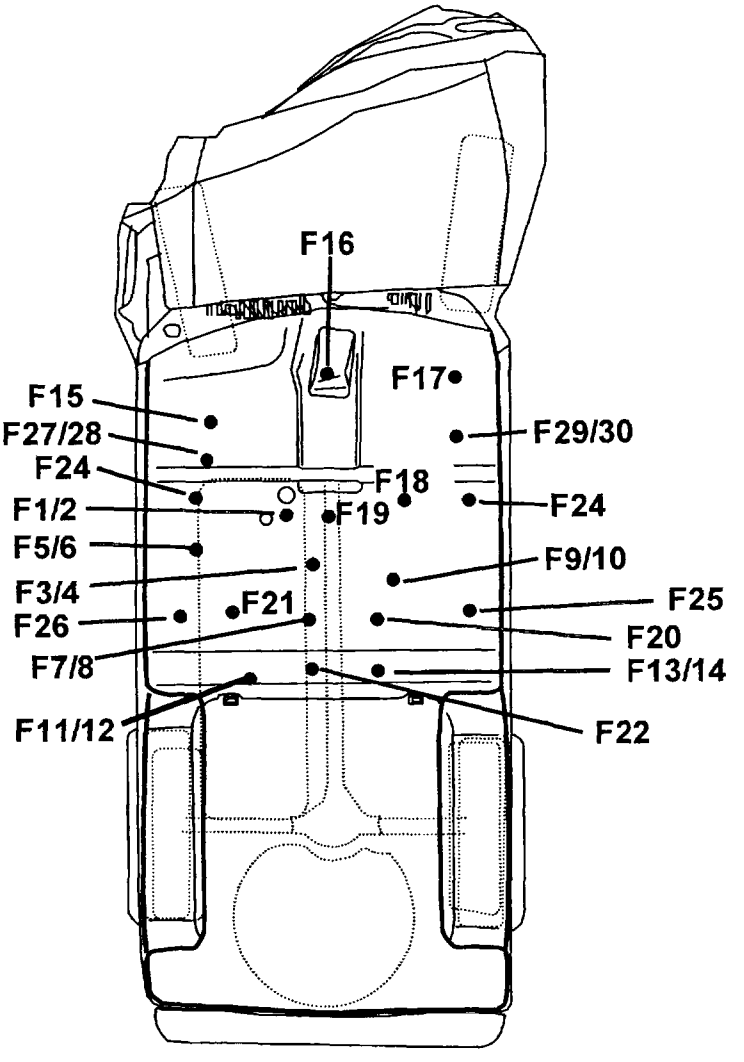

Figure F2. Fire Test F99B1403. Diagram showing the approximate locations of thermocouples on the floor panel in the Experimental Vehicle. Thermocouples F1, F3, F5, F7, F9, F11, F13, F15, F17, F18, F19, F20, F21, F22, F23, F24, F25, F26, F27, and F29 were located approximately 1 cm below the lower surface of the floor panel. Thermocouples F2, F4, F6, F8, F10, F12, F14 and F30 were attached to the upper surface of the floor panel with thermally conducting cement. Thermocouple F16 was attached to the upper surface of the manual transmission shift lever pass-through cover plate with thermally conducting cement.

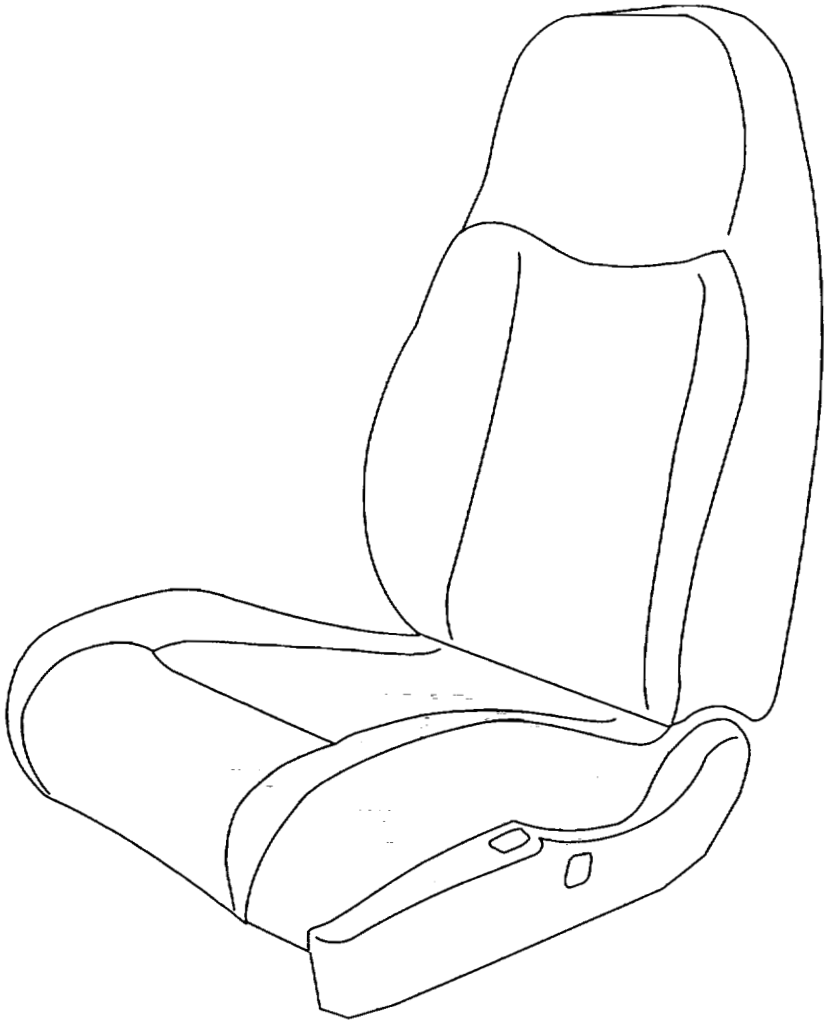

Figure F3. Fire Test F99B1403. Diagram showing the approximate locations of thermocouples below the left front seat in the Experimental Vehicle. Thermocouples FS1, FS2, FS3, and FS4 were located just below the lower surface of the foam pad in the left front seat cushion.

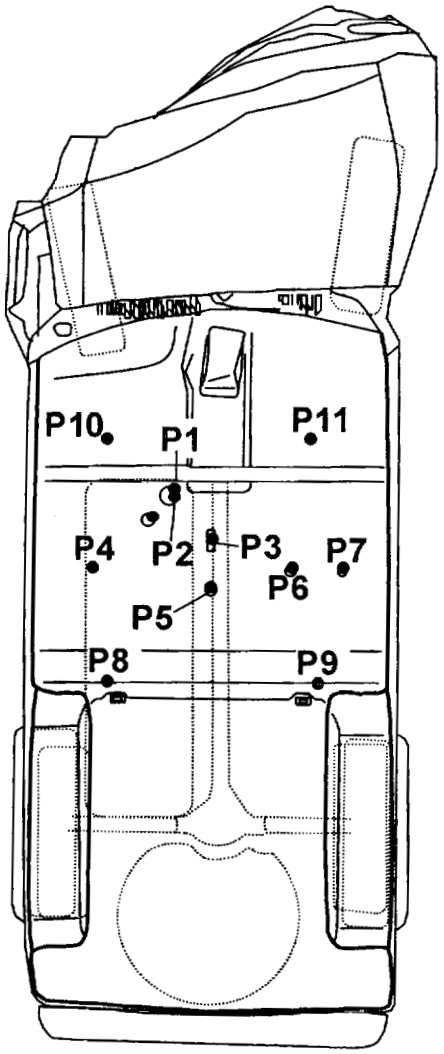

Figure F4. Fire Test F99B1403. Diagram showing the approximate locations of thermocouples above the floor pan drain hole plugs in the Experimental Vehicle. Thermocouple P1 was located in an electrical pass-through opening in the floor panel were the grommet had been dislodged in the crash test. Thermocouple P2 was located on the upper surface of a grommet in an electrical pass-through closure in the floor panel. ThermocouplesP3, P4, P5, P6, P7, P8, P9, and P10 were located on the upper surfaces of closures for drain holes in the floor panel.

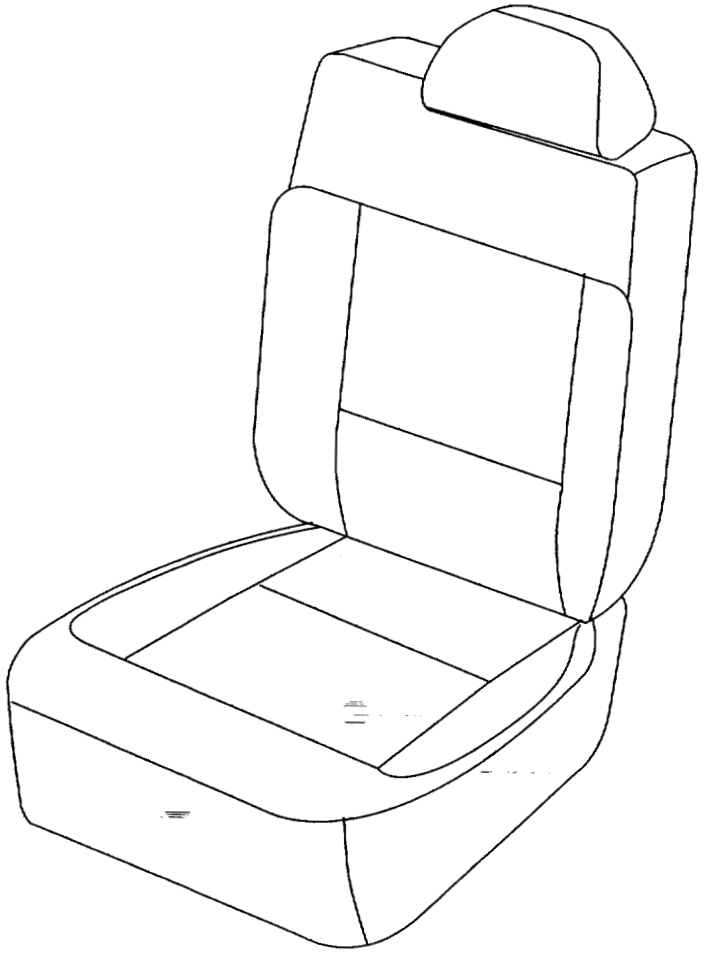

Figure F5. Fire Test F99B1403. Diagram showing the approximate locations of thermocouples under the right rear seat in the Experimental Vehicle. Thermocouples RS1, RS2, RS3, and RS4 were located just below the loser surface of the foam pad in the right rear seat cushion.

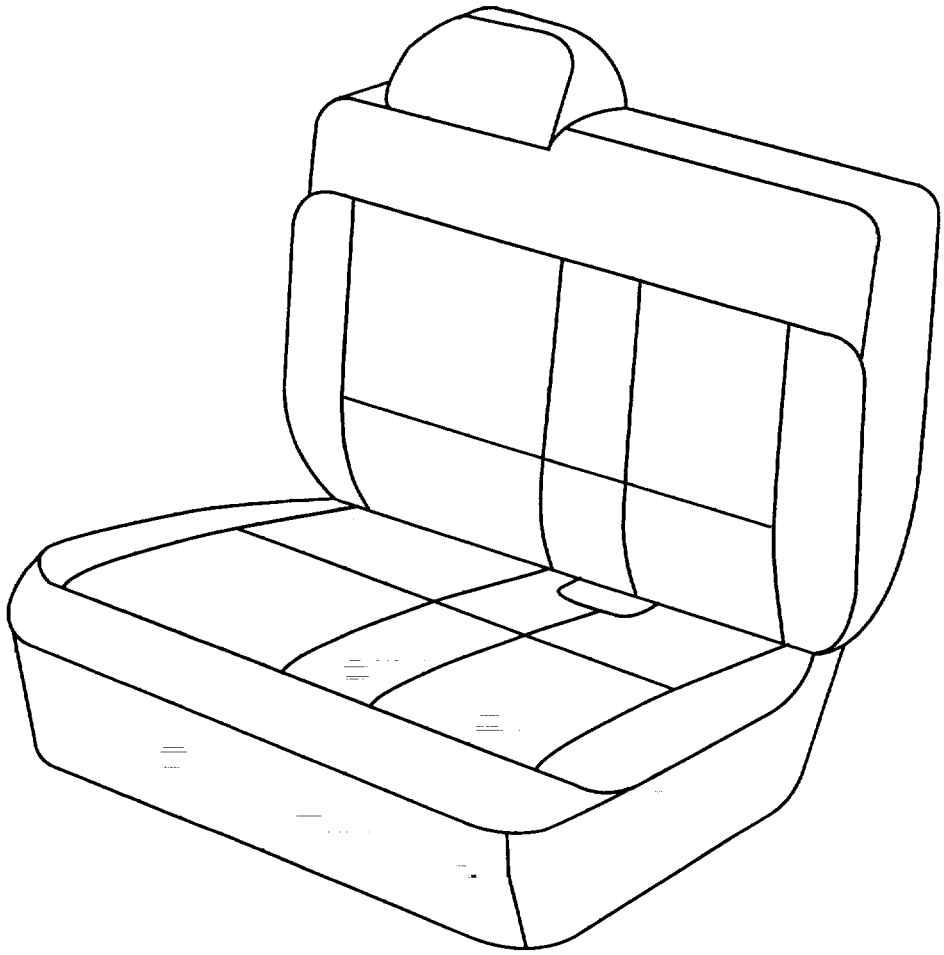

Figure F6. Fire Test F99B1403. Diagram showing the approximate locations of thermocouples under the left rear seat in the Experimental Vehicle. Thermocouples RS5, RS6, RS7, RS8, RS9, and RS10 were located just below the foam pad in the left rear seat cushion.

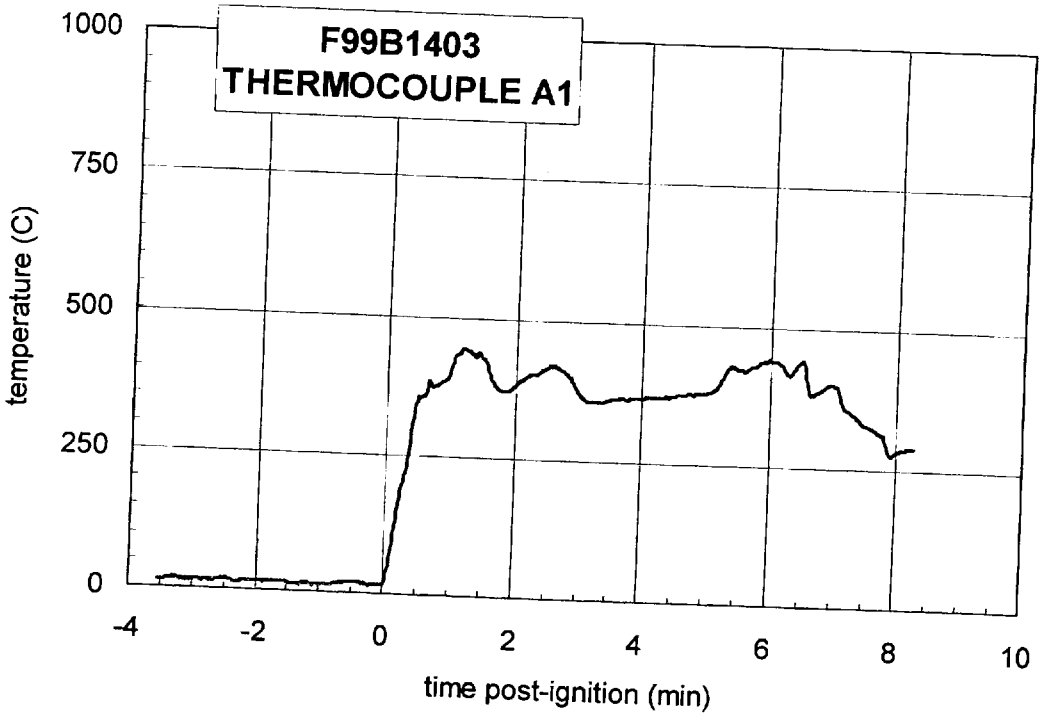

Plot F1. Fire Test F99B1403. Data plot from thermocouple A1.

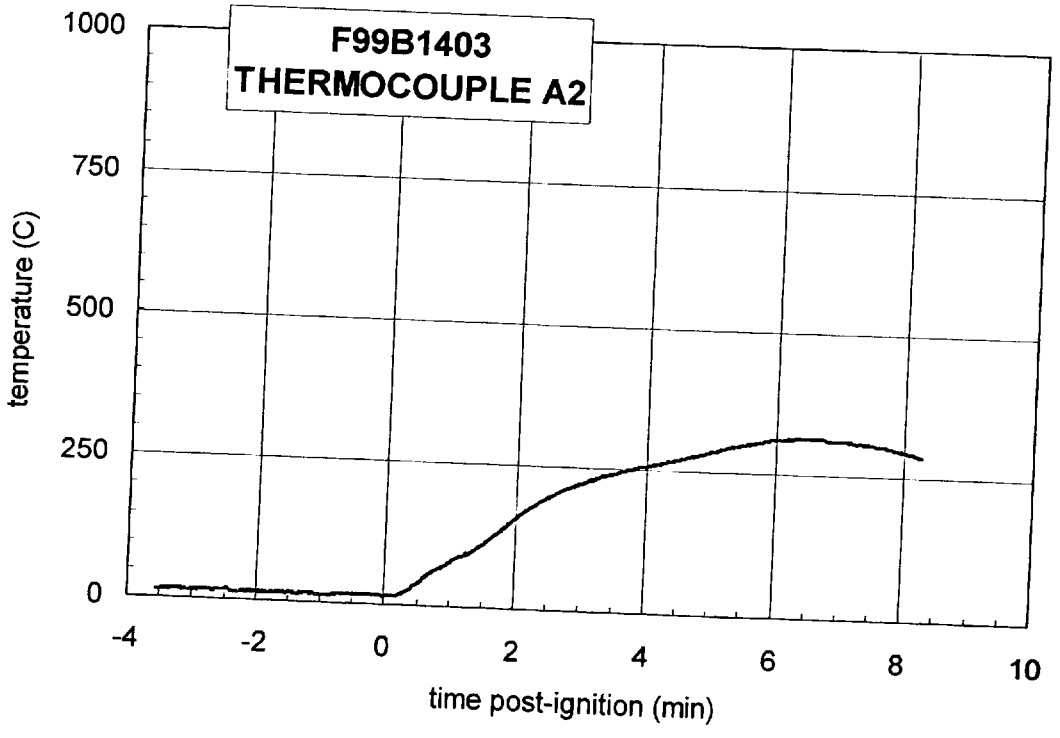

Plot F2. Fire Test F99B1403. Data plot from thermocouple A2.

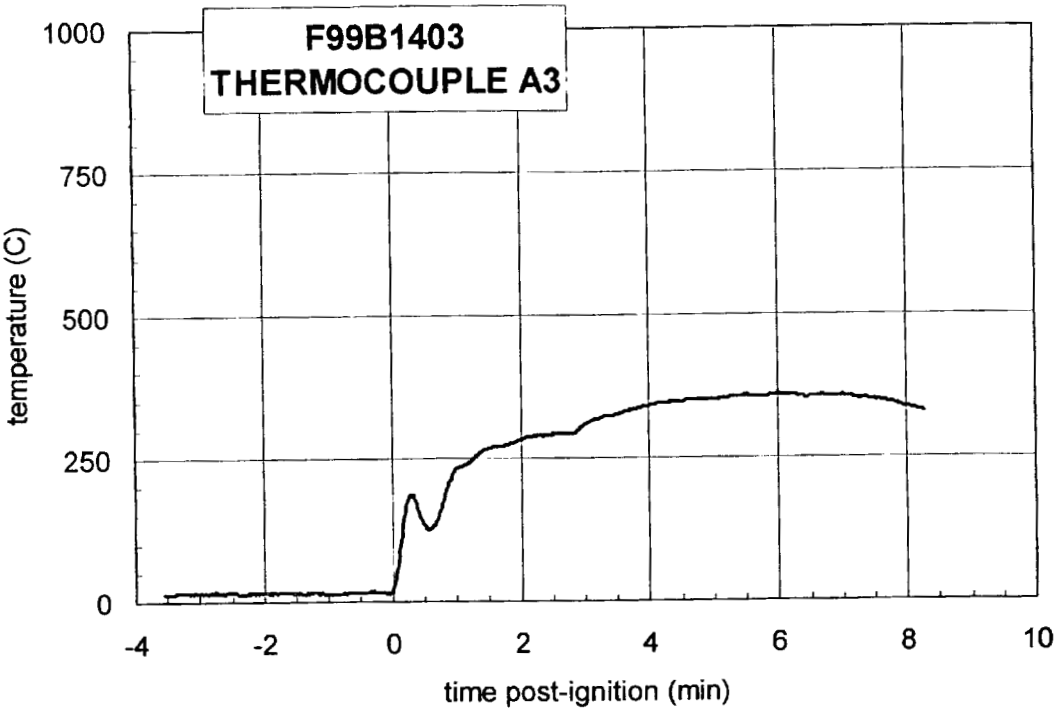

Plot F3. Fire Test F99B1403. Data plot from thermocouple A3.

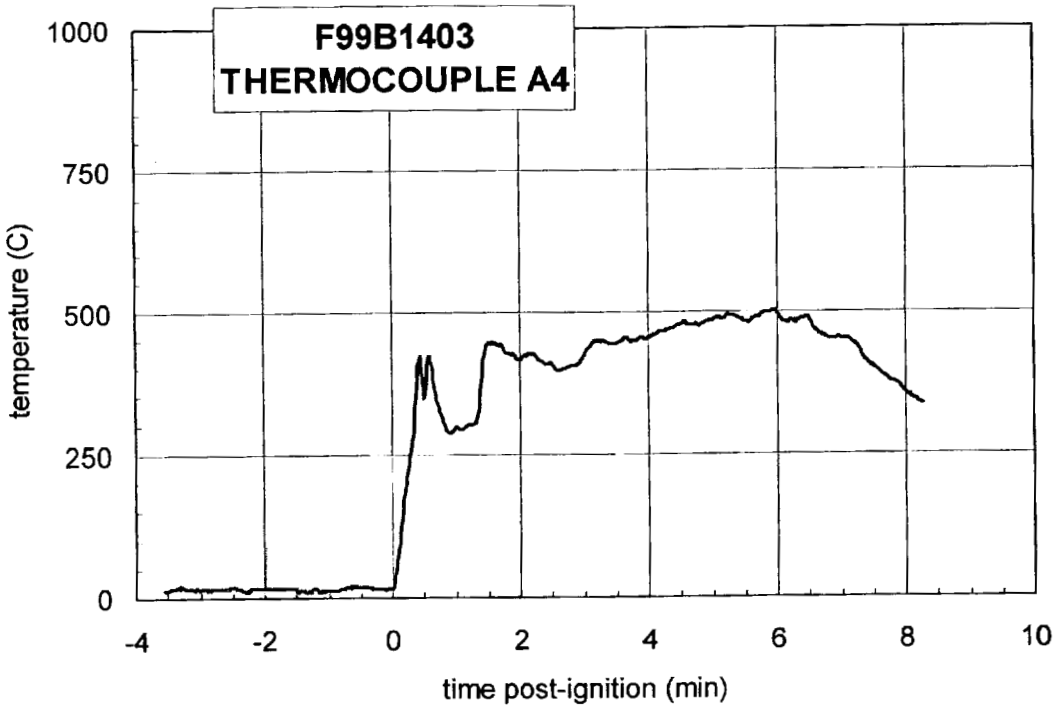

Plot F4. Fire Test F99B1403. Data plot from thermocouple A4.

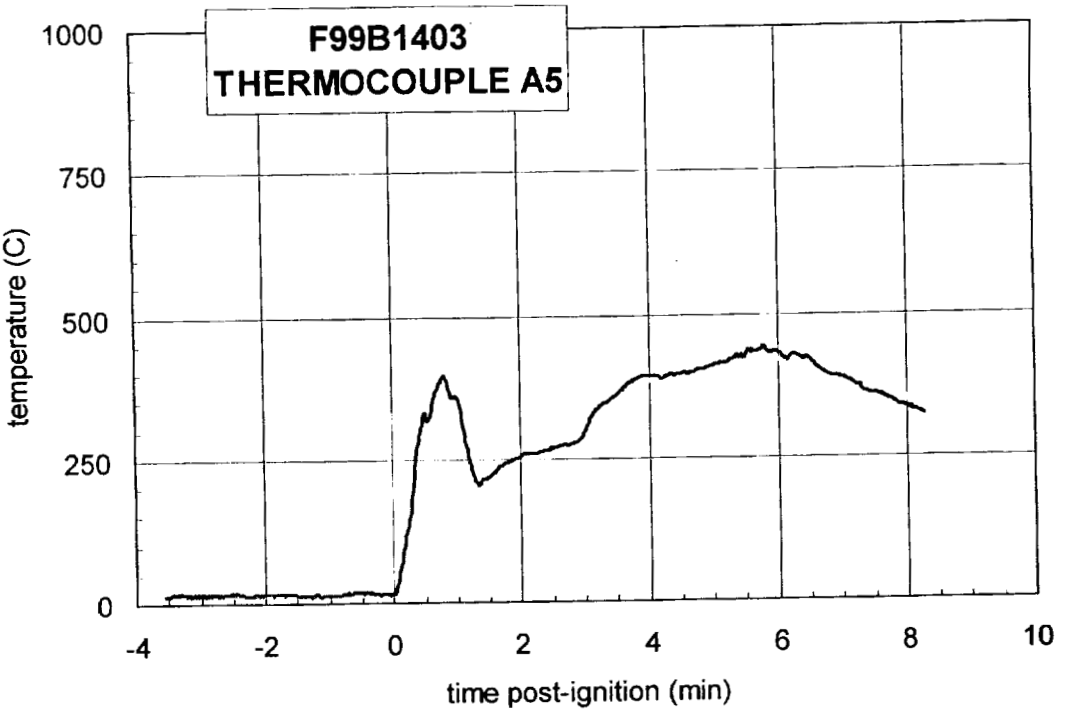

Plot F5. Fire Test F99B1403. Data plot from thermocouple A5.

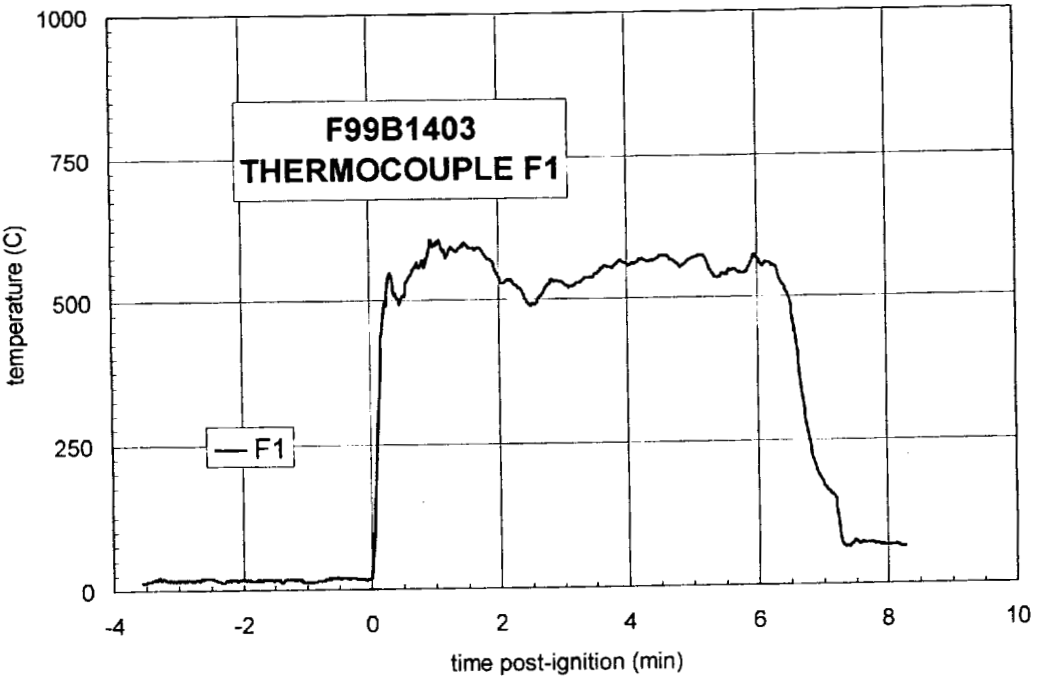

Plot F6. Fire Test F99B1403. Data plot from thermocouple F1.

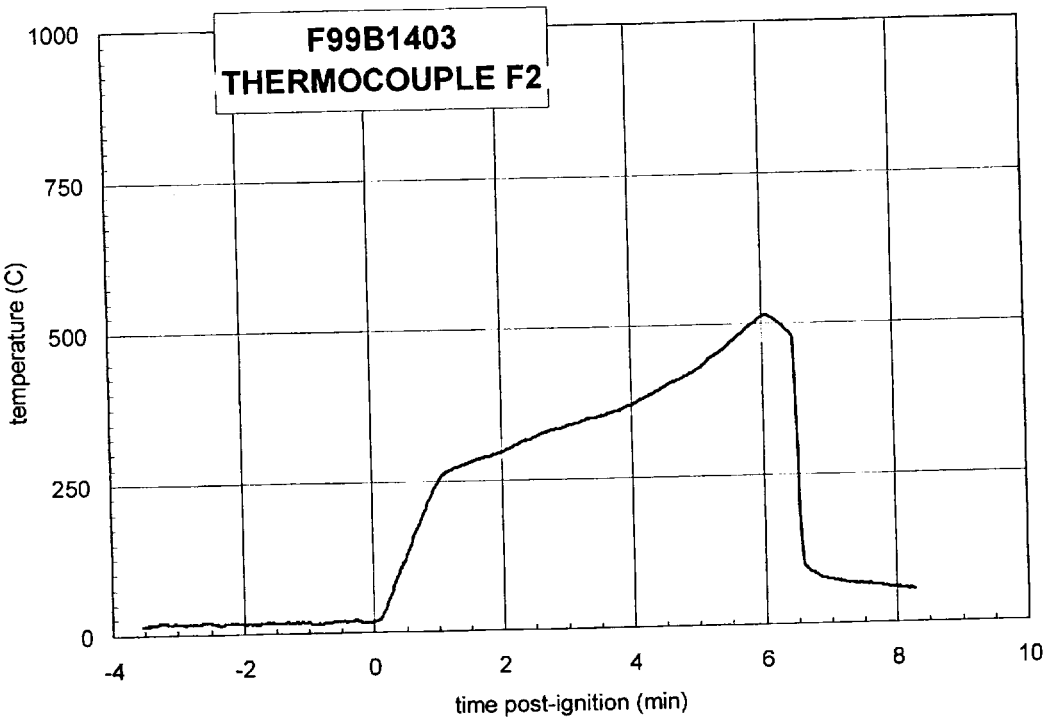

Plot F7. Fire Test F99B1403. Data plot from thermocouple F2.

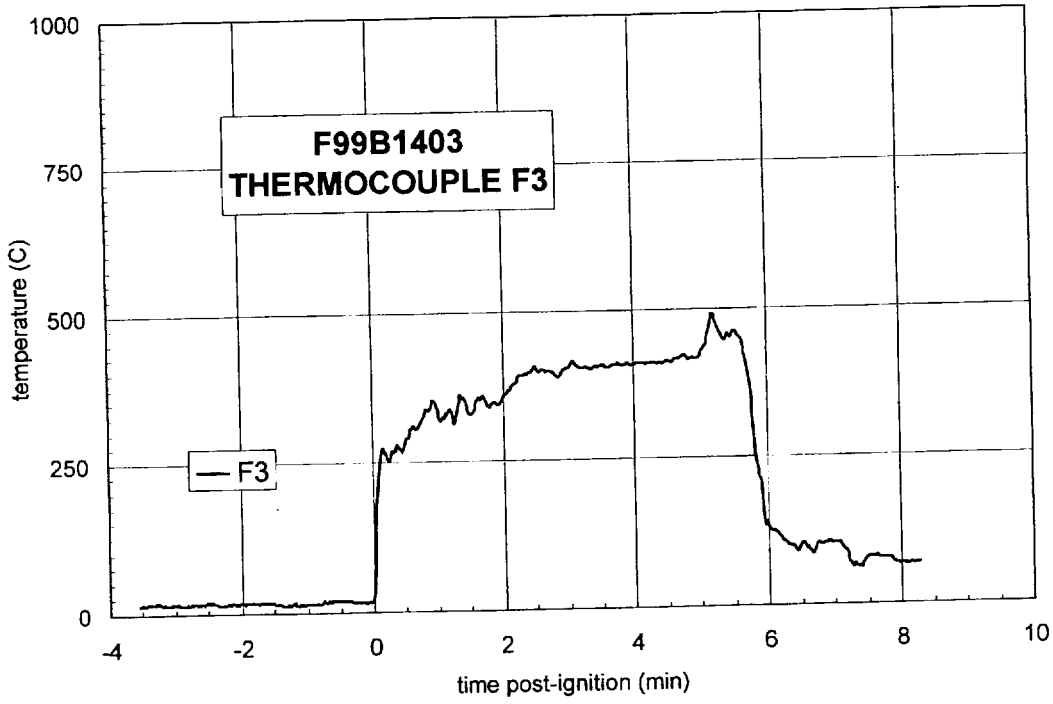

Plot F8. Fire Test F99B1403. Data plot from thermocouple F3.

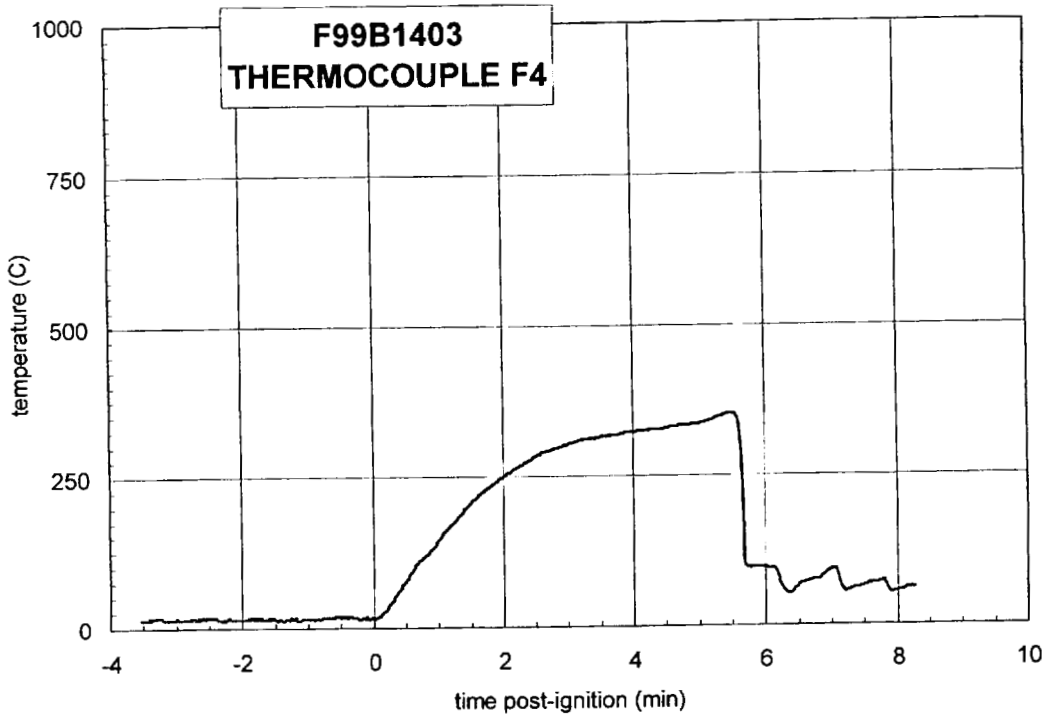

Plot F9. Fire Test F99B1403. Data plot from thermocouple F4.

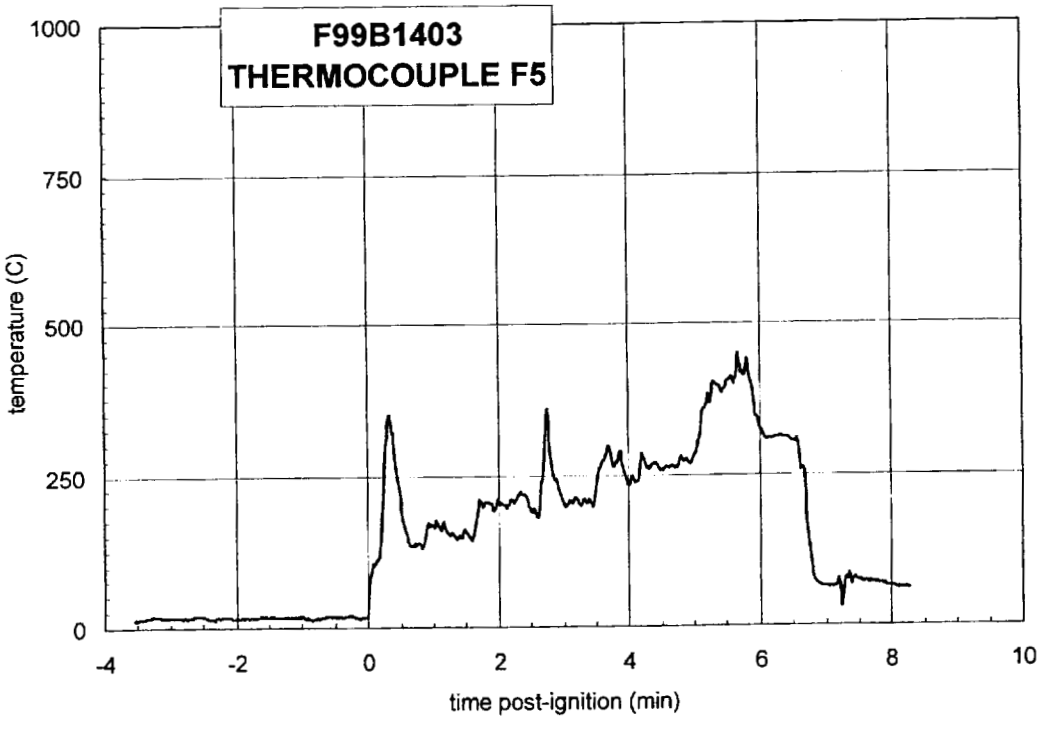

Plot F10. Fire Test F99B1403. Data plot from thermocouple F5.

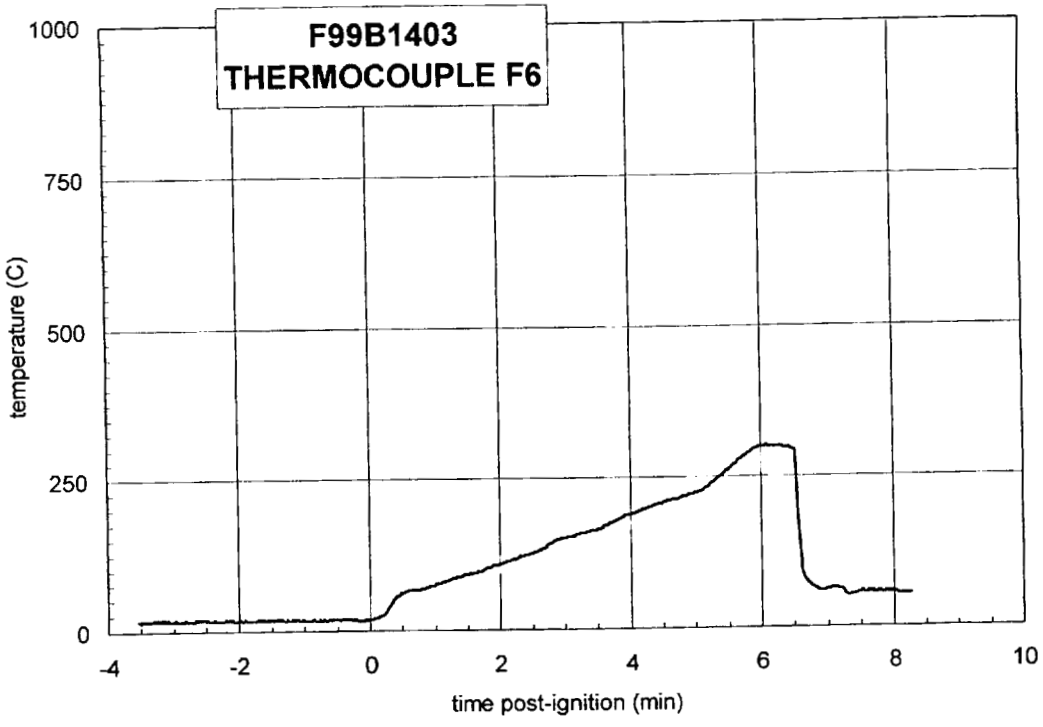

Plot F11. Fire Test F99B1403. Data plot from thermocouple F6.

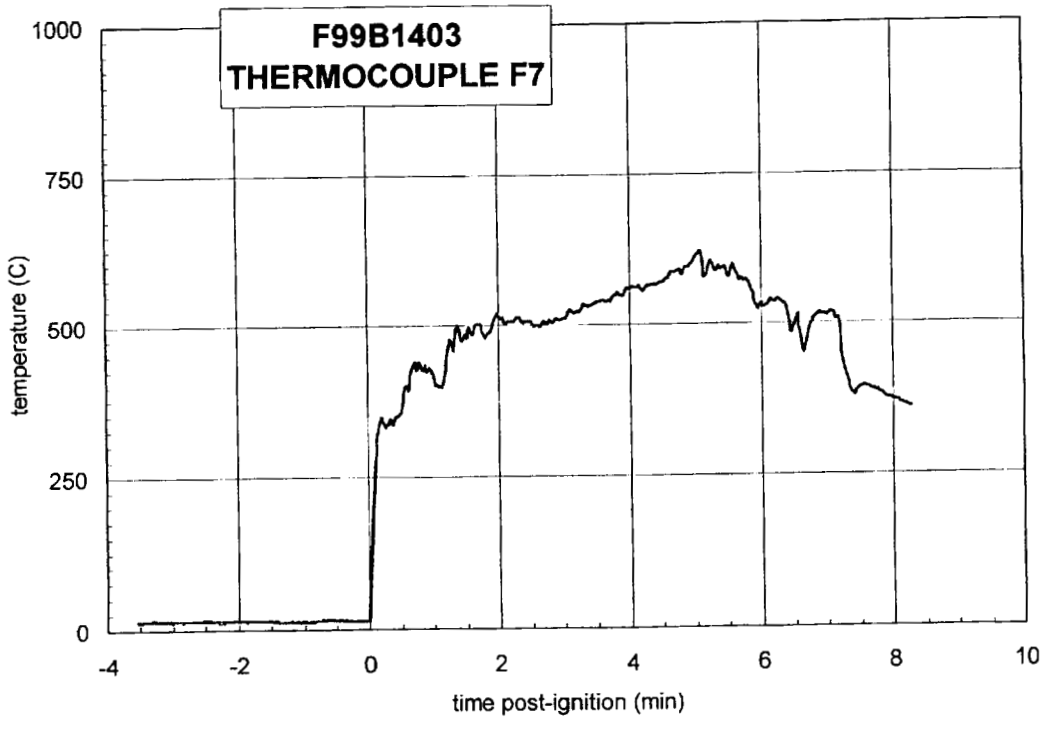

Plot F12. Fire Test F99B1403. Data plot from thermocouple F7.

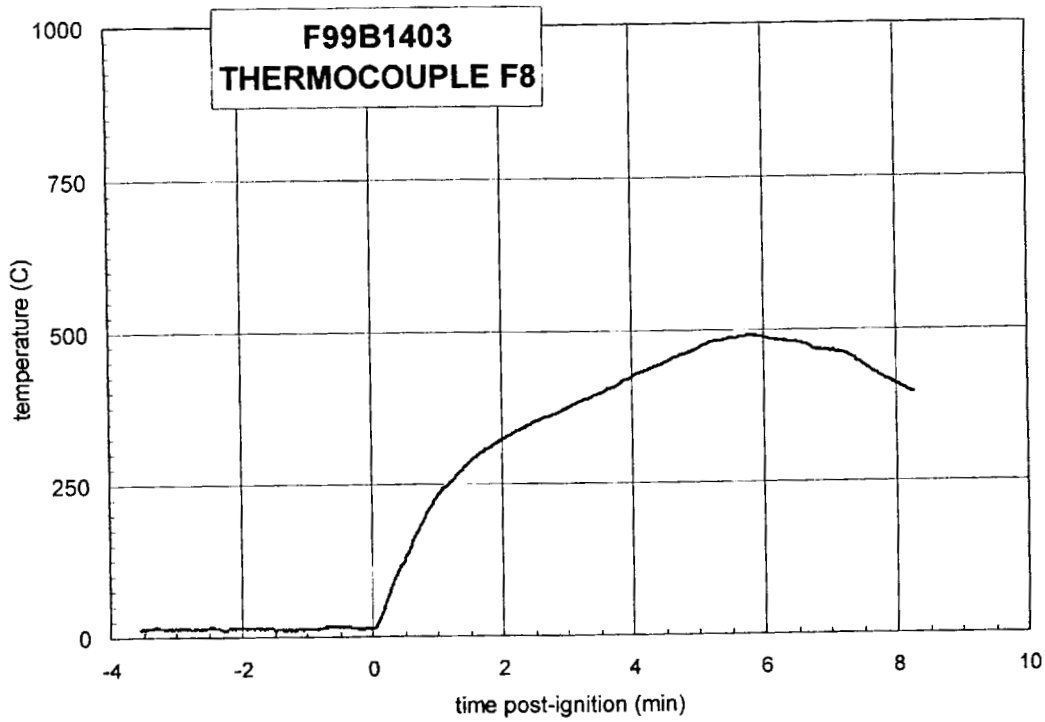

Plot F13. Fire Test F99B1403. Data plot from thermocouple F8.

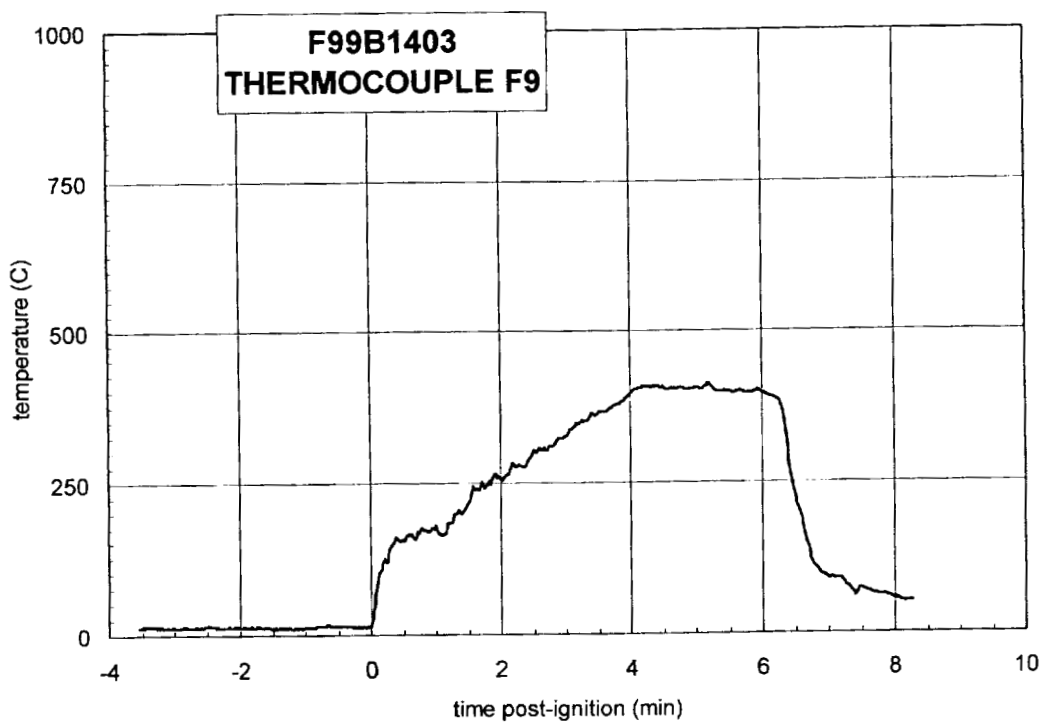

Plot F14. Fire Test F99B1403. Data plot from thermocouple F9.

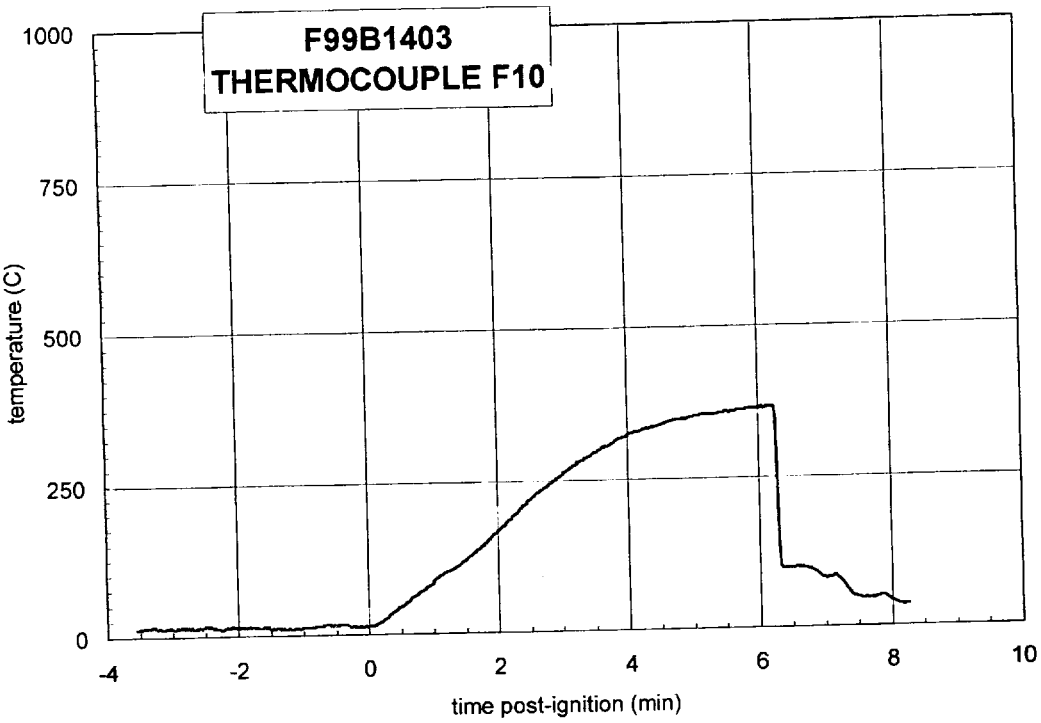

Plot F15. Fire Test F99B1403. Data plot from thermocouple F10.

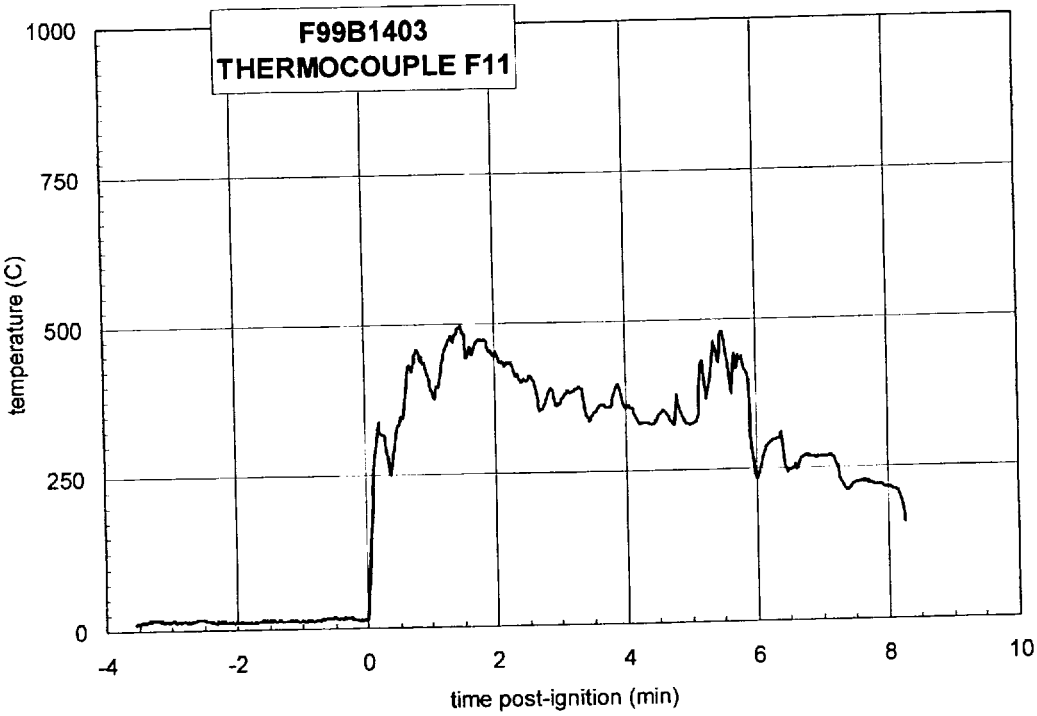

Plot F16. Fire Test F99B1403. Data plot from thermocouple F11.

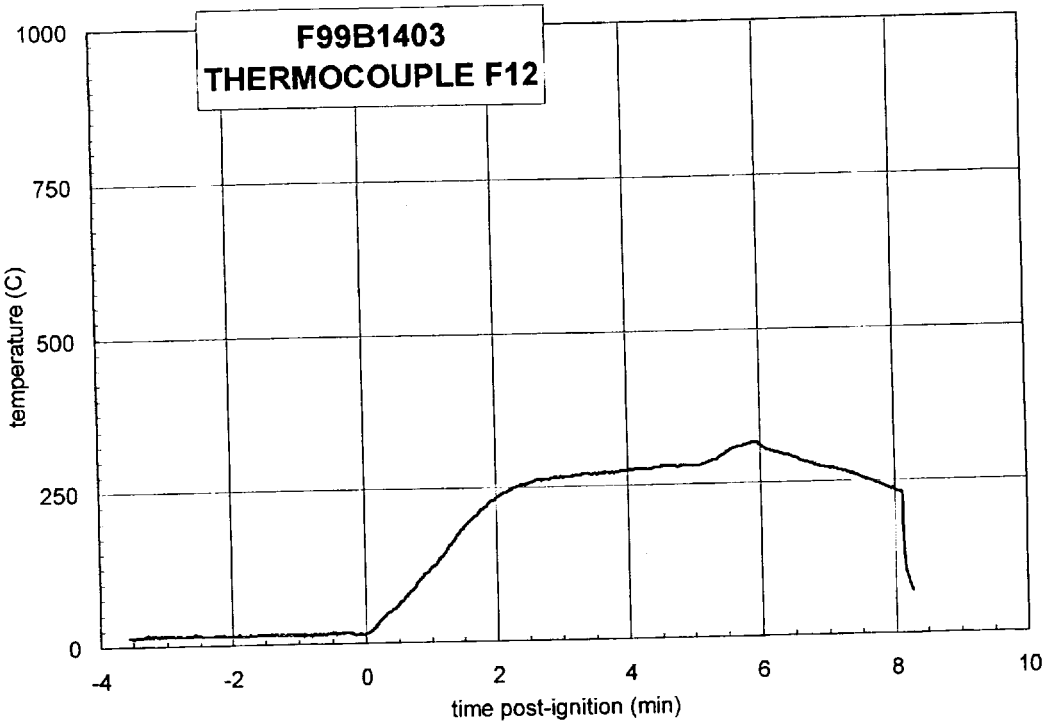

Plot F17. Fire Test F99B1403. Data plot from thermocouple F12.

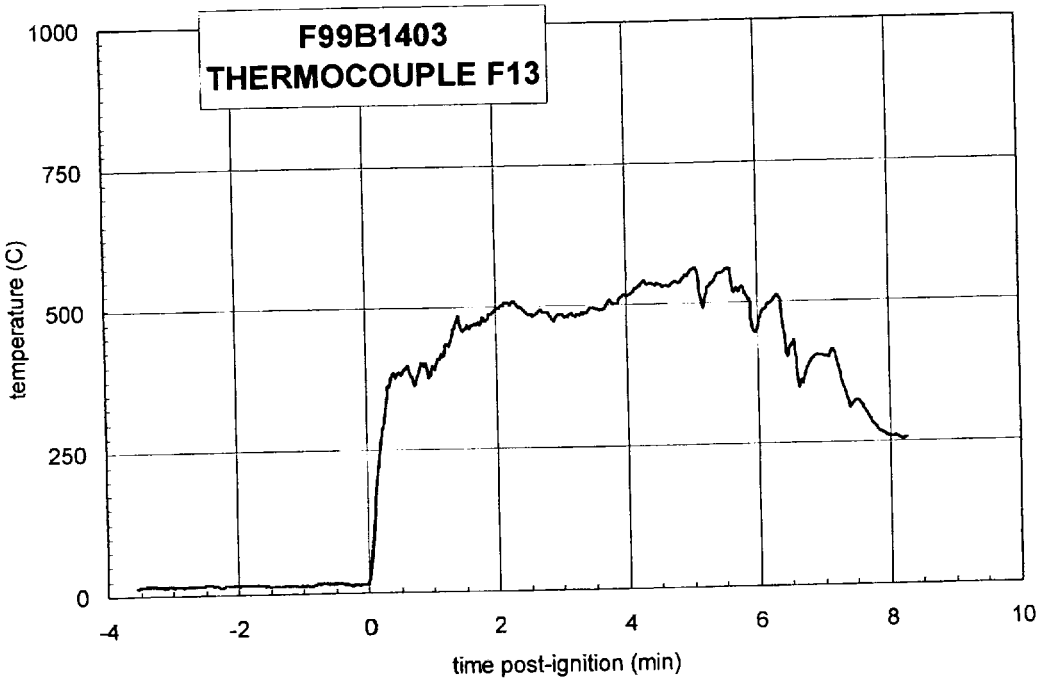

Plot F18. Fire Test F99B1403. Data plot from thermocouple F13.

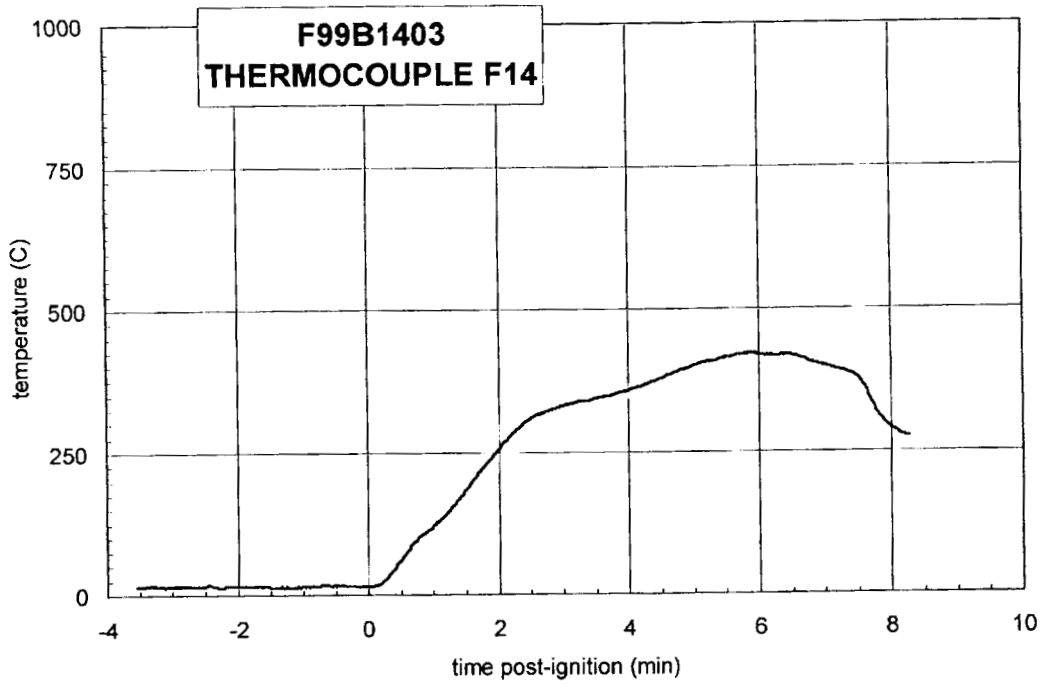

Plot F19. Fire Test F99B1403. Data plot from thermocouple F14.

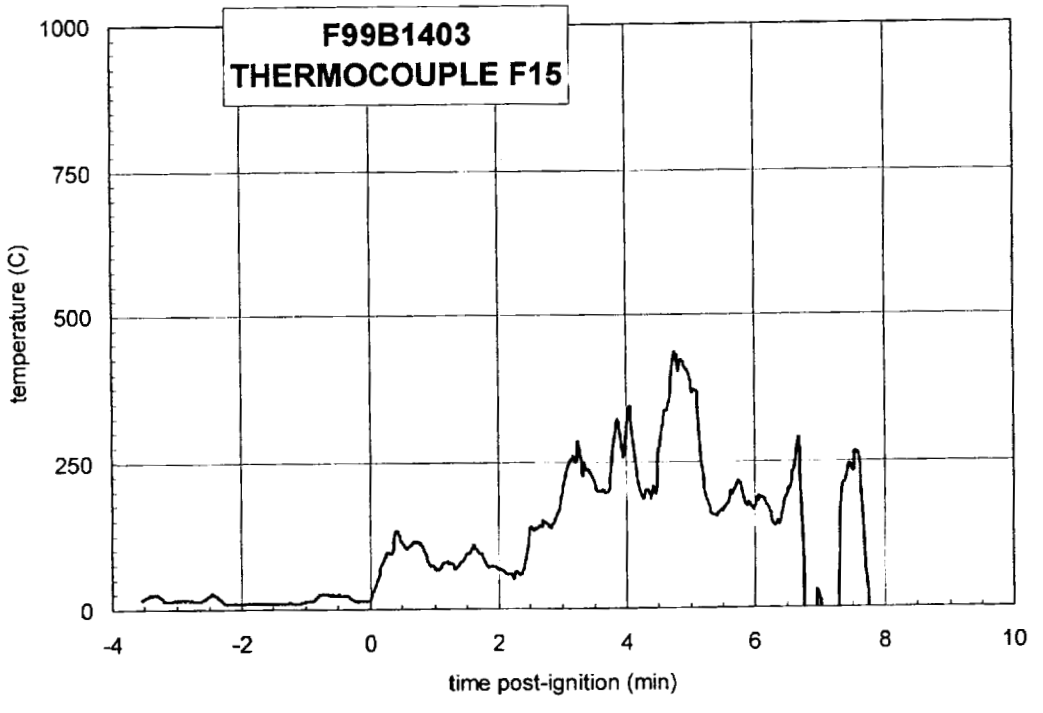

Plot F20. Fire Test F99B1403. Data plot from thermocouple F15.

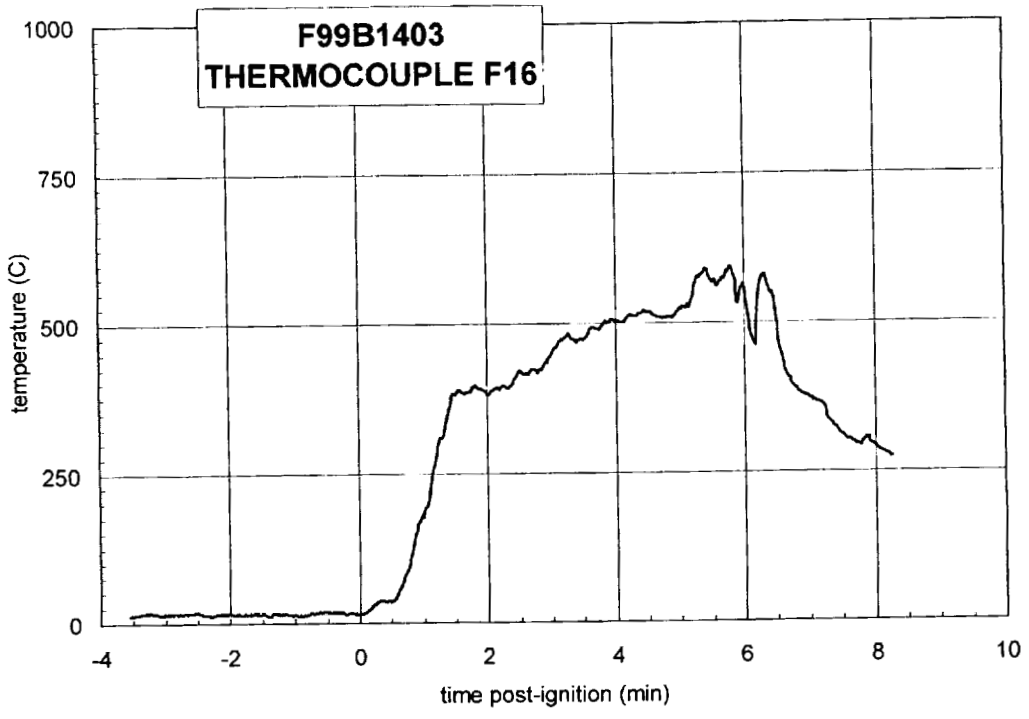

Plot F21. Fire Test F99B1403. Data plot from thermocouple F16.

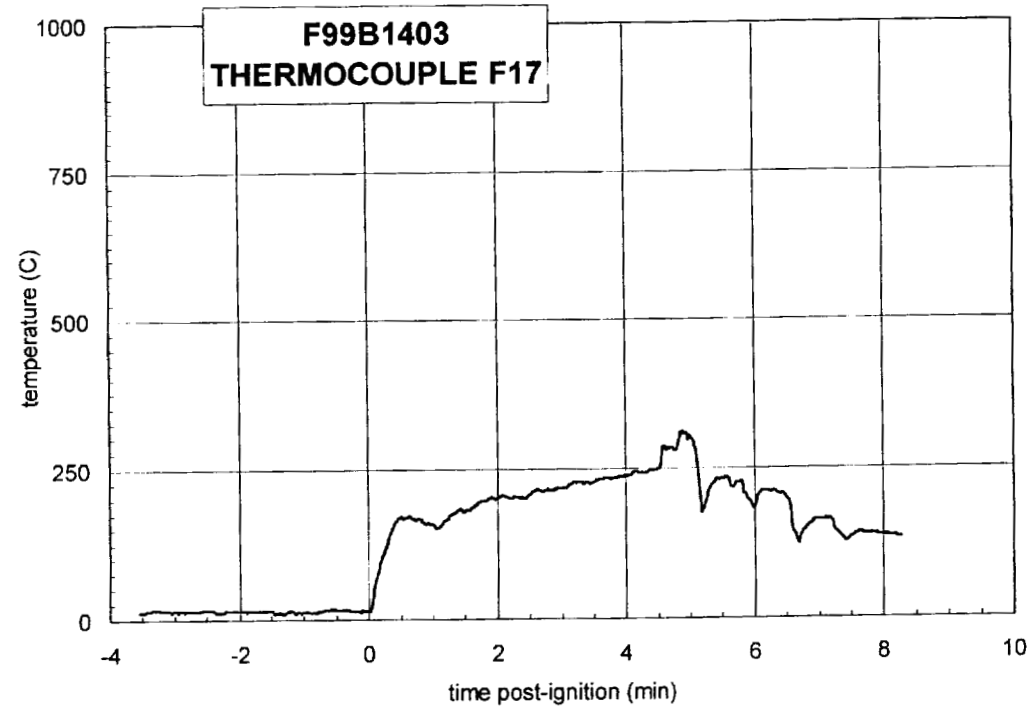

Plot F22. Fire Test F99B1403. Data plot from thermocouple F17.

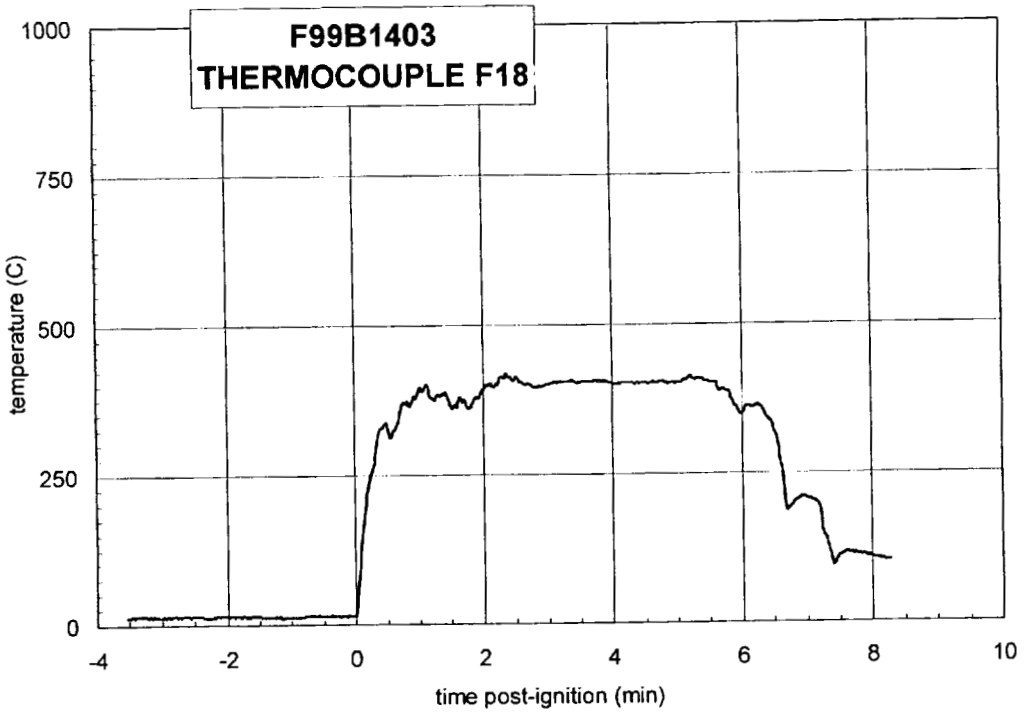

Plot F23. Fire Test F99B1403. Data plot from thermocouple F18.

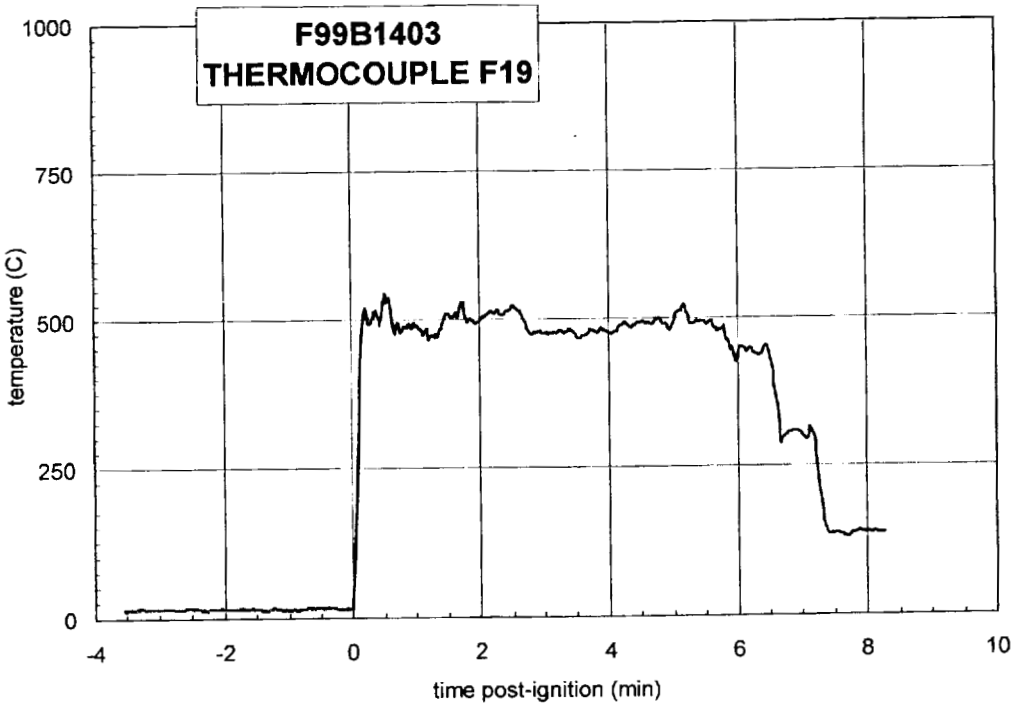

Plot F24. Fire Test F99B1403. Data plot from thermocouple F19.

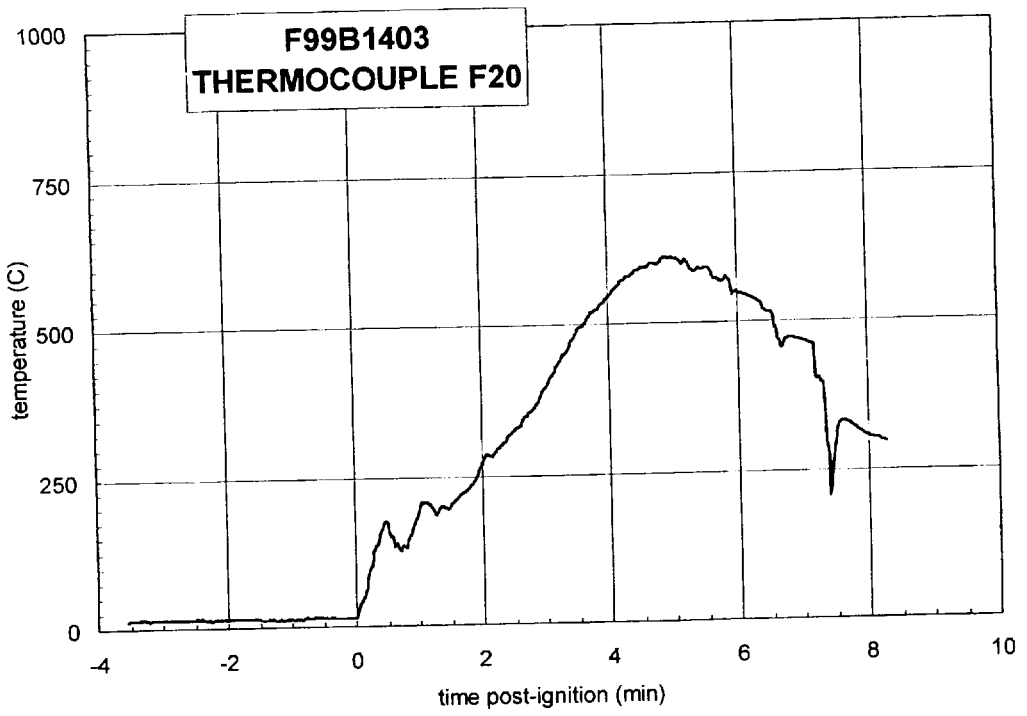

Plot F25. Fire Test F99B1403. Data plot from thermocouple F20.

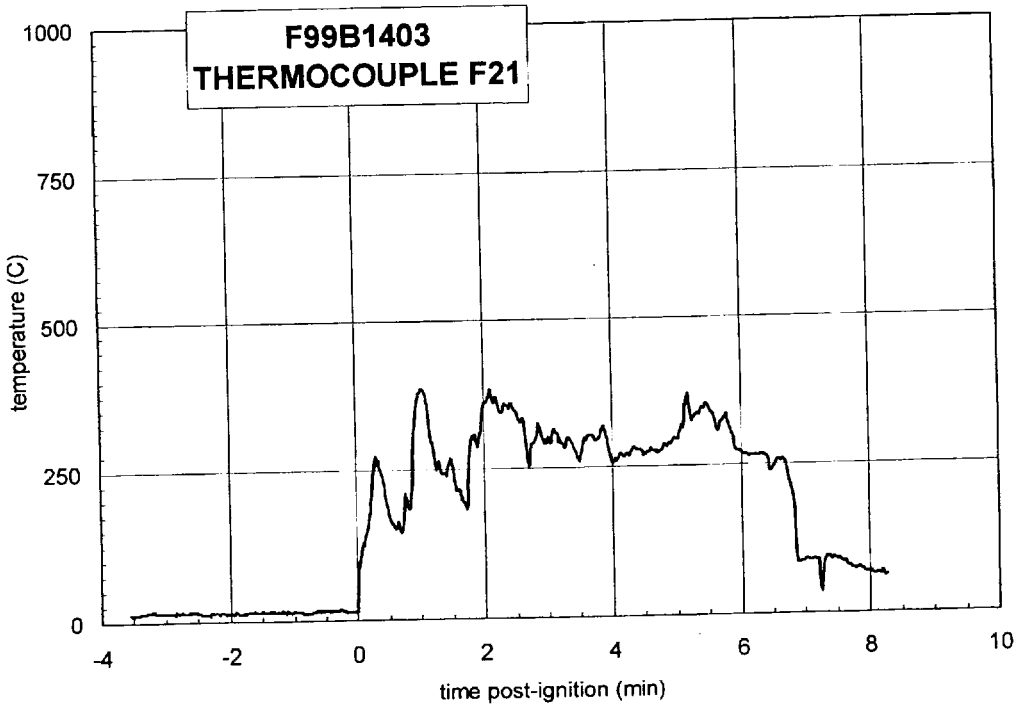

Plot F26. Fire Test F99B1403. Data plot from thermocouple F21.

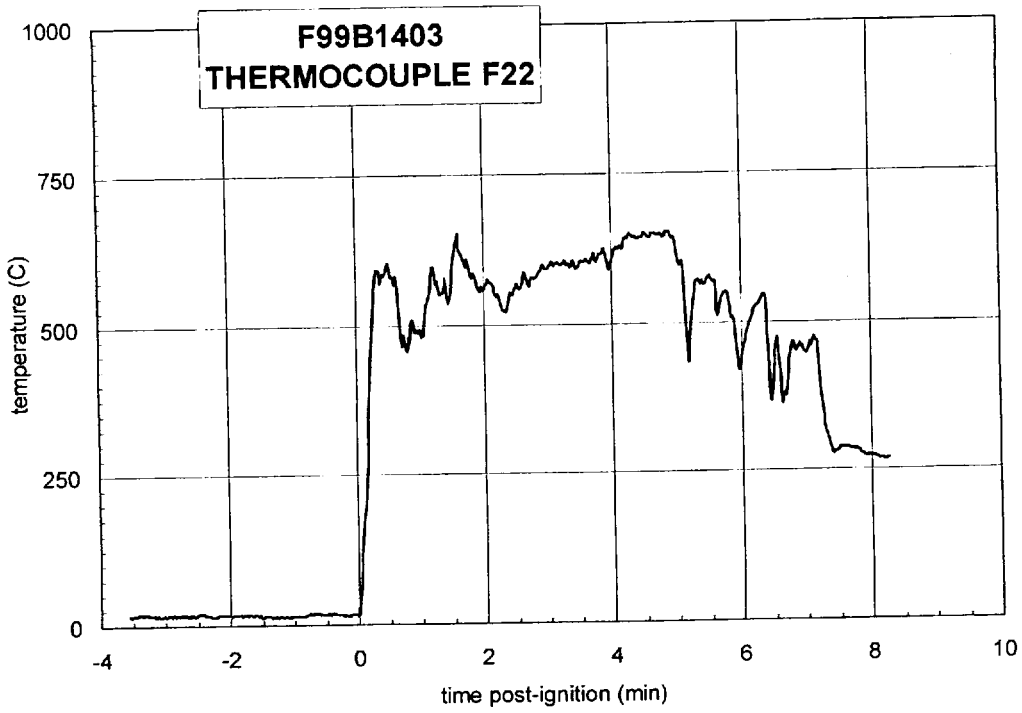

Plot F27. Fire Test F99B1403. Data plot from thermocouple F22.

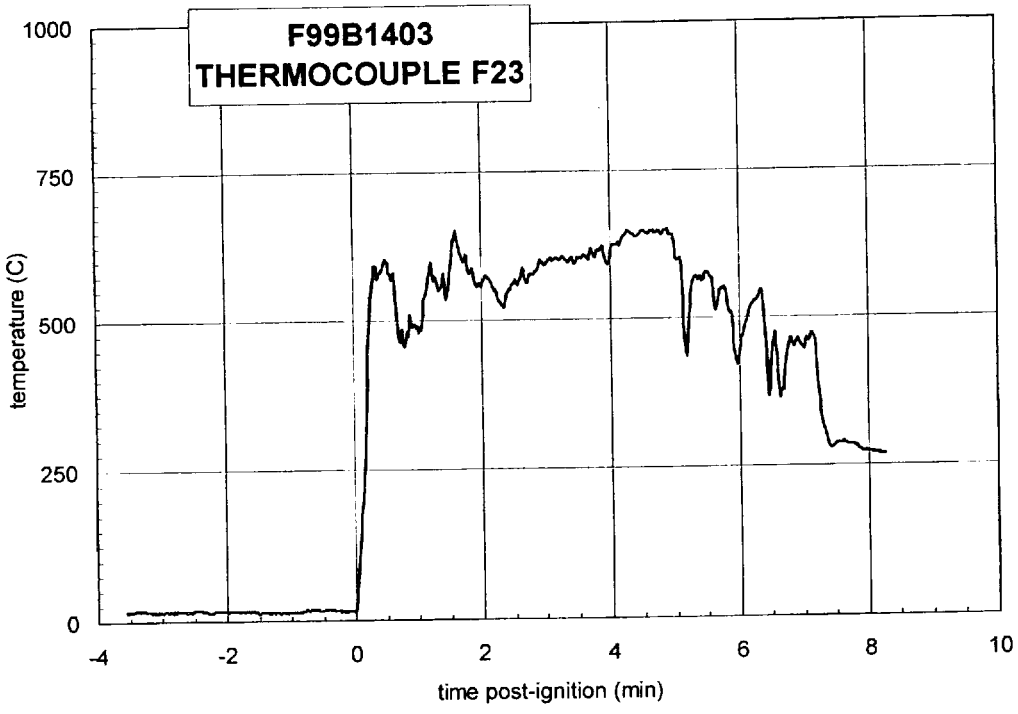

Plot F28. Fire Test F99B1403. Data plot from thermocouple F23.

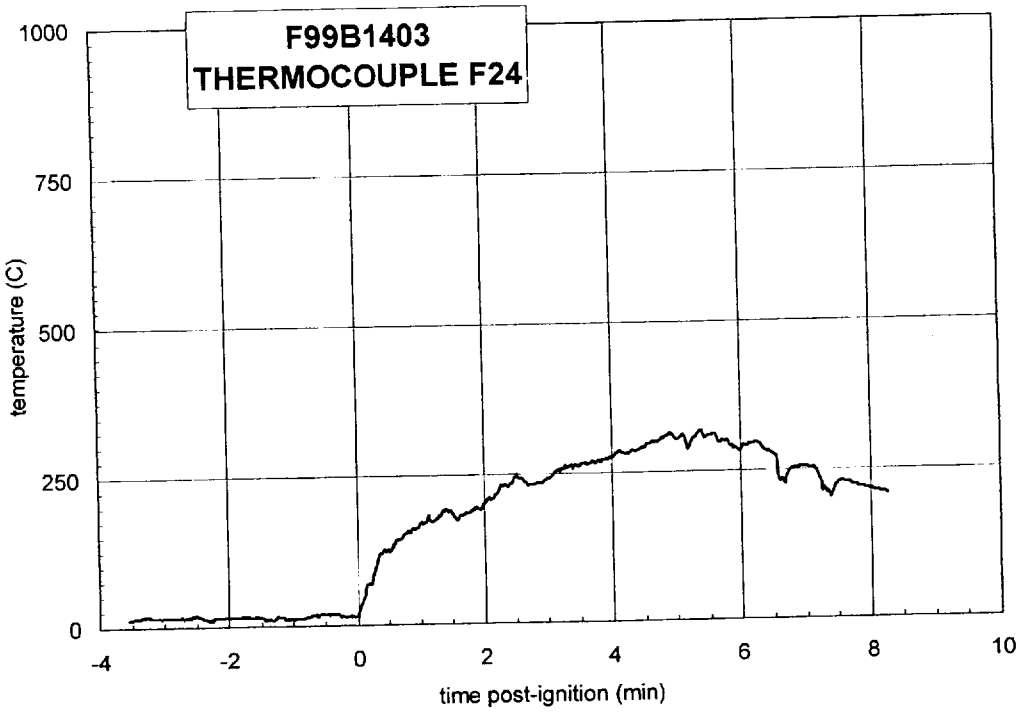

Plot F29. Fire Test F99B1403. Data plot from thermocouple F24.

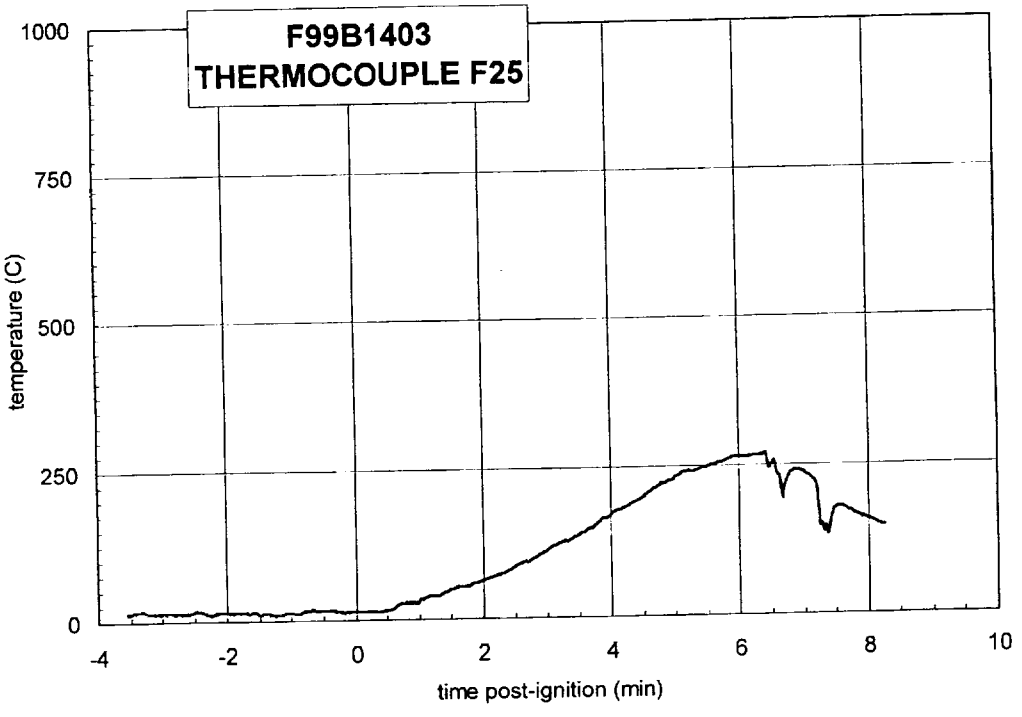

Plot F30. Fire Test F99B1403. Data plot from thermocouple F25.

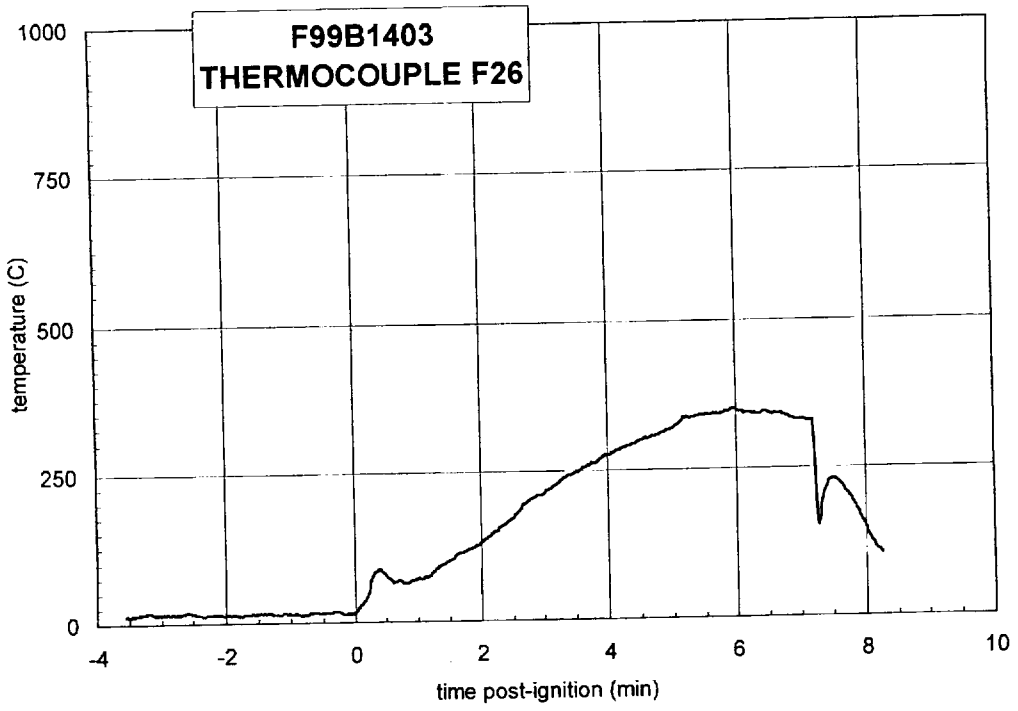

Plot F31. Fire Test F99B1403. Data plot from thermocouple F26.

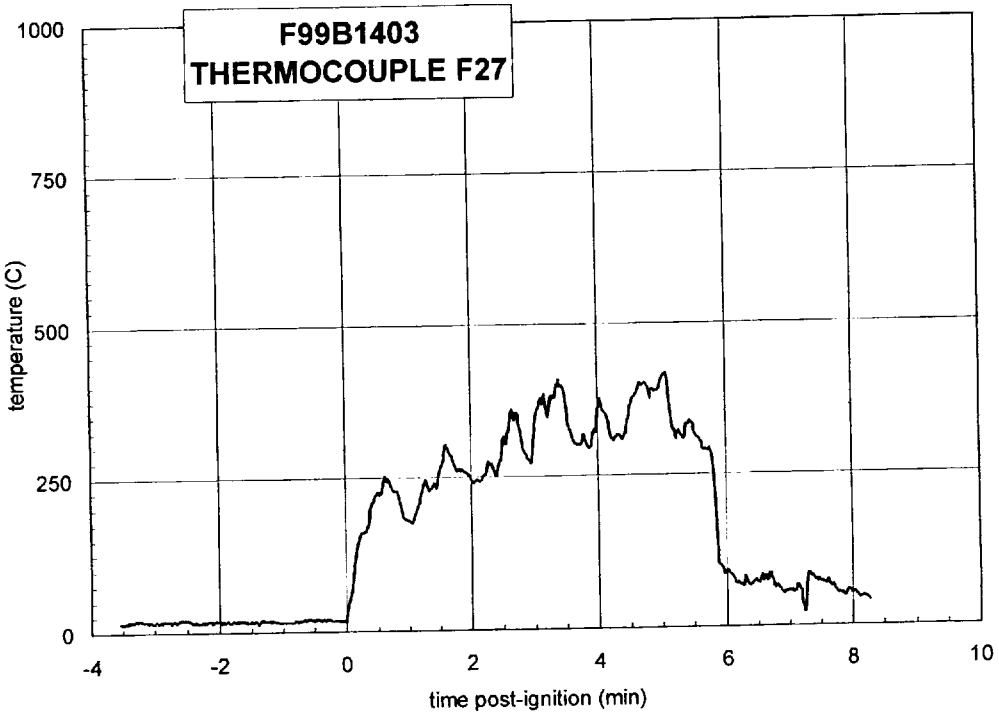

Plot F32. Fire Test F99B1403. Data plot from thermocouple F27.

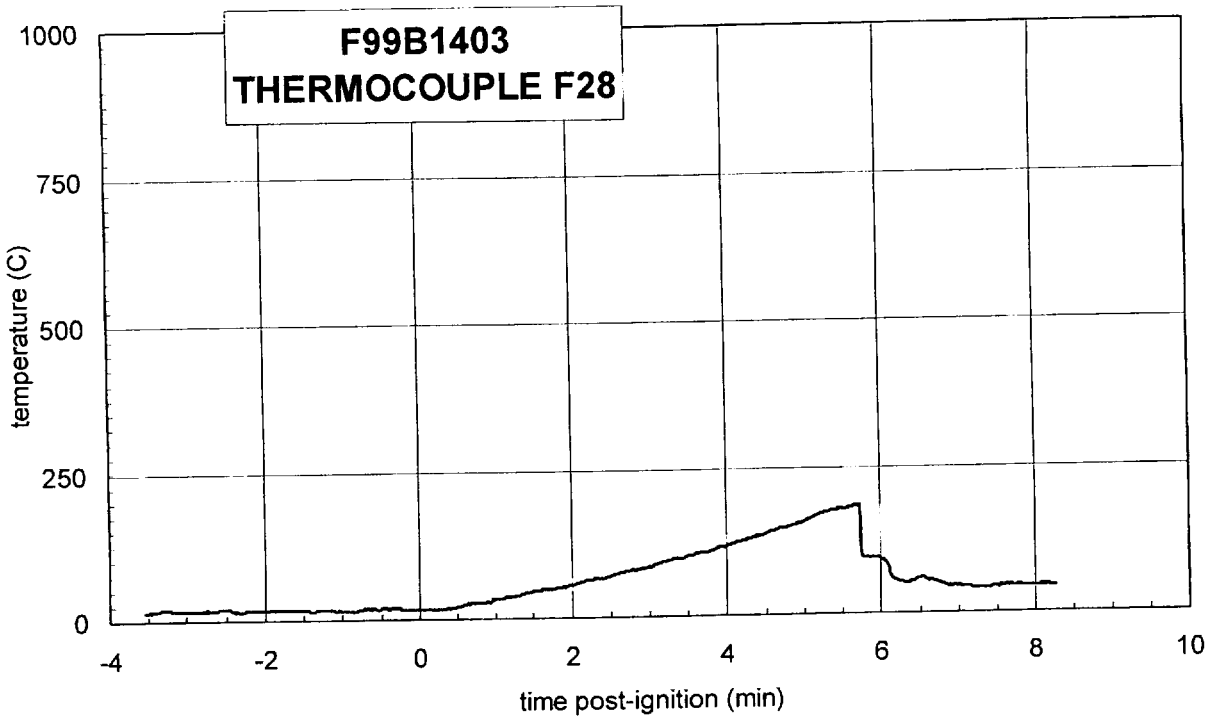

Plot F33. Fire Test F99B1403. Data plot from thermocouple F28.

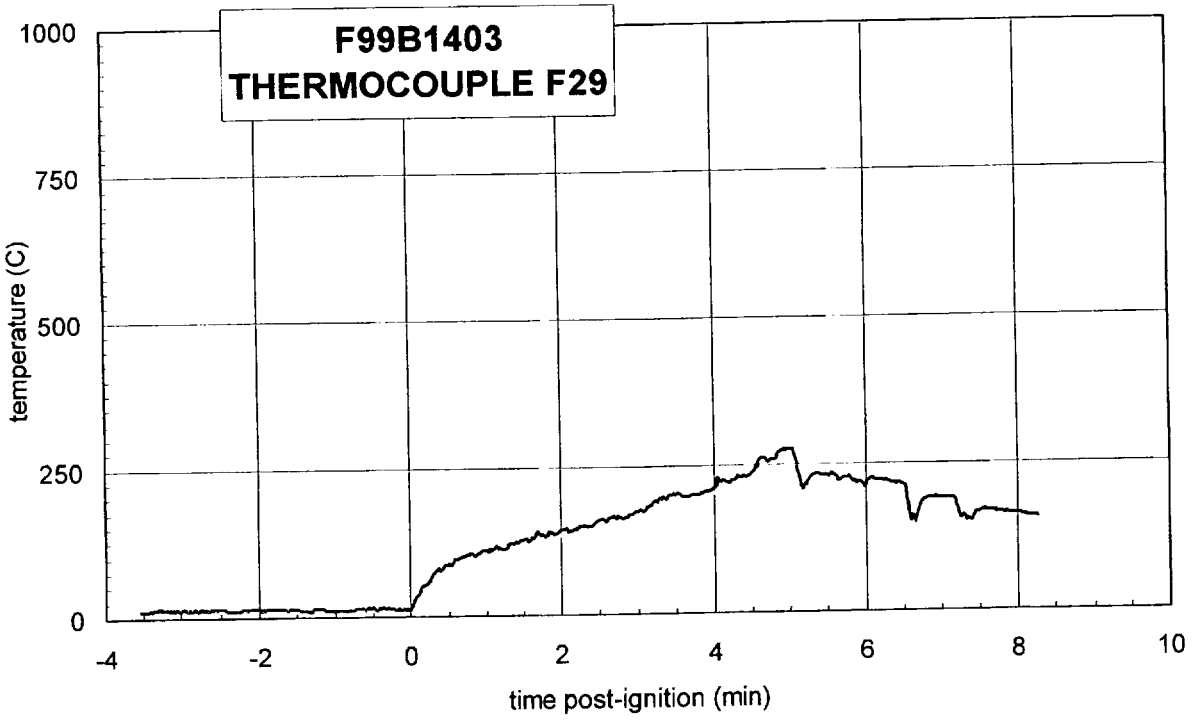

Plot F34. Fire Test F99B1403. Data plot from thermocouple F29.

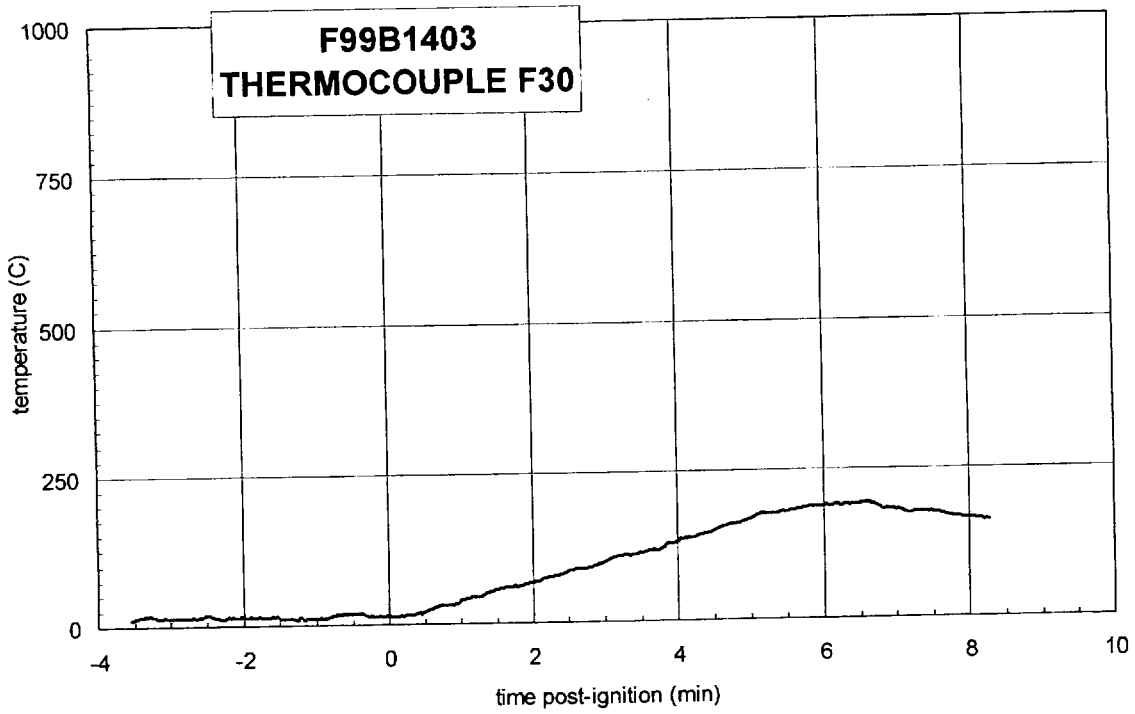

Plot F35. Fire Test F99B1403. Data plot from thermocouple F30.

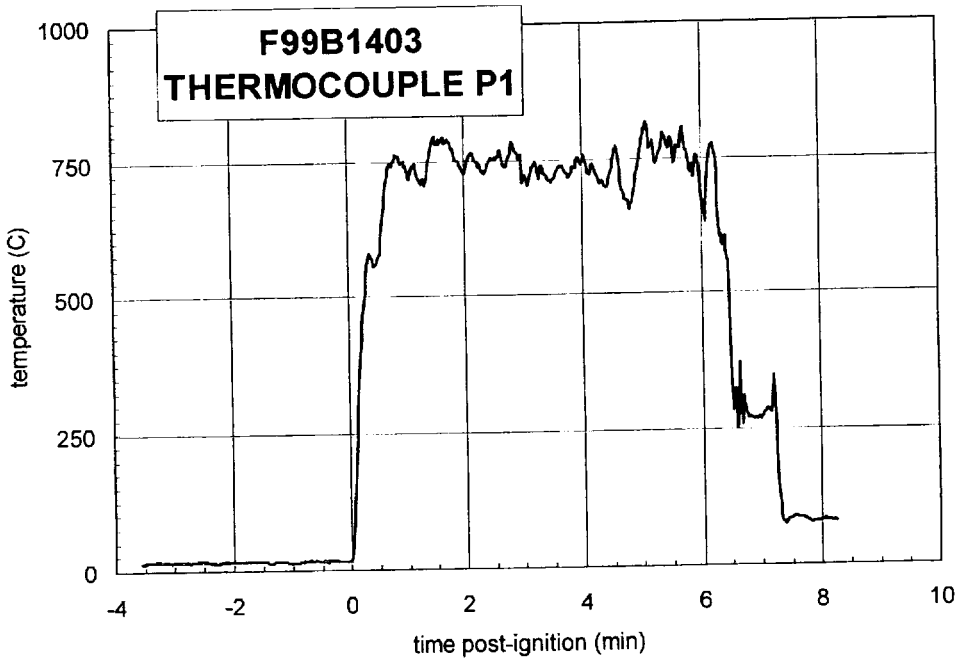

Plot F36. Fire Test F99B1403. Data plot from thermocouple P1.

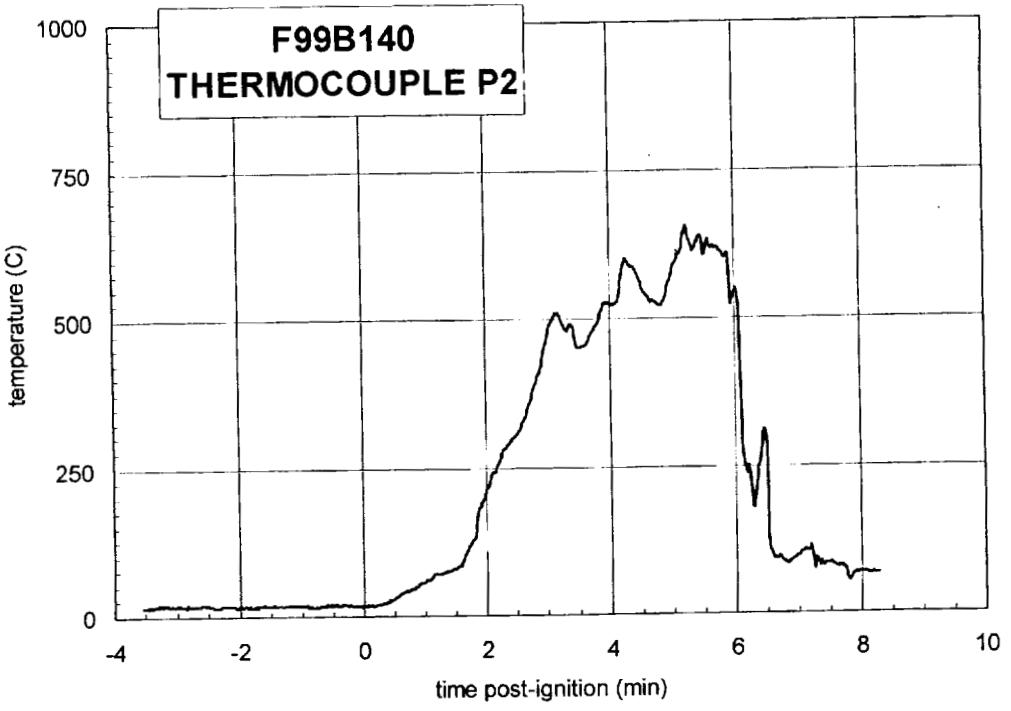

Plot F37. Fire Test F99B1403. Data plot from thermocouple P2.

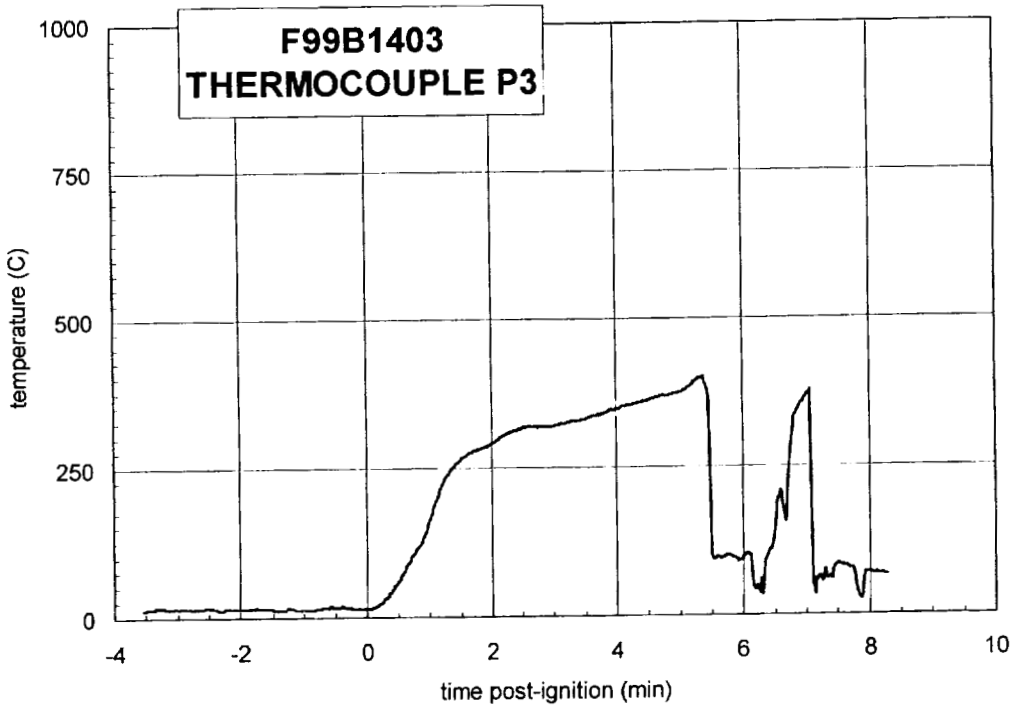

Plot F38. Fire Test F99B1403. Data plot from thermocouple P3.

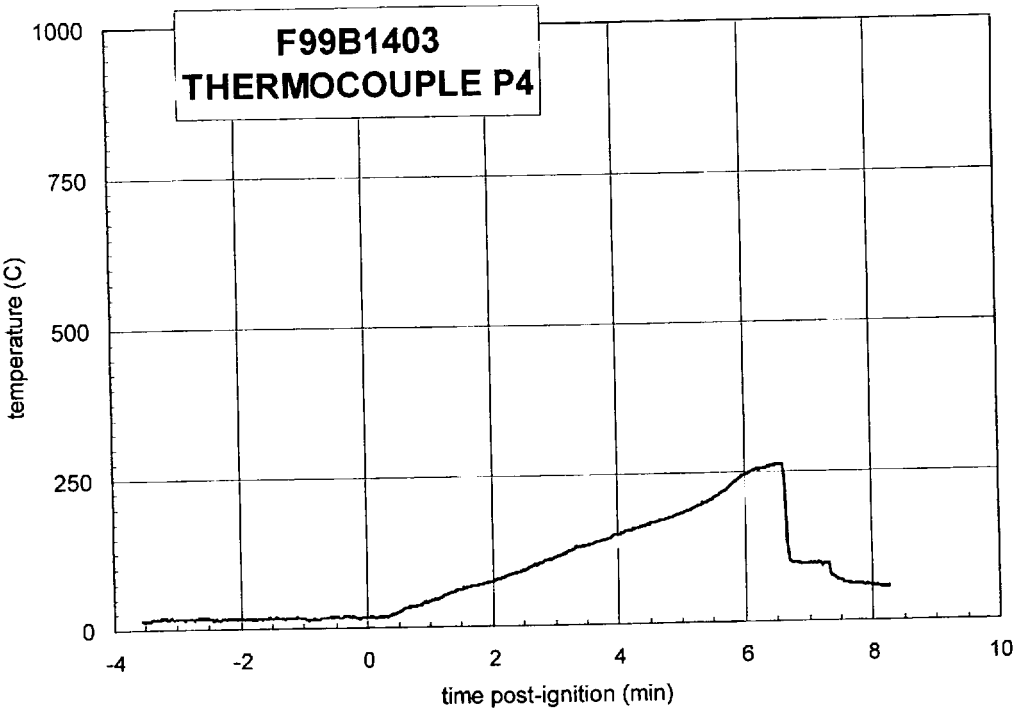

Plot F39. Fire Test F99B1403. Data plot from thermocouple P4.

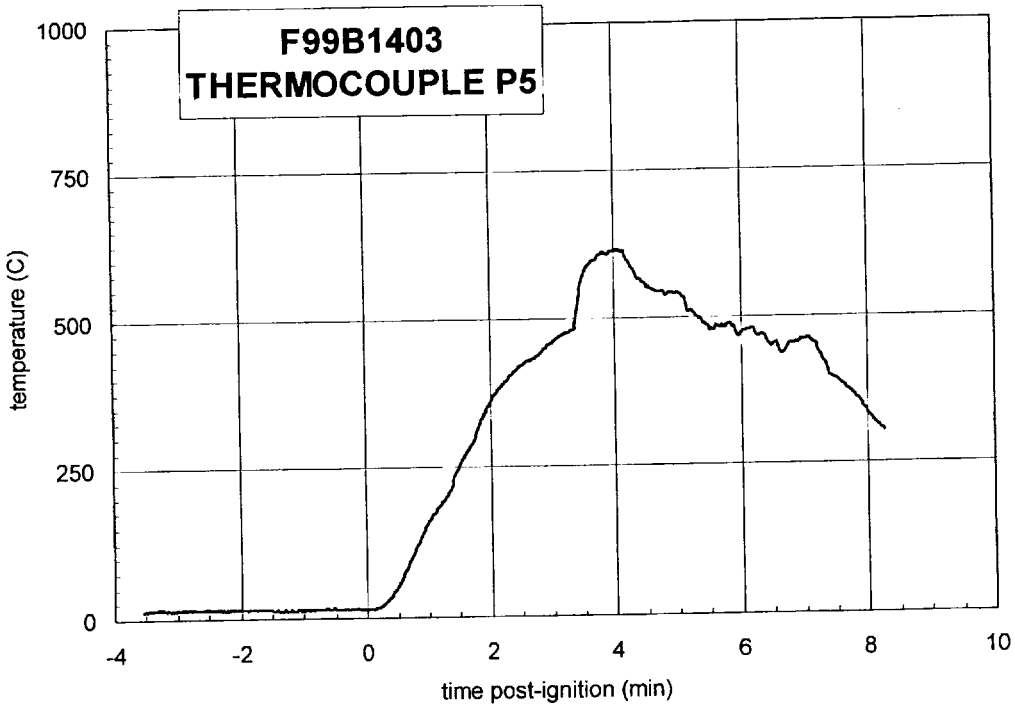

Plot F40. Fire Test F99B1403. Data plot from thermocouple P5.

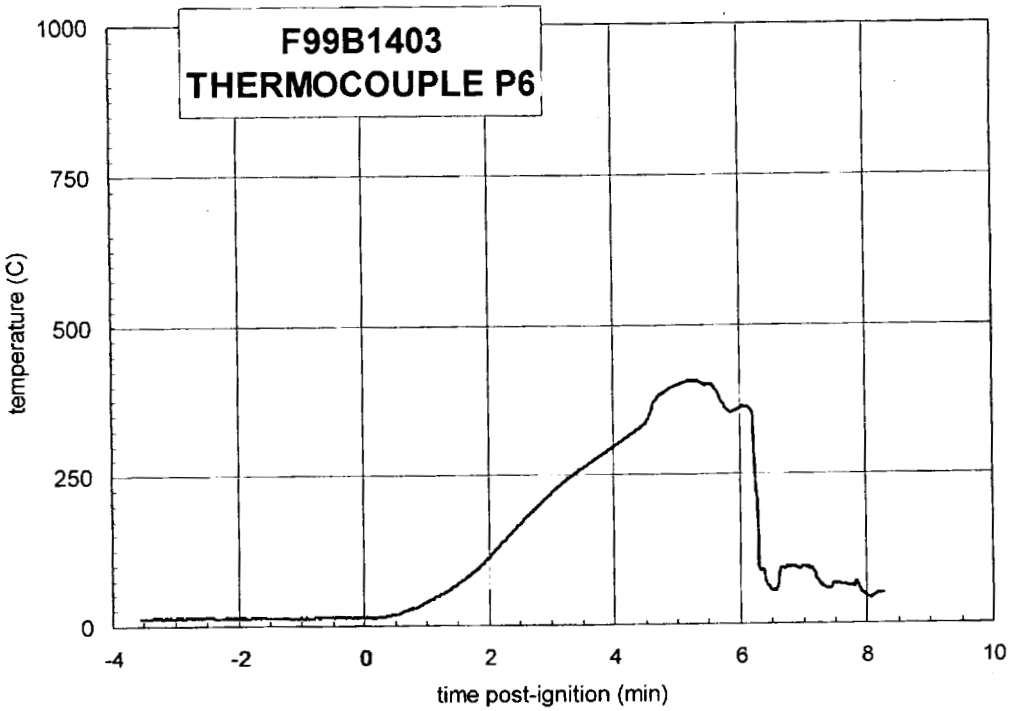

Plot F41. Fire Test F99B1403. Data plot from thermocouple P6.

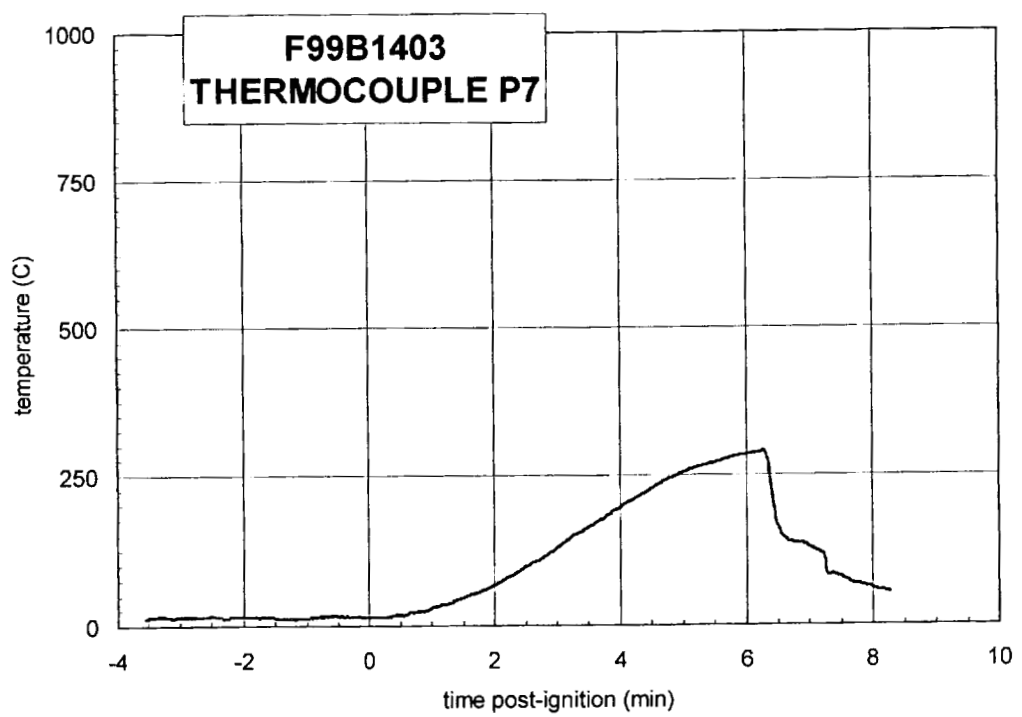

Plot F42. Fire Test F99B1403. Data plot from thermocouple P7.

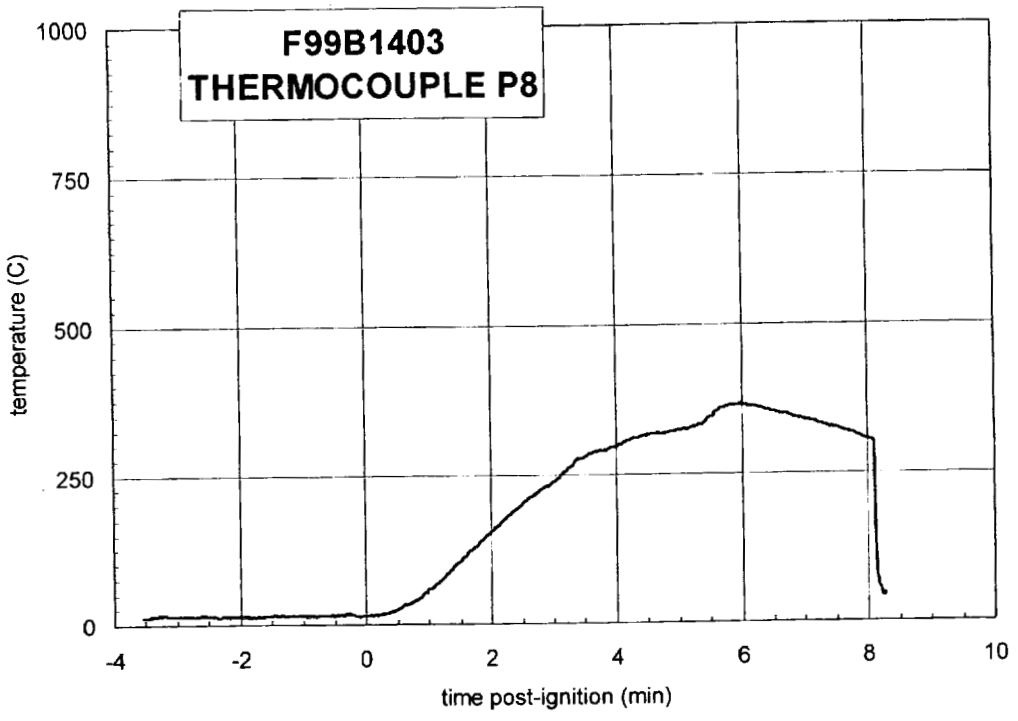

Plot F43. Fire Test F99B1403. Data plot from thermocouple P8.

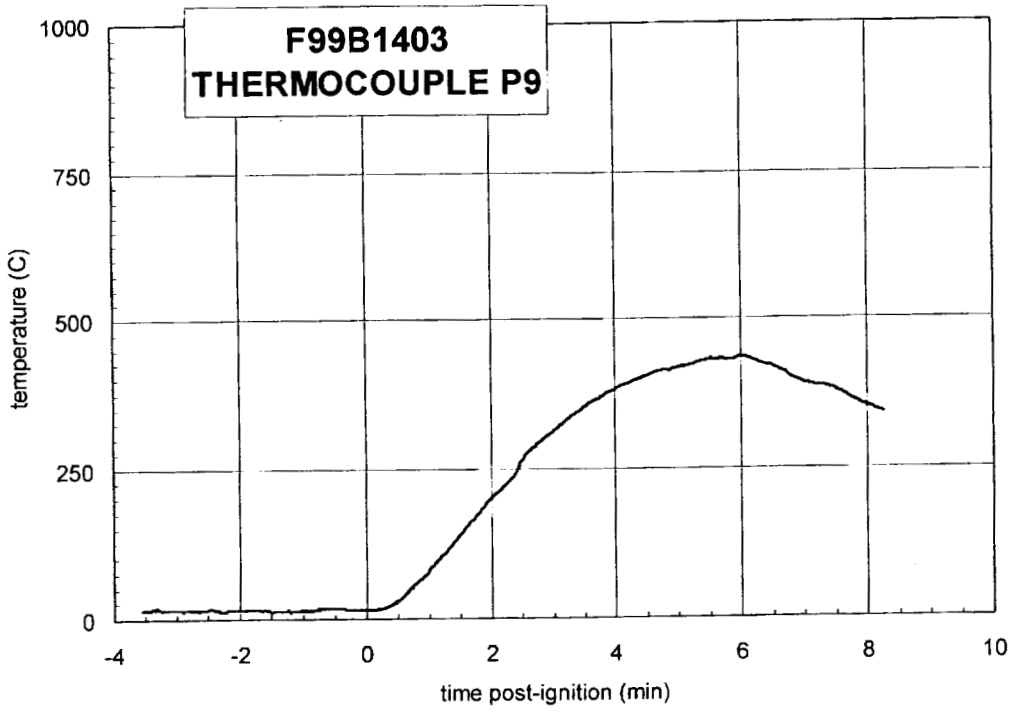

Plot F44. Fire Test F99B1403. Data plot from thermocouple P9.

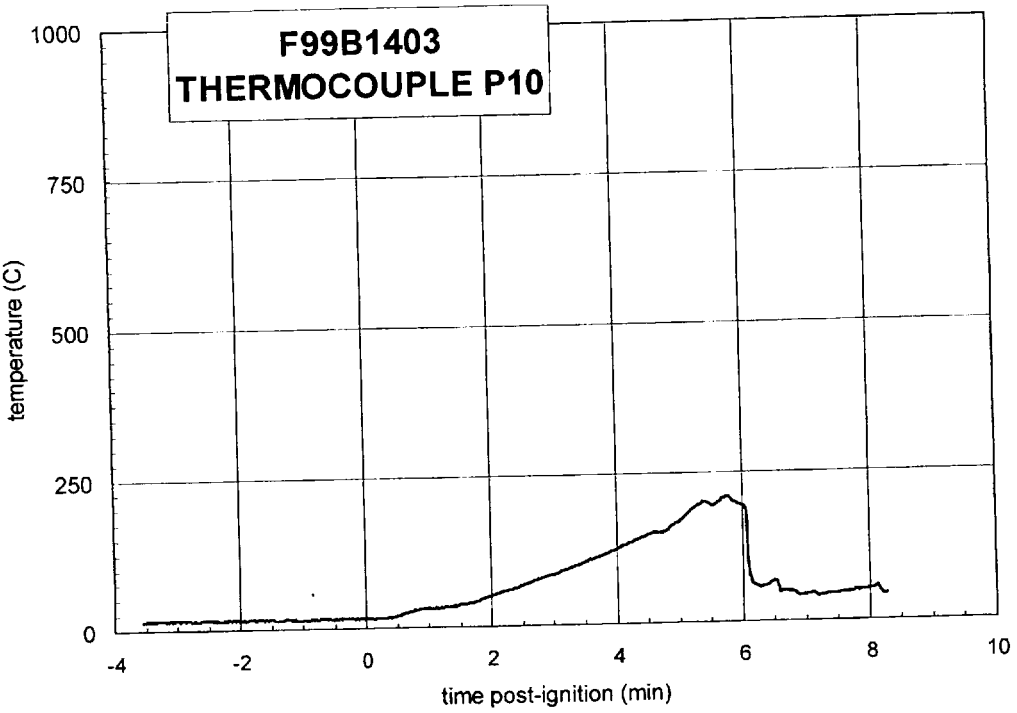

Plot F45. Fire Test F99B1403. Data plot from thermocouple P10.

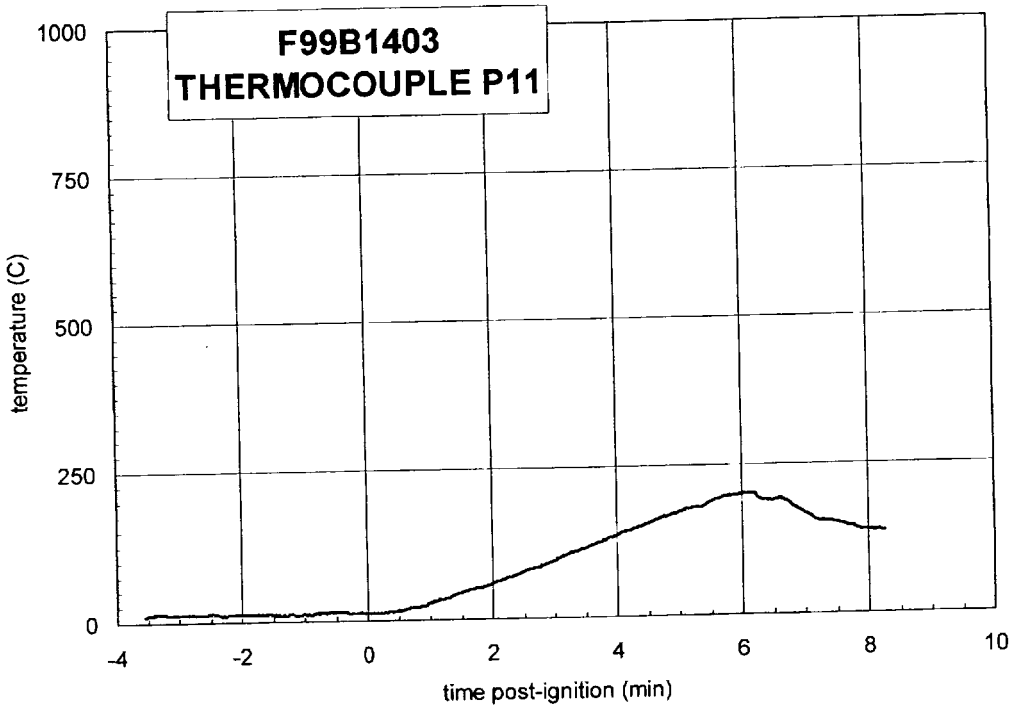

Plot F46. Fire Test F99B1403. Data plot from thermocouple P11.

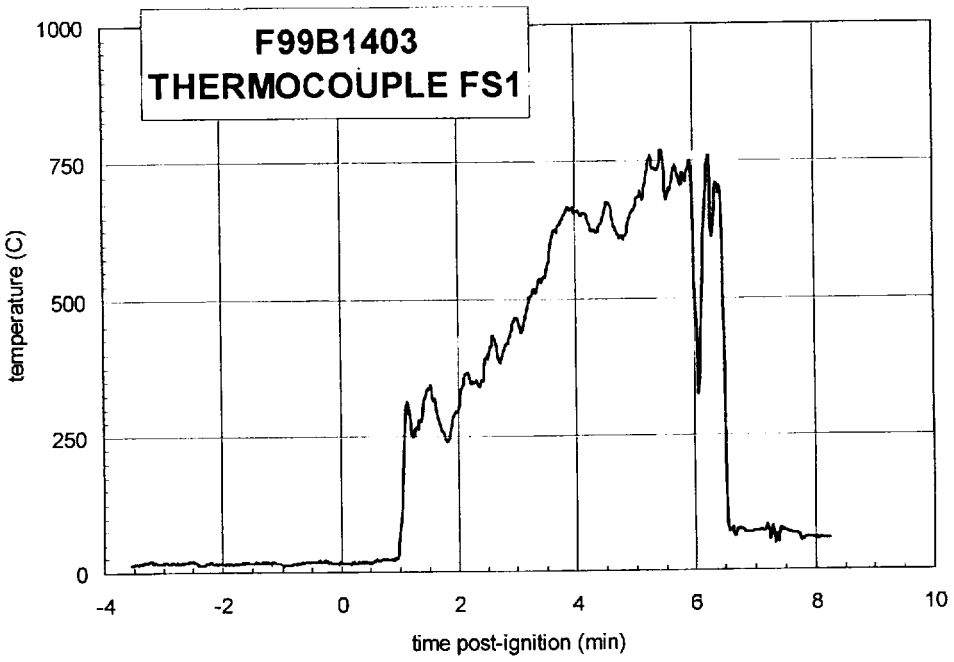

Plot F47. Fire Test F99B1403. Data plot from thermocouple FS1.

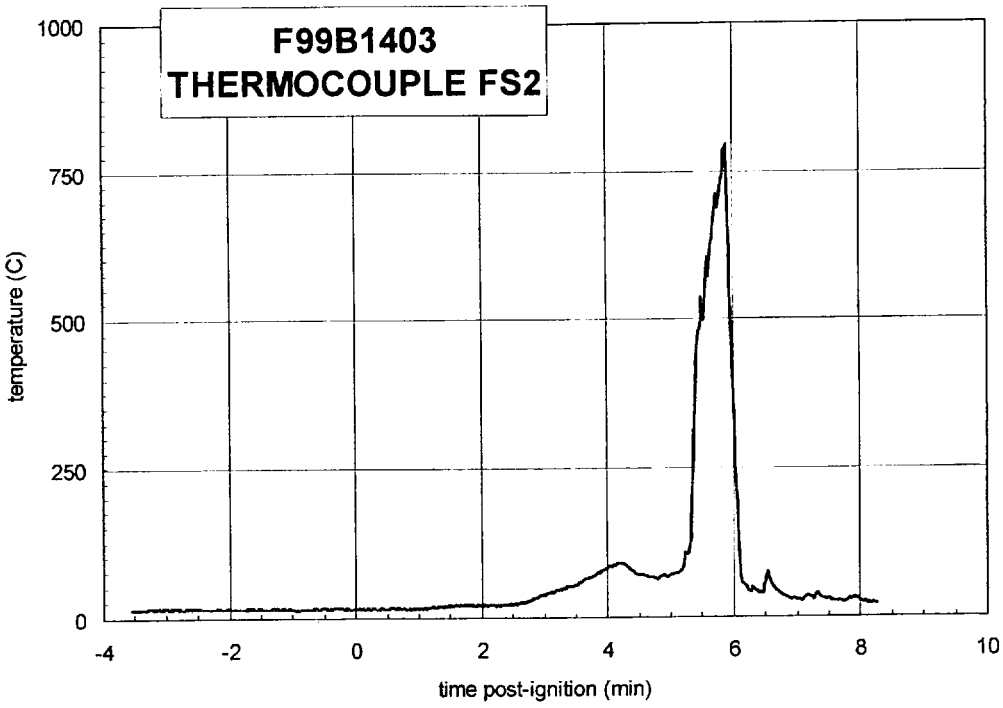

Plot F48. Fire Test F99B1403. Data plot from thermocouple FS2.

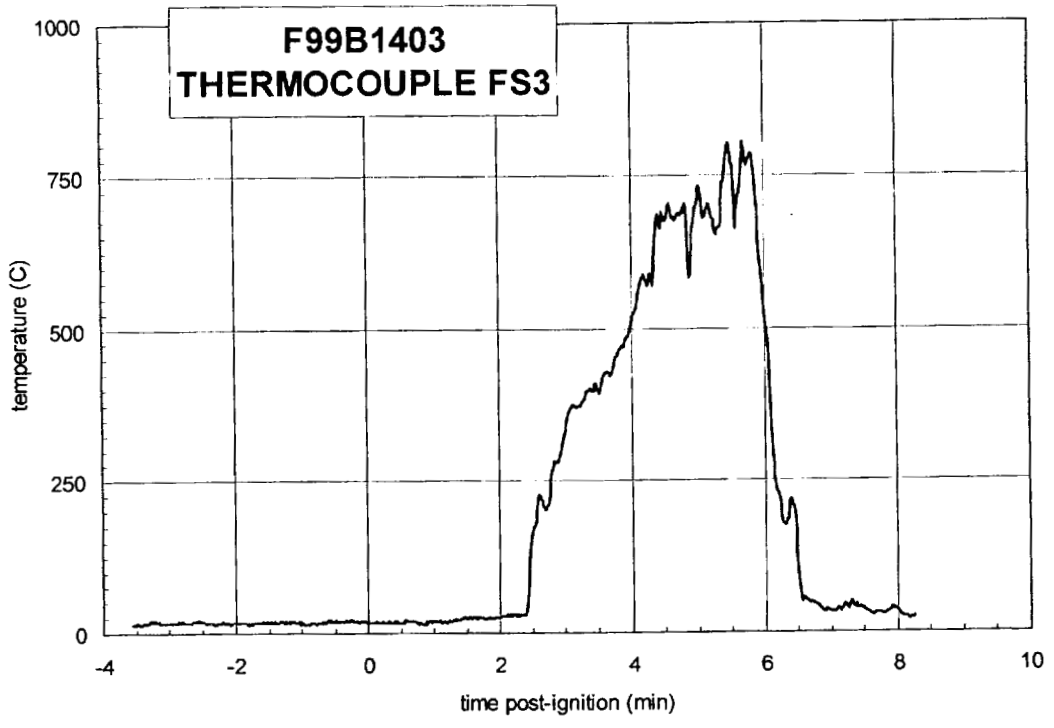

Plot F49. Fire Test F99B1403. Data plot from thermocouple FS3.

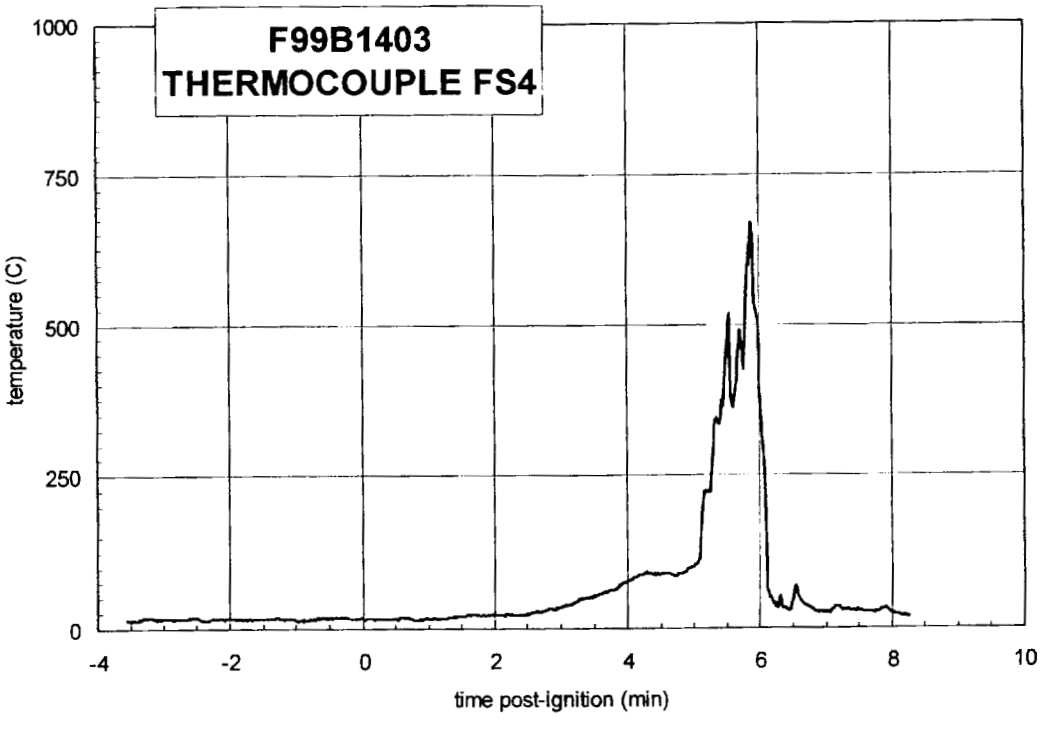

Plot F50. Fire Test F99B1403. Data plot from thermocouple FS4.

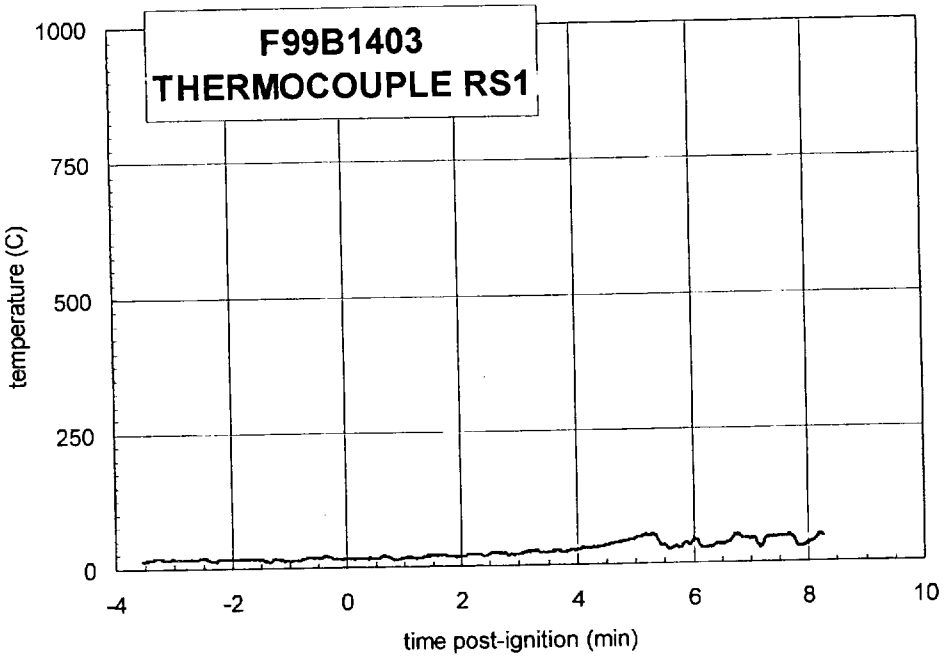

Plot F51. Fire Test F99B1403. Data plot from thermocouple RS1.

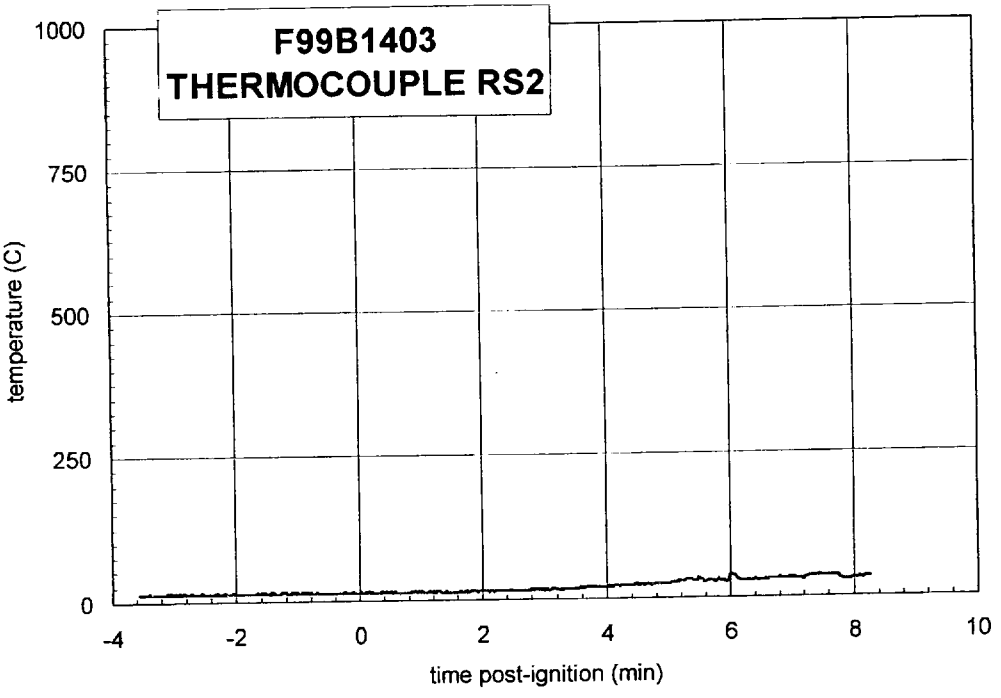

Plot F52. Fire Test F99B1403. Data plot from thermocouple RS2.

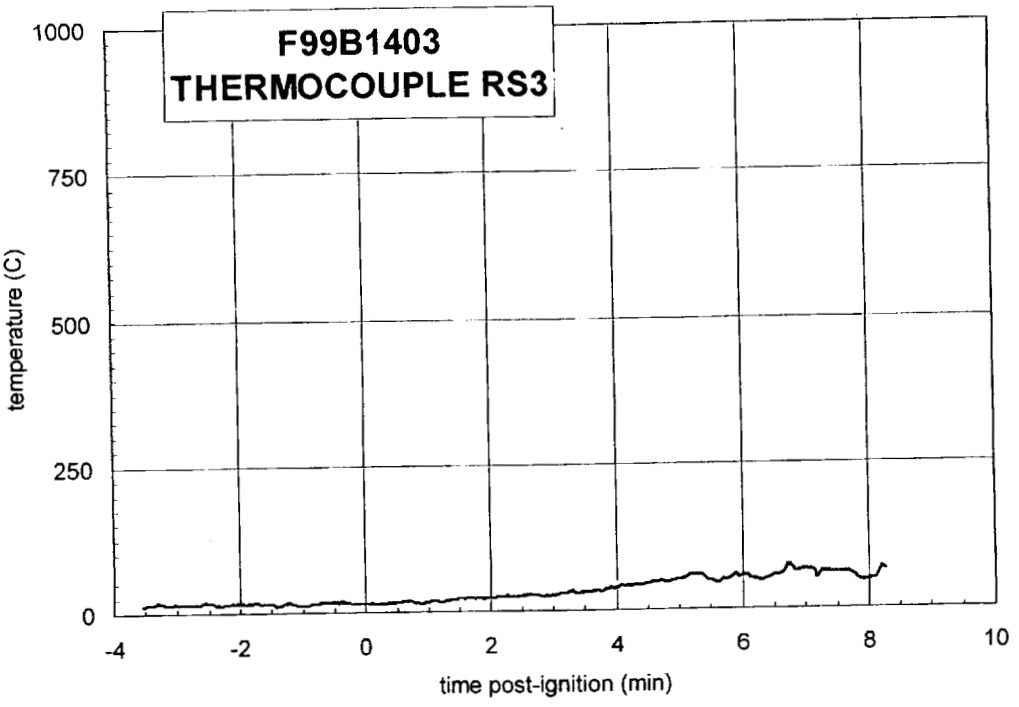

Plot F53. Fire Test F99B1403. Data plot from thermocouple RS3.

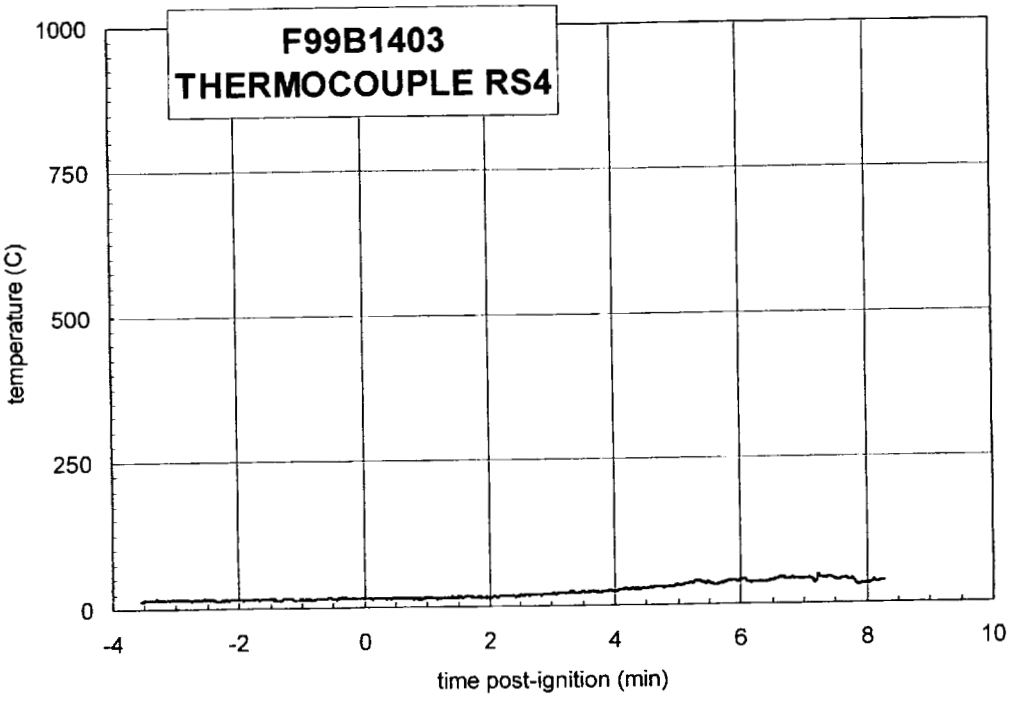

Plot F54. Fire Test F99B1403. Data plot from thermocouple RS4.

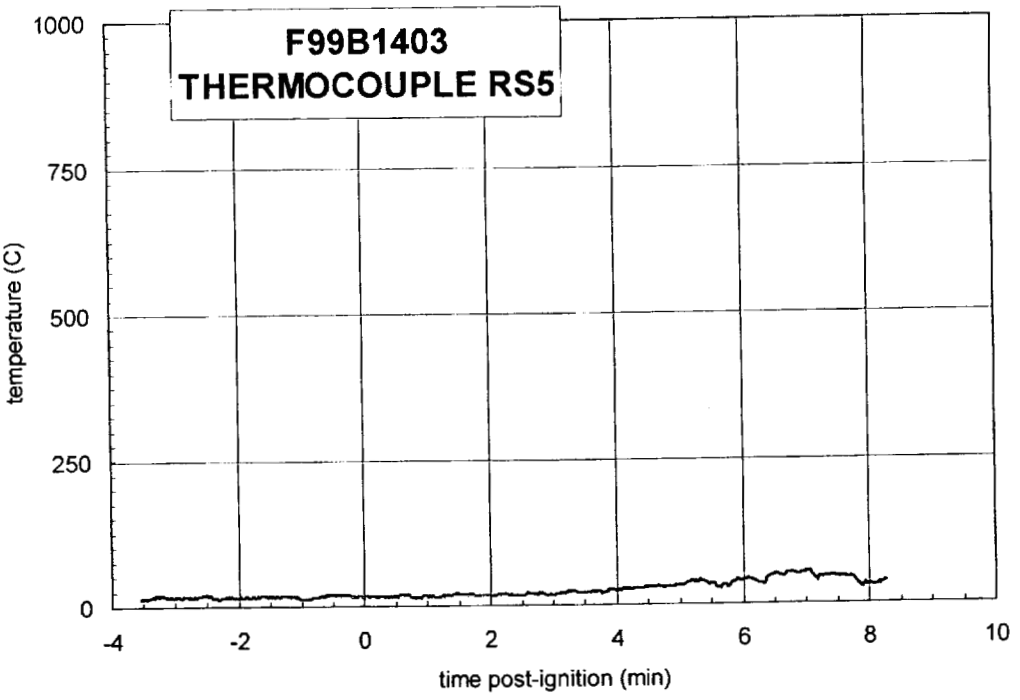

Plot F55. Fire Test F99B1403. Data plot from thermocouple RS5.

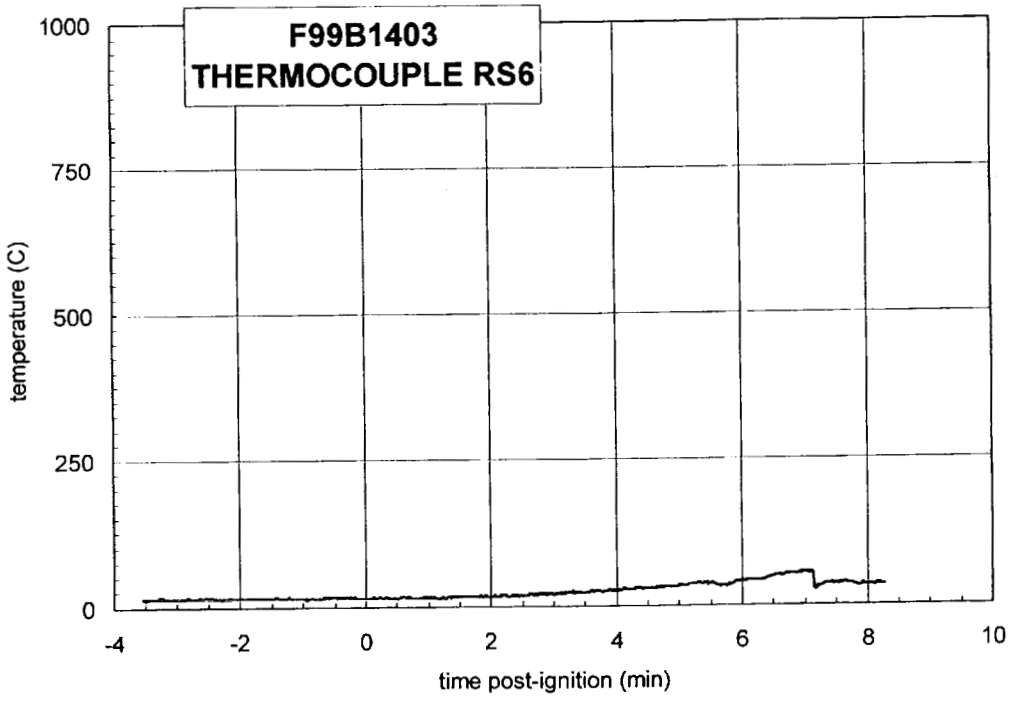

Plot F56. Fire Test F99B1403. Data plot from thermocouple RS6.

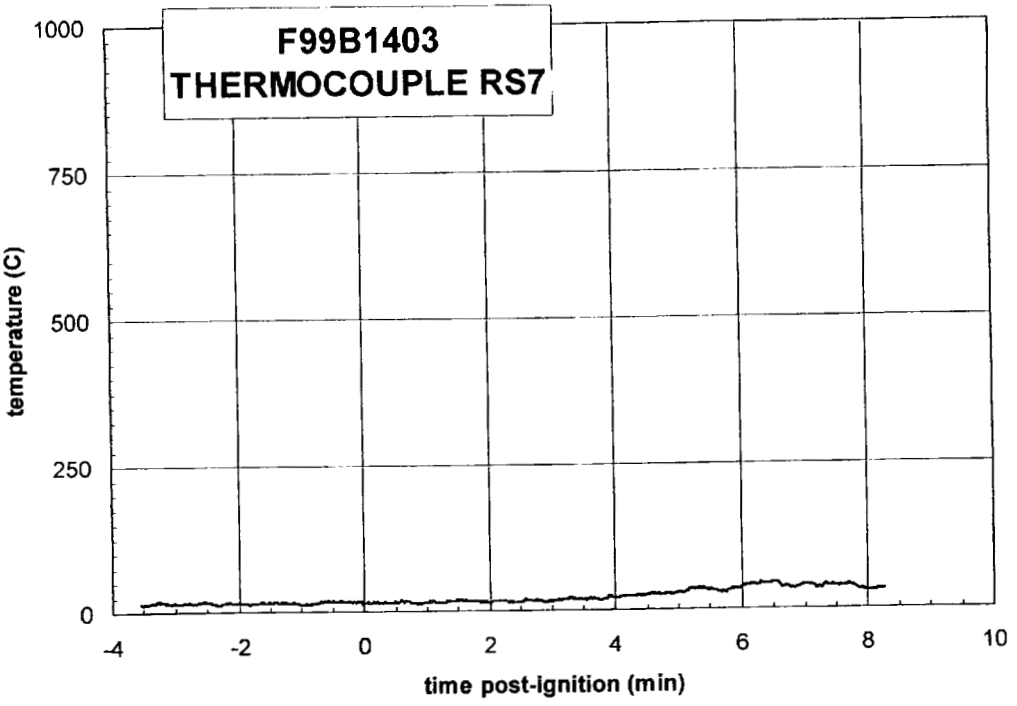

Plot F57. Fire Test F99B1403. Data plot from thermocouple RS7.

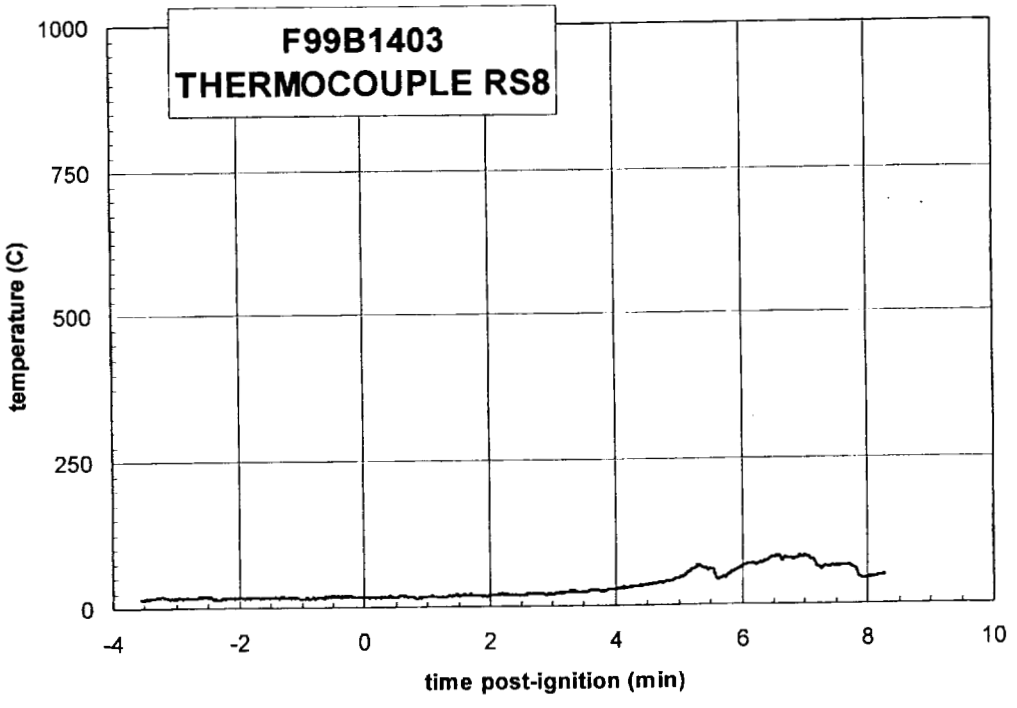

Plot F58. Fire Test F99B1403. Data plot from thermocouple RS8.

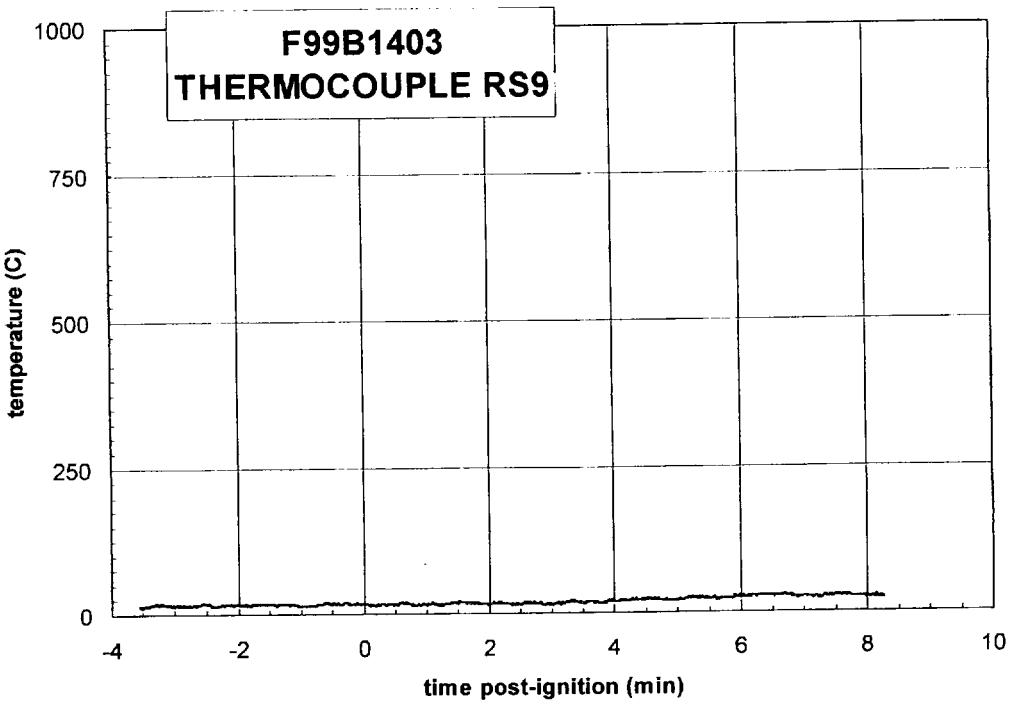

Plot F59. Fire Test F99B1403. Data plot from thermocouple RS9.

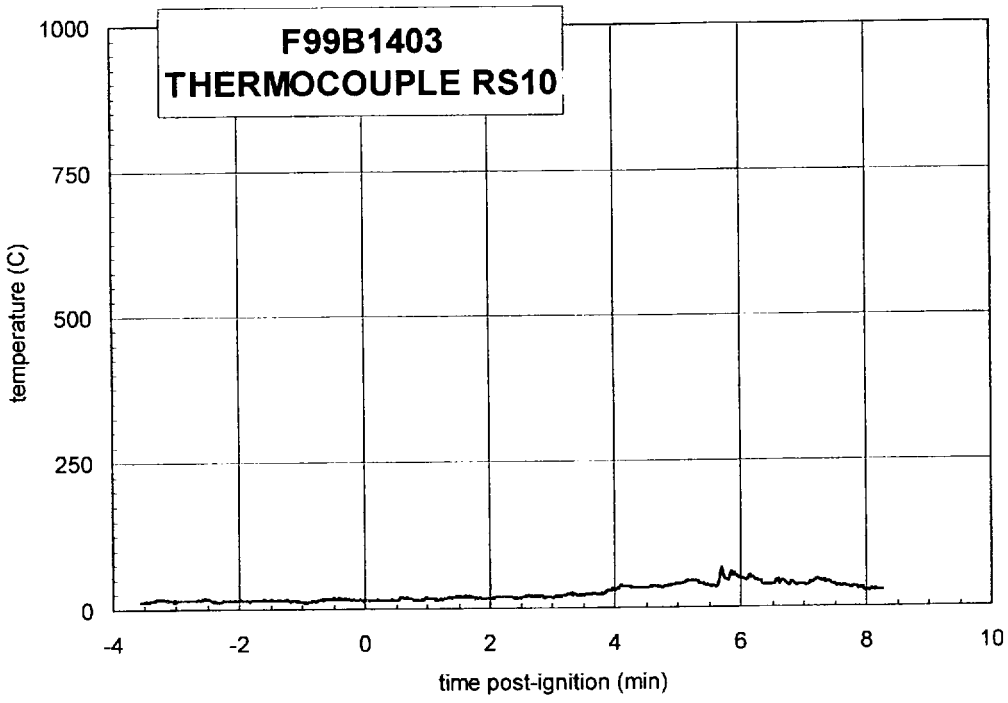

Plot F60. Fire Test F99B1403. Data plot from thermocouple RS10.

Appendix G

Fire Tests F99B1403 - Aspirated Thermocouple Data

One aspirated thermocouple assembly (Medtherm Corporation) was installed in the test vehicles (Fig. G1). The aspirated thermocouple assembly was fabricated from Inconel 600 tubing and consisted of a vertical manifold (o.d. = 0.375 in. (9.5 mm), i.d. = 0.25 in. (6.4 mm), length = 16 in. (406 mm)) with six horizontal radiation shields (o.d. = 0.25 in. (6.4 mm), i.d. = 0.19 in. (4.8 mm), length = 1.00 in. (25.4 mm)). The vertical spacing between the radiation shields along the manifold was 3 in. (75 mm). Three radial holes were drilled near the tip of each radiation shield. The holes were sized to approximately balance the airflow-rates over each thermocouple. A Type-N thermocouple inserted into each radiation shield so that the thermocouple junction was positioned approximately 0.2 in. (5.1 mm) down-stream from the inlet holes.

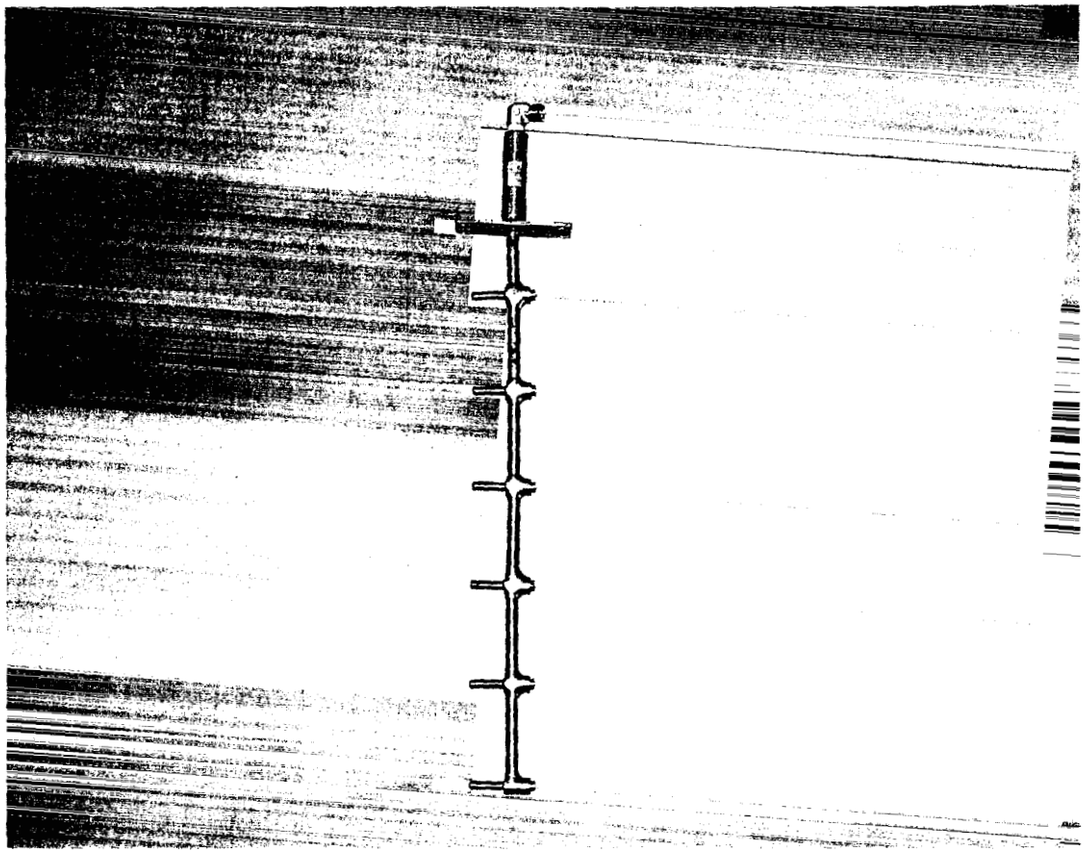

Figure G1. Fire Test F99B1403. Photograph of the aspirated thermocouple assembly used in the passenger compartment of the test vehicle.

The mounting flange of the aspirated thermocouple probe assembly was attached to the roof of the vehicle. The probe extended into the passenger compartment through a hole in the roof so that all 6 thermocouples were located below the headliner. The probe was vertical and located

along the longitudinal mid-line of the vehicle approximately equidistant from the A and B pillars. The upper-most aspirated thermocouple was approximately 0.5 in. (12 mm) below the lower surface of the headliner. The manifold was connected to a rotary-vane pump with flexible copper tubing (o.d. = 0.5 in. (12 mm), length = 15 ft. (4.6 m)). The capacity of the pump was 50 L/min at atmospheric pressure.

Figures G2 and G3 show the approximate location of the aspirated thermocouple probe assembly in the test vehicle for this test.

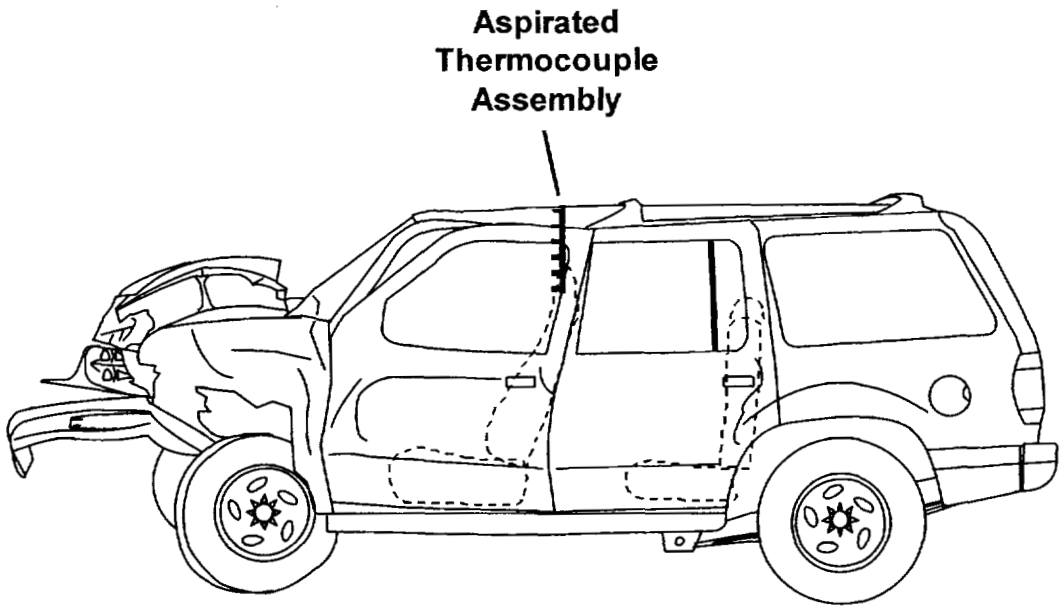

Figure G2. Fire Test F99B1403. Side view of the test vehicles showing the approximate location of the aspirated thermocouple probe assembly in the passenger compartment.

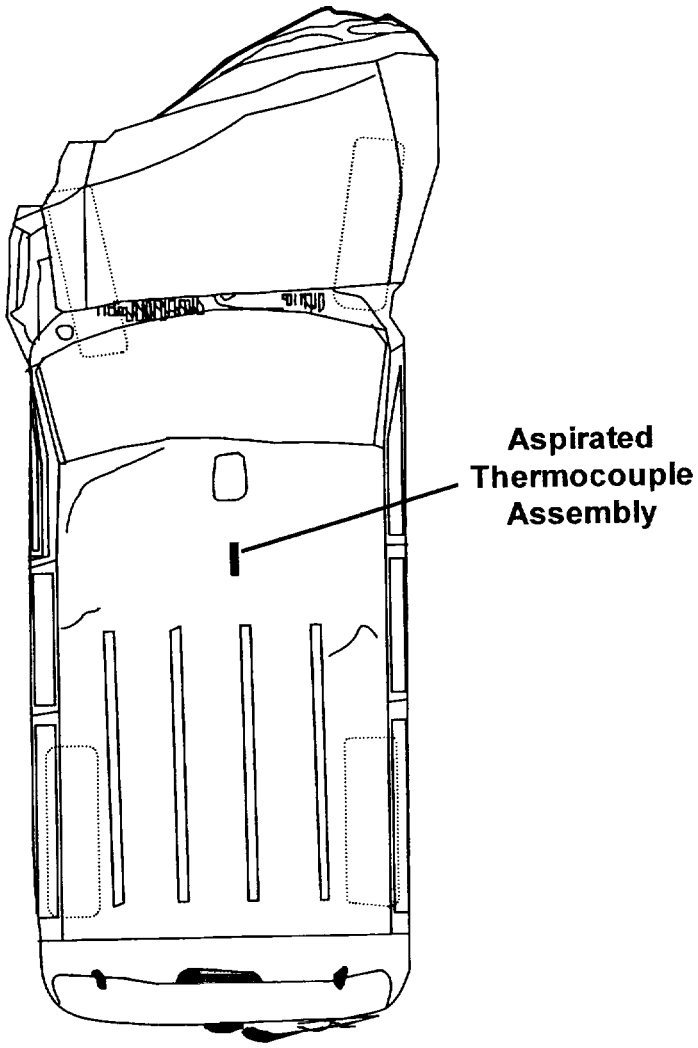

Figure G3. Fire Test F99B1403. Top view of the test vehicles showing the approximate location of the aspirated thermocouple probe assembly in the passenger compartment.

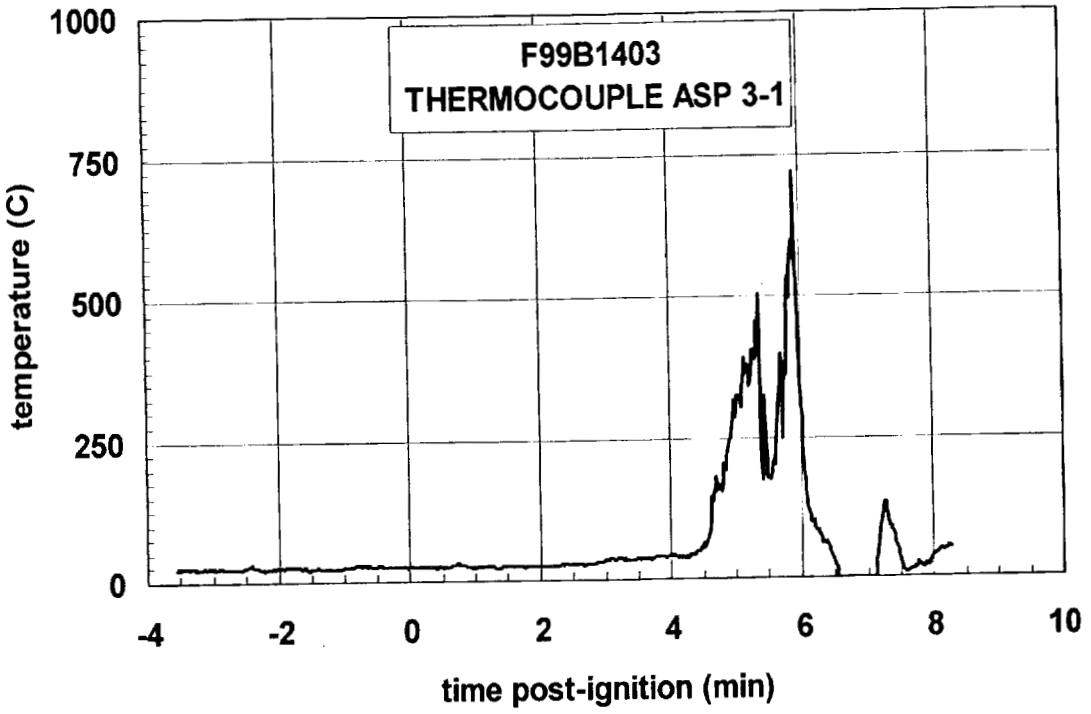

Plot G1. Fire Test F99B1401. Data plot from thermocouple ASP 3 - 1.

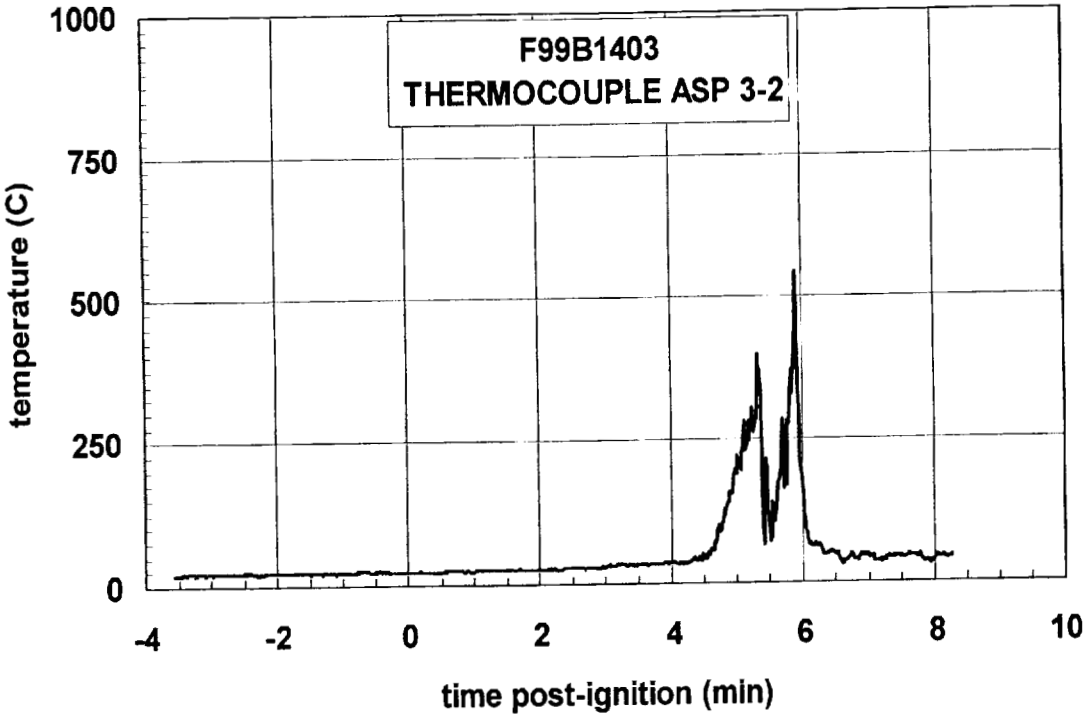

Plot G2. Fire Test F99B1402. Data plot from thermocouple ASP 3 - 2.

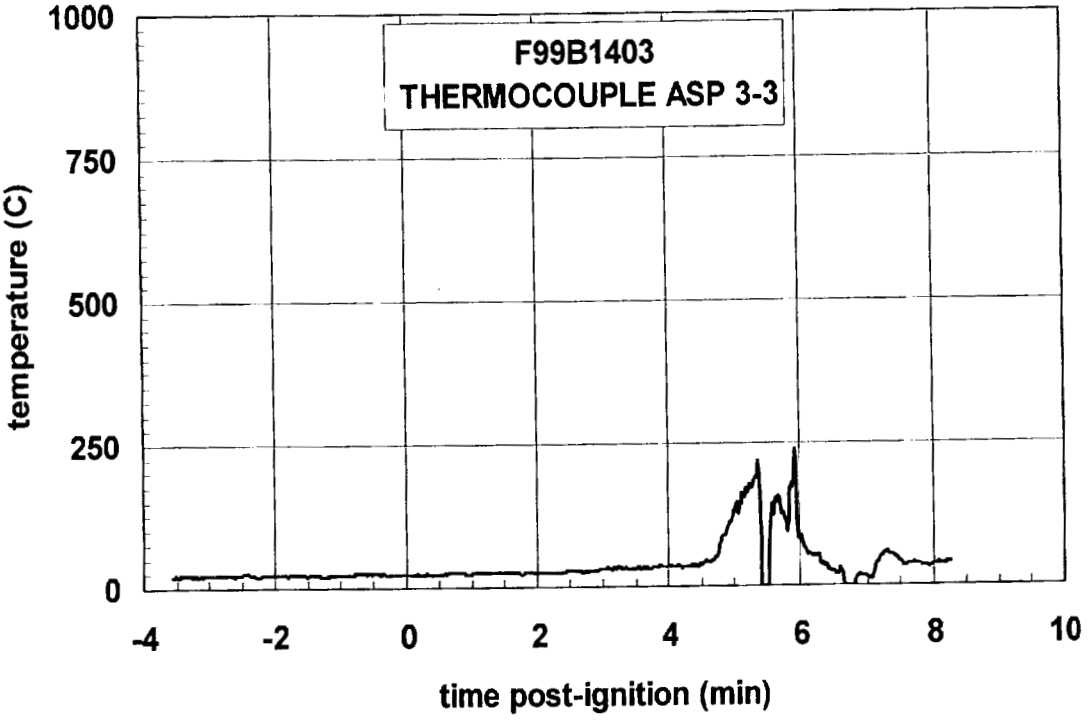

Plot G3. Fire Test F99B1401. Data plot from thermocouple ASP 3 - 3.

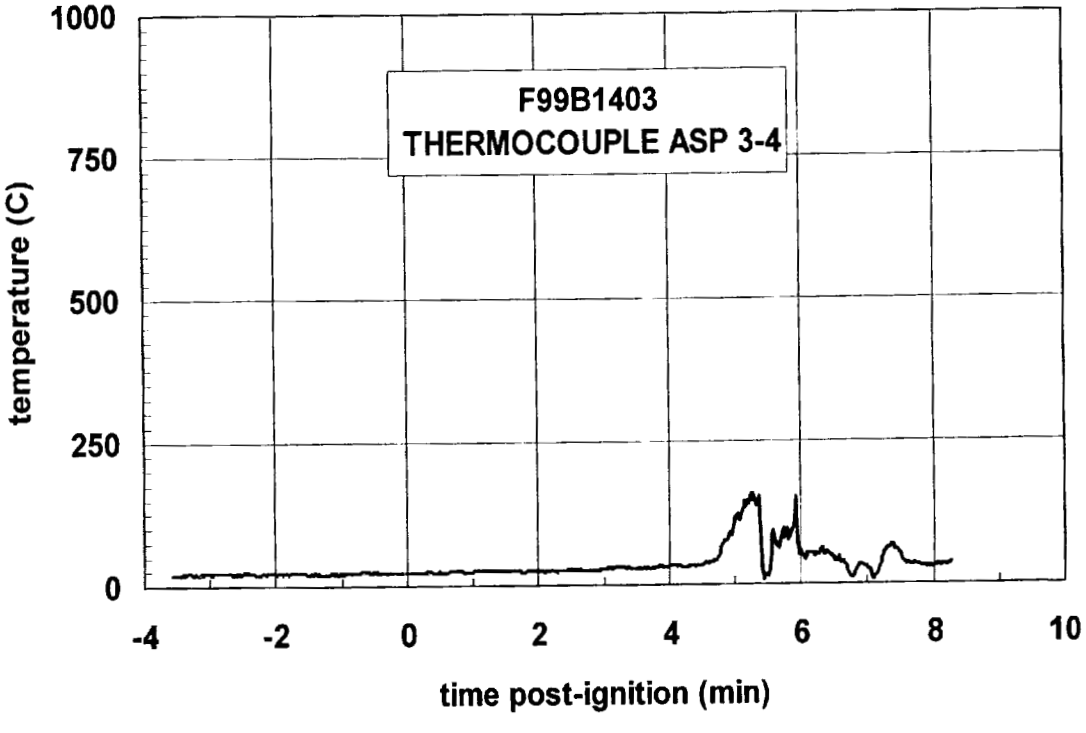

Plot G4. Fire Test F90B1402. Data plot from thermocouple ASP 3 - 4.

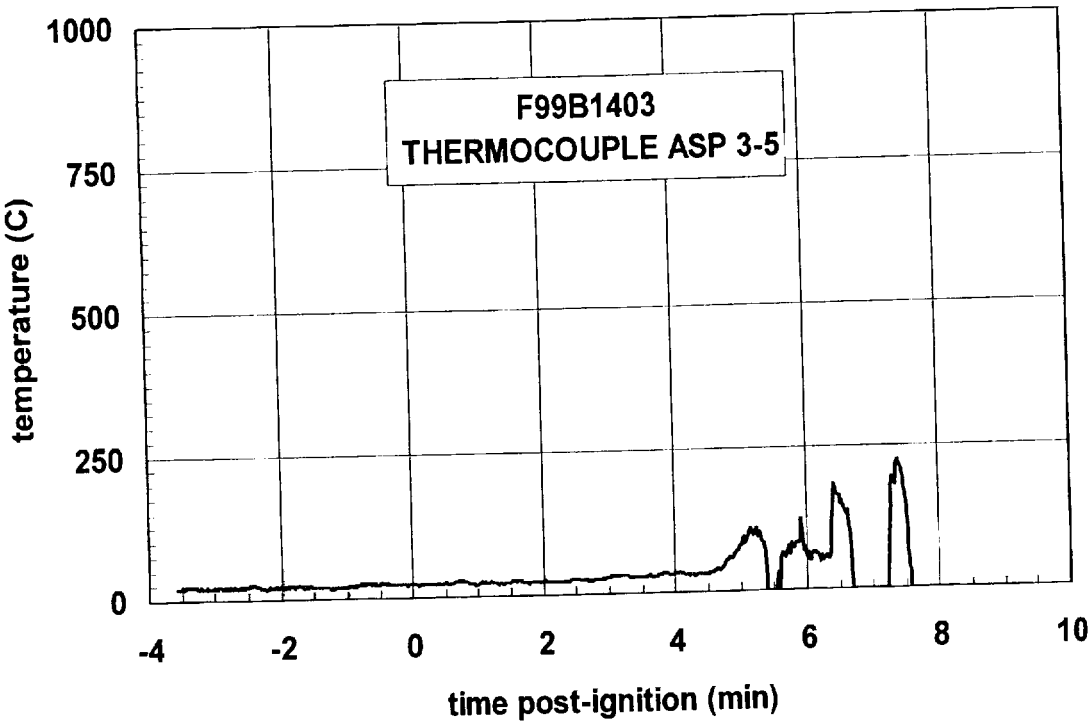

Plot G5. Fire Test F99B1401. Data plot from thermocouple ASP 3 - 5.

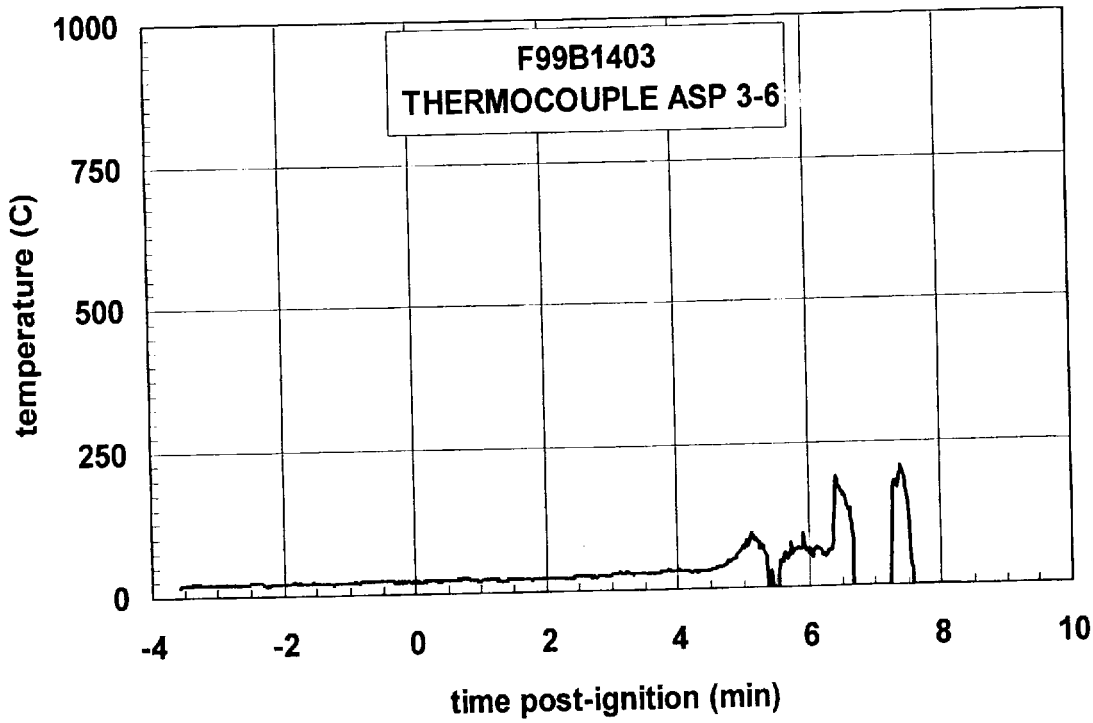

Plot G6. Fire Test F99B1402. Data plot from thermocouple ASP 3 - 6.

Appendix H

Fire Test F99B1403 - Heat Flux Transducer/Radiometer Data

A single heat-flux transducer (64 Series, Medtherm Corporation) was used to measure the heat flux to the floor pan of the test vehicle. This transducer consisted of a Schmidt-Boelter thermopile in a water-cooled copper body (diameter = 1 in. (25.4 mm), length = 1 in. (25.4 mm)). The face of the heat flux transducers was coated with high-temperature optical black paint. This transducer was calibrated to 100 kW/m^2 at a reference temperature of 80°C.

Four heat flux transducer/radiometer assemblies were used to measure the convective and radiative heat flux to four locations in the passenger comarptment. Each of these transducers contained two Schmidt-Boelter thermopiles in a water-cooled copper body (diameter = 1 in. (25.4 mm), length = 1 in. (25.4 mm)). The faces of the heat flux transducers were coated with high-temperature optical black paint. The radiometers had removable zinc selinide (ZnSe) windows (view-angle = 150°; optical transmittance range 0.4 to 4.2 μm). The HFTs and RADs in these assemblies were calibrated to 10 kW/m^2 at a reference temperature of 80°C.

The PC-based data system used to acquire data from the thermocouples (**APPENDIX H**) also was used to acquire data from the heat flux transducers and radiometers. The electrical signal wires from these transducers terminated in a 5-pin circular connector (165 Series, Amphenol). Each connector was plugged into a panel-mounted jack, which was hard wired to an analog-input multiplex expansion card (DBK-12, IOTech, Inc., Cleveland, OH). As with the thermocouples, the electrical shields on the signal cables were connected to the electronic chassis grounds on the analog-input expansion cards. The data acquisition software (DASYLab) was configured to sample each channel at a rate of 10 Hz and store the data in 10-point block averages.

Figures H1 and H2 show the approximate locations of heat flux transducer and heat flux transducer/radiometer assemblies in the test vehicle. HFT 1 was inserted through a clearance hole cut into the floor panel. The transducer face was flush with the lower surface of the floor panel. HTF/RAD10 were located approximately 30 cm above the left rear seat cushion facing downward. HFT/RAD12 was located approximately 30 cm above the above the left rear seat facing right. HFT/RAD 14 was located approximately 30 cm above the left front seat facing downward. HFT/RAD15 was located approximately 30 cm above the left front seat cushion facing upward. HTF/RAD10, HFT/RAD12, HFT/RAD 14, and HFT/RAD15 were mounted to threaded rods (diameter = ½ in.) inserted through holes drilled in the roof. The lower ends of each rod were secured to the seat cushion to stabilize the transducers during the test. Copper tubing (o.d. = 0.25 in. (6.4 mm)) was used for the cooling water supply and waste lines. The temperature of the water supplied to the HFT and HFT/RAD assemblies was approximately 80°C, and the flow rate of water through each body was approximately 100 mL/min. Thermocouples

O10, O12, O14 and O15 were located in the bodies of HFT/RAD10, HFT/RAD12, HFT/RAD14 and HFT/RAD15, respectively.

Data recorded from these transducers is shown in Plots J1 through J8.

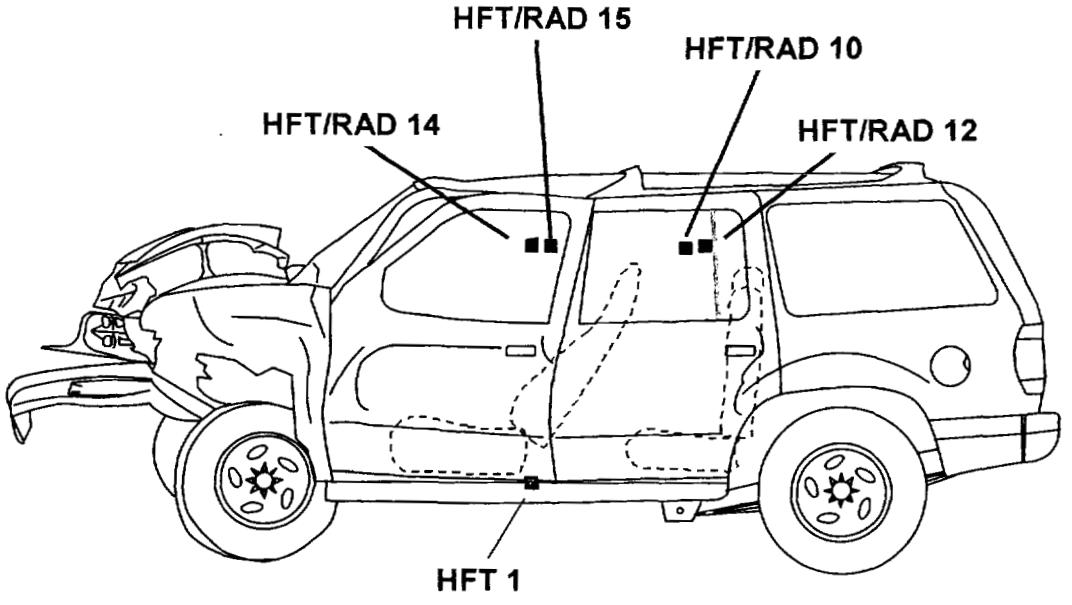

Figure H1. Fire Test F99B1403. Side view showing the approximate locations of heat flux transducer (HFT) and heat flux transducer/radiometer (HFT/RAD) assemblies in the test vehicle.

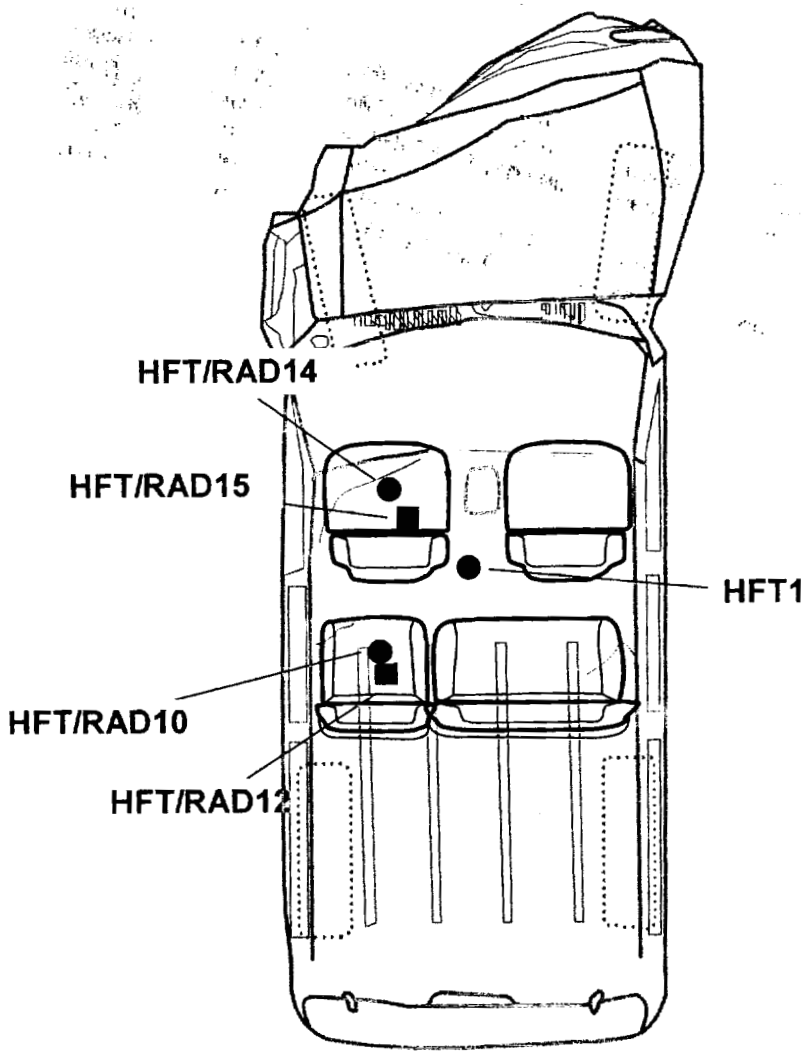

Figure H2. Fire Test F99B1403. Top view showing the approximate locations of heat flux transducer (HFT) and heat flux transducer/radiometer (HFT/RAD) assemblies in the test vehicle.

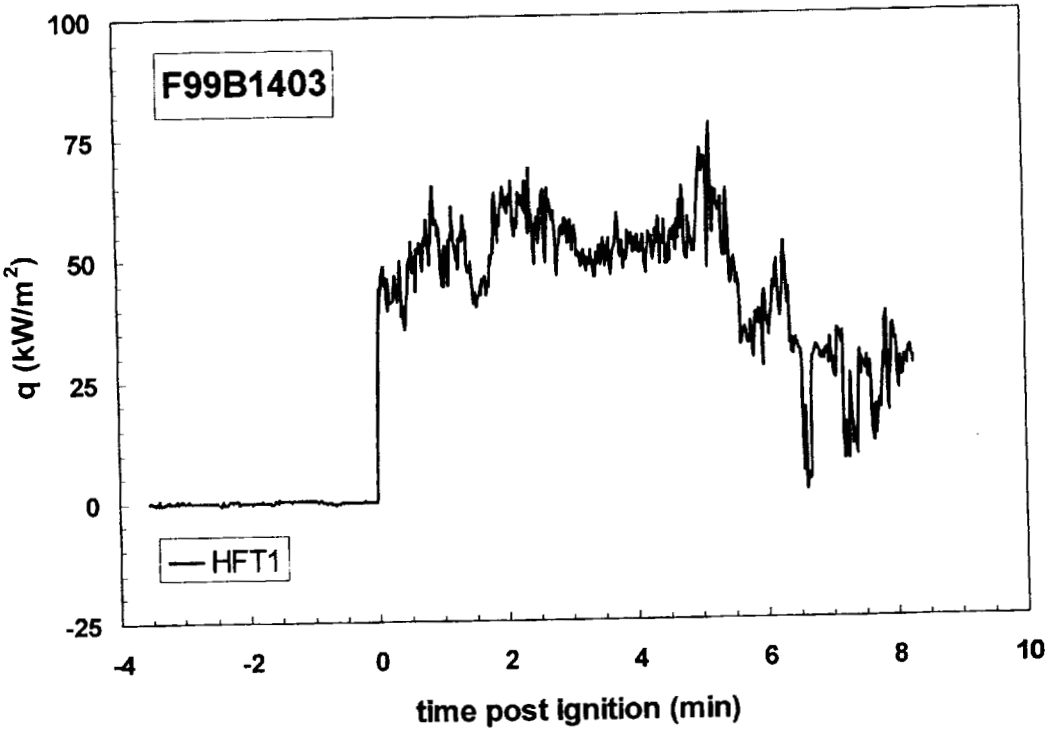

Plot H1. Fire Test F999B1403. Data plot from Heat Flux Transducer 1.

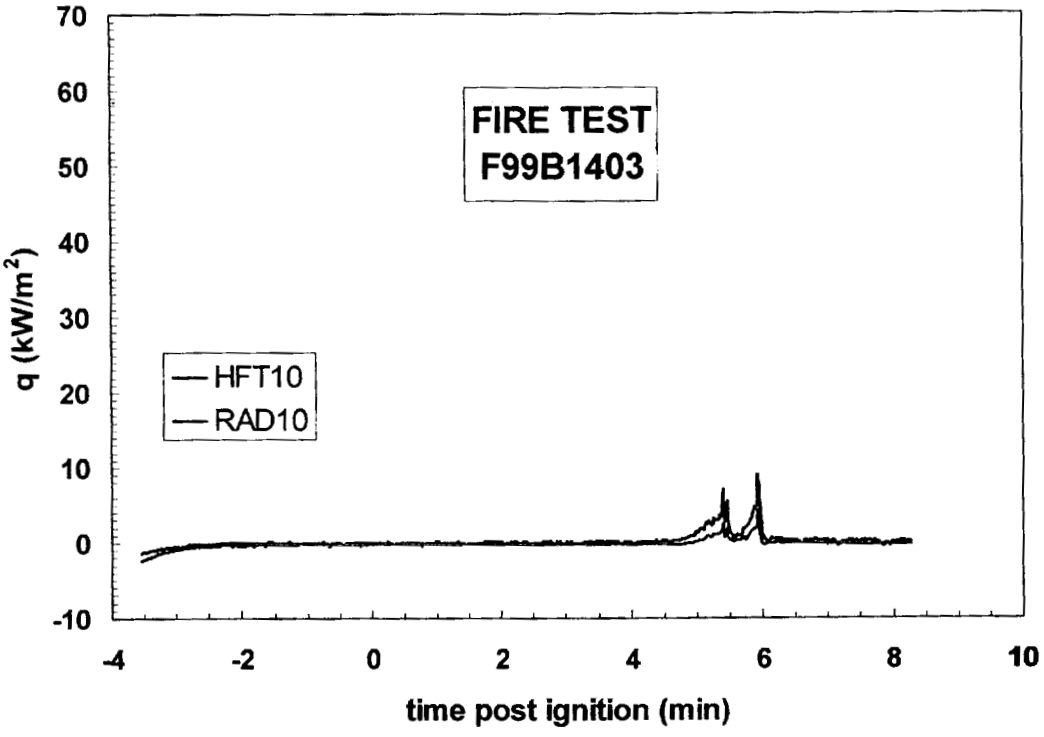

Plot H2. Fire Test F99B1403. Data plot from Heat Flux Transducer 10 and Radiometer 10.

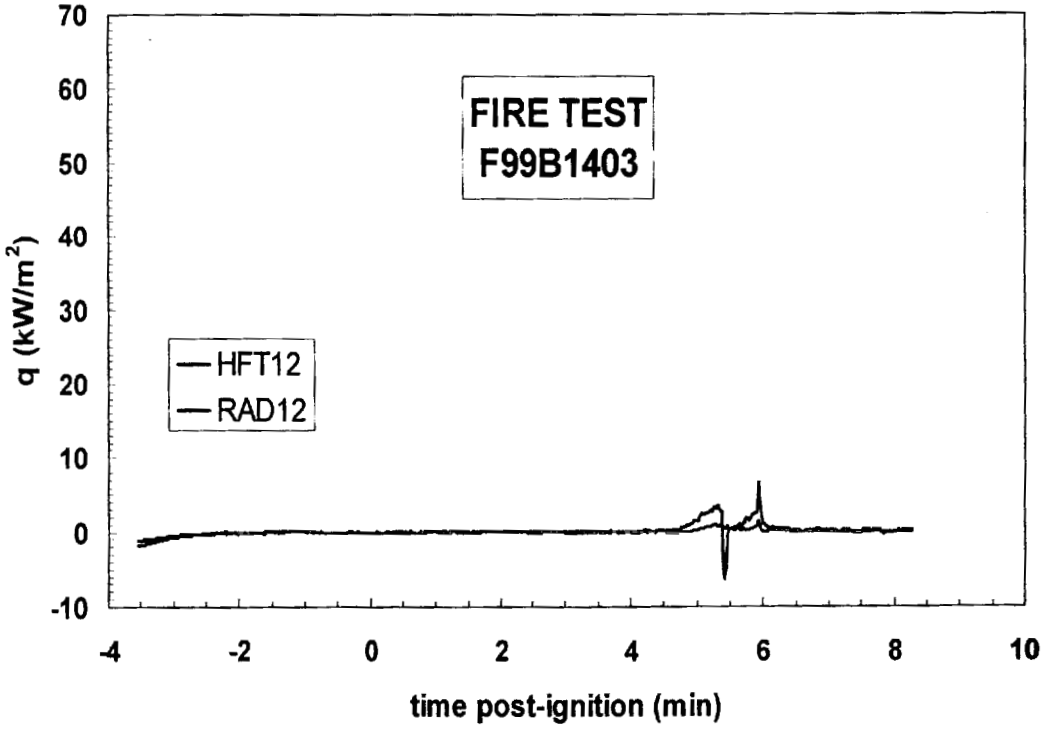

Plot H3. Fire Test F99B1403. Data plot from Heat Flux Transducer 12 and Radiometer 12.

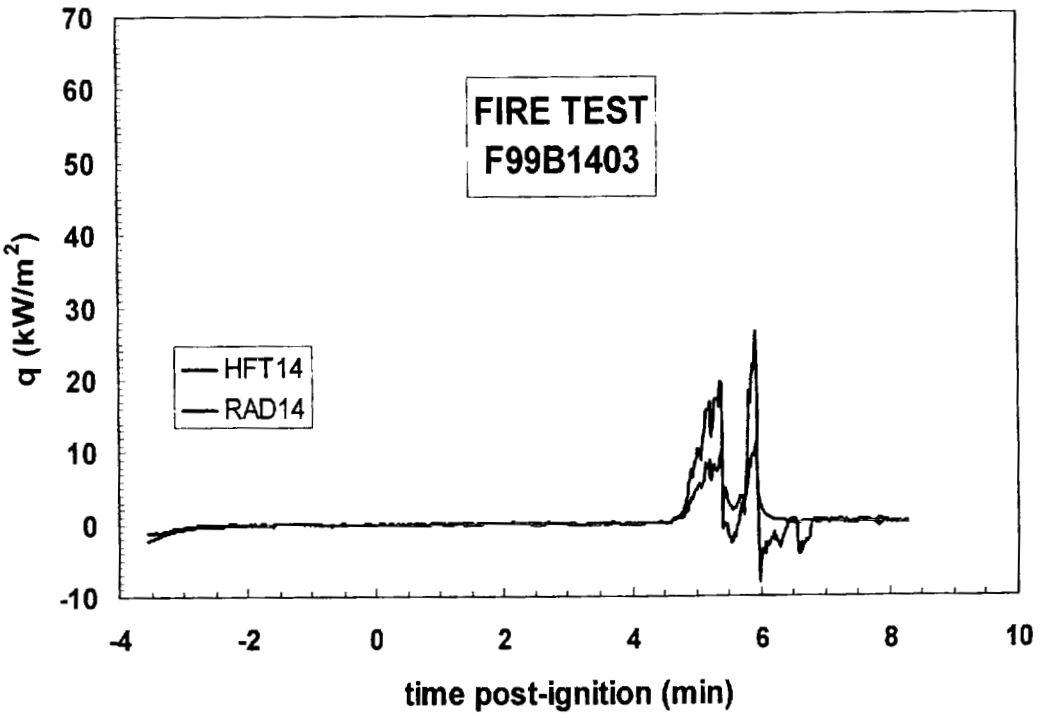

Plot H4. Fire Test F99B1403. Data plot from Heat Flux Transducer 14 and Radiometer 14.

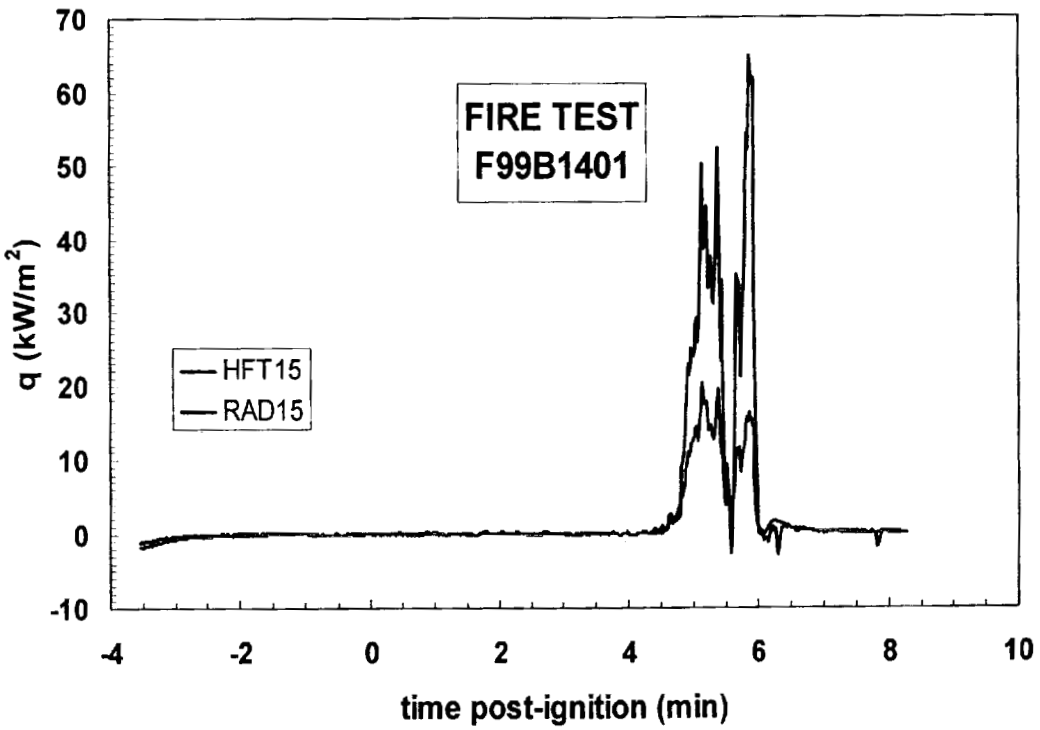

Plot H5. Fire Test F99B1403. Data plot from Heat Flux Transducer 15 and Radiometer 15.

Appendix I

Fire Test F99B1403 – Fourier Transform Infrared Spectroscopy Gas Analysis Data

The sampling-line for FTIR analysis consisted of a stainless-steel tube (o.d. = 0.250 in. (6.4 mm), i.d. = 0.125 in. (3.2 mm), l = 20 ft (6.1 m)) inserted through the roof between the front seats along the longitudinal midline of the test vehicle (Fig.'s I1 and I2). The inlet of the sample-tube extended approximately 10 in. below the headlining (Fig.'s I1 and I2). The tube was not heated. The outlet of the sample tube was connected to a heated Teflon® transfer-line (o.d. = 0.250 in. (6.4 mm), i.d. = 0.125 in. (3.2 mm), l = 75 ft. (23 m)), which was connected to the gas cell of the FTIR spectrometer. The transfer-line was heated to 105°C during the test to prevent condensation of water and water-soluble gases (*e.g.*, HCl, HCN, NO, and NO_2). An in-line stainless steel filter holder containing a quartz fiber filter (o.d. = 47 mm) was placed between the sample-tube and the transfer-line to prevent smoke particles from contaminating analytical instrumentation.

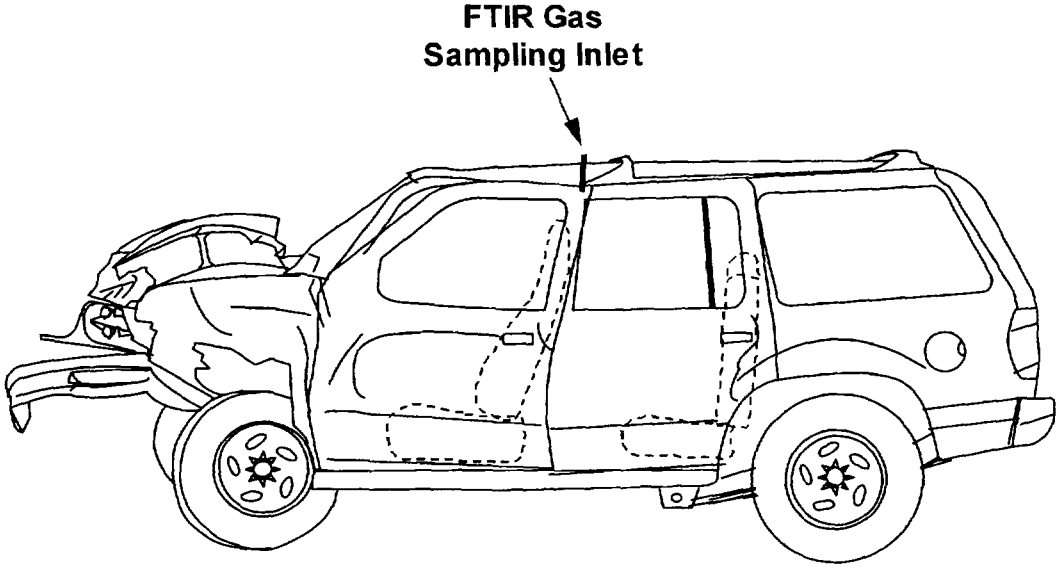

Figure I1. Fire Test F99B1403. Side-view of the test vehicle show the approximate location of the FTIR gas-sampling inlet in the passenger compartment.

The FTIR spectrometer was a Model I-1000 Series FTIR Spectrometer (MIDAC Corporation, Riverside, California), with a KBr beam-splitter; a liquid nitrogen-cooled Mercury-Cadmium-Telluride detector; and gold-surfaced aluminum optics. This instrument was fitted with a stainless steel, multiple-reflectance gas cell (path length = 10 m) with zinc selenide windows. The gas cell was heated to 105°C. The optical bench was filled with clean, dry argon and hermetically sealed. The usable spectral range of this instrument was approximately 7400-700 cm^{-1}. Pressure in the gas cell during the fire tests was measured with a Baratron pressure gauge (MKS Instruments, Burlington, MA). The spectrometer was operated at a spectral resolution of 0.5 cm^{-1}.

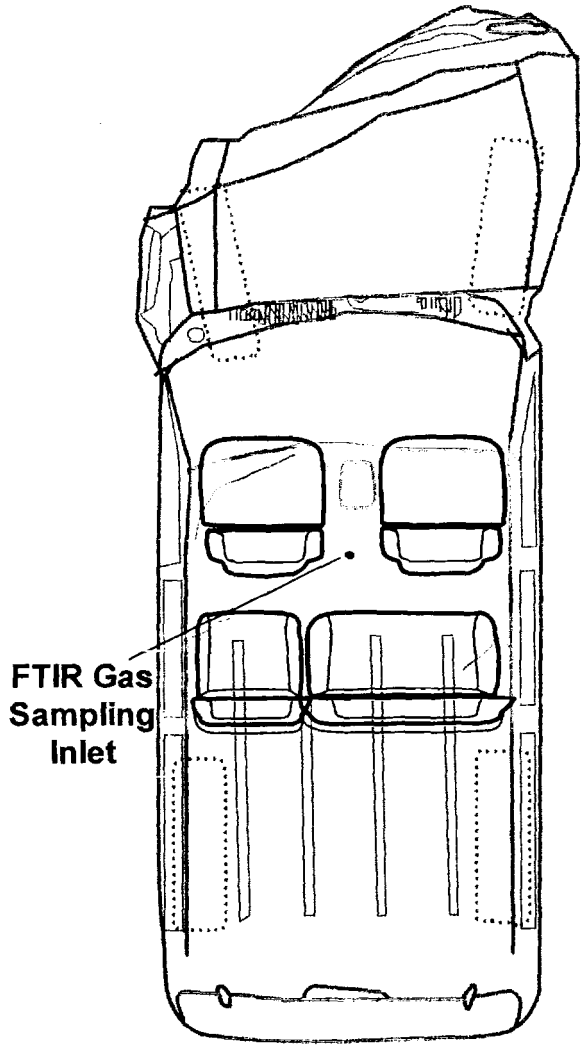

Figure I2. Fire Test F99B1403. Top view of the test vehicle showing the approximate location of the FTIR gas sampling inlet in the passenger compartment.

The sampling line and gas cell were equilibrated to a temperature of 105°C for at least 60 minutes before sample acquisition. A reference spectrum was acquired while the gas cell was evacuated. During the fire tests, the gas cell was purged continuously with air withdrawn from the passenger compartment at a flow rate of 7 L/min. Single-scan absorbance spectra were acquired and stored to disk at intervals of 10 s. After the test, the stored spectra were analyzed using the quantitative analysis software provided by the instrument manufacturer (AutoQuant, MIDAC). This software uses a Classical Least Squares algorithm to determine gas concentrations. The method developed for analysis of combustion gases was calibrated with gas standards (Scott Specialty Gases, Inc., Troy, MI). The standards were either NIST-traceable or produced by a gravimetric blending process.

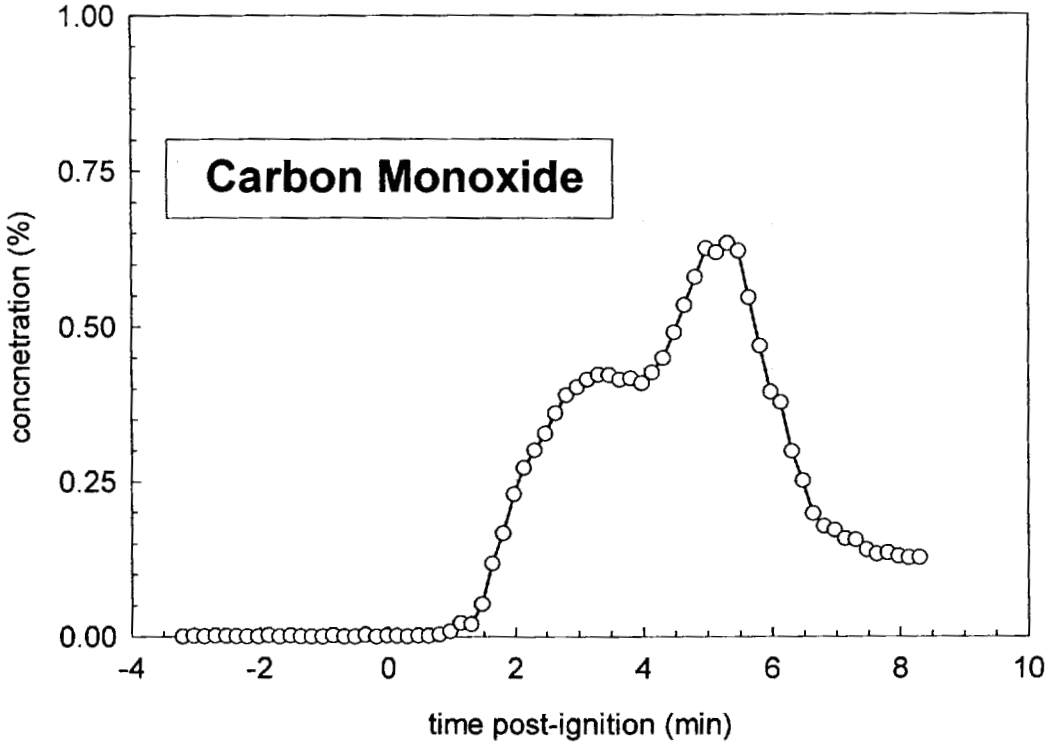

Plot I1. Fire Test F99B1403. Concentration of carbon monoxide (CO) in the passenger compartment determined by FTIR analysis.

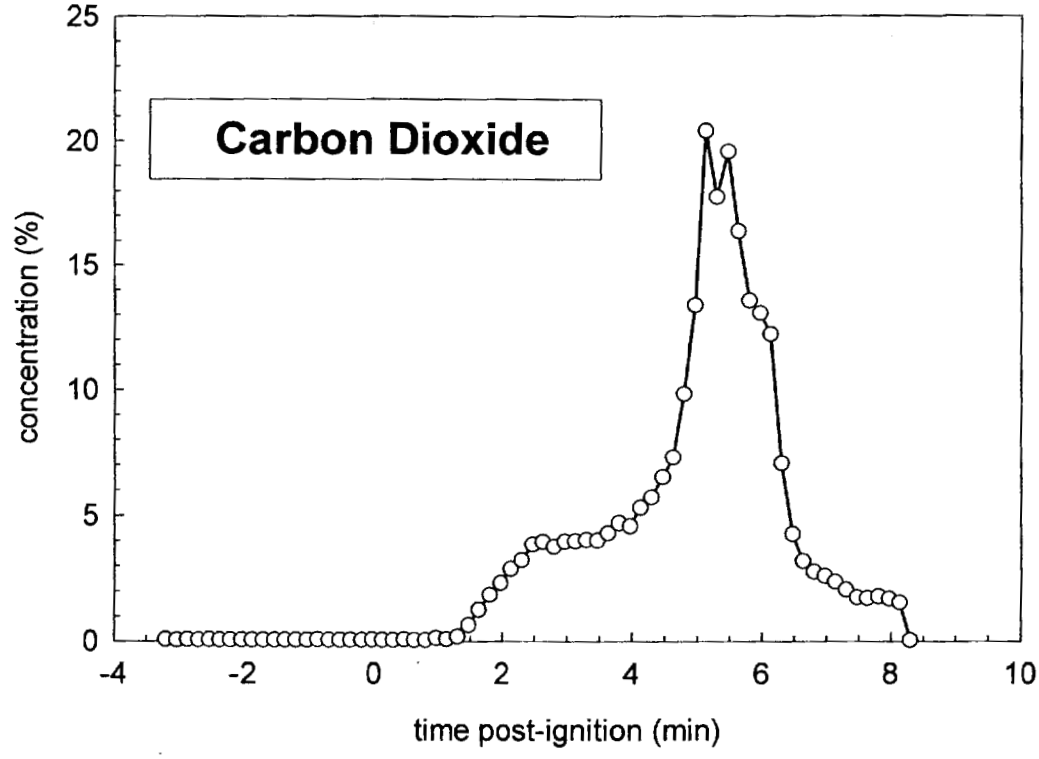

Plot I2. Fire Test F99B1403. Concentration of carbon dioxide (CO_2) in the passenger compartment determined by FTIR analysis.

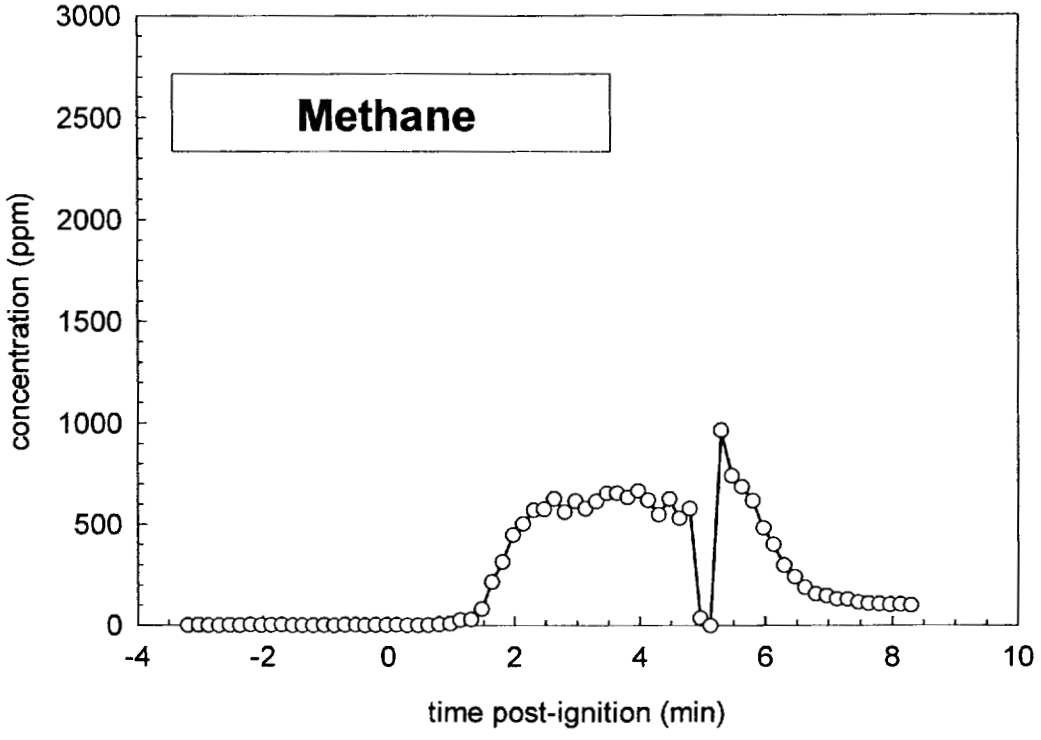

Plot I3. Fire Test F99B1403. Concentration of methane (CH_4) in the passenger compartment determined by FTIR analysis.

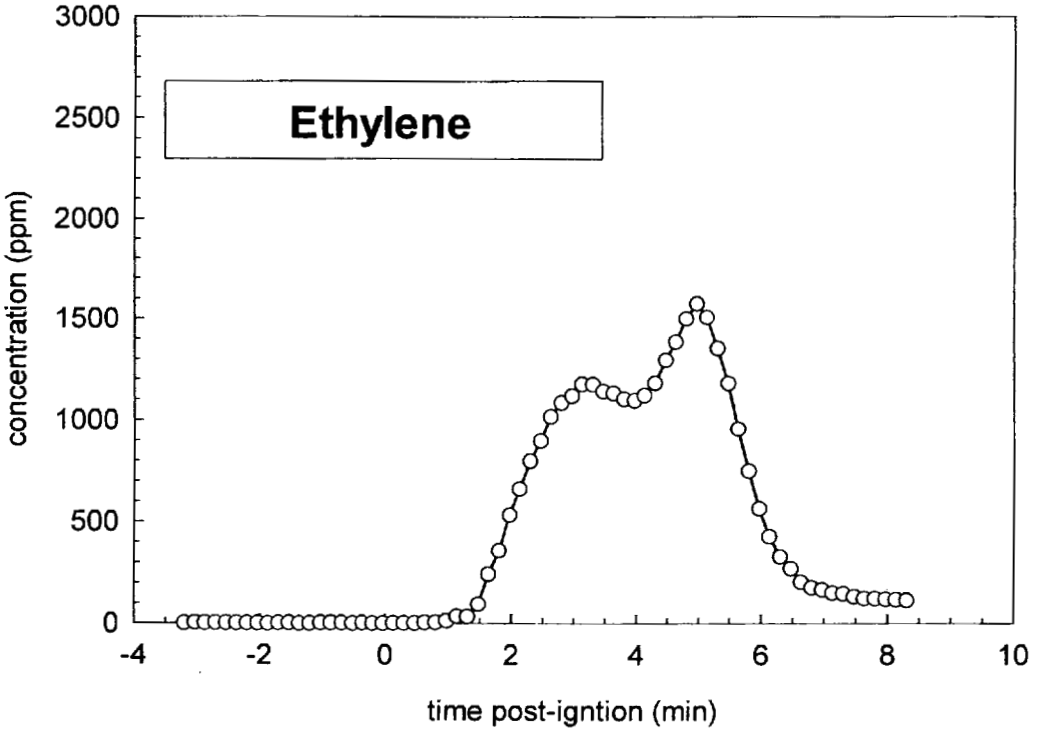

Plot I4. Fire Test F99B1403. Concentration of ethylene (C_2H_4) in the passenger compartment determined by FTIR analysis.

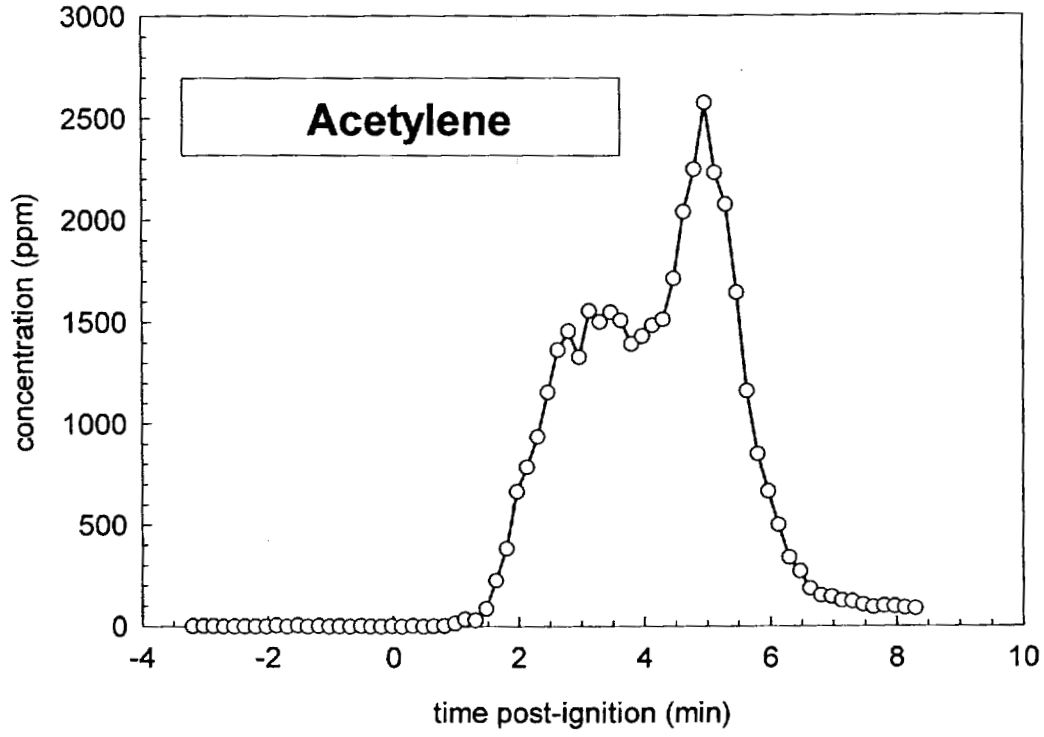

Plot I5. Fire Test F99B1403. Concentration of acetylene (C_2H_2) in the passenger compartment determined by FTIR analysis.

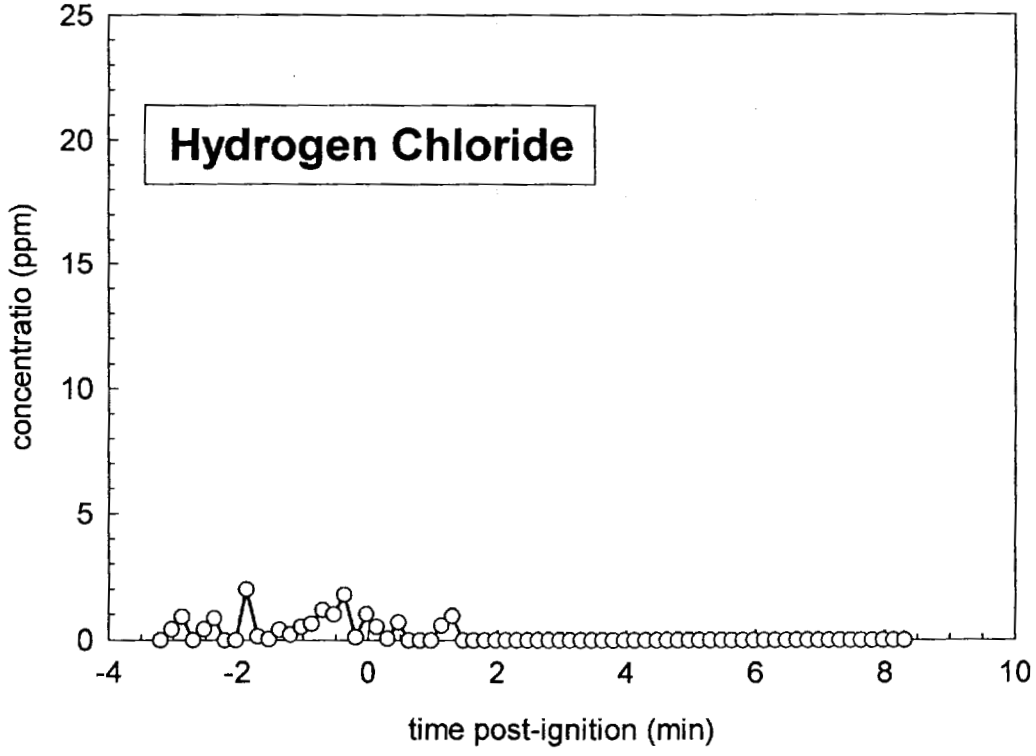

Plot I6. Fire Test F99B1403. Concentration of hydrogen chloride (HCl) in the passenger compartment determined by FTIR analysis.

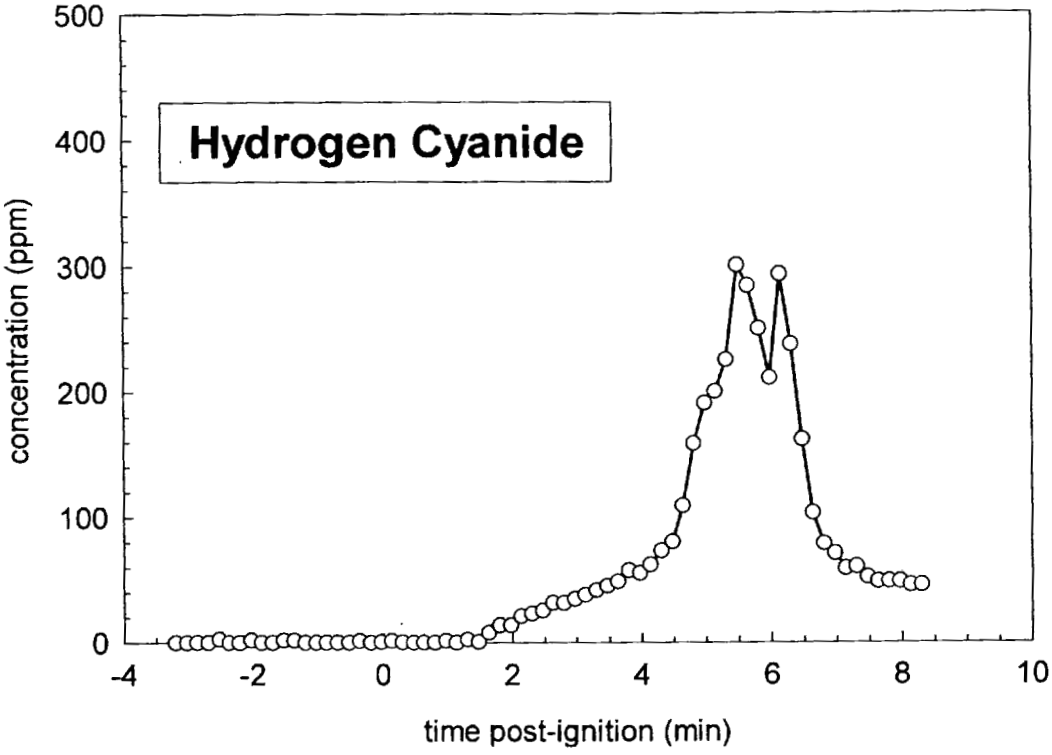

Plot I7. Fire Test F99B1403. Concentration of hydrogen cyanide (HCN) in the passenger compartment determined by FTIR analysis.

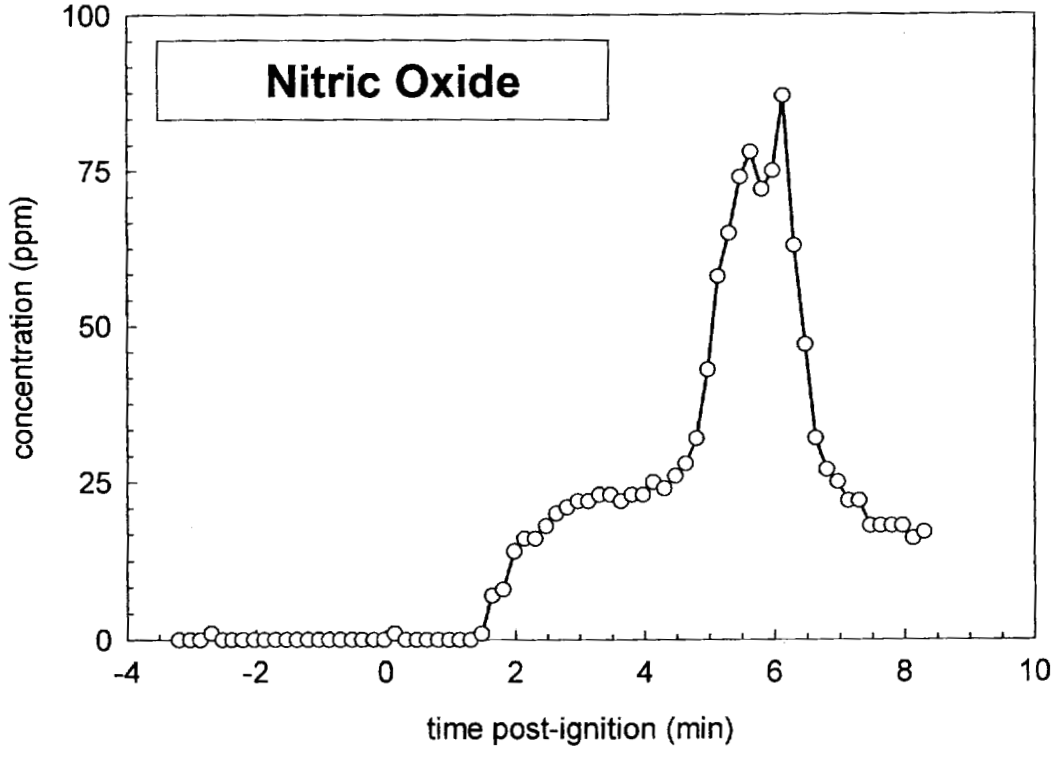

Plot I8. Fire Test F99B1403. Concentration of nitric oxide (NO) in the passenger compartment determined by FTIR analysis.

Appendix J

F99B1403 – Fire Products Collector Data

Scientific and technical personnel from Factory Mutual Research Corporation were primarily responsible for obtaining and analyzing data from the Fire Products Collector (FPC) at the Factory Mutual Test Center.

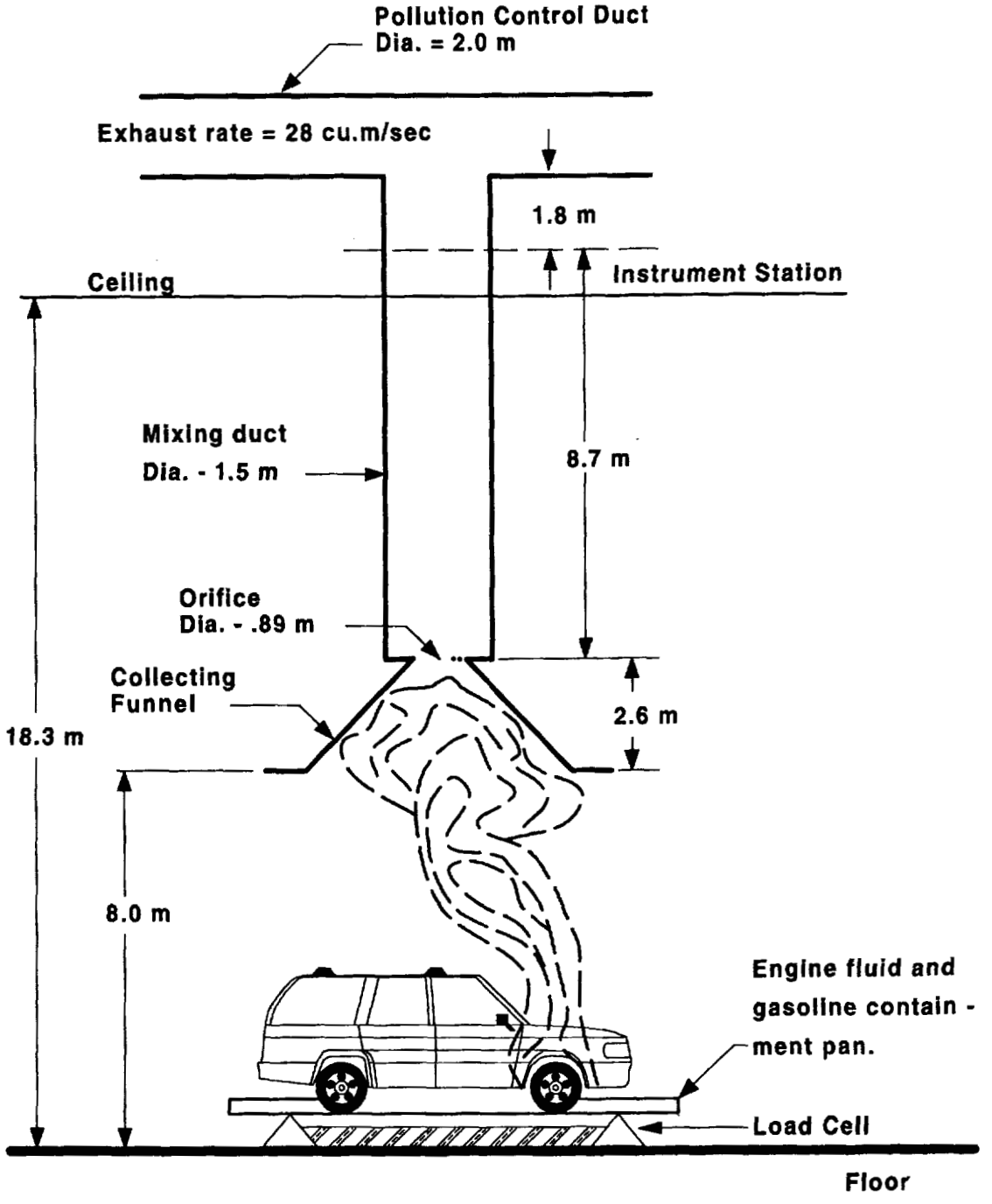

Figure J1. Fire Test F99B1403. Diagram of the test vehicle under the fire products collector at the Factory Mutual Test Center.

The Fire Products Collector was used to measure heat and combustion gases generated by the burning vehicles during these tests (Fig. J1). The FPC consisted of a collection funnel (diameter = 6.1 m), an orifice plate (hole = 0.9 m), and a vertical stainless steel sampling duct (diameter = 1.5 m). The sampling duct was connected to the air pollution control system of the Test Center. The blower of the air pollution control system induces gas flow through the sampling duct. Air enters the sampling duct via the orifice plate. The temperature, linear velocity, optical transmission, and chemical composition of the entrained gas were measured in the center of the sampling duct 8.66 m (5.7 duct diameters) downstream from the orifice plate, ensuring a flat velocity profile at the sampling location. The data acquisition system consisted of a Hewlett Packard 2313B analog-to-digital conversion sub-system interfaced to a Hewlett Packard 1000 computer.

Gas temperature in the sampling duct was measured with two Type-K thermocouples (30 gage) with exposed bead-type junctions. The thermocouple leads were housed in stainless steel tubes (o.d. = 6.4 mm). Ambient air temperature in the facility was measured by five Type-K thermocouples attached to the external surface of the duct at 2.44, 5.49, 9.14, 12.8, and 15.9 m above the floor. These thermocouples were shielded from radiation from the fire.

The linear velocity of the gas entrained in the sampling duct was measured with a Pitot ring consisting of four Pitot tubes. A static pressure tap was mounted on the inside wall of the sampling duct. The pressure difference between the Pitot ring and the static wall tap was measured with an electronic manometer (Barocel Model 1173, CGS Scientific Corporation).

The particulate concentration in the entrained air was determined from the optical transmission across the duct measured at 0.4579 μm (blue), 0.6328 μm (red), and 1.06 μm (infrared). The optical path length across the duct was 1.524 m. Gas was withdrawn from the sampling duct through a stainless steel tube (o.d. = 3.9 mm) at a flow rate of 0.17×10^{-3} m^3/s for chemical analysis. The gas flowed through a particulate filter, a water condenser, and a drying agent before entering the analyzers. Carbon dioxide (CO_2) and carbon monoxide (CO) were measured with two dedicated non-disperse infrared analyzers (Beckman Model 864 Infrared Analyzers). Oxygen (O_2) was measured with a paramagnetic oxygen analyzer (Beckman Model 755 Paramagnetic Oxygen Analyzer). Total gaseous hydrocarbons were measured with a flame ionization analyzer (Beckman Model 400 Flame Ionization Analyzer).

The rate of product release was calculated using the following relationship:

$$\left(\frac{dR_j}{dt}\right) = f_j\left(\frac{dV}{dt}\right)\rho_j = f_j\left(\frac{dW}{dt}\right)\left(\frac{\rho_j}{\rho_g}\right) \qquad \text{(J1)}$$

where $d(R_j)/dt$ is the mass release rate of product j in kg/s; f_j is the volume fraction of product j; dV/dt is the total volume flow rate of the gas entrained in the sampling duct in m^3/s; **dW/dt** is the total mass flow rate of the gas entrained in the sampling duct in kg/s; ρ_j is the density of product j in g/m^3; and ρ_g is the density of the gas entrained in the concentration measurements. The rate of oxygen consumption was calculated using equation (J1), where the volume fraction of oxygen consumed was substituted for f_j.

The volume fraction of smoke particulate was calculated from the following relationship:

$$f_s = \frac{D\lambda \times 10^{-6}}{\Omega} \qquad \text{(J2)}$$

where f_s is the volume fraction of smoke, λ is the wavelength of the light source, Ω is the extinction coefficient of particulate (a value of 0.7 was used in these calculations), and **D** is the optical density at each of the three wavelengths at which measurements were made:

$$D = \frac{\ln\left(I_0/I\right)}{L} \qquad \text{(J3)}$$

where I_0 is the intensity of light transmitted through clean air, I is the intensity of light transmitted through air containing smoke particulate, and L is the optical pathlength, which was equal to 1.524 m. A value of 1.1×10^6 g/m^3 was used for the density of smoke particulate (ρ_j) in equation (G1).

The convective heat release rate was calculated using the following relationship:

$$\left(\frac{dE_{conv}}{dt}\right) = \left(\frac{dW}{dt}\right) \times c_p \times \left(T_g - T_a\right) \qquad \text{(J4)}$$

where $d(E_{conv})/dt$ is the convective heat release rate in kW; dW/dt is the mass flow rate of the gas entrained in the sampling duct in kg/s; c_p is the heat capacity of the gas entrained in the sampling

duct at the gas temperature in kJ/(kg×K); T_g is the temperature of the gas entrained in the sampling duct in K; and T_a is the ambient air temperature in K.

The chemical heat release rate was calculated from the release rates of carbon dioxide and carbon monoxide as follows:

$$\left(\frac{dE_{ch}}{dt}\right) = \Delta H^{*}_{CO_2} \times \left(\frac{dR_{CO_2}}{dt}\right) + \Delta H^{*}_{CO} \times \left(\frac{dR_{CO}}{dt}\right) \qquad \text{(J5)}$$

where $d(E_{ch})/dt$ is the chemical heat release rate in kW; ΔH^* is the net heat of complete combustion per unit mass of carbon dioxide or carbon monoxide released in the fire in kJ/g; and dR/dt is the mass release rate of carbon dioxide or carbon monoxide in kg/s. Values of ΔH^* for carbon dioxide and carbon monoxide were obtained from the literature [J1 and J2].

The chemical heat release rate also was calculated from the oxygen consumption rate as follows:

$$\left(\frac{dE_{ch}}{dt}\right) = \Delta H^{*}_{O}\left(\frac{dC_O}{dt}\right) \qquad \text{(J6)}$$

where $d(E_{ch})/dt$ is the chemical heat release rate in kW; ΔH^*_O is the net heat of complete combustion per unit mass of O_2 consumed in kJ/g; and $d(C_O)/dt$ is the consumption rate of oxygen in kg/s. The value for ΔH^*_O was obtained from the literature [J1 and J2].

The radiative heat release rate was the difference between the chemical heat release rate and the convective heat release rate:

$$\left(\frac{dE_{rad}}{dt}\right) = \left(\frac{dE_{ch}}{dt}\right) - \left(\frac{dE_{conv}}{dt}\right) \qquad \text{(J7)}$$

where $d(E_{rad})/dt$ is the radiative heat release rate; and $d(E_{ch})/dt$ is the average chemical heat release rate calculated using equations (J5) and (J6).

The vehicle was placed in a rectangular steel pan (length = 25 ft., width = 15 ft., height = 4 in.) to prevent spilled and leaking automotive fluids from spreading in the test facility. This fluid containment pan was fabricated from two sheets of carbon steel. Angle-braces were welded to

the under-side of the pan to keep it from flexing under the weight of the vehicle. The corners of the support frame rested on load cells. Mass loss was determined from data acquired from the load cells during the test.

The fluid containment pan was lined with a layer of fiberglass-reinforced cement construction board (DuraRock, USG Corporation). A thin layer of sand was used to level the concrete board so that the grade of the surface measured from the center to the edges along the major and minor axes was no greater than 1%. The joints between boards were sealed with latex caulking.

Mass loss from the burning vehicle and any burning fluids retained by the containment pan was measured with a load cell weigh-module system. The fluid containment pan was supported by an I-beam frame with a load cell weight-module (KIS Series, BLH Electronics, Inc.) at each corner. These weight-modules contain cylindrical, double cantilever strain gauge transducers that are not generally affected by changes in mass distribution. The weight-module system was calibrated before this test by placing a series of standard weights on the fluid containment pan.

Data from the fire-products collector and load cell weight-module system are shown in Plots J1 through J5.

REFERENCES

J1. G. Heskestad. A Fire Products Collector for Calorimetry into the MW Range, Technical Report J.I. OC2E1.RA. Factory Mutual Research Corporation, Norwood, MA. June, 1981.

J2. Archibald Tewarson. "Generation of Heat and Chemical Compounds in Fires" Section 3/Chapter 4, SFPE Handbook of Fire Protection Engineering, 2nd Edition, 1995, pp. 3:53-124.

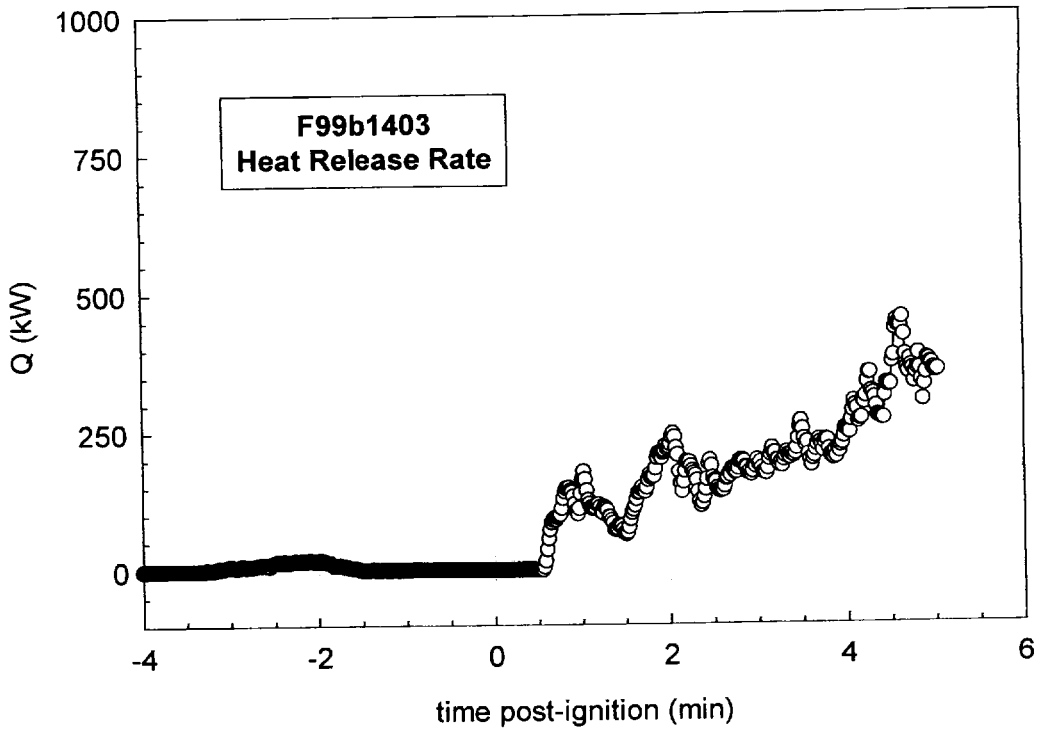

Plot J1. Fire Test F99B1403. Heat release rate measured using the Fire Products Collector.

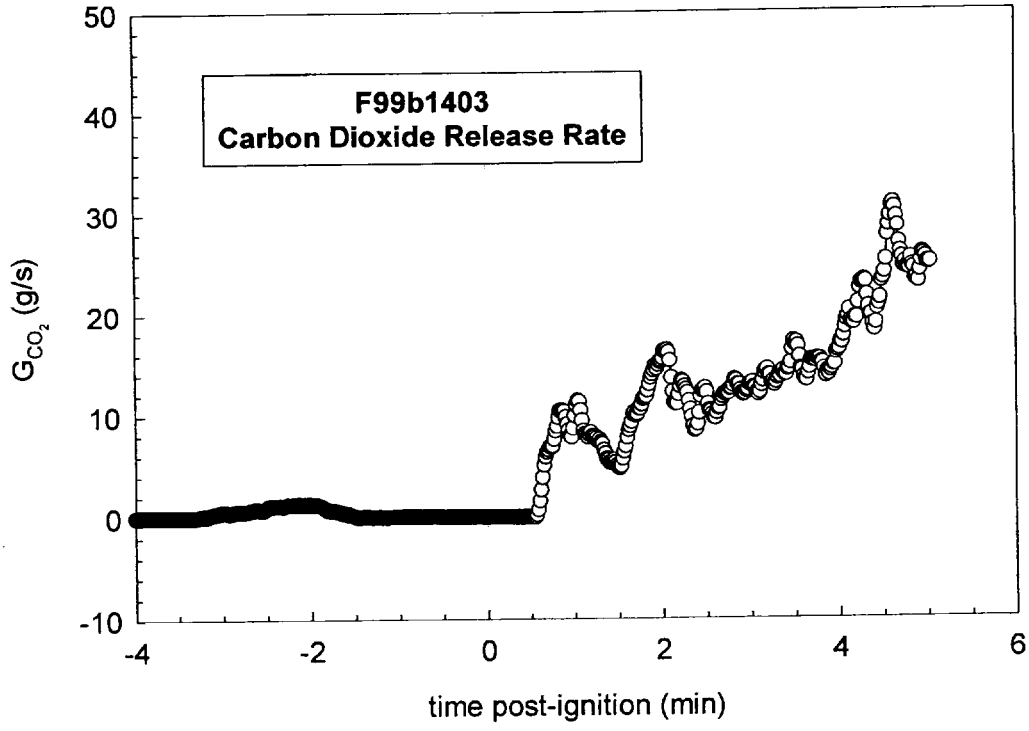

Plot J2. Fire Test F99B1403. Carbon dioxide release rate measured using the Fire Products Collector.

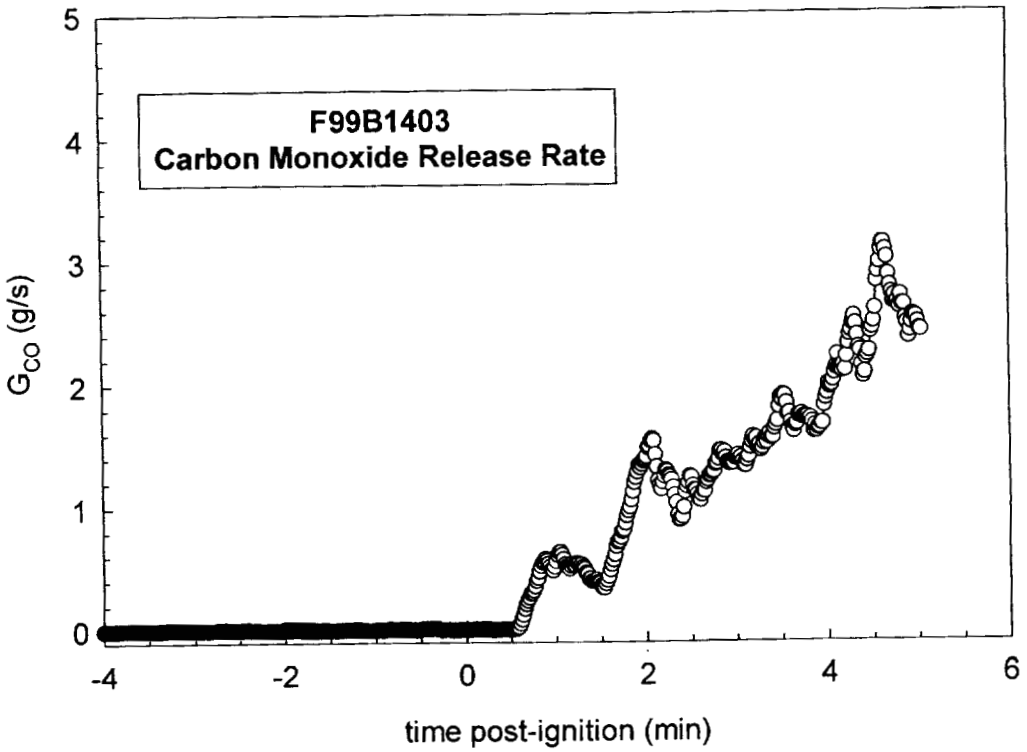

Plot J3. Fire Test F99B1403. Carbon monoxide release rate measured using the Fire Products Collector.

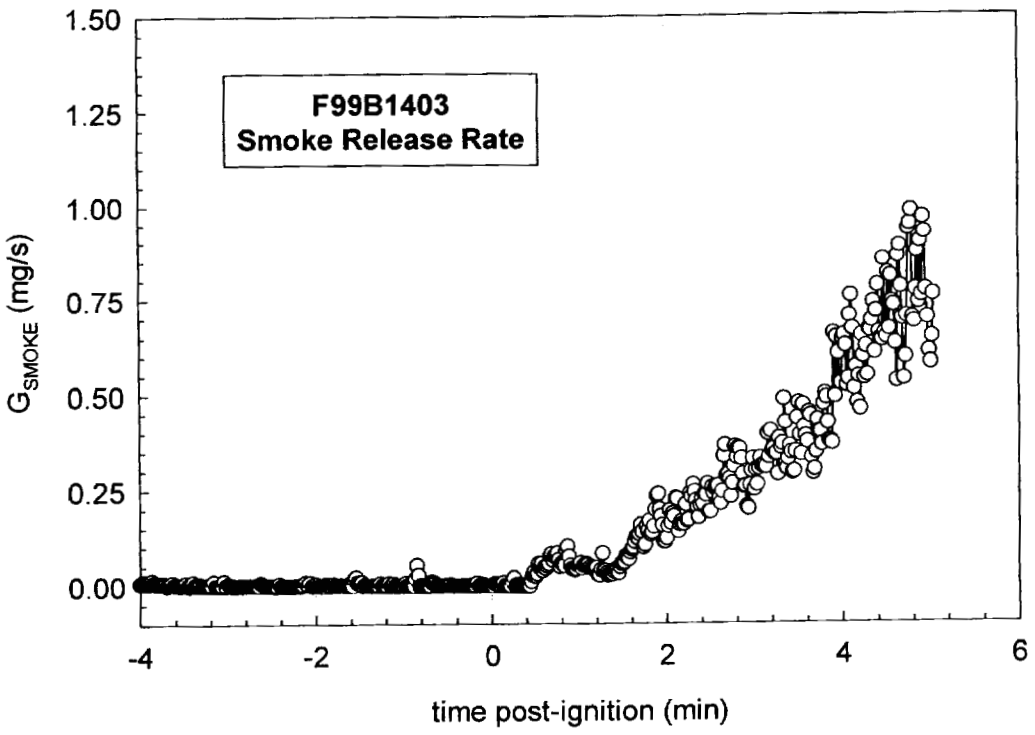

Plot J4. Fire Test F99B1403. Smoke release rate measured using the Fire Products Collector.

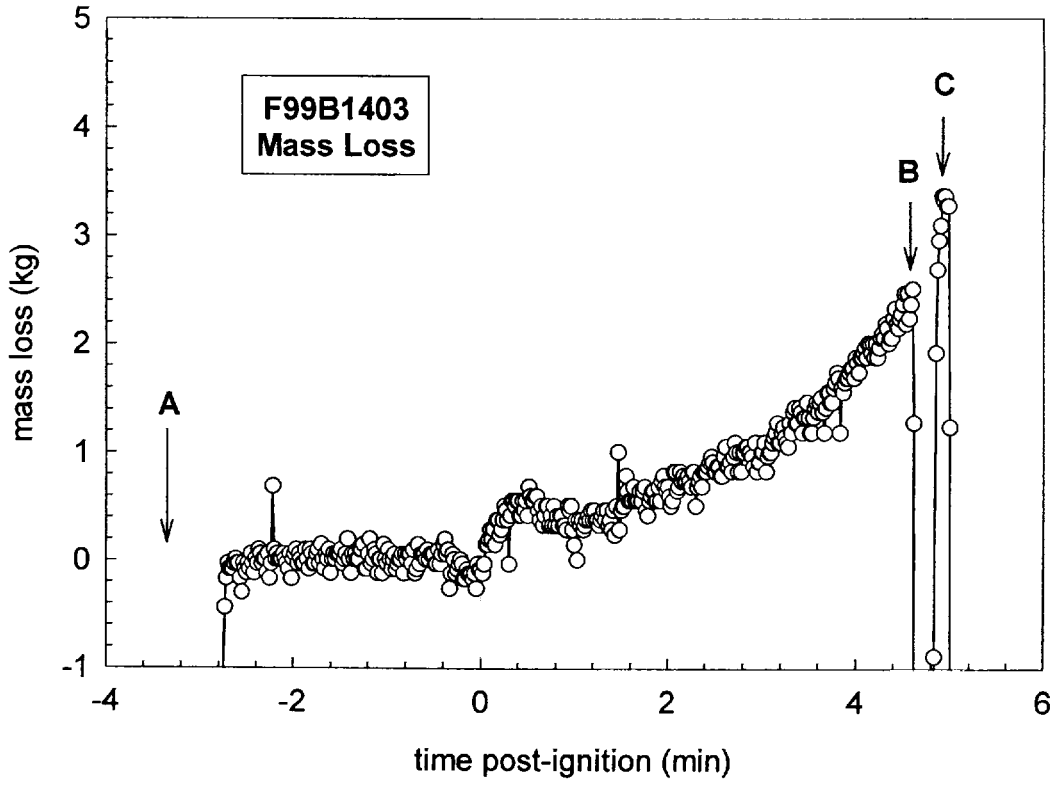

Plot J5. Fire Test F99B1403. Mass Loss from the test vehicle during the fire test.